

RAPID CONSTRUCTION OF PROTEIN CAPTURE AGENTS  
WITH CHEMICALLY DESIGNED STABILITY  
AND ANTIBODY-LIKE RECOGNITION PROPERTIES

Thesis by

Heather Dawn Agnew

In Partial Fulfillment of the Requirements

for the Degree of

Doctor of Philosophy

California Institute of Technology

Pasadena, California

2010

(Defended January 6, 2010)

© 2010

Heather D. Agnew

All Rights Reserved

## ACKNOWLEDGEMENTS

During the past five years at Caltech, I have had the opportunities to learn and grow scientifically in unprecedented ways. I owe much to my advisor Professor James R. Heath, who has been a major figure in my growth as a research scientist. His enthusiasm and intensity about science continue to motivate me to think creatively about the next big problem to solve. I was lucky to join the group during the time when Jim organized the NanoSystems Biology Cancer Center (NSBCC) between Caltech, UCLA, and the Institute for Systems Biology (ISB), which provided us students with access to resources and personnel who are leading researchers in cancer research. Jim truly has an intuition for good science, and I can only hope that I am also developing that capability through our interactions. I am very looking forward to continuing my relationship with Jim at Integrated Diagnostics.

Second, I must thank the members of my thesis committee, namely Professor Robert H. Grubbs, Professor Jacqueline K. Barton, and Professor Mark E. Davis, for being great sources of academic insight and advice, especially during this last year.

I am very grateful to the current members of my subgroup, namely Dr. Rosemary D. Rohde, Dr. Steven W. Millward, Kaycie M. Butler, and Arundhati Nag. It has been a pleasure to work with all of you, and to witness the progress we have all made in the area of protein capture agents. I must also acknowledge the scientists who gave me advice in the early days of the project, Dr. Hartmuth Kolb, Dr. Leroy Hood, and Dr. Alok Srivastava.

I must also thank the rest of the students, postdoctoral scholars, and staff in the Heath group, past and present. I thank Kevin Kan for his overall management of our lab facilities. I thank Diane Robinson for her warm advice and all of her assistance

throughout the years. I thank Dr. Gabriel A. Kwong, Dr. Steven W. Millward, and Young Shik Shin for the times we have talked about science in the office. During my early years of graduate study, I was mentored by two outstanding postdoctoral scholars, Dr. Ryan C. Bailey and Dr. Woon-Seok Yeo. I thank Ryan and Woon-Seok for their patience and guidance, and I am looking forward to great things from their independent scientific careers.

I have also had the great privilege of working with a group of amazingly bright undergraduate students, namely Abdul Ahad Tariq, Russell J. Krom, Vanessa M. Burns, Marissa Barrientos, Eric M. Johnson Chavarria, Andreea D. Stuparu, Michelle Bobrow, and Lucas Carreño. I wish them all the best in their future endeavors, and I hope that their time here gave them an opportunity to consider science as their ultimate career.

I am also very appreciative of the opportunities for collaborative research in Jim's group. I value the times I worked with Dr. Michael C. McAlpine, Dr. Mario Blanco, and Dr. William A. Goddard III on utilizing peptides as the specific recognition elements incorporated on a silicon nanowire gas-sensing device. Similarly, I appreciate the opportunity of meeting with Dr. K. Barry Sharpless, Dr. Valery V. Fokin, Dr. Jason E. Hein, and Dr. Suresh M. Pitram at The Scripps Research Institute. Barry is a wonderful teacher and mentor, and he emanates an infectious passion about science.

Since 2007, I have been interacting with Dr. Su Seong Lee, Dr. Jaehong Lim, Dr. Junhoe Cha, Sylvia Tan, Shi Yun Yeo, and Yiran Zheng from Singapore's Institute of Bioengineering and Nanotechnology. It has been really great to witness the transition of protein capture agent discovery from a strictly academic project to a significantly more high-throughput strategy.

Over the last year, I have had the privilege of working with Chang Ho Sohn, Dr. Jack L. Beauchamp, and Proteome Exploration Laboratory. I am grateful for the skills and experience I have built in mass spectrometry through this collaboration.

During meetings of the NSBCC, I have spent many enjoyable times with Dr. Michael E. Phelps and Dr. Clifton K.-F. Shen. In particular, Mike has been a source of great advice and support of my research.

During my graduate study at Caltech, several individuals have provided access to instrumentation that furthered my research. I thank Dr. Harry B. Gray and Dr. Jay R. Winkler for the use of the Beckman Institute Laser Resource Center. I thank Dr. Jost Vielmetter of the Protein Expression Center and Dr. David A. Tirrell for use of the SPR. I thank Dr. Carl S. Parker for essentially opening up his biology lab to my use. I thank Dr. David A. Baltimore for use of the ELISA plate reader. I thank Dr. Mona Shahgholi for assistance with MALDI-MS measurements. Last, I thank Genomics Facility for use of the Genepix 4200 array scanner.

Financially, I was supported by the NSF, the P.E.O. sisterhood, and Iota Sigma Pi that significantly defrayed my cost of study.

There are a few final people whom I need to thank. It has been great working with Enrica Bruno on the patenting process. I thank my parents and sisters for always being there for me. I thank Bert Lai for his encouraging and positive nature, and I am lucky to have found such a great partner to share my life with. I would finally like to acknowledge Dr. Song Tan for giving me, for the first time in my life, a feeling for exactly what it meant to perform research, and for letting me run with that.

**ABSTRACT**

This thesis describes technologies for the rapid and scalable production of high-affinity, high-specificity protein capture agents which possess the affinities and specificities of antibodies, but also exhibit improved chemical, biochemical, and physical stability. I will discuss how the chemical flexibility of comprehensive, one-bead-one-compound (OBOC) libraries of oligopeptides may be combined with *iterative in situ* click chemistry to select multi-ligand capture agents. Large OBOC libraries form the basis of individual peptide ligands, and also permit chemically designed stability through the incorporation of artificial (azide or acetylene) and non-natural amino acid building blocks. The *in situ* click chemistry method then utilizes the target protein as the catalyst, or template, for assembling its own biligand via formation of a 1,2,3-triazole linkage between two individual ligands (azide and acetylene). This process can be repeated to produce triligands, tetraligands, and other higher-order multi-ligands with an accompanying increase in affinity and specificity through cooperative interactions. Once found, multi-ligand capture agents can be produced in gram amounts via conventional synthetic methods such as the Cu(I)-catalyzed azide-alkyne cycloaddition (CuAAC). This is a general and robust strategy for the inexpensive, high-throughput construction of protein capture agents that can be exploited to detect protein biomarkers in multi-parameter clinical diagnostic assays.

While high-affinity protein capture agents represent a significant technology advance, they are just one component of what is necessary for highly multiplexed measurements of protein biomarkers. It is also important to develop or optimize the actual assay platforms that can enable sensitive multi-parameter protein measurements using these capture agents. Silicon nanowire (SiNW) nanoelectronic sensors can

provide quantitative, label-free multi-parameter measurements of protein biomarkers in real time. However, SiNW sensors can be challenging to deploy because unprotected Si forms a native oxide layer that can significantly reduce the detection sensitivity of the nanowire sensors via dielectric shielding. Another technical challenge is the development of chemistries which allow for the selective encoding of nanowire surfaces with the capture agents. To overcome these challenges, the final part of this thesis presents a general method to functionalize organic and biological molecules on highly passivated Si(111) surfaces with minimal surface oxidation.

**TABLE OF CONTENTS**

<b>LIST OF FIGURES, SCHEMES, AND TABLES</b> .....	xiii
<b>CHAPTER 1: Introduction</b> .....	1
1.1 High-Affinity Protein Capture Agents in Medical Diagnostics.....	2
1.2 Assay Platforms for Multi-Parameter Protein Measurements.....	8
1.3 References.....	12
<b>CHAPTER 2: Selection of a Multi-ligand Capture Agent for Carbonic</b>	
<b>Anhydrase II by Iterative In Situ Click Chemistry</b> .....	15
2.1 Introduction.....	16
2.2 Materials and Experimental Methods.....	18
2.2.1 Materials.....	18
2.2.2 Artificial Amino Acids.....	20
2.2.3 OBOC Oligopeptide Library Construction.....	24
2.2.4 Screening Procedures for Anchor Ligand.....	25
2.2.5 In Situ Click Screening Procedures for Biligand.....	28
2.2.6 In Situ Click Screening Procedures for Higher-Order	
Multi-ligands.....	32
2.2.7 Validation of In Situ Click/OBOC Multi-ligand	
Screening Procedures.....	32
2.2.8 Bulk Peptide Synthesis.....	33
2.2.9 On-Bead Biligand and Triligand Synthesis.....	39

2.3 Results and Discussion.....	41
2.3.1 Screening for Anchor (1°) Ligand against bCAII.....	41
2.3.2 Identification of Secondary (2°) Ligands: Biligand Screens..	43
2.3.3 Identification of Tertiary (3°) Ligands: Triligand Screens....	50
2.4 Conclusions.....	52
2.5 Acknowledgements.....	53
2.6 References.....	54

### **CHAPTER 3: Affinities, Specificities, and Implementation of Multi-ligand**

<b>Capture Agents in Standard Assays of Protein Detection.....</b>	<b>59</b>
3.1 Introduction.....	60
3.2 Materials and Experimental Methods.....	62
3.2.1 Chemicals.....	62
3.2.2 Characterization of Affinity by Fluorescence Polarization.....	62
3.2.3 Characterization of Affinity by Surface Plasmon Resonance.	63
3.2.4 Enzymatic Activity Assay of Carbonic Anhydrase II.....	65
3.2.5 Circular Dichroism of Triligand.....	65
3.2.6 Dot Blot Specificity/Sensitivity Assays of Biligand and Triligand in Serum.....	65
3.2.7 Western Blot Analysis Using Triligand.....	66
3.2.8 Sandwich (ELISA-like) Assays Using Triligand.....	67
3.3 Results and Discussion.....	67
3.3.1 Characterization of Anchor (1°) Ligand Affinities.....	68

3.3.2	Characterization of Biligand Affinities.....	70
3.3.3	Characterization of Triligand Affinities.....	74
3.3.4	Enzymatic Activity Assay of Carbonic Anhydrase II.....	74
3.3.5	Circular Dichroism of Triligand.....	77
3.3.6	Dot Blot Specificity/Sensitivity Assays of Biligand and Triligand in Serum.....	77
3.3.7	Western Blot Analysis Using Triligand.....	83
3.3.8	Sandwich (ELISA-like) Assays Using Triligand.....	86
3.4	Conclusions.....	89
3.5	Acknowledgements.....	90
3.6	References.....	91

## **CHAPTER 4: Assays for Quantifying Protein-Catalyzed Multi-ligands and**

<b>Extensions to Other Proteins.....</b>	<b>92</b>
4.1 Introduction.....	93
4.2 Materials and Experimental Methods.....	94
4.2.1 Materials.....	94
4.2.2 On-Bead Detection of In Situ Triazole Formation.....	95
4.2.3 QPCR Assay for the Detection and Quantitation of the Formation of On-Bead, Protein-Catalyzed Triligand Capture Agent.....	96
4.2.4 Selection of Biligand Capture Agent for Prostate- Specific Antigen.....	98

4.3 Results and Discussion.....	101
4.3.1 Initial Validation of Protein-Catalyzed Multi-ligand Product.	101
4.3.2 Direct Detection of Protein-Catalyzed In Situ Multi-ligand....	102
4.3.3 Strategies for Improving Signal-to-Noise Ratio during In Situ Click/OBOC Screens.....	107
4.3.4 Selection of Biligand Capture Agent for Prostate- Specific Antigen.....	112
4.4 Conclusions.....	119
4.5 Acknowledgements.....	120
4.6 References.....	121

## **CHAPTER 5: A Non-Oxidative Approach toward Chemically and**

<b>Electrochemically Functionalizing Si(111).....</b>	<b>124</b>
5.1 Introduction.....	125
5.2 Materials and Experimental Methods.....	128
5.2.1 Chemicals.....	128
5.2.2 Acetylenylation of Si(111).....	129
5.2.3 Synthesis of Electroactive Benzoquinone <b>1</b> .....	131
5.2.4 Click Reaction to Attach <b>1</b> onto Acetylene-Terminated Si(111).....	134
5.2.5 Electrochemical Activation to Attach Ferrocene Carboxylic Acid and Biotin.....	135
5.3 Surface Characterization.....	137

5.3.1 X-ray Photoelectron Spectroscopy.....	137
5.3.2 Contact Angle Goniometry.....	137
5.3.3 Electrochemical Characterization of Surface Coverages.....	138
5.3.4 Fourier-Transform Infrared Spectroscopy.....	138
5.4 Results.....	139
5.4.1 XPS Survey Scans and Contact Angle Measurements.....	139
5.4.2 High-Resolution XPS Measurements.....	139
5.4.3 Electrochemical Measurements.....	145
5.5 Discussion.....	147
5.6 Conclusions.....	154
5.7 Acknowledgements.....	154
5.8 References.....	155

<b>APPENDIX A: Iterative In Situ Click Chemistry Creates Antibody-Like Protein Capture Agents</b> ( <i>Angewandte Chemie International Edition</i> <b>2009</b> , <i>48</i> , 4944–4948).....	161
<b>APPENDIX B: Complete Hit Sequencing Results</b> .....	167
<b>APPENDIX C: Custom Edman Degradation</b> .....	176
<b>APPENDIX D: A Non-Oxidative Approach toward Chemically and Electrochemically Functionalizing Si(111)</b> ( <i>Journal of the American Chemical Society</i> <b>2006</b> , <i>128</i> , 9518–9525).....	179

**LIST OF FIGURES, SCHEMES, AND TABLES****FIGURES, Chapter 2:**

Figure 2.1. Schematic of preparing a multi-ligand capture agent.....	19
Figure 2.2. Structures of representative 1° ligands, 2° ligands, and biligands....	35
Figure 2.3. Structures of biligand anchors.....	37
Figure 2.4. Structures of 3° ligands and triligands .....	38
Figure 2.5. Results of selecting a primary or anchor ligand of bCAII.....	42
Figure 2.6. Schematic of two types of biligand screen.....	44
Figure 2.7. Identification of a 2° ligand against bCAII.....	46
Figure 2.8. Distribution of D-amino acids found in biligand hits.....	48
Figure 2.9. Binary component in situ click chemistry screen.....	49
Figure 2.10. Method to validate protein-templated formation of multi-ligand capture agent.....	51

**FIGURES, Chapter 3:**

Figure 3.1. Fluorescence polarization for a fluoresceinated anchor ligand.....	69
Figure 3.2. SPR interactions of anchor ligands with bCAII.....	71
Figure 3.3. SPR interactions of biligands with bCAII.....	73
Figure 3.4. SPR interactions of triligand with bCAII and hCAII.....	75
Figure 3.5. Enzymatic activity of bCAII in the presence of triligand.....	76
Figure 3.6. CD spectrum for triligand capture agent.....	78
Figure 3.7. Structures of biotinylated triligand and biligand anchor.....	80
Figure 3.8. Dot blot of triligand and biligand for b(h)CAII detection.....	81

Figure 3.9. Dot blot of triligand vs. antibody for b(h)CAII detection.....	82
Figure 3.10. Denaturing and non-denaturing Western blots detected with a triligand capture agent.....	85
Figure 3.11. Sandwich (ELISA-like) assay utilizing a triligand as primary capture agent for bCAII detection.....	87

#### **FIGURES, Chapter 4:**

Figure 4.1. In situ click assay for on-bead triazole formation.....	103
Figure 4.2. On-bead multi-ligand detection by QPCR.....	106
Figure 4.3. General screening strategies to improve signal-to-noise ratio and reduce number of false positives in OBOC selections.....	109
Figure 4.4. Screening and anti-screening strategies to target a particular protein epitope or modification .....	110
Figure 4.5. Two-stage in situ/click OBOC screening strategy to identify a biligand capture agent for PSA .....	111
Figure 4.6. Representative image of an in situ click/OBOC screen with enzymatic amplification.....	117
Figure 4.7. Structures of active site targeted cyclic anchor and cyclic biligand, and SPR interactions with PSA. ....	118

#### **FIGURES, Chapter 5:**

Figure 5.1. XPS data of H-C≡C-[Si(111)].....	142
Figure 5.2. High-resolution XPS spectra of H-C≡C-[Si(111)].....	143

Figure 5.3. Cyclic voltammograms (CVs) for <b>1s</b> and <b>3s</b> .....	146
Figure 5.4. ATR-FTIR characterization of H-[Si(111)] and H-C≡C-[Si(111)]..	150
Figure 5.5. Demonstration of bioattachment to acetylenylated Si(111).....	153

### **FIGURES, Appendix C:**

Figure C.1. Pulsed-Liquid cLC Extended method and gradient.....	177
Figure C.2. Final steps of Flask Normal Extended flask cycle.....	178
Figure C.3. Edman traces for artificial azide-containing amino acids.....	178

### **SCHEMES, Chapter 2:**

Scheme 2.1. Artificial amino acid synthesis.....	22
Scheme 2.2. Selection of anchor ligand by OBOC screen.....	27
Scheme 2.3. Selection of biligand by in situ click/OBOC screen.....	31
Scheme 2.4. Acetylation and click reactions for a 6-mer peptide.....	40

### **SCHEMES, Chapter 3:**

Scheme 3.1. Esterase activity of bCAII.....	76
---	----

### **SCHEMES, Chapter 5:**

Scheme 5.1. Strategy for the functionalization of Si(111).....	130
Scheme 5.2. Synthesis of electroactive benzoquinone <b>1</b> .....	132
Scheme 5.3. Steps required to non-oxidatively activate Si(111) surfaces.....	136

**TABLES, Chapter 2:**

Table 2.1. Libraries used in selecting a triligand capture agent for bCAII.....	26
Table 2.2. Screening summary.....	29

**TABLES, Chapter 5:**

Table 5.1. Measured contact angles for various Si(111) surfaces.....	140
Table 5.2. Measured molecular surface coverages for Si(111) surfaces.....	148

**TABLES, Appendix B:**

Table B.1. First-generation anchor ligand screen <b>An1</b> .....	168
Table B.2. Second-generation anchor ligand screens <b>An2a</b> and <b>An2b</b> .....	169
Table B.3. In situ biligand screen <b>Bi1</b> .....	170
Table B.4. On-bead biligand screens <b>Bi2a</b> and <b>Bi2b</b> .....	171
Table B.5. First-generation in situ triligand screen <b>Tri1</b> .....	172
Table B.6. First-generation on-bead triligand screen <b>Tri2</b> .....	173
Table B.7. Second-generation triligand screens <b>Tri3</b> and <b>Tri4</b> .....	174
Table B.8. Azide-free in situ triligand screen <b>TriX</b> (control).....	175

## **Chapter 1**

Introduction

## 1.1 High-Affinity Protein Capture Agents in Medical Diagnostics

A fundamental goal of medical diagnostics is to detect and monitor changes in biomarkers, which are substances used as an indicator of a biological state. Exemplary biomarkers are proteins, genes, mRNA, or small molecules. With the information provided by measurement of biomarkers, the current state of a patient's health can potentially be determined and predictive features can be claimed. Medical diagnostics, and in particular cancer diagnostics, is increasingly requiring measurements of large panels of biomarkers based on the complex and heterogeneous molecular composition of diseased tissues and organs. Such a multi-parameter approach, namely simultaneously measuring as many different biomarkers as possible in a single experiment, should improve the accuracy and efficiency of diagnostic assays. Through the measurement of a collection of biomarkers, multi-parameter diagnostics have the potential to offer unique molecular signatures, or fingerprints, of a patient's health status and a high level of sensitivity and specificity for diagnosing, staging, monitoring treatments over time, and predicting future disease.<sup>1</sup>

Genetic (DNA) and transcriptomic (mRNA) biomarker panels are already employed in the clinic on a routine basis, but technologies enabling the routine implementation of protein biomarker panels have lagged behind. This is quite unfortunate, as protein biomarker measurements are perhaps the most informative clinically. However, they are also by far the most expensive, in terms of cost per biomarker. In addition, the majority of the approximately 20,000 proteins in the human proteome are post-translationally modified at some stage in their existence, and such modifications can often change the basic function of the protein.<sup>2</sup> These modifications (e.g., glycosylation, phosphorylation) can only be detected by directly detecting the

modified protein. Furthermore, temporal changes in post-translational modifications, such as evolving glycosylation patterns on a given protein, have been implicated as indicators of disease stage.<sup>3</sup>

The dominant clinical technologies for detecting protein biomarkers are antibody based and, in fact, the gold standard protein assays, and the only ones that are highly reproducible from clinic to clinic and across geographical locations, require two antibodies per protein detected. These are sandwich assays, or enzyme-linked immunosorbent assays (ELISAs).<sup>4</sup> The cost and instability of antibodies generally prohibit the measurement of more than a handful of proteins in a single assay, and the cost per protein is about \$50. Nevertheless, ultimately one would like to routinely assess the levels of hundreds or more proteins for disease diagnosis, or monitor a few proteins at high frequency. This will require inexpensive protein capture agents that possess the affinities and specificities of antibodies, but also exhibit chemical, biochemical, and physical stability. A technology for the rapid and scalable production of such capture agents would revolutionize disease diagnostics. It would also significantly impact benchtop research, providing the realization of quantitative and highly multiplexed assays that can replace the pauci-parameter protein measurement approaches (e.g., Western blots) that are standard today.

Non-antibody protein capture agents have been pursued for several years. The chemical nature of such capture agents is typically limited to nucleic acids, peptides, and small molecules, but a capture agent can also incorporate lipids, carbohydrates, and even other proteins. Nucleic acid aptamers<sup>5</sup> hold promise, but possess the intrinsic limitation of chemical diversity, as there are only 4 standard nucleobases, as compared to the 20 natural amino acids from which proteins are constructed. Other issues, such as nuclease

resistance and synthetic scale-up, comprise additional hurdles in the widespread applicability of nucleic acid aptamers. On the other hand, peptides selected from phage display libraries<sup>6</sup> can offer reasonable to excellent performance. However, the L-amino acids comprising such peptides are sensitive to proteolytic cleavage. Chemical stability and water solubility can be an additional limitation as they are highly sequence dependent.

A third alternative is peptide affinity agents that are identified using one-bead-one-compound (OBOC) libraries.<sup>7</sup> This chemical library-based approach allows for the inclusion of broad classes of amino acids, including artificial and non-natural amino acids, along with peptide mimetics.<sup>8</sup> This diverse chemical flexibility can be harnessed to infer attributes including biochemical, chemical, and physical stability, and water solubility. However, compromises have to be reconciled between peptide length and library diversity, since OBOC libraries of oligopeptides are practically only  $10^5$ – $10^6$  elements in size.<sup>7</sup> In addition, even a small OBOC library of polypeptides (or polypeptide mimetics) can be challenging to build, since the synthetic purity of an on-bead peptide correlates with peptide length, and very-high purity libraries are required for affinity screening. As a result, OBOC libraries have rarely been employed for the identification of high-affinity, high-specificity protein capture agents.

Small molecule ligands can exhibit a high affinity for their protein targets, but selectivity is limited since they only sample a small part of the protein.<sup>9</sup> One small-molecule method that is relevant to the work of this thesis is that of in situ click chemistry,<sup>10</sup> which was originally developed by K. B. Sharpless and M. G. Finn. Their goal was to identify small molecule enzymatic inhibitors that could be catalytically assembled using the scaffold of the protein target itself. Some of these studies started

with a known small molecule inhibitor that was then divided into two components, each of which was expanded into a small library of building blocks. One library contained molecules functionalized with an azide group, and the other library contained molecules functionalized with an acetylene group. During the screening of the target protein against the molecular libraries, the protein plays an active role in the selection and covalent assembly of a new inhibitor. In these systems, the protein accelerates the Huisgen 1,3-dipolar “click” cycloaddition by holding elements from each library in close proximity. The protein exhibits exquisite selectivity; it only promotes the formation of a 1,2,3-triazole between those library elements that can be brought into precise molecular proximity on the protein surface. The result is a biligand inhibitor with an affinity that approaches the product of the affinities of the individual molecular components. Furthermore, the triazole itself can contribute to the binding affinity observed for this inhibitor.

In Chapters 2 and 3 of this thesis, I will discuss how the chemical flexibility of comprehensive, OBOC libraries of oligopeptides may be combined with *iterative in situ* click chemistry to select a high-affinity, high-specificity triligand capture agent against the protein biomarker carbonic anhydrase II (CA II), for both the human and bovine varieties ( $K_D \approx 45$  and  $64$  nM, respectively). Furthermore, this triligand capture agent can be used in a dot blot assay to detect those proteins at the  $\geq 20$  ng level from 10% porcine serum. Results from Western blots, sandwich (ELISA-like) assays, and protein activity assays, with the triligand implemented as the primary capture agent, are presented in Chapter 3.

The triligand is built from peptides comprised of non-natural and artificial amino acids, including amino acids containing azido and acetylene functionalities. For this

selection scheme, the OBOC method was utilized first to identify an anchor (1°) ligand for CA II which contained a terminal acetylene-containing amino acid. This screen resulted in a 7-mer peptide that binds CA II with  $K_D \approx 500 \mu\text{M}$ , which is a suitable affinity value for further maturation. Then, the protein target was utilized to template the covalent coupling between two peptide ligands, the pre-identified 1° ligand and a secondary (2°) ligand, which was selected by the protein target and the 1° ligand from a comprehensive OBOC library of 2° ligands displaying a terminal azide-containing amino acid. This in situ click chemistry screen resulted in a biligand that binds CA II with  $K_D \approx 3 \mu\text{M}$ . After modifying the biligand with a terminal acetylene-containing amino acid, this capture agent became the new anchor for selection of a 3° ligand. A final protein-templated in situ click chemistry screen between the biligand anchor and a comprehensive OBOC library of 3° ligands (azides) resulted in the triligand capture agent. Interestingly, the triligand does not bind to the enzymatically active binding site of CA II—a result that argues for the generality of this approach.

This *iterative* in situ click chemistry approach has several significant advantages over both traditional in situ click chemistry<sup>10</sup> and traditional OBOC peptide libraries<sup>7</sup> for affinity agent screening. These include: (1) Production of the capture agent requires no prior knowledge of affinity agents against the protein of interest, but can potentially take advantage of such ligands if they exist. (2) The approach permits the sampling of a very large chemical space. (3) The process can be repeated to produce tetraligands, pentiligands, and other higher-order multi-ligands with an accompanying increase in affinity and specificity from cooperative interactions. (4) The approach may be harnessed to produce branched capture agents, thus providing low molecular weight capture agents that mimic the 3-D folded structures of antibodies or polypeptides.

(5) The capture agents can be designed, *ab initio*, to contain desirable features such as chemical, biochemical, and thermal stability, water solubility, fluorophore conjugation, and ability for highly oriented attachment to a substrate or surface in a monoparameter or multiparameter assay. (6) The final capture agents may be prepared in gram quantities and stored as a powder under ambient conditions. Chapters 2 and 3 have been taken in part from *Angewandte Chemie International Edition* **2009**, 48, 4944–4948 (see also Appendix A).

Protein-templated in situ click chemistry is a low-yielding reaction requiring precise alignment of the azide and alkyne with respect to each other and the protein. Therefore, only a small fraction ( $\ll 1\%$ ) of the peptides on a particular bead will be converted to multi-ligands. In Chapter 4, both colorimetric and quantitative polymerase chain reaction (QPCR)-based methods for detection and quantitation of the formation of on-bead, protein-catalyzed multi-ligand capture agent will be discussed. The low but detectable yield per protein-catalyzed in situ click reaction—approximately 0.000005% for bCAII—confirms the exquisite demands of the process. This result encouraged us to develop more sophisticated screening strategies that incorporated anti-selections (following the selections) and also direct detection of the bead-bound products of the protein-catalyzed click reaction. In other words, we developed screens that identified the protein target, secondary screens that identified the in situ click product, and even tertiary screens that identified potential side-reactions. These new screening strategies were applied toward the selection of a biligand capture agent ( $K_D \approx 140$  nM) against the blood-based cancer biomarker prostate-specific antigen (PSA). The rapid assembly of the biligand capture agent by the protein-catalyzed process was expedited to two weeks by utilization of a previously reported anchor ligand<sup>11</sup> and the new selection/anti-

selection strategies, and demonstrates the potential feasibility of a high throughput route toward production of high-affinity, high-specificity protein capture agents.

## **1.2 Assay Platforms for Multi-Parameter Protein Measurements**

While the high-affinity protein capture agents of Chapters 2 to 4 represent a significant technology advance, they are just one component of what is necessary for highly multiplexed measurements of protein biomarkers. In addition, it is also important to develop or optimize the actual assay platforms that can enable sensitive multi-parameter protein measurements using these capture agents. There are a number of drawbacks associated with the existing gold-standard approaches. As mentioned above, the gold standard for protein diagnostic assays are ELISA assays, and the standard clinical procedures are to extract a few milliliters of blood from a patient, centrifuge that blood to separate plasma (or serum) from whole blood, and then carry out ELISA assays for one or two proteins in 96-well plate format under diffusion-limited conditions.

One drawback of this approach involves the stability of the antibodies utilized within the ELISA assays. ELISA assays require at least two antibody capture agents for detection of the protein biomarker—a monoclonal surface-immobilized antibody for protein capture, and a secondary enzyme-linked polyclonal antibody which binds to a second epitope on the protein. Binding of the secondary antibody is visualized by applying a colorimetric substrate which, for example, changes color or yields a fluorescence signal in the presence of enzyme. In Chapter 3, I will describe how peptide multi-ligands, identified by in situ click chemistry, show feasibility as capture agents in ELISA and other standard biological assays such as Western blots. Using multi-ligand capture agents instead of antibodies in these platforms avoids problems often associated

with antibody use—namely high cost, poor stability, and subtle variations in performance (e.g., sensitivity).

A second drawback of the current gold-standard clinical approach is that it is slow. During the time between blood draw and assay completion (typically a few hours to a few days), the biospecimen may degrade, so that the measured protein levels no longer reflect the patient status at the time of the blood draw. In addition, the few milliliters of blood that are drawn make it easier to handle the blood, but, in principle, the same protein assays could be accomplished with only a few microliters of plasma or serum (and thus, with a significantly reduced amount of patient discomfort).

While multi-ligand capture agents avoid the inherent problems of antibody instabilities (and potentially antibody costs), they do not change the inherently large sample volume, lengthy assay time, or number of measurement parameters per assay. The use of microfluidics to miniaturize and expedite protein assays can solve many of these problems.<sup>1a</sup> Other technologies, such as label-free nanoelectronic sensors, can provide further advantages. Silicon nanowire (SiNW) nanoelectronic sensors<sup>12</sup> can provide quantitative multi-parameter measurements from nanoliter to microliter volumes of protein biomarkers in real time. The “label-free” characteristic of these sensors means that no secondary antibodies are required to detect the binding between the protein of interest and capture agent. SiNWs fabricated by the SNAP technique<sup>13</sup> represent ultra-dense arrays of electronically addressable nanowires, where each wire may be functionalized with a different protein capture agent. When the protein of interest specifically binds to the capture agent, both the electrical conductance of the nanowire and the electrical capacitance between the nanowire and the surrounding solution is altered. These electrical changes may be directly correlated to the absolute

amount of protein in the solution. However, SiNW sensors can be challenging to deploy. For example, working with Si surfaces can be challenging because unprotected Si forms a native oxide ( $\text{SiO}_2$ ), and this insulating layer can significantly reduce the detection sensitivity of the nanowire sensors via dielectric shielding. In addition, the native oxide on silicon also has a low isoelectric point, meaning that under physiological conditions (= pH 7.4),  $\text{SiO}_2$  surfaces are negatively charged.<sup>14</sup> These surface charges can potentially limit the sensitivity of silicon nanowire field effect biosensors through Debye screening at the sensor surface.<sup>15</sup> Finally, the native oxide layer contains electrical defect sites at the Si- $\text{SiO}_2$  interface.<sup>16</sup> For high surface area devices, such as SiNWs, this phenomenon can reduce charge carrier mobilities significantly.<sup>16,17</sup>

In Chapter 5, a general method for the non-oxidative functionalization of single-crystal silicon (111) is described. To prevent the formation of this oxide, the silicon (111) surface was modified with an acetylene ( $-\text{C}\equiv\text{C}-\text{H}$ ) monolayer of  $\sim 100\%$  surface coverage. An electroactive monolayer of a benzoquinone-masked primary amine was subsequently formed on the acetylene-passivated surface via Cu(I)-catalyzed Huisgen 1,3-dipolar cycloaddition (“click” chemistry). Molecules presenting a carboxylic acid group were finally immobilized onto regions where the benzoquinone had been reduced and cleaved to reveal the underlying amine on the surface. This strategy provides a general platform to incorporate most organic and biological molecules, such as proteins, antibodies, or multi-ligand capture agents, on highly passivated silicon (111) surfaces with minimal surface oxidation. This work can be further extended toward the non-oxidative biopassivation of silicon-on-insulator (SOI) wafers, whose topmost 30–50 nm single-crystal silicon layer is the substrate in the fabrication of SiNW sensors. Chapter 5

has been taken in part from the *Journal of the American Chemical Society* **2006**, *128*, 9518–9525 (see also Appendix D).

**1.3 REFERENCES**

1. (a) Fan, R.; Vermesh, O.; Srivastava, A.; Yen, B. K. H.; Qin, L.; Ahmad, H.; Kwong, G. A.; Liu, C.-C.; Gould, J.; Hood, L.; Heath, J. R. *Nat. Biotechnol.* **2008**, *26*, 1373–1378. (b) Hood, L.; Heath, J. R.; Phelps, M. E.; Lin, B. *Science* **2004**, *306*, 640–643. (c) Phelan, M. L.; Nock, S. *Proteomics* **2003**, *3*, 2123–2134.
2. Larsen, M. R. *Methods Mol. Biol.* **2003**, *251*, 245–262.
3. Dudkin, V. Y.; Miller, J. S.; Dudkina, A. S.; Antczak, C.; Scheinberg, D. A.; Danishefsky, S. J. *J. Am. Chem. Soc.* **2008**, *130*, 13598–13607.
4. Engvall, E.; Perlmann, P. *J. Immunol.* **1972**, *109*, 129–135.
5. (a) Cox, J. C.; Hayhurst, A.; Hesselberth, J.; Bayer, T. S.; Georgiou, G.; Ellington, A. D. *Nucleic Acids Res.* **2002**, *30*, e108–e108. (b) Lee, J. F.; Hesselberth, J. R.; Meyers, L. A.; Ellington, A. D. *Nucleic Acids Res.* **2004**, *32*, D95–D100. (c) Famulok, M.; Mayer, G.; Blind, M. *Acc. Chem. Res.* **2000**, *33*, 591–599. (d) Gold, L.; Polisky, B.; Uhlenbeck, O.; Yarus, M. *Annu. Rev. Biochem.* **1995**, *64*, 1094–1110. (e) Burmeister, P. E.; Lewis, S. D.; Silva, R. F.; Preiss, J. R.; Horwitz, L. R.; Pendergrast, P. S.; McCauley, T. G.; Kurz, J. C.; Epstein, D. M.; Wilson, C.; Keefe, A. D. *Chem. Biol.* **2005**, *12*, 25–33. (f) Proske, D.; Blank, M.; Buhmann, R.; Resch, A. *Appl. Microbiol. Biotechnol.* **2005**, *69*, 367–374. (g) Thiel, K. *Nat. Biotechnol.* **2004**, *22*, 649–651.
6. Smith, G. P.; Petrenko, V. A. *Chem. Rev.* **1997**, *97*, 391–410.
7. Lam, K. S.; Lebl, M.; Krchňák, V. *Chem. Rev.* **1997**, *97*, 411–448.
8. (a) Lam, K. S.; Lebl, M.; Krchňák, V.; Wade, S.; Abdul-Latif, F.; Ferguson, R.; Cuzzocrea, C.; Wertman, K. *Gene* **1993**, *137*, 13–16. (b) Liu, R.; Marik, J.; Lam, K. S. *J. Am. Chem. Soc.* **2002**, *124*, 7678–7680. (c) Alluri, P. G.; Reddy, M. M.;

- Bachhawat-Sikder, K.; Olivos, H. J.; Kodadek, T. *J. Am. Chem. Soc.* **2003**, *125*, 13995–14004. (d) Tornøe, C. W.; Sanderson, S. J.; Mottram, J. C.; Coombs, G. H.; Meldal, M. *J. Comb. Chem.* **2004**, *6*, 312–324.
9. Fabian, M. A.; Biggs III, W. H.; Treiber, D. K.; Atteridge, C. E.; Azimioara, M. D.; Benedetti, M. G.; Carter, T. A.; Ciceri, P.; Edeen, P. T.; Floyd, M.; Ford, J. M.; Galvin, M.; Gerlach, J. L.; Grotzfeld, R. M.; Herrgard, S.; Insko, D. E.; Insko, M. A.; Lai, A. G.; Lélías, J.-M.; Mehta, S. A.; Milanov, Z. V.; Velasco, A. M.; Wodicka, L. M.; Patel, H. K.; Zarrinkar, P. P.; Lockhart, D. J. *Nat. Biotechnol.* **2005**, *23*, 329–336.
10. (a) Lewis, W. G.; Green, L. G.; Grynszpan, F.; Radić, Z.; Carlier, P. R.; Taylor, P.; Finn, M. G.; Sharpless, K. B. *Angew. Chem. Int. Ed.* **2002**, *41*, 1053–1057. (b) Manetsch, R.; Krasinski, A.; Radić, Z.; Raushel, J.; Taylor, P.; Sharpless, K. B.; Kolb, H. C. *J. Am. Chem. Soc.* **2004**, *126*, 12809–12818. (c) Bourne, Y.; Kolb, H. C.; Radić, Z.; Sharpless, K. B.; Taylor, P.; Marchot, P. *Proc. Natl. Acad. Sci. USA* **2004**, *101*, 1449–1454. (d) Kolb, H. C.; Finn, M. G.; Sharpless, K. B. *Angew. Chem. Int. Ed.* **2001**, *40*, 2004–2021. (e) Whiting, M.; Muldoon, J.; Lin, Y.-C.; Silverman, S. M.; Lindstrom, W.; Olson, A. J.; Kolb, H. C.; Finn, M. G.; Sharpless, K. B.; Elder, J. H.; Fokin, V. V. *Angew. Chem. Int. Ed.* **2006**, *45*, 1435–1439.
11. (a) Wu, P.; Leinonen, J.; Koivunen, E.; Lankinen, H.; Stenman, U.-H. *Eur. J. Biochem.* **2000**, *267*, 6212–6220. (b) Pakkala, M.; Jylhärinta, A.; Wu, P.; Leinonen, J.; Stenman, U. H.; Santa, H.; Vepsäläinen, J.; Peräkylä, M.; Närvänen, A. *J. Pept. Sci.* **2004**, *10*, 439–447. (c) Koistinen, H.; Närvänen, A.; Pakkala, P.;

- Hekim, C.; Aaltonen, J.; Zhu, L.; Laakkonen, P.; Stenman, U.-H. *Biol. Chem.* **2008**, *389*, 633–642.
12. (a) Bunimovich, Y. L.; Shin, Y.-S.; Yeo, W.-S.; Amori, M.; Kwong, G. A.; Heath, J. R. *J. Am. Chem. Soc.* **2006**, *128*, 16323–16331. (b) Zheng, G.; Patolsky, F.; Cui, Y.; Wang, W. U.; Lieber, C. M. *Nat. Biotechnol.* **2005**, *23*, 1294–1301.
13. Melosh, N.; Boukai, A.; Diana, F.; Gerardot, B.; Badolato, A.; Petroff, P.; Heath, J. R. *Science* **2003**, *300*, 112–115.
14. Hu, K.; Fan, F.-R. F.; Bard, A. J.; Hillier, A. C. *J. Phys. Chem. B* **1997**, *101*, 8298–8303.
15. (a) Lud, S. Q.; Nikolaidis, M. G.; Haase, I.; Fischer, M.; Bausch, A. R. *ChemPhysChem* **2006**, *7*, 379–384. (b) Neff, P. A.; Wunderlich, B. K.; Lud, S. Q.; Bausch, A. R. *Phys. Status Solidi A* **2006**, *203*, 3417–3423.
16. Buriak, J. M. *Chem. Rev.* **2002**, *102*, 1271–1308.
17. Israelachvili, J. *Intermolecular and Surface Forces* (London: Academic Press, 1985).

## **Chapter 2**

Selection of a Multi-ligand Capture Agent for Carbonic Anhydrase II by Iterative In Situ

Click Chemistry

## 2.1 INTRODUCTION

Protein biomarkers comprise an important aspect of *in vitro* diagnostics. Most protein detection methods rely upon antibody-based capture agents.<sup>1</sup> A high-quality antibody exhibits a high affinity and specificity for its cognate protein. However, antibodies are expensive, and can be unstable toward dehydration, pH variation, thermal shock, and many other chemical and biochemical processes.<sup>2,3</sup> In addition, antibodies are not available for many potential protein biomarkers. Thus, a major challenge is to discover an efficient and general approach for producing protein capture agents that display the positive attributes of antibodies, and exhibit a high level of chemical and biochemical stability. This is becoming an increasingly important problem as single protein-based diagnostics are being replaced by measurements of large panels of protein biomarkers.<sup>4</sup>

Several alternative protein capture agents, including oligonucleotide aptamers and phage display peptides, have been reported. Each of them have attributes as well as significant limitations.<sup>5-11</sup> A third alternative is to utilize one-bead one-compound (OBOC) peptide or peptide mimetic libraries.<sup>12-16</sup> An advantage of OBOC libraries is that chemical stability, water solubility, and other desired properties may be achieved by design. However, OBOC libraries are typically only  $10^4$ – $10^6$  elements, and so significant trade-offs are made between peptide length and library chemical diversity. Phage display methods, by contrast, produce  $\sim 10^{12}$  element peptide libraries. As a result, high-quality protein capture agents can be challenging to identify directly from standard OBOC peptide libraries.

Herein, we combine the chemical flexibility of comprehensive, OBOC libraries of oligopeptides with *in situ* click chemistry<sup>17-21</sup> to yield a target-guided,<sup>22-24</sup> potentially

general screening approach for building high-affinity protein capture agents. For this selection scheme, the protein target replaces the role of a Cu(I) catalyst for promoting the 1,3-dipolar “click” cycloaddition reaction between azide-functionalized and acetylene-functionalized peptide affinity agents. First, an anchor ( $1^\circ$ ) ligand, containing acetylene (or azido) functionality, is selected for specific binding to a protein target via standard OBOC methods. Second, the same protein target is utilized to template the covalent coupling between two peptide ligands, the pre-identified  $1^\circ$  ligand and a secondary ( $2^\circ$ ) ligand, which is selected by the protein target and the  $1^\circ$  ligand from a comprehensive OBOC library of  $2^\circ$  ligands displaying azido (or acetylene) functionality. Synthetic scale-up yields a biligand composed of the  $1^\circ$  and  $2^\circ$  ligands, joined together via the 1,2,3-triazole linker. This biligand can then be used as a new anchor ligand, and the in situ click chemistry selection may be repeated to form a triligand, and so forth. As the number of peptide ligands that comprise the multi-ligand capture agent increases, the binding affinity and specificity rapidly increase.<sup>25,26</sup> Thus, multivalent binding agents can provide a potential shortcut to high affinity.<sup>27</sup>

By instituting *iterative* in situ click chemistry selections with OBOC, we exploit both technologies to produce a triligand capture agent against human and bovine carbonic anhydrase II (hCAII and bCAII, respectively). These two proteins are >80% identical in sequence (PDB ID: 1CA2, 1V9E). Carbonic anhydrase II belongs to a family of metalloenzymes that catalyze the reversible hydration of carbon dioxide. CA II expression is induced in the endothelium of neovessels in melanoma, renal carcinoma, and other cancers.<sup>28</sup> Furthermore, CA II represents a major target antigen for stimulating an autoantibody response in melanoma patients,<sup>29</sup> and is potentially a therapeutic target

for glial tumors.<sup>30</sup> It has served as a model protein to understanding protein-ligand interactions, and is a demonstrated receptor for bivalent ligands.<sup>31–34</sup>

In this chapter, the discovery process for high-affinity protein capture agents is discussed, using the triligand capture agent for b(h)CAII as the prototype. First, the construction of OBOC libraries containing artificial amino acids is detailed. Through *iterative* OBOC and in situ click chemistry selections, specific binders of b(h)CAII are identified sequentially—1° ligands, then biligands, and finally a triligand capture agent which displays  $\geq 20$  ng sensitivity for the protein target in dilute serum. The entire screening approach is summarized in Figure 2.1.

## 2.2 MATERIALS AND EXPERIMENTAL METHODS

### 2.2.1 Materials

Fmoc-D-**X**-OH (Fmoc, fluoren-9-ylmethoxycarbonyl) (**X** = Ala, Arg(Pbf) (Pbf, pentamethyldihydrobenzofuran-5-sulfonyl), Asn(Trt) (Trt, trityl), Asp(OtBu) (*t*Bu, *tert*-butyl), Glu(OtBu), Gln(Trt), Gly, His(Trt), Ile, Leu, Lys(Boc) (Boc, *tert*-butyloxycarbonyl), Met, Phe, Pro, Ser(*t*Bu), Thr(*t*Bu), Trp(Boc), Tyr(*t*Bu), and Val) were purchased (Anaspec; San Jose, CA) and used as received. TentaGel S-NH<sub>2</sub> resins (90  $\mu$ m, 0.31 mmol/g) (Rapp-Polymere; Tübingen, Germany) were utilized for OBOC library construction. Amino acid coupling reactions were performed in 1-methyl-2-pyrrolidinone (NMP, 99%) with HATU (2-(7-Aza-1H-benzotriazole-1-yl)-1,1,3,3-tetramethylammonium hexafluorophosphate, ChemPep; Miami, FL) and *N,N'*-diisopropylethylamine (DIEA). For removal of N<sup>α</sup>-Fmoc protecting groups, a solution of 20% piperidine in NMP was used. For final deprotection of the peptide libraries, trifluoroacetic acid (TFA, 98% min. titration) and triethylsilane (TES) were used. All

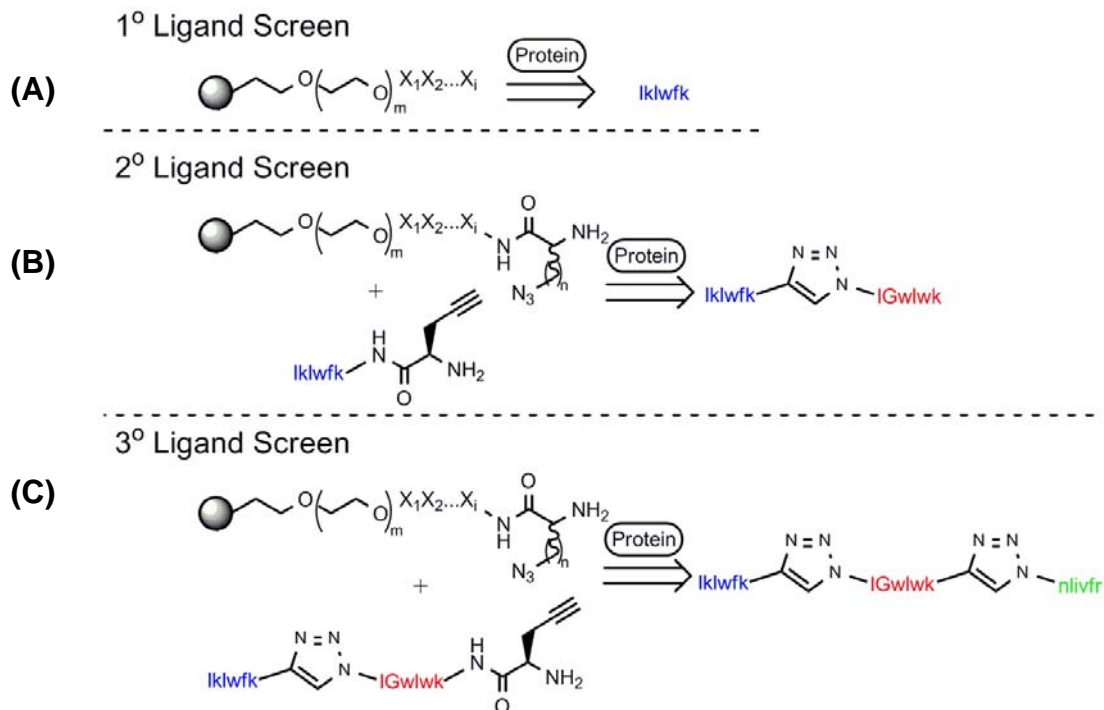


**Figure 2.1.** A schematic representation of a method for preparing a multi-ligand capture agent. **(A)** In the first step, a plurality of candidate oligopeptides in an OBOC library is contacted with a labeled target to identify an anchor (1°) ligand. **(B)** In the second step, a modified 1° ligand from the first step is contacted with the same OBOC library now appended with an azide linker to identify a secondary (2°) ligand. A biligand, formed by the 1° ligand of the first step and the 2° ligand, can be obtained. **(C)** In the third step, the screen is repeated by employing the biligand formed from the second step as the new primary ligand to allow identification of higher-order multi-ligands.

solvents and reagents were purchased from Sigma-Aldrich (St. Louis, MO) and used as received, unless otherwise noted.

OBOC libraries were synthesized using a 180-degree variable-speed shaker, fitted with small sample adapter (St. John Associates; Beltsville, MD). Fritted polypropylene solid-phase synthesis tubes were used for repeated split-mix cycles. A 24-port SPE vacuum manifold system (Grace; Deerfield, IL) was used for exchanging coupling solutions and washing the resins.

Bovine carbonic anhydrase II (bCAII, C2522), from bovine erythrocytes, lyophilized powder, was obtained (Sigma-Aldrich; St. Louis, MO) and used as received. To prepare the protein for screening, dye-labeling was accomplished with the Alexa Fluor 647 Microscale Protein Labeling Kit (Invitrogen; Carlsbad, CA) following the manufacturer's protocol for a low degree of labeling (DOL). Protein (100  $\mu$ g) was incubated with 6 mol equiv Alexa Fluor 647 succinimidyl ester for 15 min at 25 °C. Excess dye was removed by BioGel P-6 size exclusion resin (Bio-Rad; Hercules, CA). The labeled protein (bCAII-Alexa Fluor 647) was characterized by UV-Vis and mass spectrometry.

Human carbonic anhydrase II (hCAII, C6165), from human erythrocytes, lyophilized powder, was obtained (Sigma-Aldrich; St. Louis, MO) and used in affinity and specificity studies. Both bCAII and hCAII were tested by SDS gel electrophoresis, and confirmed to display a single band corresponding to 29,000 Da.

### **2.2.2 Artificial Amino Acids**

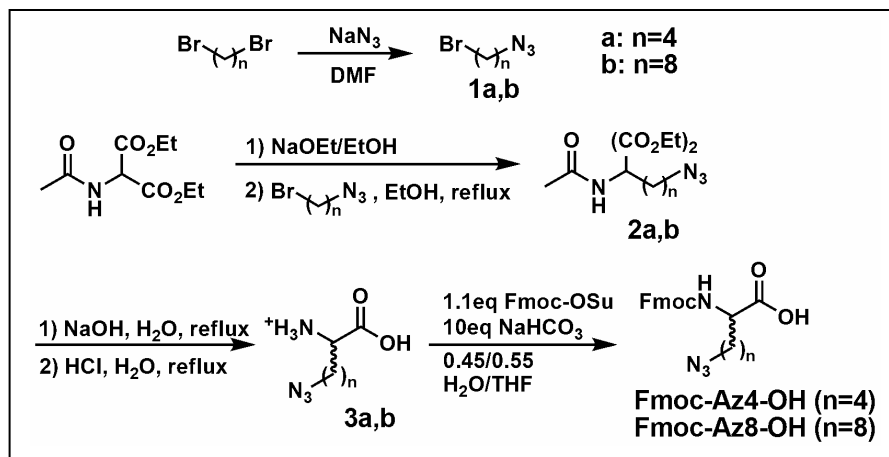
Fmoc-D-propargylglycine (Fmoc-D-Pra-OH) was acquired (Chem-Impex International; Wood Dale, IL) and used as the acetylene handle for construction of

ligands. Azide-containing amino acids Fmoc-Az4-OH (and intermediates 1a-3a) and Fmoc-Az8-OH (and intermediates 1b-3b) were synthesized using a modification of literature protocols (Scheme 2.1).<sup>35-37</sup>

**Azidobutylbromide (1a).** To a solution of 1,4-dibromobutane (123 mmol), sodium azide (61.5 mmol) was added and stirred overnight in *N,N'*-dimethylformamide (DMF) at 50 °C. The reaction was diluted with ethyl acetate, and the organic layer was washed with water, then brine, and then dried over MgSO<sub>4</sub>. The crude residue was purified by silica gel chromatography (100% hexanes) to give a product (80%) as a clear oil. <sup>1</sup>H NMR (300 MHz, CDCl<sub>3</sub>): δ 3.44 (2H, t, *J* = 6.3 Hz), 3.34 (2H, t, *J* = 6.6 Hz), 1.93-1.98 (2H, m), 1.74-1.79 (2H, m).

**Azidooctylbromide (1b).** Synthesis was carried out as described above, except 1,8-dibromooctane was used as the starting material. <sup>1</sup>H NMR (300 MHz, CDCl<sub>3</sub>): δ 3.41 (2H, t, *J* = 6.9 Hz), 3.26 (2H, t, *J* = 6.6 Hz), 1.86 (2H, p, *J* = 6.9 Hz), 1.60 (2H, p, *J* = 8.7 Hz), 1.34-1.55 (4H, m).

**Diethyl 2-acetamido-2-(4-azidobutyl)malonate (2a).** To a solution of 0.598 g (0.026 mol) sodium metal in 25 mL absolute EtOH, 5.65 g diethyl acetamidomalonate (0.026 mol) was added, following previously published procedures.<sup>35</sup> The mixture was stirred for 30 min at room temperature. By dropwise addition, azidobutylbromide **1a** (4.82 g, 0.027 mol) was added with stirring. The reaction mixture was stirred for 2 h at room temperature and refluxed for 6 h at 80 °C. After cooling overnight, the reaction mixture was concentrated to dryness, and the residue was extracted with diethyl ether. The combined ether extracts were washed with water, sat. NaHCO<sub>3</sub>, water, and brine, and were dried over MgSO<sub>4</sub> and then concentrated. Silica gel chromatography (Hex:EtOAc = 1:1) gave a product (63%) as a clear, viscous oil. <sup>1</sup>H NMR (300 MHz,



**Scheme 2.1.** Artificial amino acid synthesis.

CDCl<sub>3</sub>):  $\delta$  6.77 (1H, s), 4.24 (4H, q,  $J = 6.9$  Hz), 3.26 (2H, t,  $J = 6.9$  Hz), 2.31-2.37 (2H, m), 2.04 (3H, s), 1.59 (2H, p,  $J = 7.5$  Hz), 1.26 (6H, t,  $J = 6$  Hz), 1.16-1.27 (2H, m). ESI-MS  $m/e$  315.

**Diethyl 2-acetamido-2-(8-azidoctyl)malonate (2b).** Similar synthetic protocol as **2a** was adopted, only with azidoctylbromide **1b** serving as the starting material. <sup>1</sup>H NMR (300 MHz, CDCl<sub>3</sub>):  $\delta$  6.76 (1H, s), 4.24 (4H, q,  $J = 7.2$  Hz), 3.24 (2H, t,  $J = 6.9$  Hz), 2.27-2.33 (2H, m), 2.04 (3H, s), 1.56 (2H, p,  $J = 7.5$  Hz), 1.25 (6H, t,  $J = 7.2$  Hz), 1.06-1.16, 1.2-1.4 (10H, m). ESI-MS  $m/e$  371.

**2-Azidobutyl amino acid (3a).** Following standard methods,<sup>36</sup> the diester **2a** (2.8 mmol) in 25 mL of 10% NaOH solution was heated to reflux for 4 h. The solution was then neutralized with concentrated HCl and evaporated. The residue was dissolved in 25 mL of 1 M HCl and heated to reflux for 3 h. The solvent was reduced and extraction with MeOH afforded amino acid **3a** as the hydrochloride salt (85%). <sup>1</sup>H NMR (300 MHz, CD<sub>3</sub>OD):  $\delta$  3.98 (1H, t,  $J = 6.3$  Hz), 3.35 (2H, t,  $J = 7.8$  Hz), 1.45-1.7, 1.85-2.05 (6H, m). MALDI-MS  $m/e$  173.

**2-Azidoctyl amino acid (3b).** Synthesis was carried out as described above, using diester **2b** as the starting material. <sup>1</sup>H NMR (300 MHz, CD<sub>3</sub>OD):  $\delta$  3.94 (1H, t,  $J = 6.3$  Hz), 3.27 (2H, t,  $J = 6.9$  Hz), 1.3-1.52, 1.52-1.62, 1.8-1.98 (14H, m). ESI-MS  $m/e$  229.

**Fmoc-2-Azidobutyl amino acid (Fmoc-Az4-OH).** The amino acid **3a** (26.3 mmol) was dissolved in 0.45:0.55 H<sub>2</sub>O:THF (150 mL), and NaHCO<sub>3</sub> (22.1 g, 263 mmol) was added, following published methods.<sup>37</sup> After the mixture was cooled to 0 °C, Fmoc-OSu (9.7 g, 28.9 mmol) was added dropwise over 5 min. The reaction mixture was allowed to come to room temperature and stirred overnight. Evaporation of

THF was completed *in vacuo* and the aqueous residue was washed with diethyl ether ( $2 \times 200$  mL). The aqueous layer was then collected and acidified with conc. HCl to pH 2 before extraction with ethyl acetate ( $4 \times 100$  mL). The combined organic layers were washed with brine, dried over  $\text{MgSO}_4$ , filtered, and concentrated. The organic residue was purified by column chromatography (2% MeOH in DCM) to yield a white powder (48% yield).  $^1\text{H}$  NMR (300 MHz,  $\text{CDCl}_3$ ):  $\delta$  7.76 (2H, d,  $J = 7.5$  Hz), 7.59 (2H, d,  $J = 6.9$  Hz), 7.40 (2H, t,  $J = 7.5$  Hz), 7.31 (2H, t,  $J = 7.5$  Hz), 5.34 (1H, d,  $J = 7.8$  Hz), 4.49-4.59 (1H, m), 4.43 (2H, d,  $J = 6.6$  Hz), 4.22 (1H, t,  $J = 6.6$  Hz), 3.27 (2H, t,  $J = 6.6$  Hz), 1.3-2.0 (6H, m). ESI-MS  $m/e$  395.

**Fmoc-2-Azidoethyl amino acid (Fmoc-Az8-OH).** The amino acid **3b** was treated to Fmoc protection as described above.  $^1\text{H}$  NMR (300 MHz,  $\text{CDCl}_3$ ):  $\delta$  7.75 (2H, d,  $J = 7.5$  Hz), 7.57-7.61 (2H, m), 7.39 (2H, t,  $J = 7.5$  Hz), 7.30 (2H, t,  $J = 7.2$  Hz), 5.40 (1H, d,  $J = 8.1$  Hz), 4.42-4.52 (1H, m), 4.40 (2H, d,  $J = 7.2$  Hz), 4.21 (1H, t,  $J = 7.2$  Hz), 3.23 (2H, t,  $J = 6.9$  Hz), 1.18-1.98 (14H, m). ESI-MS  $m/e$  450.

### 2.2.3 OBOC Oligopeptide Library Construction

Randomized OBOC libraries of penta- to heptapeptides were synthesized manually via standard split-and-mix solid-phase peptide synthesis methods on  $90 \mu\text{m}$  polyethylene glycol-grafted polystyrene beads (TentaGel S-NH<sub>2</sub>, 0.31 mmol/g,  $2.86 \times 10^6$  beads/g).<sup>12-14</sup> Non-natural D-stereoisomers (denoted by lowercase one-letter amino acid code) were used at every possible position in the peptide sequence to infer intrinsic biochemical stability. At least a 5-fold excess of beads was utilized in each library synthesis to ensure adequate representation of each library element. A standard solid-phase peptide synthesis method with Fmoc chemistry was used.<sup>38</sup> All wash,

deprotection, and coupling steps were facilitated by 180-degree shaking of the resin. The resin was pre-swelled in NMP in a plastic fritted reaction vessel, and was separated into multiple aliquots. Each aliquot was reacted with 2-fold molar excess (relative to resin) of a single N<sup>α</sup>-Fmoc-amino acid. Amide coupling was initiated by addition of a 2-fold molar excess of HATU and a 6-fold molar excess of DIEA.<sup>39</sup> The coupling reaction was run for 15 min. Another 2 equiv N<sup>α</sup>-Fmoc-amino acid, 2 equiv HATU, and 6 equiv DIEA were added, and allowed to react for 15 min (“double coupling”). In some cases, “triple coupling” was performed with a third set of coupling reagents and N<sup>α</sup>-Fmoc-amino acids (Table 2.1, Libraries D, E, F, and G). Following coupling, the aliquots were thoroughly washed (5 × NMP), mixed together into a single vessel, and deprotected with 20% piperidine in NMP (30 min). The resin was thoroughly washed (5 × NMP), dried (5 × DCM), and re-divided into multiple equal-mass aliquots for the next cycle of coupling. The procedures were repeated until the desired length of peptide was attained.

The amino acid side chain protecting groups were then removed by incubation in trifluoroacetic acid (95%), water (5%), and triethylsilane (2-fold molar excess per protected side chain) for 2 h at 25 °C. The library resin was then neutralized with DMF, and washed thoroughly with DMF (5 ×), water (5 ×), methanol (MeOH, 5 ×), and methylene chloride (DCM, 5 ×),<sup>40</sup> and then dried under vacuum and stored in phosphate-buffered saline [PBS (pH 7.4)] + 0.05% NaN<sub>3</sub> at 25 °C.

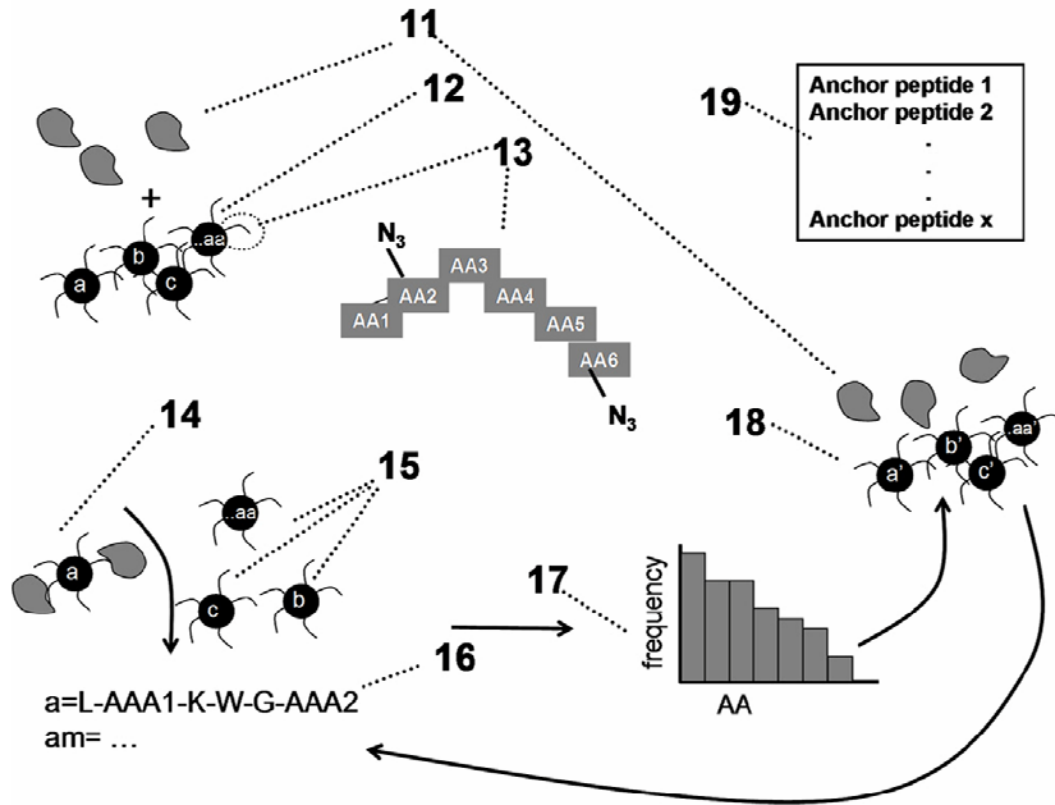
#### **2.2.4 Screening Procedures for Anchor Ligand**

A method for identifying an anchor (1°) ligand is schematically illustrated in Scheme 2.2. In particular, in the illustration of Scheme 2.2, a fluorescently labeled protein of interest (11) is screened against an OBOC library of peptides (12). Each bead

**Table 2.1.** Libraries used in selecting a triligand capture agent for bCAII.<sup>a</sup>

	<b>Formula</b>	<b>Components</b>	<b># of unique sequences</b>
<b>A</b>	$x_1x_2x_3x_4x_5$	$x_i = 19$ D-amino acids (no D-Cys)	2,476,099
<b>B</b>	$x_1x_2x_3x_4x_5x_6$	$x_i = r, k, l, w, f, h, y$	117,649
<b>C</b>	$Az_n-x_2x_3x_4x_5x_6-Az_n$	$x_i = 19$ D-amino acids (no D-Cys)  $Az_n = 1/3 Az_4, 1/3 Az_8,$ 1/3 nothing	22,284,891
<b>D</b>	$x_1x_2x_3x_4x_5x_6-Tz1-kfwlkl$	$x_i = k, l, w, f, i, G, v$	117,649
<b>Tz1 = triazole formed between Az4 (on terminal k) and D-Pra (on x<sub>6</sub>)</b>			
<b>E</b>	$x_7x_6x_5x_4x_3x_2-Tz2-kwlwGl-Tz1-kfwlkl$	$x_i = d, r, s, w, G, f, l$	117,649
<b>Tz1 = triazole formed between Az4 (on terminal k) and D-Pra (on l)</b> <b>Tz2 = triazole formed between Az4 (on terminal x<sub>2</sub>) and D-Pra (on k)</b>			
<b>F</b>	$Az_4-x_2x_3x_4x_5x_6x_7$	$x_2 = r, n, l, i;$ $x_3 = w, f, l, i;$ $x_4 = r, w, f, l, i;$ $x_5 = w, f, v, l;$	3200
<b>G</b>	$x_7x_6x_5x_4x_3x_2-Tz2-kwlwGl-Tz1-kfwlkl$	$x_6 = r, w, f, l, k;$ $x_7 = f, r$	3200

<sup>a</sup> Randomized positions are denoted by  $x_i$  (for D-amino acids) and  $Az_n$  (for azide-containing artificial amino acids).



**Scheme 2.2.** Selection of anchor ligands by OBOC screen.

contains a unique peptide (13) comprised of non-natural amino acids (D-stereoisomers) or artificial amino acids (displaying azide or acetylene functionalities). The protein (11) and the library (12) are incubated for a period of time at a particular protein concentration (Table 2.2, Screen **An1**), and the “hit” beads (14) are identified by their fluorescence using a GenePix 4200 array scanner ( $\lambda_{\text{ex}} = 635 \text{ nm}$ ). Typically 0.1% or less of the beads are identified as hit beads, and are separated manually from the non-hit beads by micropipette (15). The protein is removed from the beads by incubation with 7.5 M guanidine hydrochloride (GuHCl, pH 2.0) for 1 h, and the peptides on single hit beads are sequenced using Edman degradation<sup>41</sup> (Procise cLC Sequencing System, Applied BioSystems, Foster City, CA; see Appendix C) or MALDI-TOF/TOF mass spectrometry.<sup>42</sup>

Once the hit peptide sequences (16) are identified, a histogram (17) that correlates the amino acid frequency vs. amino acid identity is prepared. A second, more focused library (18) that uses those most commonly identified amino acids can then be prepared and re-screened against the protein (11) (Table 2.2, Screens **An2a** and **An2b**). This focused library can contain slightly longer peptides, and the screening process can involve a lower concentration of the protein (11). This process can then be repeated until the desired affinity of peptide anchor ligand (19) is achieved. The affinity of the peptide anchor ligand will depend upon the number of amino acids in the peptide, and the three-dimensional structure of the peptide, among other factors. Affinities in the order of  $10^{-4}$ – $10^{-6}$  M are typically achievable.

### **2.2.5 In Situ Click Screening Procedures for Biligand**

Identification of the secondary (2°) ligand and formation of a biligand then can

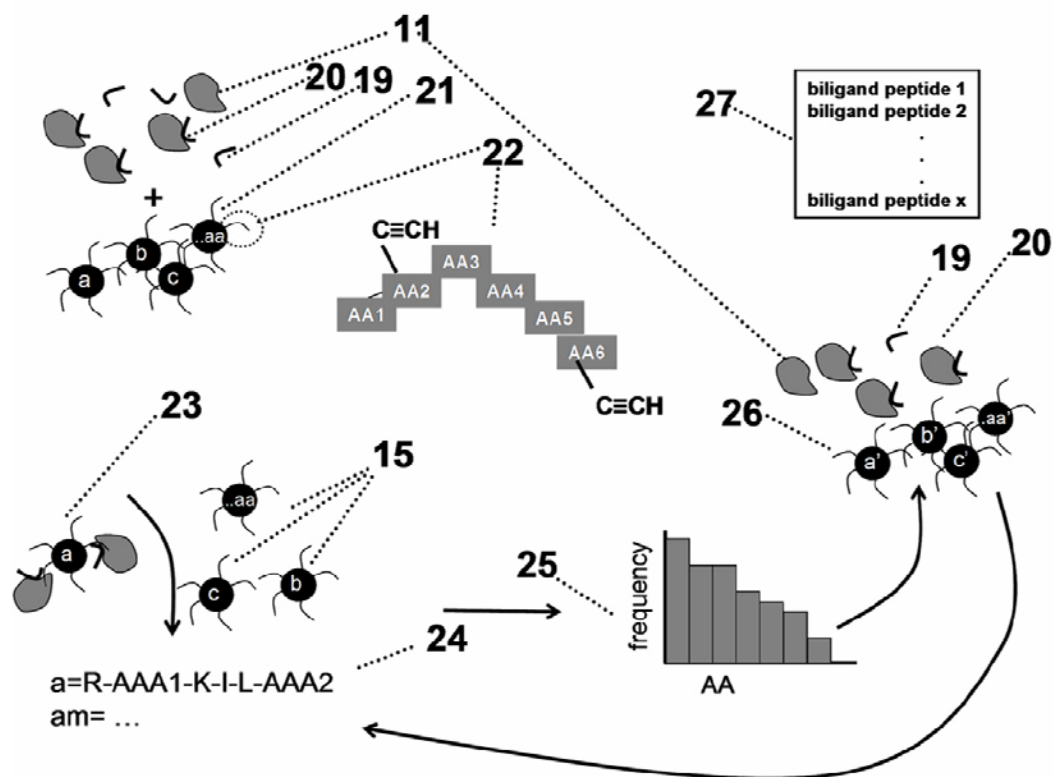
**Table 2.2.** Screening summary.<sup>a</sup>

Screen	Library	[bCAII-AF647]	Time(h)	% hit beads	Buffer	Other components
An1	A	100 nM	1 h	0.02%	PBS	N/A
An2a	B	50 nM	1 h	0.09%	PBS	N/A
An2b	B	8 nM	24 h	2 hits	PBS	N/A
Bi1	C	50 nM	2 h; 37° C (no beads) + 48 h; 37° C	0.007%	PBS + 1% DMSO (v/v)	100 μM of <b>lklwfk-(D-Pra)</b>
Bi2a	D	50 nM	17 h	0.07%	PBSTBNaN <sub>3</sub>	N/A
Bi2b	D	10 nM	17 h	0.008%	PBSTBNaN <sub>3</sub>	N/A
Tri1	C	10 nM	2 h (no beads) +15 h	0.007%	PBSTBNaN <sub>3</sub> + 1% DMSO (v/v)	100 μM of <b>(D-Pra)-kwlwGI-Tz1-kfwlkl</b>
Tri2	E	10 nM	17 h	0.008%	PBSTBNaN <sub>3</sub>	N/A
TriX	A	10 nM	17 h	0.007%	PBSTBNaN <sub>3</sub> + 1% DMSO (v/v)	100 μM of <b>(D-Pra)-kwlwGI-Tz1-kfwlkl</b>
Tri3	F	0.5 nM	2 h (no beads) +18 h	0.005% -0.01%	PBSTBNaN <sub>3</sub> + 1% DMSO (v/v)	100 μM of <b>(D-Pra)-kwlwGI-Tz1-kfwlkl</b>
Tri4	G	0.25 nM	18 h	0.005% -0.01%	PBSTBNaN <sub>3</sub>	N/A

<sup>a</sup> All screens were conducted at pH = 7.4 and T = 25 °C, unless otherwise noted.

be performed according to the method schematically illustrated in Scheme 2.3. A typical screen begins with incubation of a library (12) in PBS (pH 7.4) + 0.1% Tween 20 + 0.1% bovine serum albumin (BSA) + 0.05% NaN<sub>3</sub> (PBSTBNaN<sub>3</sub>) for 1 h, with shaking, to block non-specific protein binding.<sup>34</sup> One of the anchor ligands (19) from the screening procedures in Section 2.2.4 is added to the protein of interest (11) at a concentration that is dependent upon its binding affinity. It is desirable that this concentration of anchor ligand (19) is at least two orders of magnitude higher than the K<sub>D</sub>. All in situ click chemistry screens (Scheme 2.3) started with an initial 2 h pre-incubation of bCAII-Alexa Fluor 647 with the anchor ligand (20), which was followed by addition of the OBOC library of 2° ligands (21) and continuation of the screen (Table 2.2, Screen **Bi1**). This OBOC oligopeptide library is constructed similarly to the candidate library for anchor ligands (12), except that the azide components (22) are replaced by acetylene functionalities. Following in situ screening, beads are washed with 3 × 5 mL PBSTBNaN<sub>3</sub>, 3 × 5 mL PBS (pH 7.4) + 0.1% Tween 20, and then 6 × 5 mL PBS (pH 7.4).

As with the screening procedures in Section 2.2.4, the hit beads (23) are identified by their fluorescence and separated from the non-hit beads (15). While the hit beads can contain a certain amount of biligand formed by the protein-catalyzed coupling of bead-bound 2° ligand with anchor ligand, the majority of the peptide on the hit beads (23) is actually 2° ligand that did not participate in the “click” reaction. The protein target and excess anchor ligand are removed from the bead by incubation with 7.5 M GuHCl (pH 2.0) for 1 h, the peptide (24) on the bead is sequenced using standard methods, and a histogram (25) that correlates amino acid frequency vs. amino acid identity is constructed. A second, more focused library (26) that utilizes those most



**Scheme 2.3.** Selection of biligand by in situ click/OBOC screen. Similarly, triligands (27) may be selected by iteration of this screening method, utilizing a biligand as the anchor unit (19).

commonly identified amino acids may then be prepared and re-screened against the protein (11). Once again, the hit beads are identified via peptide sequencing (24). This second library of 2° ligands can contain slightly longer peptides, and the screening process can involve a lower concentration of the protein (11).

### 2.2.6 In Situ Click Screening Procedures for Higher-Order Multi-ligands

In situ click screening procedures operate similarly to Scheme 2.3 for identification of higher-order multi-ligands such as the triligand in Figure 2.1. The in situ click/OBOC screen for this triligand (Table 2.2, Screens **Tri1** and **Tri3**) contained an initial 2 h pre-incubation of bCAII-Alexa Fluor 647 with biligand anchor, which was followed by addition of the OBOC library of 3° ligands and continuation of the screen. As a negative control, screen **TriX** was performed with an azide-free OBOC library of 3° ligands.

### 2.2.7 Validation of In Situ Click/OBOC Multi-ligand Screening Procedures

**Binary component screen for in situ biligand.** Stock solutions of 2° ligand (azide, Az4-kiwiG, 13.1 mM) and anchor ligand (acetylene, lklwfk-(D-Pra), 2.1 mM) were prepared in DMSO. Stock solutions of bCAII and bovine serum albumin (BSA) were prepared in PBS (pH 7.4). Each reaction contained 394 μM azide, 65 μM alkyne, and 36 μM protein in 100 μL PBS (pH 7.4) + 6% DMSO (v/v). Reactions proceeded for 48 h at 37 °C, followed by 5 days at 25 °C. Reactions were quenched with 100 μL of 7.5 M GuHCl (pH 2.0), and proteins were subsequently removed by centrifugal filtration (Microcon YM-3, Millipore, Billerica, MA).

The formation of in situ biligands was identified by MALDI-MS. Control experiments were conducted (1) in the absence of bCAII, and (2) replacing bCAII with BSA, to verify that the click reaction between the azide and alkyne is specific to the bCAII protein target. A third control, performed in the absence of protein, represents the slow thermally driven reaction between solutions of azide and alkyne.

**On-bead biligand screen.** Synthesis of Library D was achieved on bead via the Cu(I)-catalyzed azide-alkyne cycloaddition (CuAAC),<sup>43-45</sup> as described in Section 2.2.9. Screens **Bi2a** and **Bi2b** (Table 2.2) were conducted using Library D following the general OBOC screening protocol described in Section 2.2.4. After initial blocking with PBSTBNaN<sub>3</sub> for 1 h, 10 nM to 50 nM bCAII-Alexa647 in PBSTBNaN<sub>3</sub> was incubated with the library for 17 h at 25 °C, with shaking. The screened beads were washed with 3 × 5 mL PBSTBNaN<sub>3</sub>, then 3 × 5 mL PBS (pH 7.4) + 0.1% Tween 20, and finally 6 × 5 mL PBS (pH 7.4). The beads were imaged for fluorescence, and the hits were selected by micropipette. After washing the hits to remove bound protein [7.5 M GuHCl (pH 2.0)], their sequences were determined by Edman degradation.

**On-bead triligand screen.** Synthesis of Libraries E and G was achieved on bead via the CuAAC, as described in Section 2.2.9. Screens **Tri2** and **Tri4** (Table 2.2) were conducted following the general OBOC screening protocol described in Section 2.2.4, using <10 nM bCAII-Alexa647 and fluorescent detection of hits.

### 2.2.8 Bulk Peptide Synthesis

Bulk synthesis of hit peptide sequences was performed on either Fmoc-Rink amide MBHA (50 μm, 0.67 mmol/g, AnaSpec) or Biotin-PEG-NovaTag resin (0.48 mmol/g; Novabiochem), on a typical resin scale of 0.2 g per sequence. Crude peptides

were precipitated with ether, and then purified to >95% by HPLC (Beckman Coulter System Gold 126 Solvent Module and 168 Detector, Fullerton, CA) on a C<sub>18</sub> reversed-phase semi-preparative column (Phenomenex Luna 10 μm, 250 × 10 mm). The pure peptides were used for affinity measurements, in situ click/OBOC screens, and binding assays. Hit peptide sequences were also re-synthesized on TentaGel S-NH<sub>2</sub> on a similar resin scale, and used for on-bead binding assays.

Installation of polyethylene glycol linkers (EG)<sub>n</sub> was achieved by Fmoc-NH-(PEG)<sub>5</sub>-COOH (22 atoms) (Novabiochem) via SPPS with standard HATU/DIEA coupling. N-terminal biotin labeling of certain sequences was achieved via SPPS with standard HATU/DIEA coupling and overnight reaction.

It should be noted that the protein-templated in situ click reaction may yield product regioisomers that are either *anti* (1,4), *syn* (1,5), or a mixture of the two geometries. Although we have not yet determined which regioisomers of the in situ click products were formed, the authentic multi-ligands synthesized by CuAAC to test affinity and specificity were definitely the 1,4-triazole (see Chapter 3).

All anchor ligands, biligands, and triligands were prepared in bulk by solid-phase synthesis, purified by HPLC, and analyzed by mass spectrometry prior to further study. Their characterization is as follows:

*lklwfk-(D-Pra)* (Figure 2.2A). MALDI-MS of the purified 1° ligand gave peaks at  $m/z$  928.7 for [M + H]<sup>+</sup> and 950.7 for [M + Na]<sup>+</sup>.

*Az4-kiwiG* (Figure 2.2B). ESI-MS of the purified 2° ligand gave peaks at  $m/z$  385.2 for [M + 2H]<sup>2+</sup> and 769.5 for [M + H]<sup>+</sup>.

*lklwfk-Tz1-kiwiG* (Figure 2.2C). MALDI-MS of the purified biligand gave a peak at  $m/z$  1808.4 for [M + H]<sup>+</sup>.

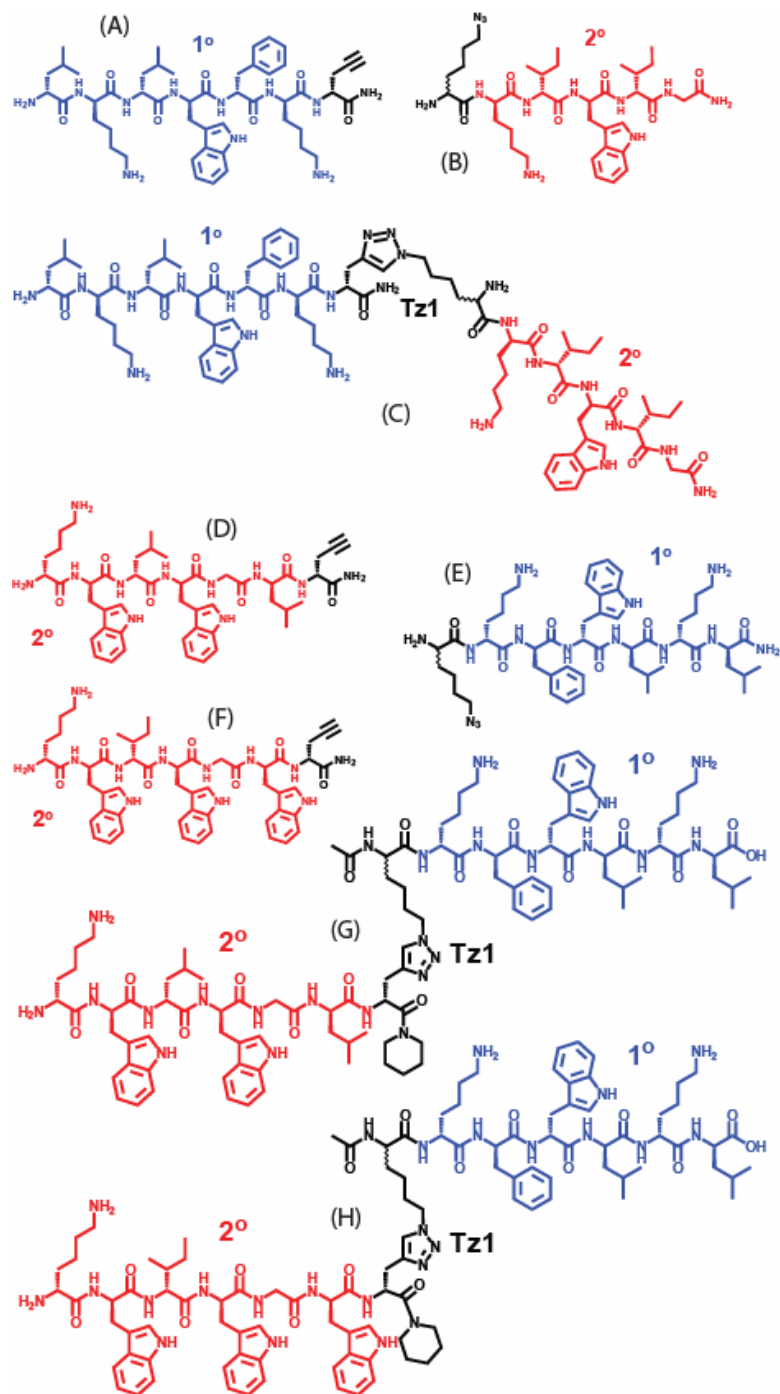


**Figure 2.2.** Structures of representative 1° ligands (**A**, **E**), 2° ligands (**B**, **D**, **F**), and biligands (**C**, **G**, **H**) which were isolated as moderate affinity binders of bCAII.

*Az4-kfwlkl* (Figure 2.2E). ESI-MS of the purified 1° ligand gave peaks at  $m/z$  329.9 for  $[M + 3H]^{3+}$ , 494.3 for  $[M + 2H]^{2+}$ , and 987.6 for  $[M + H]^+$ .

*kwlwGl-(D-Pra)* (Figure 2.2D). MALDI-MS of the purified 2° ligand gave peaks at  $m/z$  897.0 for  $[M + H]^+$ , 919.0 for  $[M + Na]^+$ , and 935.0 for  $[M + K]^+$ .

*kwiwGw-(D-Pra)* (Figure 2.2F). MALDI-MS of the purified 2° ligand gave peaks at  $m/z$  970.1 for  $[M + H]^+$  and 992.1 for  $[M + Na]^+$ .

*kwlwGl-Tz1-kfwlkl* (Figure 2.2G). MALDI-MS of the purified biligand gave a peak at  $m/z$  1993.6 for  $[M + H]^+$ .

*kwiwGw-Tz1-kfwlkl* (Figure 2.2H). MALDI-MS of the purified biligand gave peaks at  $m/z$  2066.9 for  $[M + H]^+$  and 2088.7 for  $[M + Na]^+$ .

*(D-Pra)-kwlwGl-Tz1-kfwlkl* (Figure 2.3A). ESI-MS of the purified biligand anchor gave peaks at  $m/z$  711.1 for  $[M + 3H]^{3+}$  and 1066.1 for  $[M + 2H]^{2+}$ .

*(D-Pra)-k(Boc)w(Boc)lw(Boc)Gl-Tz1-k(Boc)fw(Boc)lk(Boc)l* (Figure 2.3B). ESI-MS of the biligand anchor as the fully protected peptide gave peaks at  $m/z$  1365.3 for  $[M + 2H]^{2+}$  and 2731.6 for  $[M + H]^+$ .

*Biotin-(EG)<sub>5</sub>-(D-Pra)-kwlwGl-Tz1-kfwlkl* (Figure 2.3C). MALDI-MS of the purified biotinylated biligand anchor gave peaks at  $m/z$  1325.9 for  $[M + 2H]^{2+}$  (minor) and 2649.9 for  $[M + H]^+$  (major).

*Az4-nlivfr* (Figure 2.4A). MALDI-MS of the purified 3° ligand gave a peak at  $m/z$  914.5 for  $[M + H]^+$ .

*Az4-nlivfr-(EG)<sub>3</sub>-Biotin* (Figure 2.4B). MALDI-MS of the purified biotinylated 3° ligand gave a peak at  $m/z$  1343.8 for  $[M + H]^+$ .

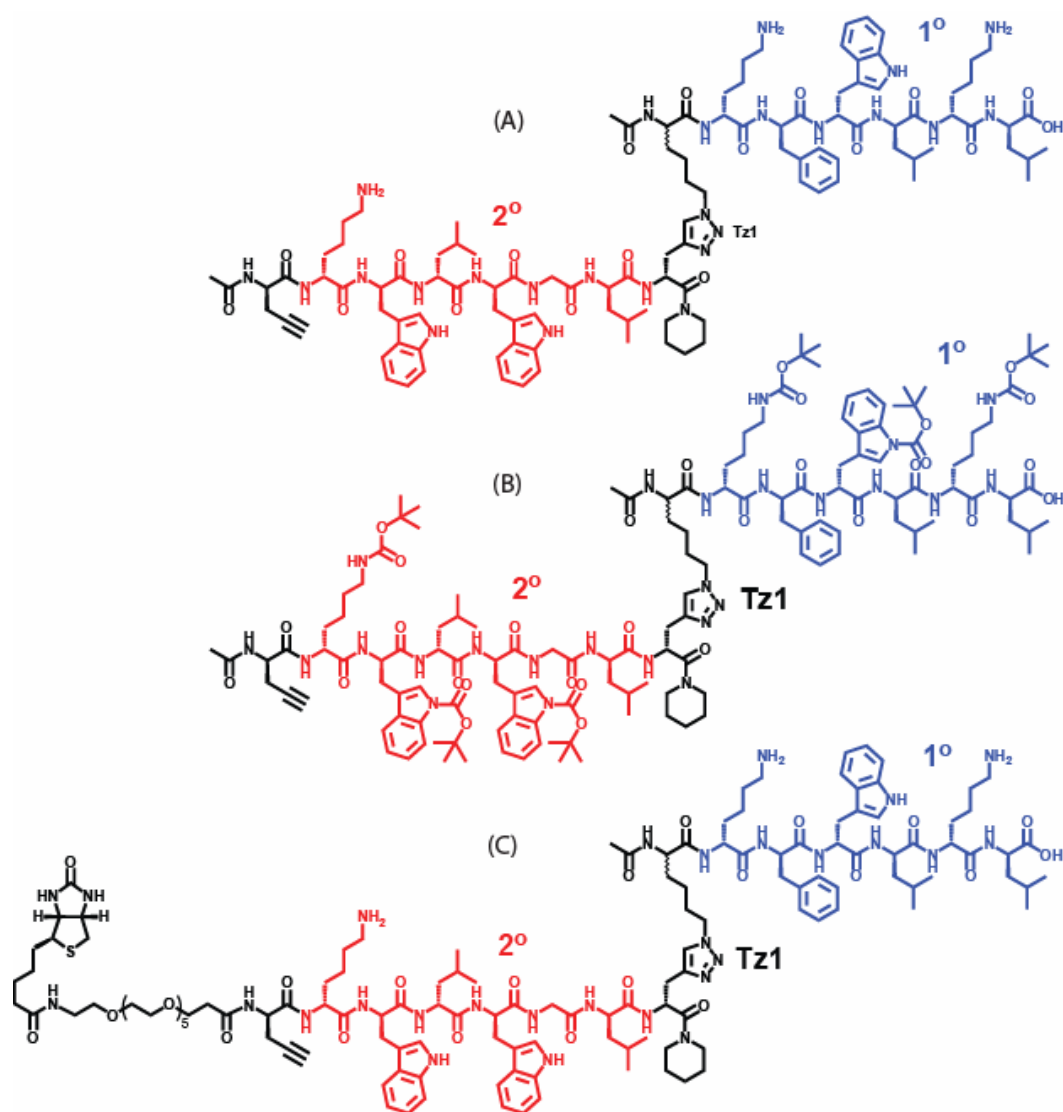


**Figure 2.3.** (A) Biligand anchor, employed for in situ click/OBOC screens. (B) Fully protected biligand anchor, used in bulk triligand synthesis. (C) Biotinylated biligand anchor, used in specificity experiments and assays for detecting on-bead, protein-templated multi-ligand.

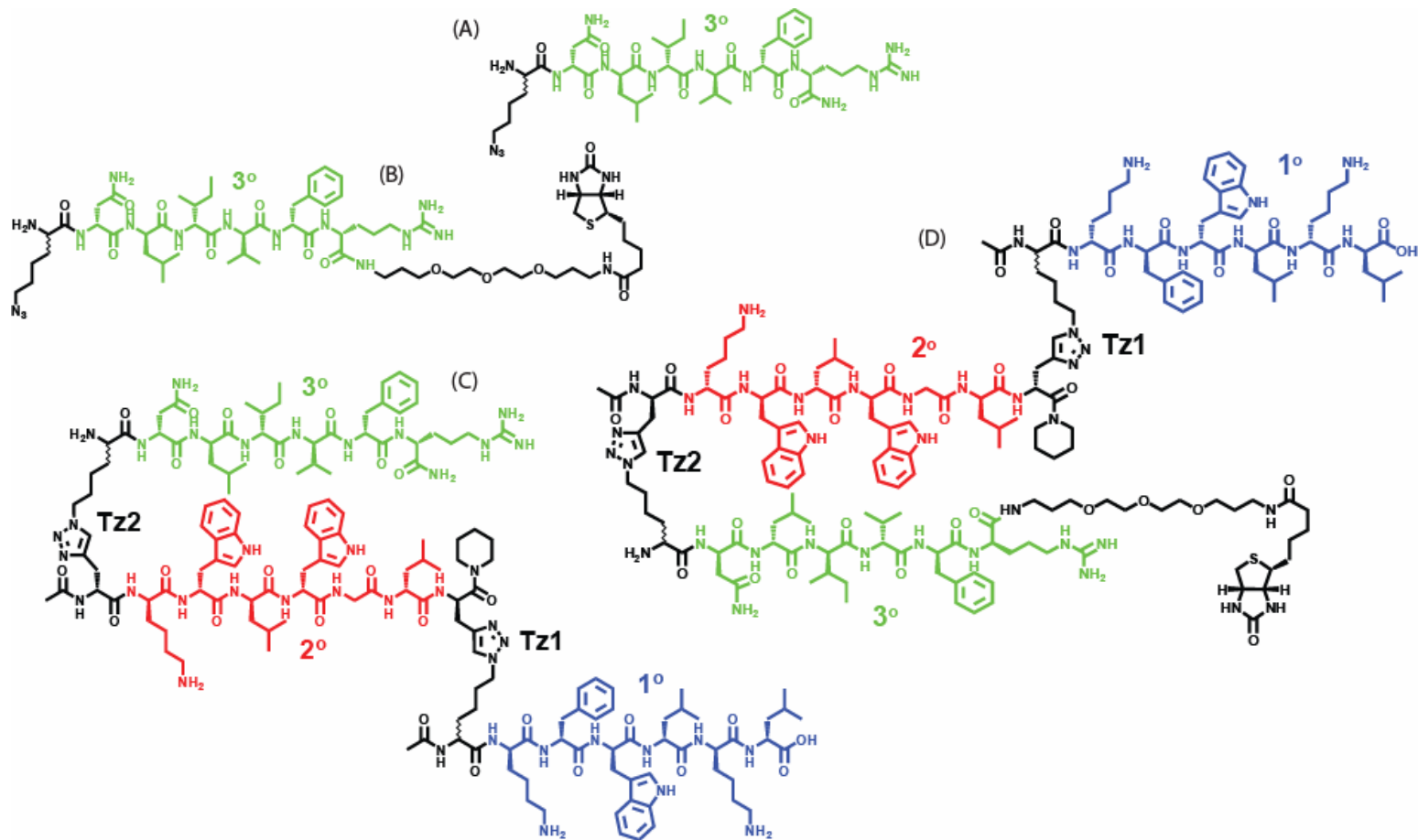


**Figure 2.4.** (A, B) Tertiary (3°) ligands. (C, D) Triligand capture agent, where the 1° ligand is colored in blue, the 2° ligand in red, and the 3° ligand in light green. The connections between the ligands are formed by 1,2,3-triazoles (Tz1 and Tz2).

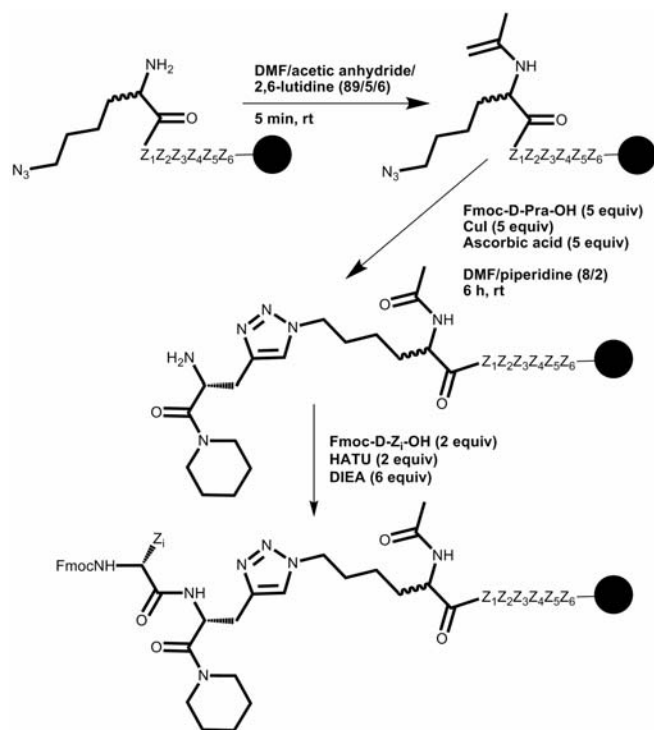
*rfviln-Tz2-kwlwGl-Tz1-kfwlkl* (Figure 2.4C). MALDI-MS of the purified triligand gave peaks at  $m/z$  1522.9 for  $[M + 2H]^{2+}$  (minor) and 3045.7 for  $[M + H]^+$  (major).

*rfviln-Tz2-kwlwGl-Tz1-kfwlkl-(EG)<sub>3</sub>-Biotin* (Figure 2.4D). MALDI-MS of the purified biotinylated triligand gave peaks at  $m/z$  1737.5 for  $[M + 2H]^{2+}$  (minor) and 3472.0 for  $[M + H]^+$  (major).

### 2.2.9 On-Bead Biligand and Triligand Synthesis

For preparing Libraries D, E, and G (Table 2.1), as well as for bulk synthesis of biligand and triligand candidates, the Cu(I)-catalyzed azide-alkyne cycloaddition (CuAAC)<sup>43-45</sup> was carried out on bead, with 4 general steps: (1) anchor ligand synthesis, (2) acetylation, (3) click reaction, and (4) addition of 2° ligand sequence. Scheme 2.4 illustrates the acetylation and click reactions for a 6-mer peptide ( $Z = \text{any amino acid}$ ). The fully protected TentaGel S-NH<sub>2</sub> bead-bound anchor ligand (0.420 g, 0.13 mmol) was capped by a solution of acetic anhydride (1 mmol) in 2,6-lutidine and DMF.<sup>46</sup> The acetylated peptide was reacted with Fmoc-D-Pra-OH (0.218 g, 0.65 mmol) in the presence of CuI (0.124 g, 0.65 mmol), L-ascorbic acid (0.114 g, 0.65 mmol), and DMF/piperidine (8/2) at 25 °C for 6 h.<sup>47</sup> The resin was washed with 5 × 5 mL Et<sub>2</sub>NCSSNa•3H<sub>2</sub>O (sodium diethyldithiocarbamate trihydrate, 1% w/v), containing 1% DIEA (v/v) in DMF to remove the coordinated copper from click reaction.<sup>48</sup>

The biligand anchor (D-Pra)-kwlwGl-Tz1-kfwlkl was synthesized on 2-chlorotriyl chloride (1.6 mmol/g) resin (Anaspec, San Jose, CA) using Scheme 2.4. The biligand anchor was released either as the fully deprotected peptide by cleavage with



**Scheme 2.4.** Acetylation and click reactions for a 6-mer peptide ( $Z = \text{any amino acid}$ ) by solid-phase synthesis. Peptide synthesis may continue via the Fmoc-protected primary amine of  $Z_1$  to generate a linear multi-ligand capture agent.

95:5 TFA:water (+ 2 mol equiv TES per side chain protecting group), or as the fully protected peptide by cleavage with 99:1 DCM:TFA.<sup>49</sup> To facilitate the on-bead click reaction, it is noted that the 1° ligand was synthesized here as Az4-kfwlkl (displaying N-terminal Az<sub>n</sub> modification), and to this sequence was coupled D-Pra and the 2° ligand to produce the linear biligand.

Triligands were synthesized by click reaction between the fully protected biligand anchor (D-Pra)-kwlwGl-Tz1-kfwlkl (0.274 g, 0.1 mmol, >95% HPLC) and bead-bound 3° ligand Az4-nlivfr (0.1 g, 0.03 mmol) using CuI (0.021 g, 0.1 mmol) and L-ascorbic acid (0.020 g, 0.1 mmol) in DMF/piperidine (8/2).

## 2.3 RESULTS AND DISCUSSION

### 2.3.1 Screening for Anchor (1°) Ligand against bCAII

The anchor (1°) ligand was selected from a two-generation screen (**An1**, **An2a**, **An2b**) as summarized in Table 2.2. For the first screen (**An1**), following Edman sequencing of hits, a histogram correlating the (position-independent) frequency of amino acid occurrence vs. amino acid identity (Figure 2.5A) suggested the importance of basic/charged (k, r) and aromatic residues (y, f, w) for an 1° ligand for bCAII. A second, more focused library (Library B) of ~10<sup>5</sup> D-peptide compounds was constructed from the most commonly occurring amino acids, as identified from screen **An1**, but expanded into a 6-mer peptide, and screened under 50 nM bCAII (**An2a**) and 8 nM bCAII (**An2b**) conditions. Figure 2.5B illustrates the results of these second-generation 1° ligand screens. The more stringent screen (**An2b**) yielded two hits, hlyflr and lklwfk. From these two candidates, one peptide (lklwfk) was arbitrarily chosen as the starting point for

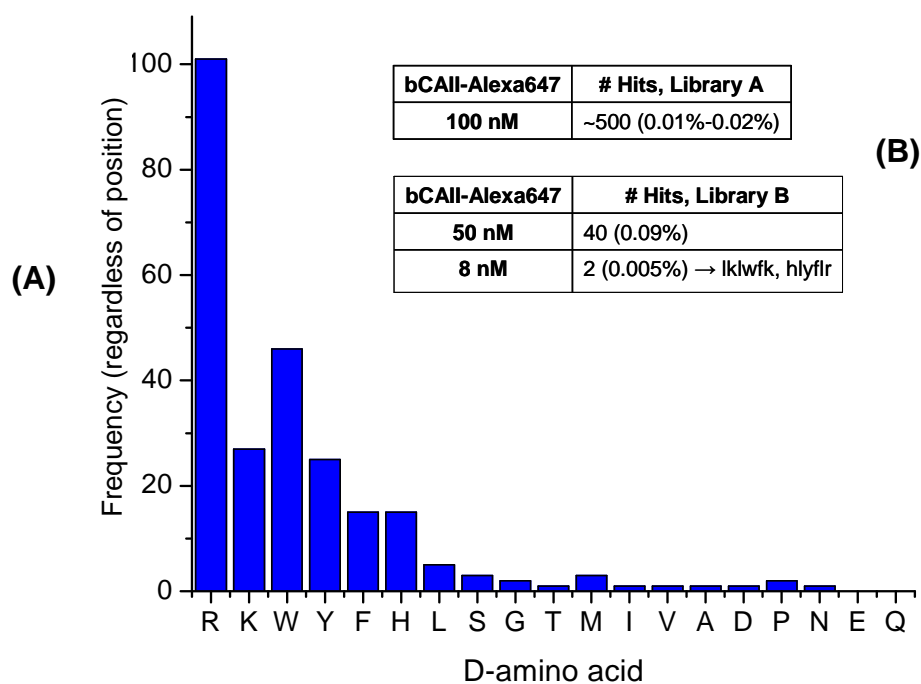


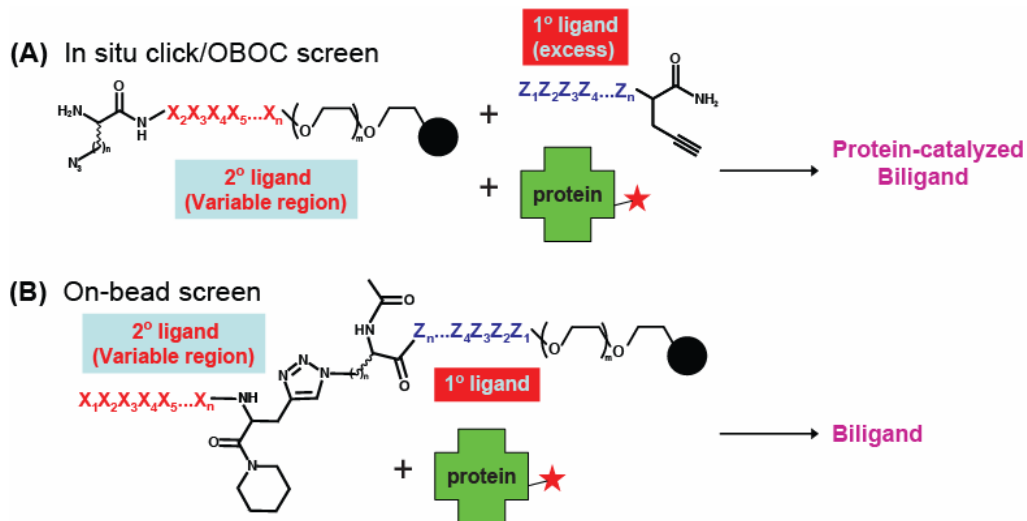
**Figure 2.5.** Results of selecting a primary or anchor ligand of bCAII. (A) Diagram plotting frequency vs. D-amino acid for 51 hit sequences isolated from screening Library A (first-generation anchor ligand screen). (B) Hit rates for Library A and B (second-generation anchor ligand) screens, leading to the selection of two anchor ligands (lklwfk and hlyflr).

a 1° ligand for use in multi-ligand screens. A complete list of 1° ligand hit sequences from OBOC selections can be found in Appendix B.

The peptide lklwfk was then functionalized with either an azide (-N<sub>3</sub>) or acetylene (-C≡C-H) terminus, fluoresceinated, and produced in bulk quantities for affinity measurements by fluorescence polarization. Chapter 3 will describe that one such 1° ligand lklwfk-(D-Pra) displays an equilibrium dissociation constant of  $K_D \approx 500 \mu\text{M}$  for its interaction with bCAII. This value is an estimate, since weak affinities are hard to quantify. Surface plasmon resonance (SPR) was also employed to measure the affinity of bCAII for Az4-kfwkl and lklwfk-(D-Pra) as 1° ligands, and a similarly low affinity was recorded (at least  $>10 \mu\text{M}$ , see Chapter 3).

### 2.3.2 Identification of Secondary (2°) Ligands: Biligand Screens

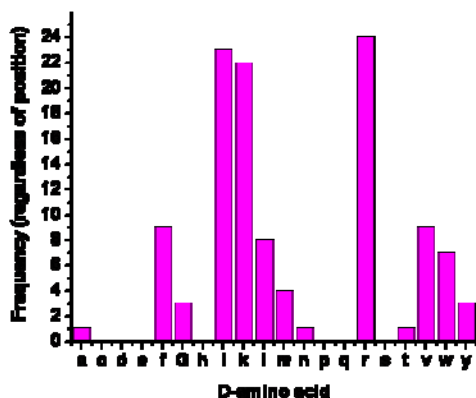
A biligand is constructed of a 2° ligand that is covalently attached, via a 1,2,3-triazole linkage, to the 1° ligand. As illustrated by Figure 2.6, secondary (2°) ligands were identified by two complementary approaches: (1) in situ click/OBOC biligand screens; (2) on-bead biligand screens. In the first approach (Figure 2.6A), the protein acts as a catalyst for the in situ click assembly of the biligand on bead. During this screen, the 1° ligand and protein coexist in solution, while the cognate library of 2° ligands is on bead. In the second approach (Figure 2.6B), the 1° ligand is covalently coupled to the on-bead library of 2° ligands via the copper(I)-catalyzed azide-alkyne cycloaddition (CuAAC). Such a library of pre-assembled biligands is screened against the protein target to discover 2° ligand candidates. The protein target is not a catalyst in this approach; this screen was used as a validation tool for comparison against the in situ click/OBOC screens.



**In situ click/OBOC biligand screen.** Based on the protein-catalyzed in situ click reactions reported by the Sharpless group<sup>17-21</sup> only those 2° ligands that bind with bCAII *and* are in close proximity with the 1° ligand, *and* are in the correct orientation, will react to form the 1,2,3-triazole product. Figure 2.7A illustrates the result of the first-generation in situ biligand screen **Bi1** against bCAII, which utilized 100 μM lklwfk-(D-Pra) as the 1° ligand and a comprehensive azide-modified Library C. From histogram and raw analysis of hits, a 2° ligand Az4-kiwiG emerged as the best candidate, since its inherent motif was repeated several times. Figure 2.7B shows an abbreviated list of the hit sequences isolated from screening Library C against 50 nM bCAII-Alexa647 (**Bi1**). A complete list of biligand hit sequences from the in situ click/OBOC screens can be found in Appendix B.

The very high sequence homology observed here was not witnessed for the 1° ligand screens, but is characteristic of all of the in situ biligand and triligand (see Section 2.3.3) screens discussed in this thesis. Note also that all of the peptides in Figure 2.7B contain at least one azide group, although, statistically, over one-third of the OBOC library does not contain azide groups at positions 1 or 7. The high sequence homology, coupled with the persistence of azide groups in the selected 2° ligands, provides strong circumstantial evidence that the in situ click/OBOC screen worked to produce a biligand.

**On-bead biligand screen.** On-bead biligand screens (**Bi2a** and **Bi2b**) were carried out utilizing a focused CuAAC biligand library (Library D) that was prepared based on the sequencing results from screen **Bi1**. All 2° ligand sequences obtained by screens **Bi2a** and **Bi2b** (Table 2.2) also display striking sequence homology. Several sequences were repeated more than once, including kwlwGl and kwiwGw. A residue-



(A)

	Az <sub>n</sub>	x <sub>2</sub>	x <sub>3</sub>	x <sub>4</sub>	x <sub>5</sub>	x <sub>6</sub>	Az <sub>n</sub>
hit1	Az4	k	i	w	i	G	
hit2	Az8	r	l	w	v	G	Az4
hit3	Az8	r	r	r	k	r	Az8
hit4	Az4	l	l	v	i	k	Az4
hit5	Az4	m	i	l	i	k	
hit6	Az8	i	i	i	m	r	Az4
hit7	Az8	i	i	i	w	r	Az8
hit8	Az4	n	v	i	i	f	
hit9	Az4	i	f	l	v	k	Az8
hit10	Az4	k	i	w	i	G	Az8
hit11	Az4	r	r	k	f	r	Az8
hit12	Az4	r	v	w	l	r	Az8
hit13	Az8	k	y	r	r	r	Az4
hit14	Az8	r	r	k	v	w	Az4
hit15	Az4	i	f	l	v	k	Az8
hit16		k	r	k	r	f	Az4
hit17	Az8	k	i	w	i	k	

(B)

**Figure 2.7.** Identification of a 2° ligand by in situ click/OBOC screening against bCAII. (A) Diagram illustrating frequency (y-axis) of D-amino acids (x-axis) for 2° ligand candidates of a biligand isolated from screening Library C in the presence of the 1° ligand lklwfk-(D-Pra) and bCAII (screen **Bi1**). (B) Abbreviated list of the 2° ligand sequences isolated from the screen of Figure 2.7A.

by-residue histogram analysis (Figure 2.8) of all 2° ligand hits illustrates a strong preference for only one particular amino acid at each residue position—1 (k), 2 (w), 4 (w), and 5 (G)—in the 2° ligand component of the biligand capture agent. The distribution of D-amino acids illustrated in Figure 2.8, based on the analysis of 37 biligand hit beads, suggests this consensus sequence k-w-x<sub>3</sub>-w-G (where x<sub>3</sub> = hydrophobic amino acid). A complete list of biligand hit sequences from the on-bead biligand screens can be found in Appendix B.

Several methods were employed to characterize the properties of biligand candidates. First, homology derived from the 2° ligand sequences from both the in situ click/OBOC and on-bead screens provided clues. Second, the three candidate biligands—kwlwGI-Tz1-kfwlkl, kwiwGw-Tz1-kfwlkl, and lklwfk-Tz1-kiwiG—were synthesized in bulk, and their binding affinities for bCAII were measured by SPR. Chapter 3 will describe that an equilibrium dissociation constant of  $K_D \approx 3 \mu\text{M}$  (bCAII) was determined for the best-binding biligand kwlwGI-Tz1-kfwlkl. This value is two orders of magnitude greater than the affinity for the 1° ligand alone, meeting our goal of affinity enhancement.

**Binary component screen for in situ biligand.** Finally, the in situ click/OBOC biligand screening method can be validated by a binary component screen. The 1° ligand lklwfk-(D-Pra) and 2° ligand Az4-kiwiG were combined in solution in the presence of protein target. The bCAII-catalyzed assembly of biligand is typically monitored by analytical methods such as LC/MS.<sup>17-21</sup> Here, MALDI-MS was used to monitor the extent of this reaction over several days (Figure 2.9). The bCAII-catalyzed biligand product is marked with an arrow. While it was encouraging that the

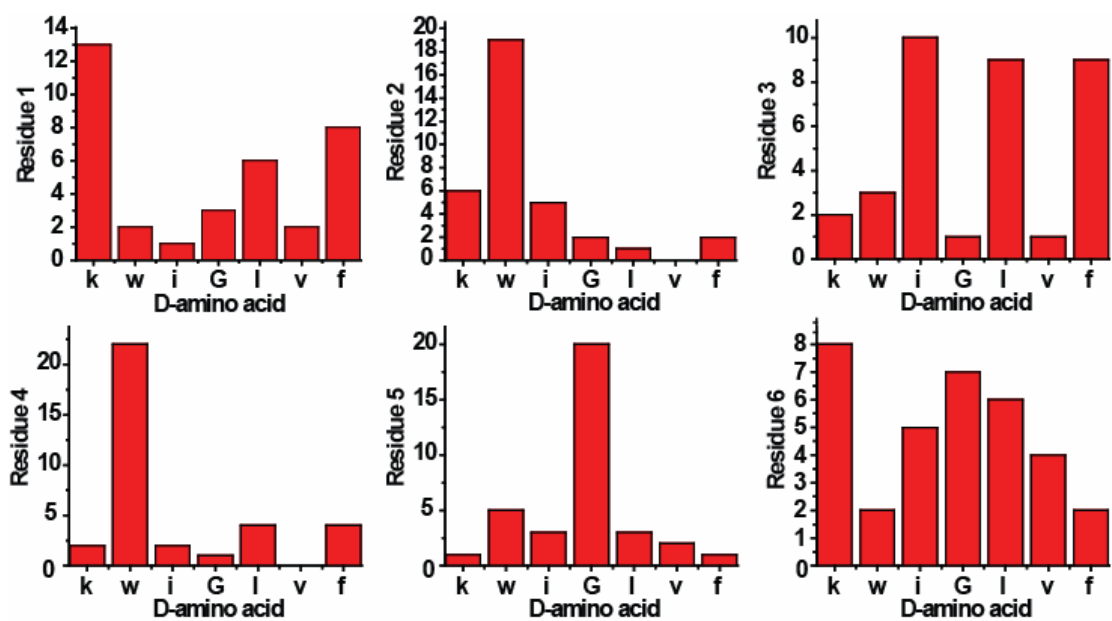


**Figure 2.8.** Distribution of D-amino acids found in positions 1 to 6 based on the analysis of 37 biligand hit beads from screens **Bi2a** and **Bi2b**.

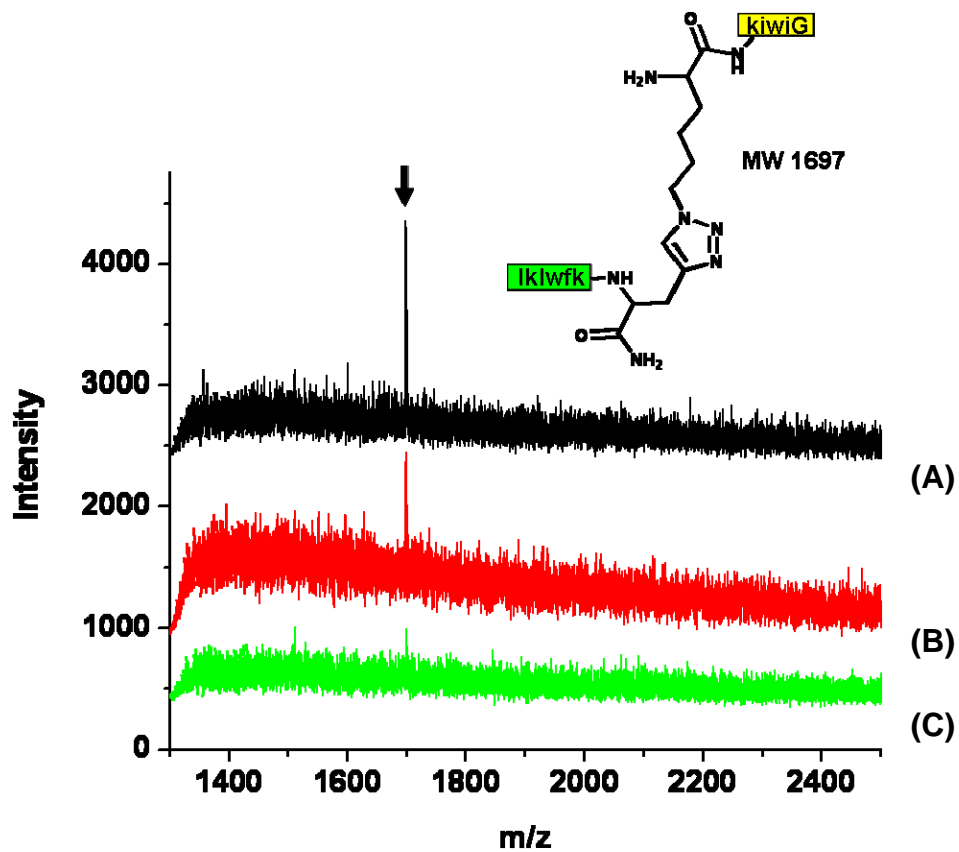


**Figure 2.9.** Binary component in situ click chemistry screen of 1° ligand lklwfk-(D-Pra) and 2° ligand Az4-kiwiG, illustrating bCAII-catalyzed formation of biligand (marked by arrow). (A) Bovine carbonic anhydrase II (bCAII). (B) Bovine serum albumin (BSA) control. (C) Buffer-only (no protein) control.

background reactions (BSA, no protein) were less, the MALDI-MS result did not provide quantitative measurement of the signal-to-noise ratio and overall yield for the bCAII-catalyzed reaction. Methods to quantitatively assess these were developed at the triligand level and are discussed in detail in Chapter 4.

### 2.3.3 Identification of Tertiary (3°) Ligands: Triligand Screens

Once a biligand is identified, that biligand can serve as the new anchor ligand, as illustrated in Figure 2.1, and *the same OBOC library* may be employed to identify a triligand. This process may be repeated with the same OBOC library until a multi-ligand with the desired affinity and specificity is reached. With the biligand (D-Pra)-kwlwGl-Tz1-kfwlkl serving as the anchor ligand, the Figure 2.1 in situ click/OBOC screen was repeated with Library C (Table 2.1) to identify a triligand rfviln-Tz2-kwlwGl-Tz1-kfwlkl (Figure 2.4C). It is crucial to note that the comprehensive Library C was applied again here, demonstrating the versatility of this type of general library.

For the case of the triligand screens, a histogram charting the position-dependent frequency of amino acids observed in the hit beads was generated. The consensus tertiary (3°) ligand was Az4-nlivfr (Figure 2.4A). Figure 2.10 shows position-dependent histograms for the first-generation in situ click/OBOC screens, for peptides (a) with and (c) without an azide-containing amino acid, to generate a triligand. For the in situ screen (**Tri1**, Figure 2.10A), one-third of the beads had no azide at the  $x_1$  or  $x_7$  positions, but interestingly, all hit beads contained an azide. On the other hand, the first- and second-generation on-bead CuAAC library screens (**Tri2** and **Tri4**, Figure 2.10B), where the 3° ligand variable region was coupled via CuAAC (Tz2) to the biligand, yielded independent validation of the in situ result. The final, consensus triligand sequence is

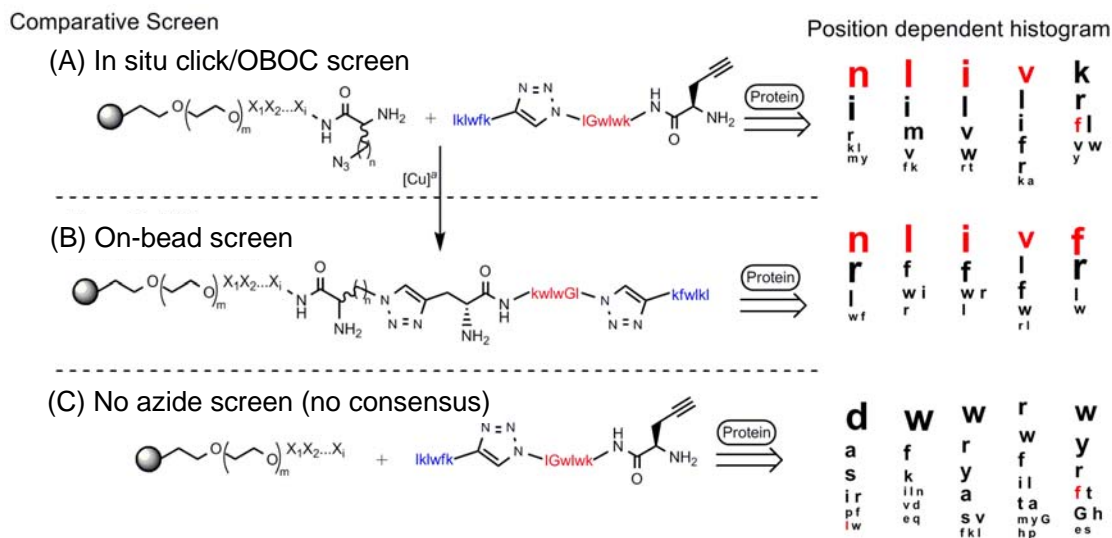


**Figure 2.10.** Method to validate protein-templated formation of a multi-ligand capture agent. Position-dependent histograms are illustrated for the first-generation in situ click/OBOC screens, for tertiary ligands (A) with and (C) without an azide-containing amino acid, to generate a triligand. First- and second-generation on-bead CuAAC library screens (B) independently confirmed the in situ result. The final consensus triligand sequence is indicated in red. Sample size: *in situ* = 25 hits; *in situ no azide* = 24 hits; *CuAAC library* = 21 hits.

<sup>a</sup> CuAAC conditions: Fully protected (D-Pra)-kwlwG1-Tz1-kfwlkl (0.274 g, 0.1 mmol, >98% HPLC), 0.03 mmol Library C, CuI (0.021 g, 0.1 mmol), and L-ascorbic acid (0.020 g, 0.1 mmol) were stirred in DMF/piperidine (8/2) overnight at 25 °C.

indicated by red font. Both this on-bead triligand screen, and the in situ click/OBOC screen, yielded *the same* consensus sequence and confirmed the equivalence of the two types of screens.

In the absence of azide (Figure 2.10C), the in situ triligand screens yielded completely different, and much less homologous, hit sequences. This phenomenon resulted from the prevention of triligand capture agent formation by click chemistry (control screen **TriX**). This screen illustrates the importance of the azide and acetylene functional groups, and their specific interaction on the surface of the target to produce a multi-ligand capture agent.

The consensus 3° ligand obtained by second-generation in situ screen **Tri3** resembles almost exactly the 3° ligand isolated by the first-generation screen (**Tri1**). Such sequence homology is unique to the in situ screens, which display target-guided selection. A complete list of triligand hit sequences from the in situ click/OBOC screens and on-bead triligand screens can be found in Appendix B.

The interaction between bCAII and triligand rfviln-Tz2-kwlwGl-Tz1-kfwlkl (Figure 2.4C) was measured by SPR. Chapter 3 will describe that equilibrium dissociation constants of  $K_D \approx 45$  nM (hCAII) and  $K_D \approx 64$  nM (bCAII) were determined, and represent a fifty-fold affinity enhancement from the protein/biligand interaction.

## 2.4 CONCLUSIONS

It was our goal to develop a high-affinity protein capture agent with high affinity and specificity through the iterative conjugation of modest affinity peptides using in situ click chemistry. An affinity enhancement due to in situ click conjugation was apparent at each screening level. Even for a weakly binding anchor ligand ( $K_D \approx 500$   $\mu$ M), the

hits from biligand screens displayed high sequence homologies and affinities ( $K_D \approx 3$  to  $10 \mu\text{M}$ ). Both types of biligand screens, in situ and on-bead, demonstrated this effect, suggesting that although the mechanism of the selection is different, the hits identified are essentially equivalent.

At the triligand level, a similar concept was explored. When the peptide ligand became approximately larger than a 15-mer, the OBOC library size was practically limited to <5 million sequences, and the in situ screen (**Tri1**) became the only way to sample increasing diversity and length. Based on analysis of sequence homology, we discovered that the final triligand capture agent reflected in situ assembly, as the on-bead CuAAC triligand library (Table 2.2, Library E) was not comprehensive.

The final triligand capture agent (Figure 2.4C) was demonstrated to bind to bCAII and hCAII with affinities of  $K_D \approx 64 \text{ nM}$  and  $K_D \approx 45 \text{ nM}$ , respectively, and in Chapter 3, we will provide evidence that it is a specific binder for the enzyme.

## 2.5 ACKNOWLEDGEMENTS

This work was completed in collaboration with Rosemary D. Rohde, Steven W. Millward, Arundhati Nag, Wook-Seok Yeo, Jason E. Hein, Suresh M. Pitram, Abdul Ahad Tariq, Vanessa M. Burns, Russell J. Krom, Valery V. Fokin, and K. Barry Sharpless.

**2.6 REFERENCES**

1. Borrebaeck, C. A. K. *Immunol. Today* **2000**, *21*, 379–382.
2. Kodadek, T.; Reddy, M. M.; Olivos, H. J.; Bachhawat-Sikder, K.; Alluri, P. G. *Acc. Chem. Res.* **2004**, *37*, 711–718.
3. Blow, N. *Nature* **2007**, *447*, 741–744.
4. (a) Fan, R.; Vermesh, O.; Srivastava, A.; Yen, B. K. H.; Qin, L.; Ahmad, H.; Kwong, G. A.; Liu, C.-C.; Gould, J.; Hood, L.; Heath, J. R. *Nat. Biotechnol.* **2008**, *26*, 1373–1378. (b) Hood, L.; Heath, J. R.; Phelps, M. E.; Lin, B. *Science* **2004**, *306*, 640–643. (c) Phelan, M. L.; Nock, S. *Proteomics* **2003**, *3*, 2123–2134.
5. Smith, G. P.; Petrenko, V. A. *Chem. Rev.* **1997**, *97*, 391–410.
6. Cox, J. C.; Hayhurst, A.; Hesselberth, J.; Bayer, T. S.; Georgiou, G.; Ellington, A. D. *Nucleic Acids Res.* **2002**, *30*, e108–e108.
7. McCauley, T. G.; Hamaguchi, N.; Stanton, M. *Anal. Biochem.* **2003**, *319*, 244–250.
8. Lee, J. F.; Hesselberth, J. R.; Meyers, L. A.; Ellington, A. D. *Nucleic Acids Res.* **2004**, *32*, D95–D100.
9. Gold, L.; Polisky, B.; Uhlenbeck, O.; Yarus, M. *Annu. Rev. Biochem.* **1995**, *64*, 763–797.
10. Burmeister, P. E.; Lewis, S. D.; Silva, R. F.; Preiss, J. R.; Horwitz, L. R.; Pendergrast, P. S.; McCauley, T. G.; Kurz, J. C.; Epstein, D. M.; Wilson, C.; Keefe, A. D. *Chem. Biol.* **2005**, *12*, 25–33.
11. Proske, D.; Blank, M.; Buhmann, R.; Resch, A. *Appl. Microbiol. Biotechnol.* **2005**, *69*, 367–374.
12. Lam, K. S.; Lebl, M.; Krchňák, V. *Chem. Rev.* **1997**, *97*, 411–448.

13. Furka, A.; Sebestyén, F.; Asgedom, M.; Dibó, G. *Int. J. Pept. Protein Res.* **1991**, *37*, 487–493.
14. Geysen, H. M.; Mason, T. J. *Bioorg. Med. Chem. Lett.* **1993**, *3*, 397–404.
15. Alluri, P. G.; Reddy, M. M.; Bachhawat-Sikder, K.; Olivos, H. J.; Kodadek, T. J. *Am. Chem. Soc.* **2003**, *125*, 13995–14004.
16. Reddy, M. M.; Bachhawat-Sikder, K.; Kodadek, T. *Chem. Biol.* **2004**, *11*, 1127–1137.
17. Lewis, W. G.; Green, L. G.; Grynszpan, F.; Radić, Z.; Carlier, P. R.; Taylor, P.; Finn, M. G.; Sharpless, K. B. *Angew. Chem. Int. Ed.* **2002**, *41*, 1053–1057.
18. Manetsch, R.; Krasinski, A.; Radić, Z.; Raushel, J.; Taylor, P.; Sharpless, K. B.; Kolb, H. C. *J. Am. Chem. Soc.* **2004**, *126*, 12809–12818.
19. Bourne, Y.; Kolb, H. C.; Radić, Z.; Sharpless, K. B.; Taylor, P.; Marchot, P. *Proc. Natl. Acad. Sci. USA* **2004**, *101*, 1449–1454.
20. Mocharla, V. P.; Colasson, B.; Lee, L. V.; Röper, S.; Sharpless, K. B.; Wong, C.-H.; Kolb, H. C. *Angew. Chem. Int. Ed.* **2005**, *44*, 116–120.
21. Whiting, M.; Muldoon, J.; Lin, Y.-C.; Silverman, S. M.; Lindstrom, W.; Olson, A. J.; Kolb, H. C.; Finn, M. G.; Sharpless, K. B.; Elder, J. H.; Fokin, V. V. *Angew. Chem. Int. Ed.* **2006**, *45*, 1435–1439.
22. Kehoe, J. W.; Maly, D. J.; Verdugo, D. E.; Armstrong, J. I.; Cook, B. N.; Ouyang, Y.-B.; Moore, K. L.; Ellman, J. A.; Bertozzi, C. R. *Bioorg. Med. Chem. Lett.* **2002**, *12*, 329–332.
23. Ramstrom, O.; Lehn, J. M. *Nature Rev. Drug Discov.* **2002**, *1*, 26–36.
24. Poulin-Kerstien, A. T.; Dervan, P. B. *J. Am. Chem. Soc.* **2003**, *125*, 15811–15821.

25. Jain, A.; Huang, S. G.; Whitesides, G. M. *J. Am. Chem. Soc.* **1994**, *116*, 5057–5062.
26. Mammen, M.; Choi, S. K.; Whitesides, G. M. *Angew. Chem. Int. Ed.* **1998**, *37*, 2755–2794.
27. Kodadek, T.; Reddy, M. M.; Olivos, H. J.; Bachhawat-Sikder, K.; Alluri, P. G. *Acc. Chem. Res.* **2004**, *37*, 711–718.
28. Parkkila, S.; Rajaniemi, H.; Parkkila, A.-K.; Kivelä, J.; Waheed, A.; Pastoreková, S.; Pastorek, J.; Sly, W. S. *Proc. Natl. Acad. Sci. USA* **2000**, *97*, 2220–2224.
29. Yoshiura, K.; Nakaoka, T.; Nishishita, T.; Sato, K.; Yamamoto, A.; Shimada, S.; Saida, T.; Kawakami, Y.; Takahashi, T. A.; Fukuda, H.; Imajoh-Ohmi, S.; Oyaizu, N.; Yamashita, N. *Clin. Cancer Res.* **2005**, *11*, 8201–8207.
30. Haapasalo, J.; Nordfors, K.; Järvelä, S.; Bragge, H.; Rantala, I.; Parkkila, A.-K.; Haapasalo, S. *Neuro-Oncol.* **2007**, *9*, 308–313.
31. Krishnamurthy, V. M.; Kaufman, G. K.; Urbach, A. R.; Gitlin, I.; Gudiksen, K. L.; Weibel, D. B.; Whitesides, G. M. *Chem. Rev.* **2008**, *108*, 946–1051.
32. Jude, K. M.; Banerjee, A. L.; Haldar, M. K.; Manokaran, S.; Roy, B.; Mallik, S.; Srivastava, D. K.; Christianson, D. W. *J. Am. Chem. Soc.* **2006**, *128*, 3011–3018.
33. Melkko, S.; Scheuermann, J.; Dumelin, C. E.; Neri, D. *Nat. Biotechnol.* **2004**, *22*, 568–574.
34. Wilkinson, B. L.; Bornaghi, L. F.; Houston, T. A.; Innocenti, A.; Supuran, C. T.; Poulsen, S.-A. *J. Med. Chem.* **2006**, *49*, 6539–6548.
35. Chenault, H. K.; Dahmer, J.; Whitesides, G. M. *J. Am. Chem. Soc.* **1989**, *111*, 6354–6364.

36. van Hest, J. C. M.; Kiick, K. L.; Tirrell, D. A. *J. Am. Chem. Soc.* **2000**, *122*, 1282–1288.
37. Lee, H.-S.; Park, J.-S.; Kim, B. M.; Gellman, S. H. *J. Org. Chem.* **2003**, *68*, 1575–1578.
38. (a) I. Coin, M. Beyermann, M. Bienert, *Nat. Protocols* **2007**, *2*, 3247–3256.  
(b) Fields, G. B.; Noble, R. L. *Int. J. Pept. Protein Res.* **1990**, *35*, 161–214.
39. Carpino, L. A.; El-Faham, A.; Minor, C. A.; Albericio, F. *J. Chem. Soc., Chem. Commun.* **1994**, 201–203.
40. Dixon, S. M.; Li, P.; Liu, R.; Wolosker, H.; Lam, K. S.; Kurth, M. J.; Toney, M. *D. J. Med. Chem.* **2006**, *49*, 2388–2397.
41. (a) Edman, P. *Acta Chem. Scand.* **1950**, *4*, 283–293. (b) Laursen, R. A. *Eur. J. Biochem.* **1971**, *20*, 89–102. (c) Niall, H. D. *Methods Enzymol.* **1973**, *27*, 942–1010.
42. Lee, S. S.; Lim, J.; Cha, J.; Yeo, S. Y.; Tan, S.; Agnew, H. D.; Heath, J. R. *Anal. Chem.* **2010**, *82*, 672–679.
43. Rostovtsev, V. V.; Green, L. G.; Fokin, V. V.; Sharpless, K. B. *Angew. Chem. Int. Ed.* **2002**, *41*, 2596–2599.
44. Tornøe, C. W.; Christensen, C.; Meldal, M. *J. Org. Chem.* **2002**, *67*, 3057–3064.
45. Tornøe, C. W.; Meldal, M. “Peptidotriazoles: Copper(I)-catalyzed 1,3-dipolar cycloadditions on solid-phase” in *Peptides: The Wave of the Future* (Lebl, M.; Houghten, R. A., editors), Kluwer, Dordrecht, 2001, p. 263.
46. Atherton, E.; Sheppard, R. C. in *Solid Phase Peptide Synthesis—A Practical Approach*, Oxford University Press, USA, 1989, p. 136.
47. Zhang, Z.; Fan, E. *Tetrahedron Lett.* **2006**, *47*, 665–669.

48. Weterings, J. J.; Khan, S.; van der Heden, G. J.; Drijfhout, J. W.; Melief, C. J. M.; Overkleeft, H. S.; van der Burg, O. H.; Ossendorp, F.; van der Marel, G. A.; Filippov, D. V. *Bioorg. Med. Chem. Lett.* **2006**, *16*, 3258–3261.
49. García-Martín, F.; Bayó-Puxan, N.; Cruz, L. J.; Bohling, J. C.; Albericio, F. *QSAR Comb. Sci.* **2007**, *26*, 1027–1035.

### **Chapter 3**

Affinities, Specificities, and Implementation of Multi-ligand Capture Agents in Standard

Assays of Protein Detection

### 3.1 INTRODUCTION

In Chapter 2, the screening methodology for discovery of a triligand capture agent for a specific target, namely human and bovine carbonic anhydrase II (hCAII and bCAII, respectively), was explored as a proof of concept. During the course of multi-ligand development, measurements of binding affinity, specificity, and other physicochemical properties for the isolated ligands were performed. Characterization of hit-derived compounds provided guidance on selecting the most suitable anchor ligand(s), evaluating the quality of the screen, and deciding how many screens to perform. The resultant triligand rfviln-Tz2-kwlwGl-Tz1-kfwlkl was further studied for efficacy as a capture and detection reagent in standard assays including dot blot, Western blot, and sandwich (ELISA-like) assay. Through their potential to remove reliance on antibodies, multi-ligand capture agents may directly impact quantitative biology through such implementation in standard assays for protein detection.

The binding affinities describing the interaction between b(h)CAII and the anchor ligands, biligands, and triligands have been characterized via several techniques, including fluorescence polarization and surface plasmon resonance (SPR). The terms “binding affinity” or “affinity” as used herein indicate the strength of the binding between a ligand and protein target (CA II), and is expressed as an equilibrium dissociation constant ( $K_D$ ). Binding affinities are influenced by non-covalent intermolecular interactions between the two molecules such as hydrogen bonding, electrostatic interactions, hydrophobic interactions, and van der Waals forces. The smaller the dissociation constant, the more tightly bound is the ligand, or the better the binding affinity between the two molecules.

Specificities of multi-ligands have been demonstrated and optimized in one case (dot blot). The term “specificity,” with reference to the binding of a ligand to a protein target (CA II), refers to the recognition, contact, and formation of a stable complex between the first molecule and the second molecule, together with substantially less to no binding interaction with other molecules that may be present. With the protein target spiked in serum, dot blots, Western blots, and sandwich (ELISA-like) assays were employed to compare specificities of antibody vs. multi-ligand. Detection sensitivities of triligand vs. biligand vs. anchor ligand were also studied. As anticipated, the triligand  $\text{rfviln-Tz2-kwlwGl-Tz1-kfwlkl}$  was the most sensitive, detecting CA II at the  $\geq 20$  ng level from 10% porcine serum.

Physicochemical properties of multi-ligands provide additional information on utility of capture agents in various biological assays. Circular dichroism (CD) measurements indicated that the 1,2,3-triazole linker (Tz1 and Tz2) in a multi-ligand induces formation of a random coil structure, which is likely to influence the mechanism of binding to the protein target. On the other hand, an activity assay of bCAII was utilized to assess capacity for active site binding by multi-ligands. In addition, non-natural amino acids in the form of D-stereoisomers were found to be useful ligand building blocks because they are not susceptible to enzymatic degradation. Because the multi-ligands can be chemically synthesized and stored as a lyophilized powder, they have long shelf lives ( $>1$  yr). Since we have highly modular chemical control over capture agent synthesis, additional molecules or functional groups (e.g., fluorophores, small molecules, oligonucleotides, haptens, and other proteins) can be installed in desired locations to provide desired chemical or biological activity. Similarly, if ultra-

high affinity (e.g.,  $K_D \approx \text{pM}$ ) is a desired goal, the triligand can potentially be matured into a tetraligand capture agent via another iteration of the in situ click/OBOC screen.

## 3.2 MATERIALS AND EXPERIMENTAL METHODS

### 3.2.1 Chemicals

For bulk biligand and triligand synthesis (see Chapter 2), acetylation reagents (acetic anhydride, 2,6-lutidine, and *N,N*-dimethylformamide) were purchased from Sigma-Aldrich (St. Louis, MO). For the on-bead Cu(I)-catalyzed click reaction, copper(I) iodide, L-ascorbic acid, and sodium diethyldithiocarbamate trihydrate were purchased from Sigma-Aldrich (St. Louis, MO).

Fluorescein isothiocyanate (FITC) was obtained from AnaSpec. D-biotin and 4-nitrophenyl acetate were obtained from Sigma-Aldrich (St. Louis, MO).

### 3.2.2 Characterization of Affinity by Fluorescence Polarization

The N-terminus of the anchor ligand was labeled with FITC following published protocols.<sup>1</sup> After resin cleavage, the crude fluoresceinated anchor ligand was precipitated with ether and then purified to >95% by  $C_{18}$  reversed phase HPLC.

Luminescence spectra were recorded by Fluorolog2 spectrofluorimeter (Jobin Yvon, Longjumeau, France) in the Beckman Institute Laser Resource Center (Pasadena, CA). All samples contained 6  $\mu\text{M}$  fluoresceinated anchor ligand and a concentration gradient of bCAII (0.2 to 800  $\mu\text{M}$ ) in PBS (pH 7.4) + 3% (v/v) DMSO. Stock protein and anchor ligand concentrations were verified by UV-Vis using  $\epsilon_{280}$  (bCAII) = 57,000  $\text{M}^{-1}\text{cm}^{-1}$  or  $\epsilon_{494}$  (FITC, 0.1 N NaOH) = 68,000  $\text{M}^{-1}\text{cm}^{-1}$  for fluoresceinated anchor ligand. After incubation for 1 h at 25 °C in the dark, samples were excited at

488 nm (2-nm band-pass), and luminescence spectra were obtained between 500 and 700 nm (4-nm band-pass). All measurements were taken at 2-nm intervals with 0.5 s integration times at 25 °C. All luminescence spectra were subjected to background subtraction.

The ratio of sensitivities (G) for the vertically and horizontally plane-polarized light in the system was calculated by the equation  $G=I_{HH}/I_{HV}$  using the  $I_{HH}$  and  $I_{HV}$  luminescence spectra obtained from a peptide-only sample. The luminescence spectra  $I_{VV}$  and  $I_{VH}$  were integrated, and the fluorescence polarization value (P) was calculated by applying Equation (1). The polarization value, P, being a ratio of light intensities, is dimensionless, and is sometimes expressed in millipolarization units (1 polarization unit = 1000 mP Units).

$$P = \frac{I_{VV} - GI_{VH}}{I_{VV} + GI_{VH}} \quad (1)$$

The polarization values were fitted with a sigmoidal dose-response curve using Origin 6.1 (Northampton, MA).

### 3.2.3 Characterization of Affinity by Surface Plasmon Resonance

Affinity measurements were performed using a Biacore T100 SPR (Caltech Protein Expression Center, Pasadena, CA) and research grade CM5 sensor chips (GE Healthcare). The instrument was first primed with HBS-P<sup>+</sup> [10 mM HEPES, 150 mM NaCl, 0.05% Tween20 (pH 7.4)] + 3% DMSO. Flow cell 1 was used as a reference to subtract nonspecific binding, drift, and the bulk refractive index, while flow cell 2 (or 3) was immobilized with bCAII (or hCAII) following standard procedures. A 1:1 mixture of 0.4 M EDC and 0.1 M NHS was used to activate flow cell 2, and 0.25 mg/mL bCAII

solution [prepared in 10 mM sodium acetate (pH 5.0)] was injected.<sup>2</sup> Similarly, flow cell 3 was immobilized with hCAII following standard procedures using 0.25 mg/mL hCAII prepared in 10 mM sodium acetate (pH 5.5) buffer.<sup>3</sup> Immobilization levels of ~4000 RU were achieved using a flow rate of 100  $\mu$ L/min over 420 s. The instrument was then primed using running buffer (HBS-P<sup>+</sup> + 3% DMSO). Prior to the peptide analyte experiment, 8 buffer-alone cycles were completed to establish baseline stabilization.

Triligands were dissolved in HBS-P<sup>+</sup> + 3% DMSO buffer to produce 2  $\mu$ M peptide stock solutions for each peptide, which were serially diluted by a factor of 2 to produce a concentration series down to 0.1 nM. Biligands were dissolved in HBS-P<sup>+</sup> + 3% DMSO buffer to produce 5  $\mu$ M peptide stock solutions for each peptide, which were serially diluted by a factor of 2 to produce a concentration series down to 2 nM. Anchor (1<sup>o</sup>) ligands were dissolved in HBS-P<sup>+</sup> + 3% DMSO buffer to produce ~10  $\mu$ M peptide stock solutions for each peptide, which were serially diluted by a factor of 2 to produce a concentration series down to 300 nM. For a given affinity measurement, these series of peptide solutions successively were injected into flow cell 2 (or 3) for 120 to 180 s of contact time, 300 s of dissociation time, and 200 s of stabilization time using a flow rate of 100  $\mu$ L/min at 25  $^{\circ}$ C. Data processing and affinity analysis, including background subtraction, was performed using Biacore T100 evaluation software (Version 2.0.1, Biacore). Equilibrium dissociation constant ( $K_D$ ) values for 1:1 binding were extracted by nonlinear regression fitting of the data to Equation (2).

$$RU_{eq} = RU_{max}[peptide]/(K_D + [peptide]), \quad (2)$$

where  $RU_{eq}$  is the measured response unit at a certain peptide analyte concentration and  $RU_{max}$  is the maximum response unit.

### 3.2.4 Enzymatic Activity Assay of Carbonic Anhydrase II

Following previous methods,<sup>4</sup> solution assays for esterase activity were conducted with 1.4  $\mu\text{M}$  bCAII, 5  $\mu\text{M}$  triligand rfviln-Tz2-kwlwGl-Tz1-kfwlkl, and 50  $\mu\text{M}$  4-nitrophenyl acetate (4-NPA) in Tris buffer composed of 9 mM Tris-HCl and 81 mM NaCl + 9% acetonitrile (v/v) + 1% DMSO (v/v). Control assays were conducted in the absence of triligand, and in the absence of protein. The hydrolysis of 4-NPA was monitored over a time course of 60 min, with absorbance measurements taken every 6 min.

### 3.2.5 Circular Dichroism of Triligand

Circular dichroism spectra were measured by Aviv 62AD Spectropolarimeter (Aviv Associates, Lakewood, NJ) in a 1 mm cuvette at 25 °C. Measurements of 15  $\mu\text{M}$  triligand rfviln-Tz2-kwlwGl-Tz1-kfwlkl in 100 mM Tris-HCl (pH 7.5) were recorded between 200 and 260 nm with a band-pass of 1.5 nm.

### 3.2.6 Dot Blot Specificity/Sensitivity Assays of Biligand and Triligand in Serum

For these tests, Biotin-PEG-NovaTag resin (0.48 mmol/g; Novabiochem) was utilized for bulk synthesis of C-terminal biotin-labeled multi-ligands (Figure 3.7). After resin cleavage, the crude biotinylated multi-ligand was precipitated with ether and then purified to >95% by C<sub>18</sub> reversed phase HPLC.

The b(h)CAII antigens were prepared as 1 mg/mL stocks in PBS (pH 7.4). A dilution series of antigen was applied to a nitrocellulose membrane, typically ranging from 2  $\mu\text{g}$  to 0.5 ng per spot. The membrane was blocked at 4 °C overnight in 5% milk in Tris-buffered saline (TBS) [25 mM Tris, 150 mM NaCl, 2 mM KCl (pH 8.0)]. The

membrane was then washed with TBS. The biotinylated multi-ligand was prepared at 1  $\mu$ M in 10% porcine serum in TBS + 0.1% DMSO (v/v) and incubated over the membrane at 4 °C overnight. After washing with TBS for 1 h, 1:3000 Streptavidin-HRP (Abcam, Cambridge, MA) prepared in 0.5% milk/TBS was added to the membrane and incubated for 1 h. After washing with TBS for 1 h, the membrane was developed with SuperSignal West Pico Chemiluminescent Enhancer and Substrate Solutions (Pierce, Rockford, IL) and then immediately exposed to HyBlot CL AR film.

### 3.2.7 Western Blot Analysis Using Triligand

For denaturing Western blot analysis, bCAII-spiked porcine serum was electrophoresed on a 12% Tris-HCl PAGE gel (Bio-Rad; Hercules, CA) in 1  $\times$  TGS [25 mM Tris, 192 mM glycine, 0.1% (w/v) SDS, pH 8.3]. Samples were prepared in Laemmli Sample Buffer (Bio-Rad) containing 0.05% (v/v) 2-mercaptoethanol, and boiled before electrophoresis. Gels were transferred to nitrocellulose in 1  $\times$  TGS containing 20% methanol, over 1 h at 100 V.

For native Western blot analysis, bCAII-spiked porcine serum was electrophoresed on a 12% Tris-HCl PAGE gel (Bio-Rad; Hercules, CA) in 1  $\times$  TG [25 mM Tris, 192 mM glycine, pH 8.3]. Samples were prepared in Native Sample Buffer (Bio-Rad) for electrophoresis. Gels were transferred to nitrocellulose in 1  $\times$  TG containing 20% methanol, over 3 h at 100 V.

After transfer, the nitrocellulose membrane was blocked at 4 °C overnight in 5% milk/TBS. The membrane was then washed with TBS. The biotinylated triligand rfviln-Tz2-kwlwGl-Tz1-kfwlkl-(EG)<sub>3</sub>-Biotin was prepared at 1  $\mu$ M in 0.5% milk/TBS + 0.1% (v/v) DMSO and incubated over the membrane overnight at 4 °C. Alternately, a

separate membrane was probed with 1:4000 primary antibody (biotinylated anti-bCAII; Rockland Immunochemicals, PA) for 1 h at 4 °C. After washing with TBS for 1 h, 1:3000 Streptavidin-HRP prepared in 0.5% milk/TBS was added to the membranes and incubated for 1 h. After washing with TBS for 1 h, the membranes were developed with SuperSignal West Pico Chemiluminescent Enhancer and Substrate Solutions (Pierce; Rockford, IL) and then immediately exposed to HyBlot CL AR film.

### **3.2.8 Sandwich (ELISA-like) Assays Using Triligand**

Reacti-Bind Streptavidin high binding capacity coated 96-well plates (~125 pmol biotin/well; Pierce, Rockford, IL) were utilized for this experiment. The biotinylated multi-ligand was prepared at 3  $\mu$ M in 0.5% milk/TBS, and incubated for 1 h at 25 °C. After washing each well with 5% milk/TBS (3  $\times$ ), the plate was filled with 5% milk/TBS and blocked for 1 h at 25 °C. A serial dilution of bCAII antigen was prepared in 10% porcine serum, ranging from 1 mM to 1 pM, and incubated for 1 h at 25 °C. After washing each well with 5% milk/TBS (3  $\times$ ), 1:1000 polyclonal anti-bCAII, HRP conjugate (Abcam, Cambridge, MA) was added to each well in blocking buffer and incubated for 30 min at 25 °C. After washing each well with 5% milk/TBS (3  $\times$ ), chromogenic substrate TMB (3,3',5,5'-tetramethylbenzidine) was supplied to each well. After 20 min, the reaction was quenched with 1 M H<sub>2</sub>SO<sub>4</sub> and analyzed by absorbance at 450 nm on a plate reader.

## **3.3 RESULTS AND DISCUSSION**

With the addition of each ligand to the capture agent, the affinity and the specificity of that capture agent for its cognate protein rapidly increase. The screen

illustrated by Figure 2.1 was used to identify lklwfk-(D-Pra) as the anchor ligand and kwlwGl-Tz1-kfwlkl as the biligand, and ultimately implemented (D-Pra)-kwlwGl-Tz1-kfwlkl as the new anchor ligand for identification of a triligand rfviln-Tz2-kwlwGl-Tz1-kfwlkl against bCAII, according to the methods described in Chapter 2.

### 3.3.1 Characterization of Anchor (1°) Ligand Affinities

**Fluorescence polarization.** To determine the binding affinity of the anchor (1°) ligands lklwfk-(D-Pra) and Az4-kfwlkl, fluorescence polarization was employed. Fluorescence polarization is a measure of the extent of molecular rotation by a fluorescent ligand during the period between excitation and emission with plane polarized light.<sup>5</sup> Free ligands rotate quickly and tumble in and out of plane during their excited states. Therefore, they have low polarization values upon excitation. When a ligand is bound to a receptor (i.e., protein), the molecule remains largely stationary, and so the rotation of the ligand is smaller in its excited state, and hence high polarization values are observed. In these experiments, ligands are typically labeled with a fluorescent dye of a high quantum yield, such as FITC (~4 ns excited lifetime).

The results of a fluorescence polarization experiment to characterize the interaction between bCAII and a fluoresceinated lklwfk-(D-Pra) are shown in Figure 3.1. The fluoresceinated anchor ligand was titrated with increasing concentrations of the protein target (0.2 to 800  $\mu$ M). In high bCAII concentration, most fluoresceinated anchor ligands are bound to the protein. This fluorescent ligand-protein complex will exhibit high fluorescence polarization. However, as less bCAII is titrated, increasing amounts of free fluoresceinated anchor ligand will exist in the solution. These unbound anchor ligands will contribute to a low fluorescence polarization reading. Therefore, by

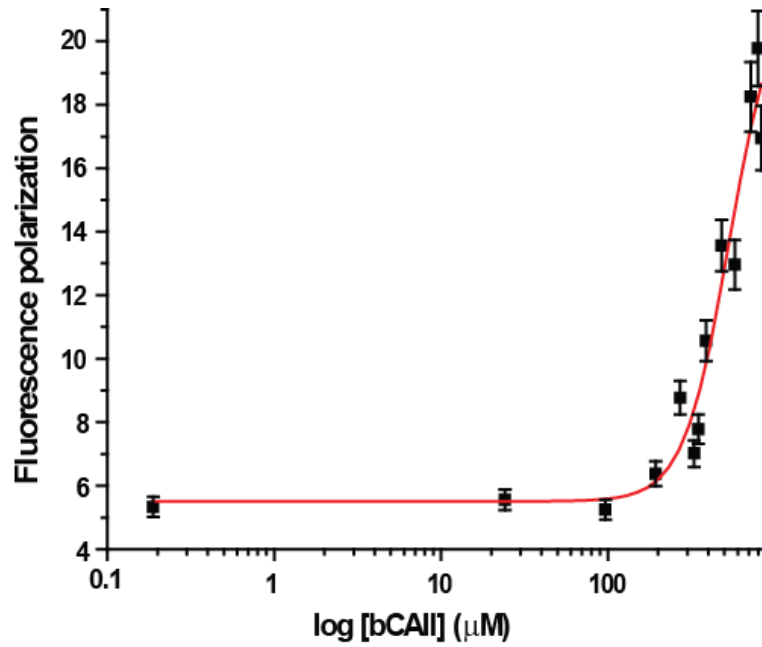


**Figure 3.1.** Fluorescence polarization binding isotherm for the anchor ligand lklwfk-(D-Pra), showing  $K_D \approx 500 \mu\text{M}$ . For fluorescence polarization experiments, the anchor ligand was labeled with FITC at the N-terminus. All samples contained  $6 \mu\text{M}$  FITC-anchor ligand and varying concentrations of bCAII (0.2 to  $800 \mu\text{M}$ ).

fitting the fluorescence polarization against the protein concentration, a value of  $K_D \approx 500 \mu\text{M}$  was extrapolated to describe the strength of the bCAII/anchor ligand interaction.

**Surface plasmon resonance.** The binding affinities of 1° ligands lklwfk-(D-Pra) and Az4-kfwlkl were also determined by SPR, and confirm the previous fluorescence polarization result. In SPR, real-time, label-free optical sensing of biomolecular binding events may be achieved through measurements of thickness (and refractive index) of films adsorbed on gold substrates.<sup>6</sup> A transducing medium is usually formed on the gold substrate film through surface-immobilized biomolecules (e.g., receptors). Changes in the refractive index of this transducing layer are induced by the binding of analyte to the biomolecule. Measurement in binding response over time yields sensorgrams which can be fitted for  $K_D$  and kinetics following a Langmuir binding isotherm.

In Figure 3.2, sensorgrams depict the interaction of surface-immobilized bCAII with increasing concentration (300 nM to  $\sim 10 \mu\text{M}$ ) of 1° ligands (A) lklwfk-(D-Pra) and (B) Az4-kfwlkl. The analyte responses were quite weak, demonstrating  $K_D > 10^{-5} \mu\text{M}$  binding affinities for both 1° ligands, and represent a limit for Biacore analysis. Since weak affinities are hard to quantify, this value is only an estimate.

### 3.3.2 Characterization of Biligand Affinities

Three candidate biligands were obtained by screening bCAII. One biligand (lklwfk-Tz1-kiwiG) is the result of an in situ click/OBOC screen between a comprehensive bead library of azides, anchor ligand lklwfk-(D-Pra), and bCAII. Two biligands (kwlwGl-Tz1-kfwlkl and kwiwGw-Tz1-kfwlkl) are the result of an on-bead

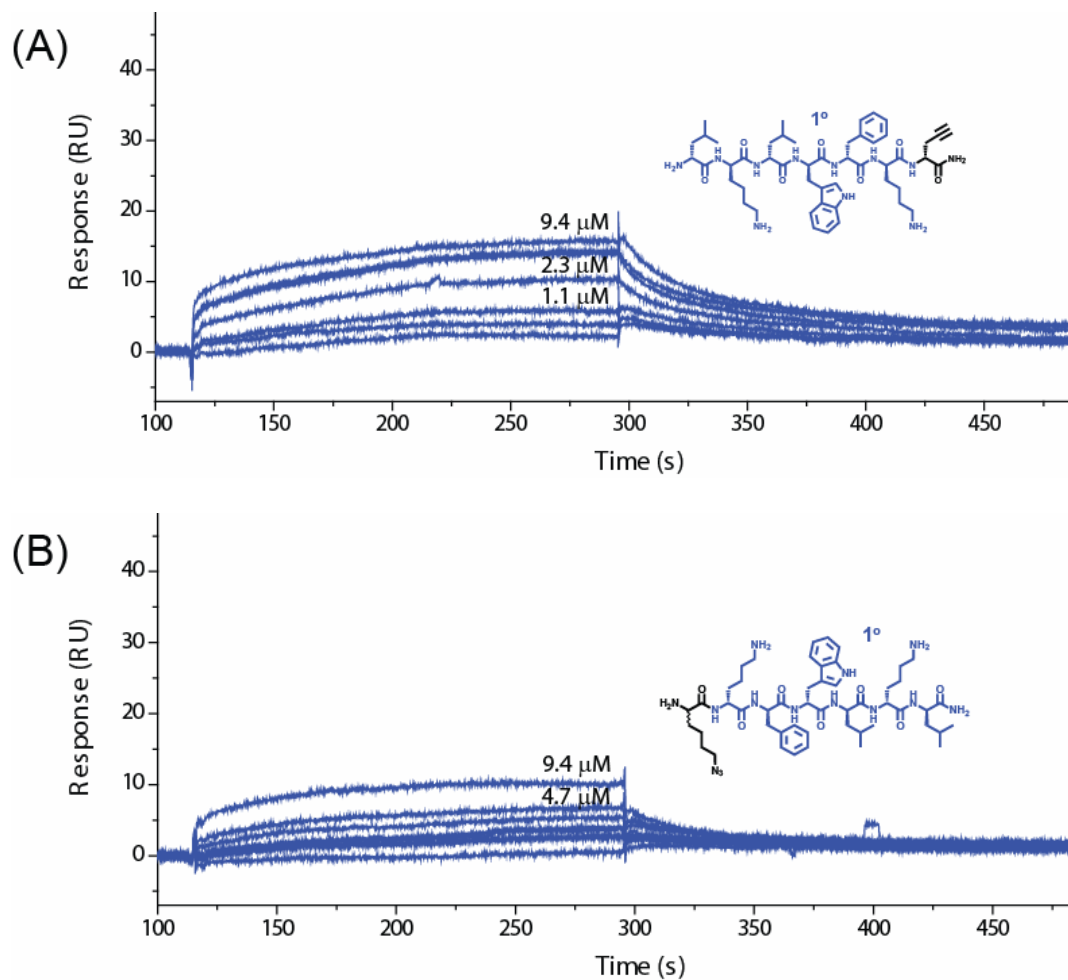


**Figure 3.2.** SPR response sensorgrams obtained with increasing concentration (300 nM to  $\sim 10 \mu\text{M}$ ) of 1° ligands (A) lklwfk-(D-Pra) and (B) Az4-kfwlkl demonstrate  $K_D > 10\text{-}\mu\text{M}$  binding affinities to immobilized bCAII.

CuAAC biligand library screen. These three biligands were synthesized in bulk, and their binding affinities for bCAII were measured using SPR.

The binding responses (Figure 3.3A-B) reveal  $K_D \approx 10^{-6}$  M affinity of two biligands toward bCAII. In particular, sensorgrams obtained with increasing concentration (2 nM to 5  $\mu$ M) of the biligands (A) kwlwG1-Tz1-kfwlkl and (B) lklwfk-Tz1-kiwiG demonstrate 3- $\mu$ M and 11- $\mu$ M binding affinities, respectively. This proves that the in situ click/OBOC screen, whose selected biligand is depicted in Figure 3.3B, and the on bead CuAAC biligand library screen, whose selected biligand is depicted in Figure 3.3A, converge on similar biligand sequences with similar affinities, further validating our selection approach. Furthermore, the SPR data for the best-binding biligand kwlwG1-Tz2-kfwlkl (Figure 3.3A), with an extrapolated affinity of  $K_D \approx 3$   $\mu$ M, represents a  $\sim$ 100-fold improvement over the binding affinity for 1<sup>o</sup> ligand interaction with the same protein.

In Figure 3.3C, SPR response sensorgrams for biligand kwiwGw-Tz1-kfwlkl are represented. These data were irregular and illustrated a significant amount of non-specific binding at high analyte concentrations (i.e., evidenced by RU exceeding  $R_{max}$  and high background binding on flow cell 1, data not shown). As this biligand sequence differs from the best-binding biligand of Figure 3.3A by only two residues (Res3: l $\rightarrow$ i and Res6: l $\rightarrow$ w), we have indirect evidence of the apparently high binding specificity of bCAII for only certain sequences.

In view of the above considerations, the biligand anchor (D-Pra)-kwlwG1-Tz1-kfwlkl was synthesized. The D-propargylglycine linker was installed at the N-terminus of the peptide, to minimize perturbation to the linear biligand sequence. In the presence

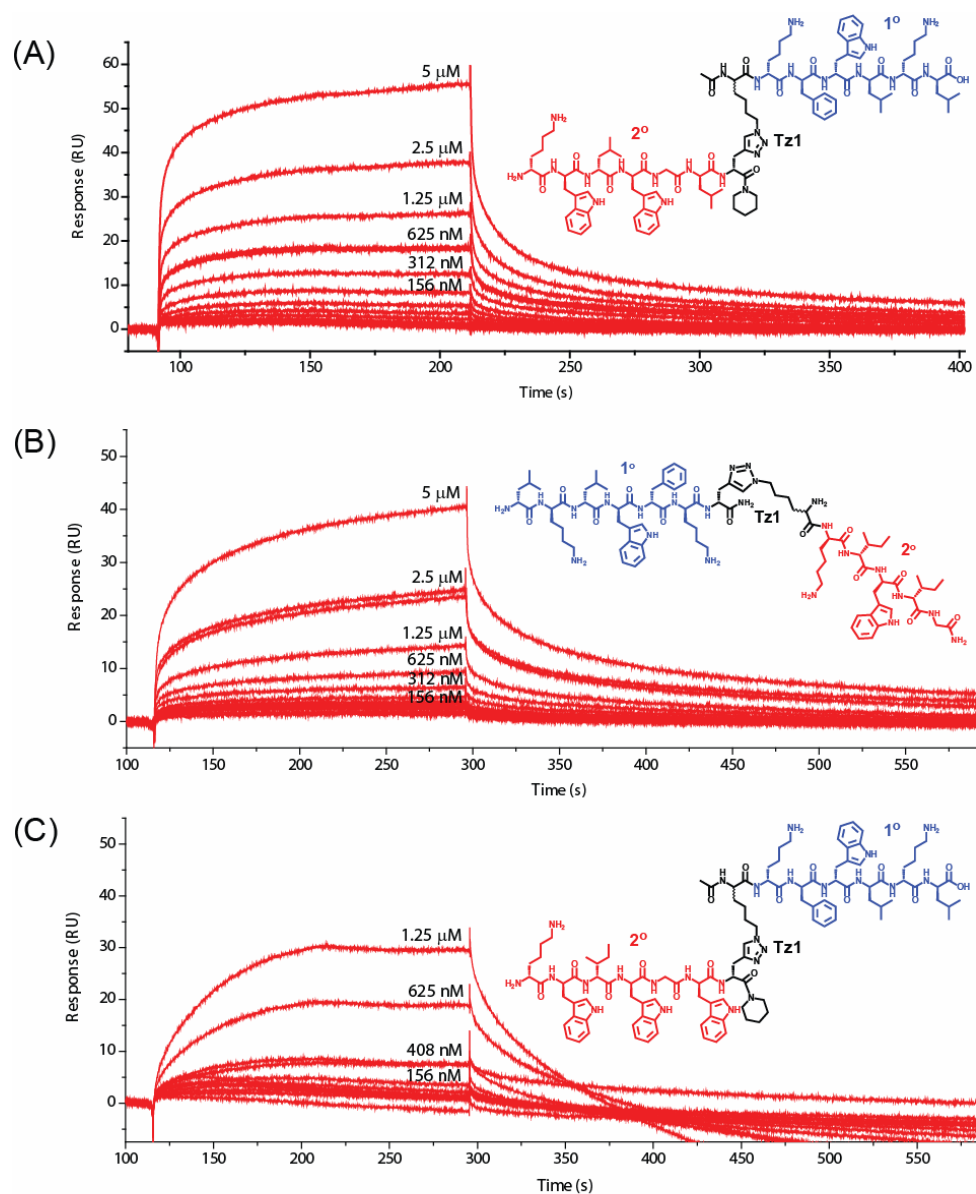


**Figure 3.3.** SPR response sensorgrams obtained with increasing concentration (2 nM to 5 μM) of the biligands (A) kwlwGI-Tz1-kfwlkl and (B) lklwfk-Tz1-kiwiG demonstrate 3-μM and 11-μM binding affinities, respectively, to immobilized bCAII. (C) Sensorgrams for biligand kwiwGw-Tz1-kfwlkl were irregular and illustrated a significant amount of non-specific binding.

of this new anchor unit, an in situ click/OBOC screen between bCAII and the same bead library of azides was performed to identify triligand candidates.

### 3.3.3 Characterization of Triligand Affinities

Only one candidate triligand was obtained by screening bCAII, because the sequence rfviln-Tz2-kwlwGl-Tz1-kfwlkl was repeated several times in both generations of in situ click/OBOC screen. This consensus triligand (Figure 3.4A) was synthesized in bulk and its binding affinity for both bCAII and hCAII was measured using SPR. The binding responses (Figure 3.4B-C) reveal  $K_D \approx 45$  nM (for hCAII) and  $K_D \approx 64$  nM (for bCAII). These equilibrium dissociation constants represent a 50-fold affinity enhancement compared to the interaction between biligand and target, and  $>10^3$ -fold affinity enhancement compared to the binding of 1° ligand and target (see Figures 3.1-3.3, for comparison).

### 3.3.4 Enzymatic Activity Assay of Carbonic Anhydrase II

**Nature of triligand binding to bCAII.** The active site of bCAII possesses an intrinsic esterase activity which can be monitored spectrophotometrically.<sup>4</sup> Specifically, bCAII catalyzes the hydrolysis of 4-nitrophenyl acetate (4-NPA) to 4-nitrophenol (4-NP), whose absorption can be monitored at 400 nm. The enzyme-catalyzed hydrolysis proceeds at a range of pH and serves as a test for active site binding by common inhibitors (Scheme 3.1). We utilized this assay to study the functional activity of bCAII as an esterase in the presence and absence of the triligand rfviln-Tz2-kwlwGl-Tz1-kfwlkl. The activity assay was performed to qualitatively assess the possibility of active site binding by the triligand.

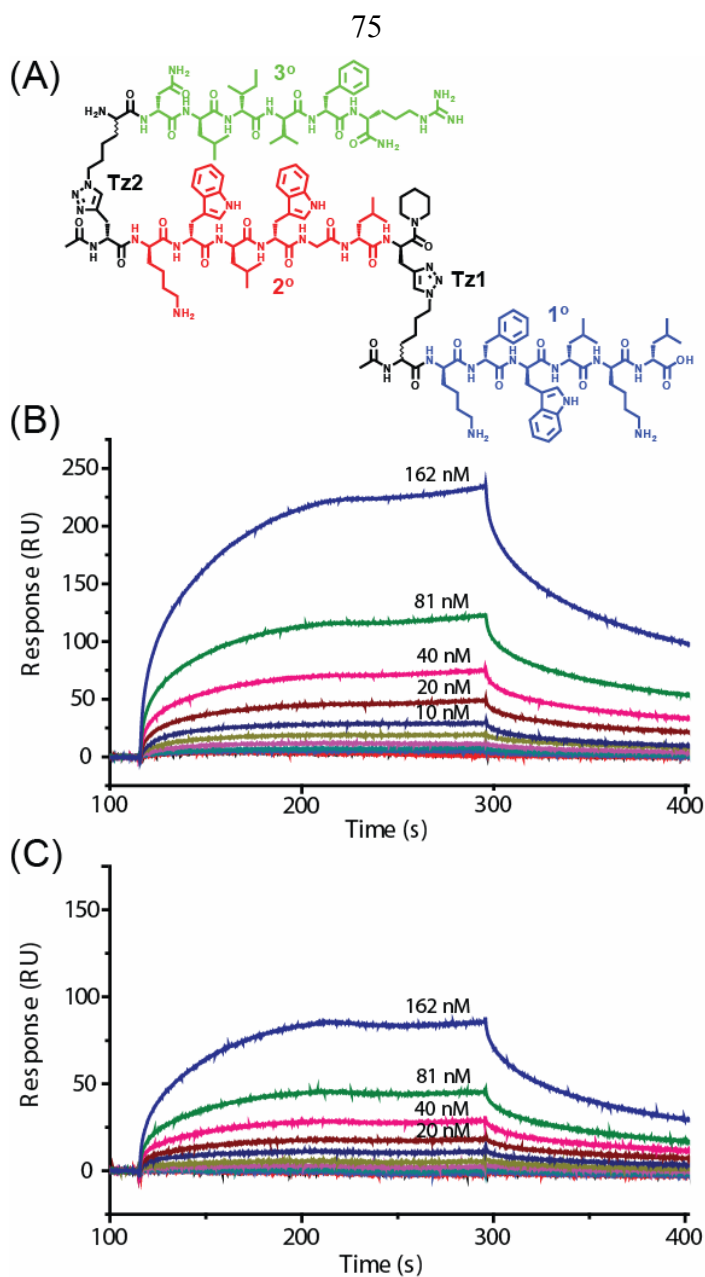
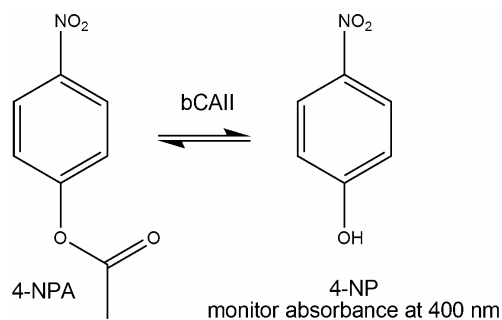


**Figure 3.4.** (A) Triligand capture agent, rfviln-Tz2-kwlwGI-Tz1-kfwlkl. SPR response sensorgrams with increasing peptide concentration (0.1 to 162 nM) characterize triligand binding to immobilized human (B) and bovine (C) CA II targets, respectively. Data analysis of this biomolecular interaction provided values of  $K_D \approx 45$  nM (hCAII) and  $K_D \approx 64$  nM (bCAII).



**Scheme 3.1.** Esterase activity of bCAII, using 4-NPA as the hydrolytic substrate.

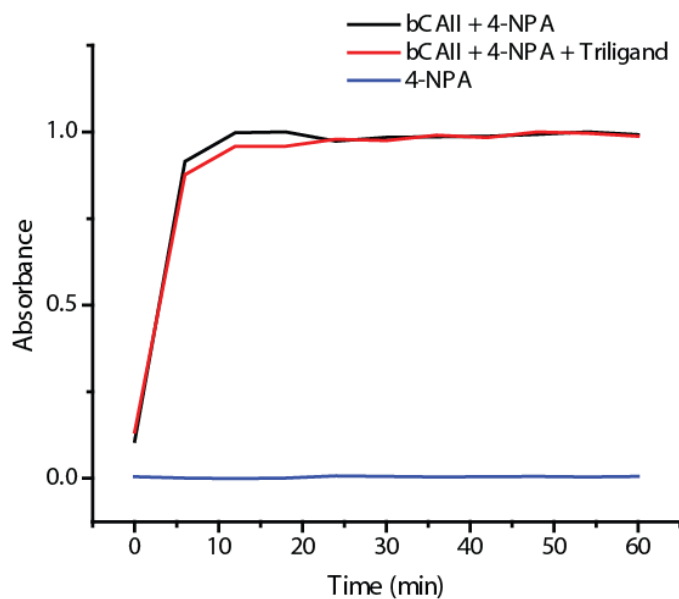


**Figure 3.5.** Enzymatic activity of bCAII in the presence of the triligand rfviln-Tz2-kwlwGl-Tz1-kfwkl. Absorbance data monitor the bCAII-catalyzed hydrolysis of 4-NPA to 4-NP ( $\epsilon = 18,400 \text{ M}^{-1}\text{cm}^{-1}$  at 400 nm) at the protein active site. Experiments were performed with (red) and without (black) capture agent. Additionally, an assay was performed in the presence of 4-NPA alone (blue) to determine the slow background hydrolysis of the ester in aqueous solution.  $[\text{bCAII}] = 1.4 \mu\text{M}$ ,  $[\text{Triligand}] = 5 \mu\text{M}$ , and  $[\text{4-NPA}] = 50 \mu\text{M}$  in Tris buffer [9 mM Tris-HCl, 81 mM NaCl, 9% acetonitrile (v/v), 1% DMSO (v/v)].

The experimental results are presented in Figure 3.5. Regardless of whether the assay contained triligand, there was an initial “burst” in 4-NP formation, followed by a slow increase in the product formation over the 60 min. Because there were no appreciable changes in the bCAII esterase activity when the triligand capture agent was included in the assay, apparently this peptide binds to an epitope distinct from the bCAII active site.

### 3.3.5 Circular Dichroism of Triligand

Circular dichroism (CD) measures the differential absorption of left- and right-handed circularly polarized light in solutions of optically active molecules such as peptides, proteins, and nucleic acids. For peptides and proteins, secondary structures such as  $\alpha$ -helix and  $\beta$ -sheet are easily resolved by CD. The signature peaks for an  $\alpha$ -helix and  $\beta$ -sheet can be found at 222 and 208 nm, respectively.<sup>7</sup>

The triligand rfviln-Tz2-kwlwGI-Tz1-kfwkl was characterized as a random coil by CD (Figure 3.6). The unfolded random coil structure may be a reflection that this oligopeptide was assembled linearly through successive protein-templated in situ click screens. Since the random coil is not one specific shape, but a statistical distribution of shapes, this conformation suggests the idea that, in the absence of specific, stabilizing interactions with the protein target, the oligopeptide will “sample” all possible conformations randomly.<sup>8</sup>

### 3.3.6 Dot Blot Specificity/Sensitivity Assays of Biligand and Triligand in Serum

Dot blots are a common method for detecting proteins. The sensitivity and

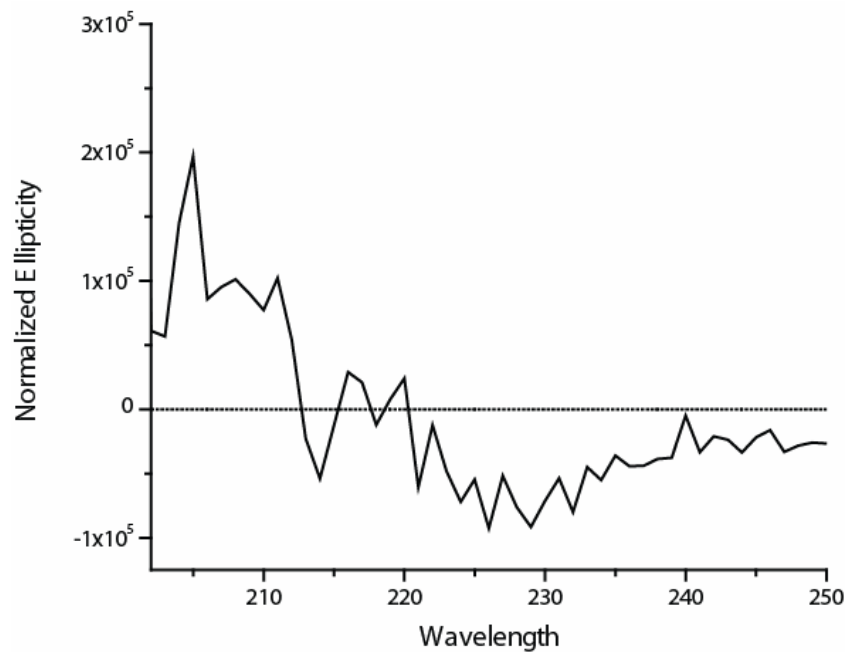


**Figure 3.6.** CD spectrum for triligand rfviln-Tz2-kwlwG1-Tz1-kfwlkl, acquired at  $15 \mu\text{M}$  in  $100 \text{ mM}$  Tris-HCl (pH 7.5). Lack of signature peaks at 222 nm (for  $\alpha$ -helix) and 208 nm (for  $\beta$ -sheet) indicates that the peptide structure is that of a random coil.

specificity of multi-ligand capture agents for detecting b(h)CAII in complex environments were demonstrated through the use of dot blot experiments in 10% porcine serum. For a dot blot, the solution containing the protein of interest is simply deposited onto an absorbent membrane material (typically nitrocellulose). The capture agent (typically an antibody, or one of the multi-ligands of Figure 3.7) is labeled with biotin, and then exposed to the entire nitrocellulose membrane. The membrane is washed to remove unbound material, and then horseradish peroxidase (HRP)-labeled streptavidin is added, attaching to the protein-bound biotin. Optical methods are typically utilized to detect this binding. Because we conducted dot blots experiments with the multi-ligand capture agent in dilute serum, both sensitivity and specificity may be addressed in a single assay.

Results for the dot blot to use the triligand (Figure 3.7A) and the biligand anchor (Figure 3.7B) to detect hCAII and bCAII from dilute porcine serum are shown in Figure 3.8. It is noted that bCAII and hCAII are >80% identical by sequence (PDB ID: 1CA2, 1V9E), and so both proteins were expected to be captured in this assay. The results of this assay illustrate ~20 ng b(h)CAII detection sensitivity by the triligand in 10% porcine serum, while ~0.2  $\mu$ g hCAII detection sensitivity is attained by the biligand anchor when the assay is performed under similar conditions. We reason that the sensitivity correlates with overall affinity of the capture agent, and so it is no surprise that the triligand is the more sensitive binder. Similarly, these results suggest that through the in situ click/OBOC screening method, we build specificity into our multi-ligands with each screening iteration.

We also wanted to directly compare binding specificity of the triligand (Figure 3.7A) against a commercially available antibody. Figure 3.9 shows the results of dot

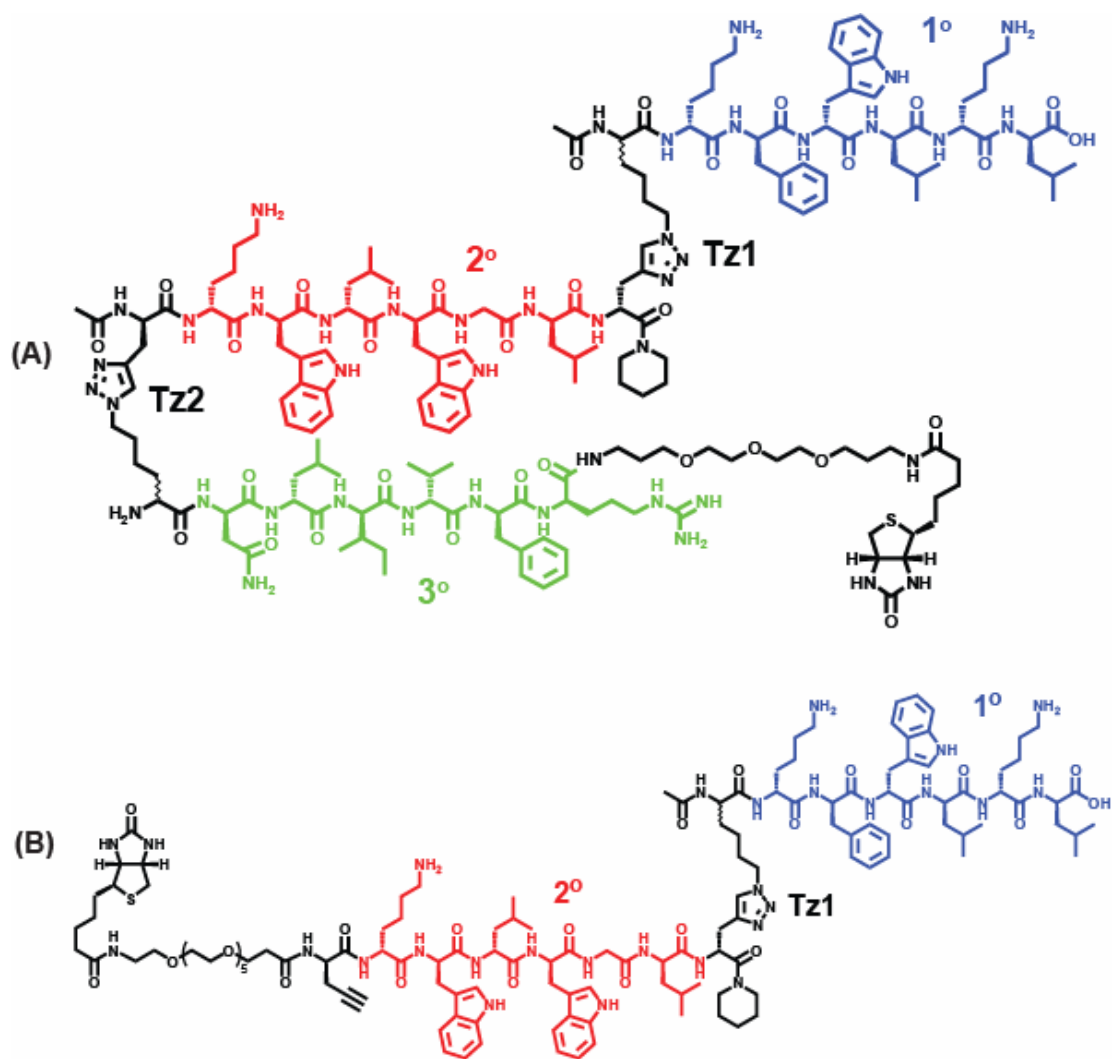


**Figure 3.7.** Biotin conjugates of the (A) triligand rfviln-Tz2-kwlwGl-Tz1-kfwlkl and (B) biligand anchor (D-Pra)-kwlwGl-Tz1-kfwlkl. These capture agents were implemented in dot blots, Western blots, and sandwich (ELISA-like) assays of bCAII.

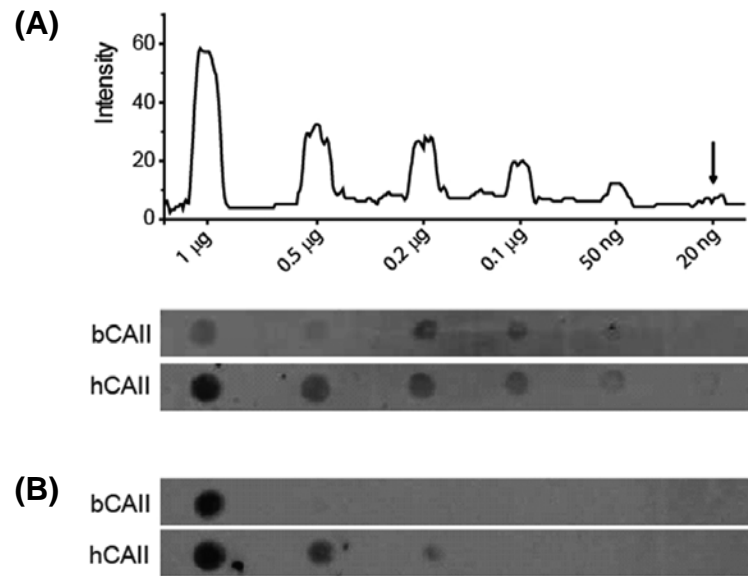


**Figure 3.8.** (A) Dot blot illustrating ~20 ng b(h)CAII detection sensitivity by the triligand of Figure 3.7A in 10% porcine serum. When the biligand anchor of Figure 3.7B is used as the primary capture agent in 0.1% serum (B), the sensitivity is reduced by more than 10-fold.

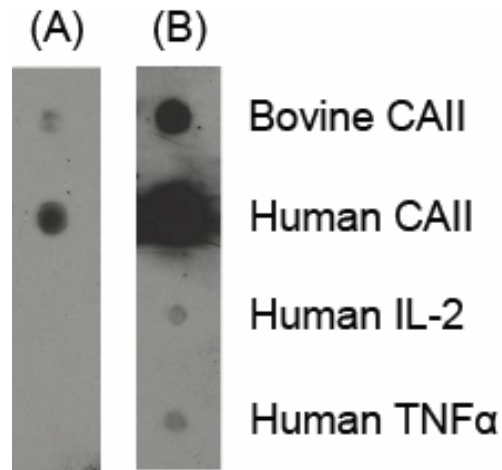


**Figure 3.9.** Results of dot blots performed in 0.5% milk/TBS where the (A) triligand of Figure 3.7A or (B) polyclonal anti-bCAII were utilized as the primary capture agent. (A) The triligand appears to be specific for CA II. (B) The polyclonal antibody displays an apparent cross-reactivity with unrelated proteins. Proteins = 2  $\mu$ g per spot.

blots performed in 0.5% milk/TBS where the (A) triligand (Figure 3.7A) or (B) polyclonal anti-bCAII were utilized as the primary capture agent. Besides bCAII and hCAII, two human secreted proteins interleukin-2 (IL-2) and TNF $\alpha$  were included in the protein panel. We also tested bovine serum albumin (BSA) as the spotted antigen in a separate blot, and neither triligand nor antibody displayed detectable cross-reactivity (data not shown). While the triligand displayed a high degree of specificity for CA II in the blot of Figure 3.9, the antibody showed an apparent cross-reactivity for the unrelated human proteins. This result is not surprising, as polyclonal antibodies generally sample diffuse epitopes. However, qualitative analysis of spot intensity suggests that the antibody is the more sensitive capture agent. From the results of Figures 3.8-3.9, we conclude that the triligand capture agent displays a comparable, or even better, specificity for b(h)CAII than the antibody, but the sensitivity remains to be optimized.

### **3.3.7 Western Blot Analysis Using Triligand**

The Western blot is another common method for detecting proteins. For the standard Western blot, proteins are subjected to denaturing gel electrophoresis and transfer to nitrocellulose. For the native Western blot, proteins are exposed to non-denaturing conditions for both electrophoresis and transfer. Antibody or multi-ligand capture agents are then used to interrogate the proteins on the nitrocellulose membrane. After specific binding of the capture agent to the target, a secondary detection agent is added to specifically bind to the capture agent. The secondary detection agent (e.g., streptavidin-HRP) often exhibits chemiluminescence which allows visualization of the results on film.

Demonstrations of Western blots to detect bCAII, with direct comparisons between the triligand (Figure 3.7A) and a commercial antibody, are shown in Figure 3.10. The denaturing Western blot of Figure 3.10A, utilizing polyclonal anti-bCAII as the primary capture agent, shows ~50 ng bCAII detection sensitivity. Curiously, on the same gel (Figure 3.10B), bCAII was not detected by the triligand. This result suggests that the triligand capture agent recognizes a 3-D protein epitope that is destroyed when the protein is subjected to denaturing conditions.

To test this hypothesis, native Western blots were performed under similar, but non-denaturing, conditions. We also took this opportunity to interrogate specificity by utilizing the antibody and triligand capture agents as probes against bCAII spiked in dilute serum. The native gel of Figure 3.10C details the electrophoresed bCAII and serum proteins. When this native gel was transferred and probed with polyclonal anti-bCAII (Figure 3.10D), bCAII and a serum protein (MW  $\approx$  30-35 kDa) are detected. We hypothesize that this upper band may be one of the related isozymes CA I or CA III, which show 58%-60% identity with each other and with CA II in amino acids at similar positions.<sup>9</sup> Furthermore, CA I is five to six times as abundant as CA II in erythrocytes.<sup>9</sup> When the same native blot is probed with the triligand of Figure 3.7A (Figure 3.10E), only bCAII is detected, illustrating triligand specificity for native bCAII epitopes. Even in the presence of serum, native Western analysis suggests that the triligand is potentially more specific than the commercial anti-bCAII antibody, and this result confirms our previous dot blot analysis.

It should be noted that the detection sensitivity for the triligand in the native Western blot is not as high as in the dot blot (1  $\mu$ g vs. 20 ng bCAII). Under non-denaturing conditions, the gel transfer step requires high voltage and is still inefficient,

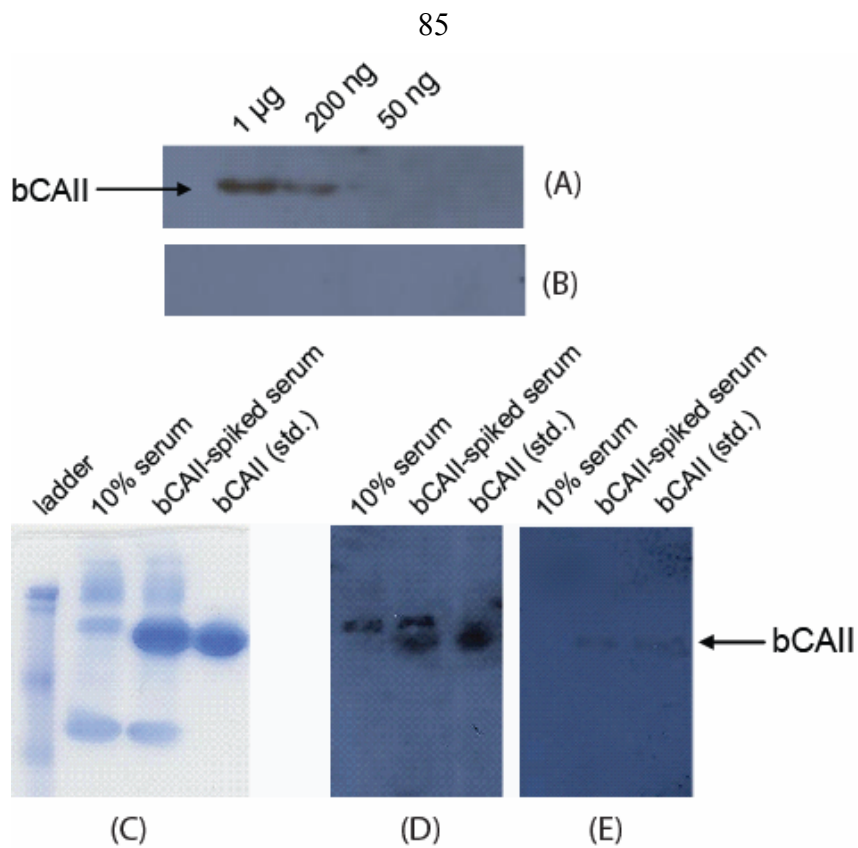


**Figure 3.10.** Results of Western blots performed under denaturing (**A**, **B**) and non-denaturing conditions (**C**, **D**, **E**). (**A**) The denaturing Western blot, utilizing polyclonal anti-bCAII as the primary capture agent, shows ~50 ng bCAII detection sensitivity. (**B**) On the same gel, bCAII was not detected by the triligand of Figure 3.7A. (**C**) The native PAGE gel was stained with Coomassie, and details total protein content. (**D**) When this native gel is transferred and probed with polyclonal anti-bCAII, bCAII and a serum protein (MW  $\approx$  30-35 kDa) are detected. (**E**) When the same native blot is probed with the triligand of Figure 3.7A, only bCAII is detected, illustrating triligand specificity for native bCAII epitopes. bCAII loading (**C**, **D**, **E**) = 1  $\mu$ g per lane.

as the proteins are only natively charged. The poor transfer leads to the perceived reduction in sensitivity by the triligand in the native Western blot.

### **3.3.8 Sandwich (ELISA-like) Assays Using Triligand**

The sandwich assay is a third common method for detecting proteins. Sandwich assays typically rely on two antibodies, a primary capture antibody (1°) and a labeled detection antibody (2° antibody), for detecting the protein of interest. In a typical ELISA sandwich assay, the 1° antibody is typically coated onto a surface, such as the surface of a well within a 96-well plate. A solution (e.g., serum, urine, etc.) expected to contain a particular target protein is added to the well. The target protein is then allowed to diffuse to the surface where it is captured by the 1° antibody. The 2° antibody is then added to the same well. This antibody is designed to bind to an orthogonal binding site, or epitope, of the target protein. Furthermore, this 2° antibody is labeled in a way that allows for the antibody/protein/antibody sandwich to be detected optically or by some other means.

For optical detection, the label is often an optically absorbent chromophore or a fluorescent dye molecule, and that label is often attached to the 2° antibody directly. The label is then detected by absorbance or fluorescence, and the signal intensity is proportional to the amount of protein captured in the assay. Alternatively, the 2° antibody may be conjugated to biotin, and in that case, a labeled protein (e.g., streptavidin-HRP) is added subsequently to visualize the biotin. Other methods are possible, such as utilizing a gold nanoparticle as a label instead of the fluorescent or optically absorbent molecule, or using a radioactive molecule as the label, where the final detection is completed using a scintillation counter or appropriately sensitized film.

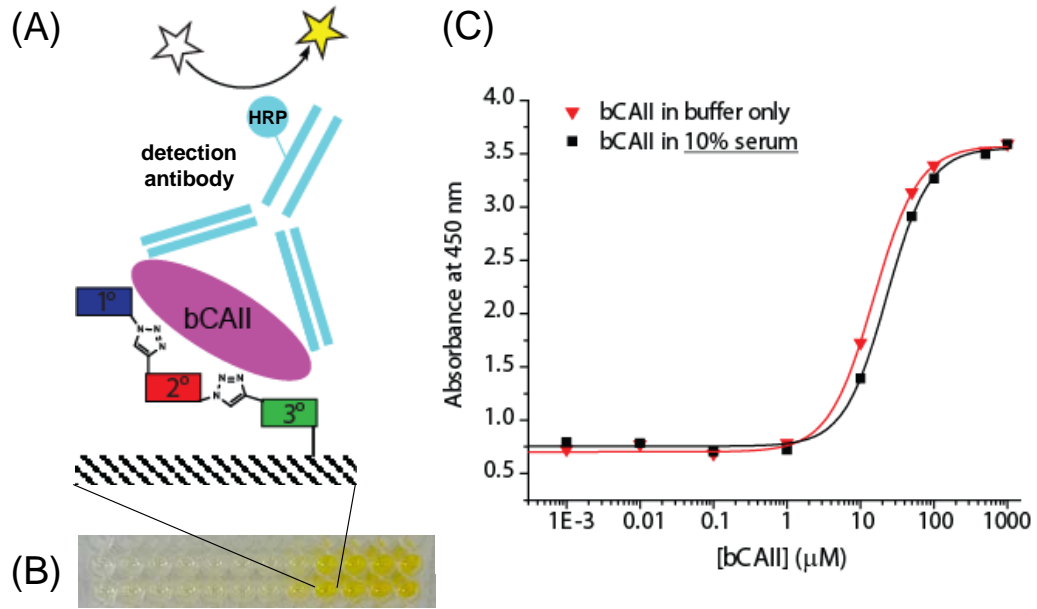


**Figure 3.11.** (A) Schematic illustration of the structure of fully assembled ELISA-like sandwich absorbance assays using the triligand of Figure 3.7A to detect bCAII protein. (B) Experimental data of ELISA assays at varying concentrations of bCAII as performed in the wells of a 96-well plate. Increasing bCAII concentration is detected as an increasing yellow color. (C) Diagrams illustrating two assay conditions. The target is presented in 0.5% milk/TBS (red curve) or in 10% porcine serum (black curve) to yield a sandwich assay with an analytical sensitivity of  $\sim 10 \mu\text{M}$  ( $\sim 300 \mu\text{g/mL}$ ).

Demonstration of sandwich-type ELISA assays on streptavidin-functionalized microtiter plates to detect bCAII using a combined commercial antibody (2° capture agent) and triligand of Figure 3.7A (as the 1° capture agent) is shown in Figure 3.11. Two assay conditions were used to compare the detection sensitivity for bCAII in buffered solution vs. a background of dilute serum (Figure 3.11C). For the sandwich assay performed with bCAII presented in 0.5% milk/TBS (red curve), the analytical sensitivity is  $\sim 10 \mu\text{M}$  ( $\sim 300 \mu\text{g/mL}$ ). This result is similar to the sandwich assay performed with bCAII presented in dilute serum (black curve), which further illustrates the utility of multi-ligand capture agents in standard assays of protein detection.

Our triligand sandwich (ELISA-like) assay, however, does not yet approach the analytical sensitivity expected for most commercial sandwich assays ( $\sim 1 \text{ pg/mL}$ ). There are several areas for optimization of the Figure 3.11 assay. First, it is possible that the triligand of Figure 3.7A and the commercial polyclonal anti-bCAII (HRP conjugate) are not an optimized reagent pair. We did not test whether these two capture agents compete for similar (or the same) binding epitopes on bCAII before performing the sandwich assay. Competition of this kind would translate to reduced sensitivity. Second, our sandwich assay was an absorbance assay using TMB (3,3',5,5'-tetramethylbenzidine) as the chromophore to visualize bound proteins. Absorbance ELISAs are not nearly as sensitive as fluorescence ELISAs. It has been reported that a five- to six-fold enhancement in signal-to-noise ratio at a given analyte concentration and a two- to five-fold enhancement in sensitivity, as reflected by relative limits of detection, may be achieved with fluorogenic substrates.<sup>10</sup> Third, the background absorbance is high (0.6 Abs units), potentially masking sensitivity for the lower bCAII concentrations. This background may be caused by insufficient washing during the assay, or possibly use of

too much polyclonal anti-bCAII (HRP conjugate). Polyclonal antibodies display a higher risk of cross-reactivity since their epitopes are less precisely defined, and so there may have been some background binding to the serum- or milk-based proteins present in our assay.

### 3.4 CONCLUSIONS

As a companion to Chapter 2, this chapter focused on the properties and results of using multi-ligand capture agents in standard assays of protein detection. Measurements by fluorescence polarization and SPR served as direct evidence of the kind of affinity enhancement that one can achieve through multivalent binding interactions. Starting from lklwfk-(D-Pra) ( $K_D \approx 500 \mu\text{M}$ ) as the anchor ( $1^\circ$ ) ligand, moderate affinity biligands such as kwlwGl-Tz1-kfwlkl ( $K_D \approx 3 \mu\text{M}$ ) were assembled by in situ click chemistry and represent a  $\sim 100$ -fold affinity improvement. Using biligand (D-Pra)-kwlwGl-Tz1-kfwlkl as the new anchor unit, a triligand capture agent (rfviln-Tz2-kwlwGl-Tz1-kfwlkl,  $K_D \approx 50 \text{ nM}$ ) was isolated by in situ click/OBOC selection and represents a 50-fold affinity enhancement compared to the interaction between biligand and target, and a  $>10^3$ -fold overall affinity enhancement compared to the binding of  $1^\circ$  ligand and target. Interestingly, this triligand does not bind the active site of bCAII, but rather to a separate generalized epitope, and apparently the random coil structure of this peptide may become stabilized by specific binding with the target.

Protein capture agents should exhibit both an affinity for their cognate protein, as well as a specificity for detecting that protein in complex environments. Multi-ligands show initial efficacy as capture agents in standard assays including dot blot, Western blot, and sandwich (ELISA-like) assay. The triligand was found to detect  $\geq 20 \text{ ng CA II}$

in porcine serum as illustrated by dot blot. The triligand was also found to detect  $\geq 1 \mu\text{g}$  CA II from porcine serum in a non-optimized native Western blot. Curiously, the triligand only recognizes a 3-D (native) protein epitope which argues for the exquisite nature of the in situ click/OBOC discovery process. Non-optimized sandwich (ELISA-like) absorbance assays using the triligand for bCAII capture and a polyclonal anti-bCAII for detection yield an analytical sensitivity of  $\sim 10 \mu\text{M}$  ( $\sim 300 \mu\text{g/mL}$ ). These feasibility demonstrations show great promise toward the routine implementation of protein capture agents in basic research and as medical diagnostic tools.

### **3.5 ACKNOWLEDGEMENTS**

This work was completed in collaboration with Rosemary D. Rohde, Steven W. Millward, Arundhati Nag, Wook-Seok Yeo, Jason E. Hein, Suresh M. Pitram, Abdul Ahad Tariq, Vanessa M. Burns, Russell J. Krom, Valery V. Fokin, and K. Barry Sharpless.

**3.6 REFERENCES**

1. Yin, H.; Litvinov, R. I.; Vilaire, G.; Zhu, H.; Li, W.; Caputo, G. A.; Moore, D. T.; Lear, J. D.; Weisel, J. W.; DeGrado, W. F.; Bennett, J. S. *J. Biol. Chem.* **2006**, *281*, 36732–36741.
2. Papalia, G. A.; Leavitt, S.; Bynum, M. A.; Katsamba, P. S.; Wilton, R.; Qiu, H.; Steukers, M.; Wang, S.; Bindu, L.; Phogat, S.; Giannetti, A. M.; Ryan, T. E.; Pudlak, V. A.; Matusiewicz, K.; Michelson, K. M.; Nowakowski, A.; Pham-Baginski, A.; Brooks, J.; Tieman, B. C.; Bruce, B. D.; Vaughn, M.; Baksh, M.; Cho, Y. H.; De Wit, M.; Smets, A.; Vandersmissen, J.; Michiels, L.; Myszka, D. *G. Anal. Biochem.* **2006**, *359*, 94–105.
3. Svedhem, S.; Enander, K.; Karlsson, M.; Sjöbom, H.; Liedberg, B.; Löfås, S.; Mårtensson, L.-G.; Sjöstrand, S. E.; Svensson, S.; Carlsson, U.; Lundström, I. *Anal. Biochem.* **2001**, *296*, 188–196.
4. Pocker, Y.; Stone, J. T. *Biochemistry* **1967**, *6*, 668–678.
5. Nasir, M. S.; Jolley, M. E. *Comb. Chem. High Throughput Screen* **1999**, *2*, 177–190.
6. Homola, J.; Yee, S. S.; Gauglitz, G. *Sens. Actuators, B* **1999**, *54*, 3–15.
7. Jasnoff, A.; Fersht, A. *Biochemistry* **1994**, *33*, 2129–2135.
8. Gokce, I.; Woody, R. W.; Anderluh, G.; Lakey, J. H. *J. Am. Chem. Soc.* **2005**, *127*, 9700–9701.
9. Sly, W. S.; Hu, P. Y. *Annu. Rev. Biochem.* **1995**, *64*, 375–401.
10. Meng, Y.; High, K.; Antonello, J.; Washabaugh, M. W. Zhao, Q. *Anal. Biochem.* **2005**, *345*, 227–236.

## **Chapter 4**

### Assays for Quantifying Protein-Catalyzed Multi-ligands and Extensions to Other Proteins

## 4.1 INTRODUCTION

Protein-templated in situ click chemistry is a low-yielding reaction, as it requires precise alignment of the azide and alkyne with respect to each other and the protein. Therefore, only a small fraction ( $\ll 1\%$ ) of the peptides on a particular bead will be converted to multi-ligands. Previously in Chapters 2 and 3, I discussed the discovery of a triligand capture agent, possessing antibody-like attributes, for the model protein, bCAII. We initially validated the in situ click assembly by analysis of sequence homology and binary component screens (monitored by MALDI-MS). However, challenges remained in developing direct, quantitative assays to assess the yield of multi-ligand capture agent following the in situ click/OBOC screen. Such quantitative assays define the signal-to-noise ratio for the in situ click/OBOC selection, since background chemical processes can also contribute to “false” hits. In this chapter, we will explore different assays for detecting on-bead, protein-templated triligand, such as colorimetric and quantitative polymerase chain reaction (QPCR) assays. The low but detectable yield per protein-catalyzed in situ click reaction—approximately 0.000005% for bCAII—confirms the exquisite demands of the process, and also provides guidance for the types of methods that can improve the signal-to-noise ratio for the in situ click/OBOC screening process.

This result encouraged us to develop more sophisticated screening strategies for improving signal-to-noise ratio during in situ click/OBOC screens. Such strategies incorporated anti-selections (following the selections) so as to remove hits that resulted from potential side reactions. The strategies also included the direct detection of the bead-bound products of the protein-catalyzed click reaction. Such product-based screens provide information that is highly complementary to that obtained from screens in which

hits are identified according to the presence of the target (i.e., the fluorescently labeled protein) on bead. These strategies were able to take advantage of the modular construction of the multi-ligand capture agents. As one example, by site-specific labeling the anchor (1°) ligand with biotin, we have a label that permits the direct monitoring of the in situ click reaction between 1° ligand and bead-bound 2° ligands. The use of this label is described in some detail within this chapter. In a second example, through the use of a labeled antibody, we can probe for bead-bound proteins during an in situ click/OBOC screen. These new screening strategies were applied toward the in situ click/OBOC selection of a biligand capture agent ( $K_D \approx 140$  nM) against the blood-based protein biomarker prostate-specific antigen (PSA). The rapid assembly of the biligand capture agent by the protein-catalyzed process was expedited to two weeks by utilization of a previously reported anchor ligand<sup>1</sup> and the new selection/anti-selection strategies, and demonstrates the feasibility of a high-throughput route toward production of high-affinity, high-specificity protein capture agents.

## **4.2 MATERIALS AND EXPERIMENTAL METHODS**

### **4.2.1 Materials**

**Proteins.** Bovine and human carbonic anhydrase II (bCAII, C2522; hCAII, C6165), from erythrocytes, lyophilized powder, were obtained (Sigma-Aldrich; St. Louis, MO) and used as received. Human transferrin (Tf) and bovine serum albumin (BSA,  $\geq 98\%$ ) were also purchased from Sigma-Aldrich as lyophilized powders. Prostate-specific antigen (PSA) was isolated by Scripps Laboratories (San Diego, CA) and shipped as a lyophilized powder. PSA activity was confirmed by an optical assay

employing the chymotrypsin substrate Suc-Arg-Pro-Tyr-pNA (AnaSpec, San Jose, CA; pNA = p-nitroaniline) as a chromogenic substrate.

#### 4.2.2 On-Bead Detection of In Situ Triazole Formation

A biotin conjugate of the biligand anchor was prepared by modifying the N-terminus with an ethylene glycol linker (Fmoc-NH-(PEG)<sub>5</sub>-COOH, EMD Biosciences) followed by biotin, by standard SPPS. A stock solution of this biotinylated biligand anchor Biotin-(EG)<sub>5</sub>-(D-Pra)-kwlwGI-Tz1-kfwlkl (1.25 mM, alkyne) was prepared in DMSO (EG = ethylene glycol). Stock solutions of bCAII (30 μM) and hCAII (30 μM) were prepared in 50 mM Tris-Cl buffer (pH 7.2). For control experiments, stock solutions of human transferrin (Tf, 30 μM) and bovine serum albumin (BSA, 30 μM) were prepared in 50 mM Tris-Cl buffer (pH 7.2), and Biotin-RPRAAA-Pra (1.25 mM, alkyne with no documented affinity for CA II) was prepared in DMSO. The consensus 3° ligand Az4-nlivfr (azide) was synthesized in bulk on TentaGel S-NH<sub>2</sub> beads. Each in situ click reaction contained 0.5 mg beads appended with 3° ligand, 30 μM biotinylated peptide-alkyne, and 15 μM protein in a final volume of 50 μL 50 mM Tris-Cl buffer (pH 7.2) + 2.5% DMSO (v/v). In situ click reactions proceeded for 24 h at 25 °C with shaking. Reactions were quenched with 50 μL 7.5 M guanidine hydrochloride (GuHCl, pH 2.0). Following incubation with GuHCl (pH 2.0) for 1 h, the beads were washed with 10 × 200 μL water, leaving only covalently bound peptides (3° ligand and biotinylated in situ triligand) on the bead.

To prepare for the enzyme-linked, colorimetric assay,<sup>2</sup> beads were washed with 3 × 100 μL Blocking Buffer (25 mM Tris-Cl, 10 mM MgCl<sub>2</sub>, 150 mM NaCl, 14 mM 2-mercaptoethanol, 0.1% (w/v) BSA, 0.1% (v/v) Tween 20, pH 7.5). Beads were then

incubated in Blocking Buffer for 1 h with shaking. Alkaline phosphatase-streptavidin (AP-SA, Promega) was introduced at 1:300 dilution in Blocking Buffer to bind to any potential bead-bound biotinylated triligand. This AP-SA solution was incubated for 1 h with shaking. Excess AP-SA was then removed by washing the beads with  $3 \times 300 \mu\text{L}$  Wash 1 Buffer (25 mM Tris-Cl, 10 mM  $\text{MgCl}_2$ , 150 mM NaCl, 14 mM 2-mercaptoethanol, pH 7.5), followed by  $2 \times 250 \mu\text{L}$  Wash 2 Buffer (25 mM Tris-Cl, 14 mM 2-mercaptoethanol, pH 7.5). Beads were developed for 2 h in  $50 \mu\text{L}$  of the chromogenic substrate BCIP (5-bromo-4-chloro-3-indoyl phosphate, Promega).

#### **4.2.3 QPCR Assay for the Detection and Quantitation of the Formation of On-Bead, Protein-Catalyzed Triligand Capture Agent**

The Streptavidin-oligo reagent was prepared as described below: SAC expression was performed according to previously published protocols.<sup>3</sup> Prior to use, stock SAC (streptavidin-cysteine) was buffer exchanged to Tris buffered saline (TBS) containing 5 mM Tris(2-carboxyethyl) phosphine hydrochloride (TCEP) using desalting columns (Pierce). MHPH (3-N-Maleimido-6-hydraziniumpyridine hydrochloride, Solulink) in DMF was added to SAC at a molar excess of 300:1. In parallel, SFB in DMF (succinimidyl 4-formylbenzoate, Solulink) was added in a 40:1 molar excess to the 5' aminated oligo. The mixtures were allowed to react at room temperature for 3 to 4 h. Excess MHPH and SFB were removed and samples were buffer exchanged to citrate buffer (50 mM sodium citrate, 150 mM NaCl, pH 6.0) using Zeba desalting spin columns (Pierce). The SFB-labeled oligo was then combined in a 20:1 molar excess with the derivatized SAC and allowed to react for 2 to 3 h at room temperature before transferring to overnight incubation at 4 °C. Unreacted oligos were removed using a

Pharmacia Superdex 200 gel filtration column at 0.5 mL/min isocratic flow of PBS. Fractions containing the SAC-oligo conjugates were concentrated using 10K MWCO concentration filters (Millipore). The synthesis of SAC-oligo constructs was verified by non-reducing 8% Tris-HCl SDS-PAGE.

The triligand-containing beads were prepared as described in Section 4.2.2. After dissociation of the target, 0.5 mg beads were washed 10 times in water and resuspended in Blocking Buffer (0.15% BSA (w/v), 0.1% Tween-20, 150  $\mu$ g/mL sheared salmon sperm DNA, in PBS pH 7.4). The beads were washed with  $3 \times 100 \mu$ L Blocking Buffer and incubated for 1 h at 25 °C in 100  $\mu$ L Blocking Buffer. The beads were then filtered and washed twice more in 100  $\mu$ L Blocking Buffer. Streptavidin-oligo (100  $\mu$ L of 170 ng/mL dilution prepared in Blocking Buffer) was added and the beads were incubated for 1 h at 25 °C. The beads were washed 5 times in 250  $\mu$ L Blocking Buffer followed by 3 washes in 250  $\mu$ L PBS. The beads were resuspended in dH<sub>2</sub>O and spotted on a glass slide. After evaporation, the beads were manually picked and placed in thin-walled PCR tubes.

Quantitative PCR (QPCR) was carried out on a Bio-Rad Real-Time PCR system. To each tube containing 1 to 5 individual beads was added 12.5  $\mu$ L iQ SYBR Green Supermix (Bio-Rad), 11.5  $\mu$ L dH<sub>2</sub>O, 100 nM Forward Primer (5'...TAATACGACTCACTATAGGGACAATTACTATTTACAATTACA...3' –SEQ ID NO: 2), and 100 nM Reverse Primer (5'...ACCGCTGCCAGACCCCGATTGGCCTGGGAGACGAACTCG...3' –SEQ ID NO: 3). Real-time PCR was carried out for 30 cycles with the following thermal profile: 94 °C, 30 s, 50 °C, 45 s, 72 °C, 60 s. A standard curve was generated using known template concentrations ranging from 0.01 nM to 0.01 pM. The Ct values for each of the known concentrations were plotted

against the log of the template concentration to generate a linear standard curve which was then used to determine the concentration of oligo in each of the sample tubes. This was adjusted based on the number of oligonucleotide templates present per streptavidin tetramer as estimated by SDS-PAGE.

#### **4.2.4 Selection of Biligand Capture Agent for Prostate-Specific Antigen**

**Two-stage in situ click/OBOC screen with biotinylated cyclic anchor.** The comprehensive 5-mer Library X, displaying an N-terminal azidoalkyl amino acid, is first blocked overnight (0.2 g TentaGel scale) at 25 °C in Blocking Buffer (25 mM Tris-Cl, 10 mM MgCl<sub>2</sub>, 150 mM NaCl, 0.1% (w/v) BSA, 0.1% (v/v) Tween 20, pH 7.5). Then, 5 to 40 nM PSA is prepared with 2.5 μM biotin-labeled cyclic anchor (Biotin-(EG)<sub>5</sub>-Pra-cy(CVFAHNYDYLVLC), Figure 4.7A) in 1 to 3 mL Blocking Buffer. The protein and cyclic anchor were allowed to incubate for 1 h at 25 °C. This solution was subsequently combined with the blocked portion of Library X. After screening for 1 h at 25 °C, the library/PSA complex was washed with 5 × 3 mL Blocking Buffer to remove excess target and then incubated with a primary antibody for 1 h at 25 °C [mouse monoclonal anti-PSA, clone PS2 or PS6 (#M86433M or #M86111M, Meridian Life Science, Saco, ME)]. Primary antibodies were prepared at 1:5000 to 1:50,000 dilution in Blocking Buffer. Beads were then washed with 5 × 3 mL Blocking Buffer to remove excess primary antibody, and then incubated with a secondary antibody [anti-mouse IgG, alkaline phosphatase (AP)-conjugated, at 1:5000 dilution in Blocking Buffer; Cell Signaling] in Blocking Buffer for 30 min at 25 °C. Excess secondary antibody was removed by washing the beads with 5 × 3 mL Blocking Buffer, followed by 5 × 3 mL Wash 1 Buffer (25 mM Tris-Cl, 10 mM MgCl<sub>2</sub>, 700 mM NaCl, pH 7.5), and last by

5 × 3 mL Wash 2 Buffer (25 mM Tris-Cl, pH 7.5). Beads were developed for 30 to 90 min in the chromogenic substrate BCIP:NBT (Promega, #S3771), freshly prepared in Alkaline Phosphatase Buffer [100 mM Tris-HCl (pH 9.0), 150 mM NaCl, 1 mM MgCl<sub>2</sub>], as recommended by the vendor. The darkest purple beads (“initial hits”) are selected by micropipette, washed with 7.5 M guanidine hydrochloride (GuHCl pH 2.0) for 1 h to remove bound protein, then with 10 × 500 μL water. Beads are then decolorized overnight by incubation in DMF. After the purple dye has completely dissociated from the beads, the initial hits are re-swollen for at least 12 h in Blocking Buffer before moving on to the next step.

The second screen for direct detection of on-bead protein-templated biligand is achieved by incubating the initial hits with AP-SA (Promega) at 1:300 dilution in Blocking Buffer for 45 min at 25 °C. Excess AP-SA is removed by washing the beads with 5 × 3 mL Blocking Buffer, followed by 5 × 3 mL Wash 1 Buffer (25 mM Tris-Cl, 10 mM MgCl<sub>2</sub>, 700 mM NaCl, pH 7.5), and last by 5 × 3 mL Wash 2 Buffer (25 mM Tris-Cl, pH 7.5). Beads are developed for 30 to 90 min in the chromogenic substrate BCIP:NBT as described above. The darkest purple beads (“true hits”) are selected by micropipette, washed with 7.5 M GuHCl (pH 2.0) for 1 h to remove bound protein, then with 10 × 500 μL water. Following this wash, the purple hit beads are analyzed directly by Edman degradation, and the sequences of the candidate 2° ligands are determined.

**Synthesis of cyclic biligand candidates.** Click reactions were performed in solution between cyclic anchor and 2° ligand. To begin, HPLC-purified cyclic anchor Biotin-(EG)<sub>5</sub>-Pra-cy(CVFAHNYDYLVLC) (EG = ethylene glycol, cy = denotes cyclized sequence) was dissolved in DMF to make a stock of 15 to 30 mM. Similarly, HPLC-

purified 2° ligands (Az8-iiydt, Az8-kyydt, and Az8-iyiet) were each dissolved in DMF to make a stock of 15 to 30 mM. In 200  $\mu$ L of 4:1 DMF:H<sub>2</sub>O, the in-solution reaction was set up with the following final concentrations: 2 mM Cyclic anchor, 3 mM 2° ligand, 3 mM CuI, 10 mM Ascorbic acid, 10 mM TBTA [Tris-(benzyltriazolylmethyl)amine]. TBTA is a ligand which accelerates catalysis while simultaneously protecting and stabilizing the copper(I) from oxidation, thus further improving the efficiency of the CuAAC.<sup>4</sup> After overnight reaction at 25 °C, the entire crude mixture was loaded onto the HPLC, and cyclic biligands were isolated at approximately 30% B (where A = H<sub>2</sub>O/0.1% TFA and B = ACN/0.1% TFA). Non-optimized yield was >25%.

It should be noted that the protein-templated in situ click reaction may yield product regioisomers that are either *anti* (1,4), *syn* (1,5), or a mixture of the two geometries. Although we have not yet determined which regioisomers of the in situ click products were formed, the authentic multi-ligands synthesized by CuAAC were definitely the 1,4-triazole [Tz1 = triazole formed between Pra (appended from the cyclic anchor) and Az8 (on the 2° ligand)]. After bulk synthesis, cyclic biligands were purified by HPLC and analyzed by MS prior to use. Their characterization is as follows:

*Biotin-(EG)<sub>5</sub>-Tz1-cy(CVFAHNYDYLVLC)-iiydt.* MALDI-MS of the purified biotinylated cyclic biligand gave a peak at  $m/z$  2982.9 for [M + H]<sup>+</sup>.

*Biotin-(EG)<sub>5</sub>-Tz1-cy(CVFAHNYDYLVLC)-kyydt* (Figure 4.7B). MALDI-MS of the purified biotinylated cyclic biligand gave a peak at  $m/z$  2998.9 for [M + H]<sup>+</sup>.

*Biotin-(EG)<sub>5</sub>-Tz1-cy(CVFAHNYDYLVLC)-iyiet.* MALDI-MS of the purified biotinylated cyclic biligand gave a peak at  $m/z$  2946.0 for [M + H]<sup>+</sup>.

**Characterization of affinity by surface plasmon resonance.** SPR experiments were performed as described in Chapter 3, with a few minor modifications. Here, PSA [30 to 60  $\mu\text{g/mL}$  in 10 mM sodium acetate (pH 5.5)] was immobilized to  $\sim 3000$  RU on the CM5 chip using a running buffer of HBS-P<sup>+</sup> [10 mM HEPES, 150 mM NaCl, 0.05% Tween20 (pH 7.4)]. Cyclic biligands were dissolved in HBS-P<sup>+</sup> buffer to produce 2.5  $\mu\text{M}$  stock solutions for each peptide, which were then serially diluted by a factor of 2 to produce a concentration series down to 0.3 nM. Cyclic anchor ligands were dissolved in HBS-P<sup>+</sup> buffer to produce 10  $\mu\text{M}$  stock solutions for each peptide, which were then serially diluted by a factor of 2 to produce a concentration series down to 1 nM. For a given affinity measurement, these series of peptide solutions successively were injected into flow cell 2 (or 3) for 360 s of contact time, 300 s of dissociation time, and 200 s of stabilization time using a flow rate of 50  $\mu\text{L/min}$  at 25 °C. Data processing and affinity analysis, including background subtraction, was performed using Biacore T100 evaluation software (Version 2.0.1, Biacore) as before.

## **4.3 RESULTS AND DISCUSSION**

### **4.3.1 Initial Validation of Protein-Catalyzed Multi-ligand Product**

Protein catalyzed, multi-ligand capture agents were prepared according to the scheme of Figure 2.1. When an in situ multi-ligand screen was carried out as illustrated in Figure 2.1, only a very small fraction of the on-bead n-order ligands were covalently coupled to the solution-phase 1<sup>o</sup> ligand by the protein. Analysis of the n-order ligands on the bead using standard methods yields information largely about the sequences of the n-order ligands themselves, since they comprise >99% of the molecules bound to the bead, and not the complete multi-ligand. For previously published in situ click

chemistry screens, the triazole product was identified using chromatographic separation followed by mass spectrometry.<sup>5-9</sup> For the case of the in situ click/OBOC biligand screens (Figure 2.1), the binary component screen was adopted. This was not a broadly applicable method, but showed efficacy in one exemplary case, which was discussed in Chapter 2 (Figure 2.9). Thus, alternative strategies were developed for demonstrating that the protein-catalyzed multi-ligand capture agent selections are indeed successful.

Two alternative strategies include: sequence homology analysis, and assays involving amplification of one or more labeled ligands. For both the first-generation biligand and triligand screens, a striking result was the extremely high sequence homology that was observed for the hit beads. For example, for the first 17 hit beads sequenced from screen **Bi1**, two peptides were identical, and a third peptide varied by only a single amino acid (see Appendix B). For screen **Tri1** (against the same library), the most commonly observed amino acids by position almost exactly reflect the consensus sequence identified in the second generation (focused) screen **Tri3** (see Appendix B). Such sequence homology was unique to in situ click/OBOC screens, and argues that these screens generate highly selective hits.

#### **4.3.2 Direct Detection of Protein-Catalyzed In Situ Multi-ligand**

**Assays with labeled ligands.** An enzyme-linked, colorimetric assay was developed for detecting on-bead, protein-templated multi-ligand (Figure 4.1). This approach relies upon appending a small molecule, such as biotin, to the solution-phase anchor (1°) ligand that is used in the screen. Once the screen has been completed, the small molecule will be covalently functionalized on only those beads that contain the protein-catalyzed multi-ligand. That small molecule can then provide a handle for

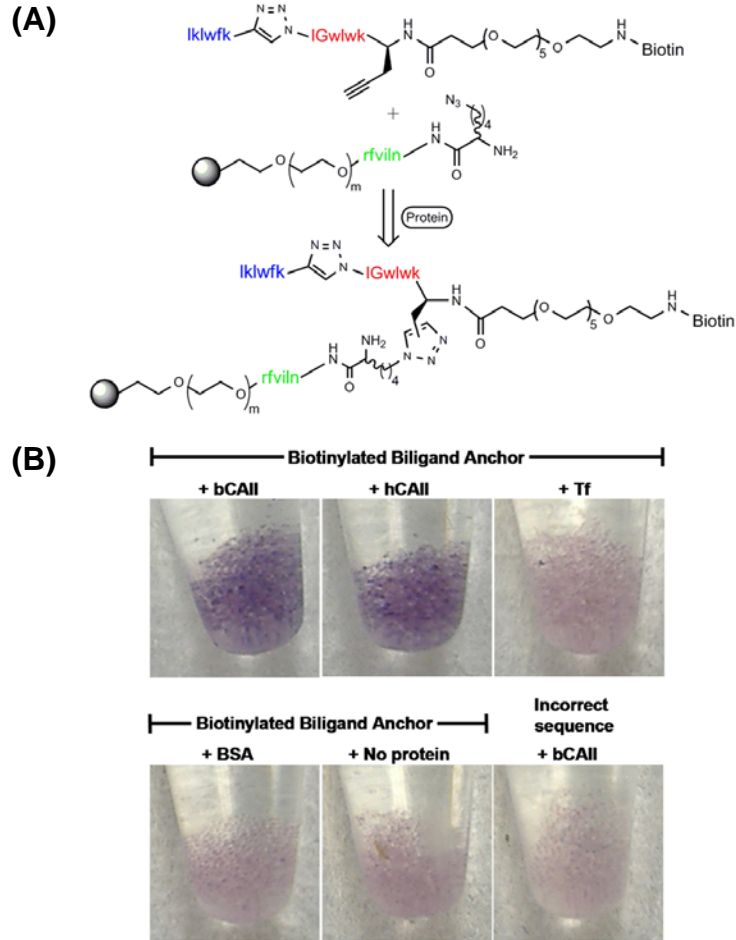


**Figure 4.1.** (A) Schematic of in situ click assay for on-bead triazole formation, using a biotinylated biligand anchor (D-Pra)-kwIwGl-Tz1-kfwlkl. (B) Purple beads are visualized as a positive indicator of triazole formation.

building up a chemical construct that can generate some detectable signal. The most successful approaches will rely on signals that can be amplified. For example, if an enzyme is appended to the small molecule, and then that enzyme can be utilized to catalyze some chemical process, which in turn represents an amplified signature of the on-bead protein-catalyzed multi-ligand. The product molecules from the enzymatic reaction can be uniquely colored, fluoresce or have some other unusual chemical or physical property that can be detected, thus providing evidence for the formation of the on-bead multi-ligand product. Results of such an assay, utilized to detect the on-bead formation of the triligand shown as the product of the 3<sup>o</sup> ligand screen of Figure 2.1, are presented in Figure 4.1.

In particular, the illustration of Figure 4.1A shows the schematic of in situ click assay for on-bead triazole formation, using a biotinylated biligand anchor Biotin-(EG)<sub>5</sub>-(D-Pra)-kwlwGl-Tz1-kfwlkl. After dissociation of the protein target, Figure 4.1B shows that treatment with alkaline phosphatase-streptavidin (AP-SA) then BCIP (5-bromo-4-chloro-3-indoyl phosphate) yields purple beads as a positive indicator of multi-ligand formation. In situ triligand was only formed in the presence of b(h)CAII protein, and not when the protein was human transferrin (Tf), BSA, or absent. Also, triligand is not observed when the biligand anchor sequence is incorrect.

**QPCR assay for the detection and quantitation of the formation of on-bead, protein-catalyzed multi-ligand protein capture agent.** Quantitative polymerase chain reaction (QPCR) enables both detection and quantification of oligonucleotide templates (as an absolute or relative copy number) through real-time monitoring of the intercalation of double-stranded DNA-binding fluorescent dyes during template

amplification. Fluorescence emission during the elongation step of each cycle is proportional to the amount of PCR product and enables direct monitoring of the PCR reaction. The resulting PCR curve is used to define the exponential phase of the reaction, which is a prerequisite for accurate calculation of the initial copy number at the beginning of the reaction.<sup>10</sup> Real-time PCR assays are characterized by a wide dynamic range of quantification, a high technical sensitivity (< 5 copies of template oligo) and a high precision (< 2% standard deviation).<sup>11,12</sup>

To quantify the formation of on-bead, protein-catalyzed triligand obtained by the assay of Figure 4.1A, it was necessary to transform the biotin label into an oligonucleotide label. The PCR-based assay shown in Figure 4.2 is a variation of the enzymatic assay where AP-SA is replaced with streptavidin conjugated to a small template oligonucleotide (5'...NH<sub>2</sub>-(CH<sub>2</sub>)<sub>6</sub>-GGGACAATTACTATTTACAATTACAATGCTCACGTGGTACGAGTTCGTCTCCCAGG...3' –SEQ ID NO: 1). Binding of this reagent to biotinylated triligand results in the recruitment of the template oligonucleotide to the bead surface where it can be amplified by PCR. The extent of amplification (i.e., number of PCR cycles required to produce a band) is directly proportional to the amount of oligonucleotide at the bead surface, providing a quantitative readout of the assembled triligand and hence the efficiency of the in situ click reaction.

The results shown in Figure 4.2 are roughly in line with the colorimetric AP-SA assays. The percent yield for the bCAII-catalyzed click reaction between biotinylated biligand anchor (D-Pra)-kwlwGl-Tz1-kfwlkl and 3° ligand Az4-nlivfr may be estimated as 0.000005% from the QPCR assay of Figure 4.2. This takes into account a stoichiometry of 4 oligos per streptavidin tetramer, and estimates that single beads

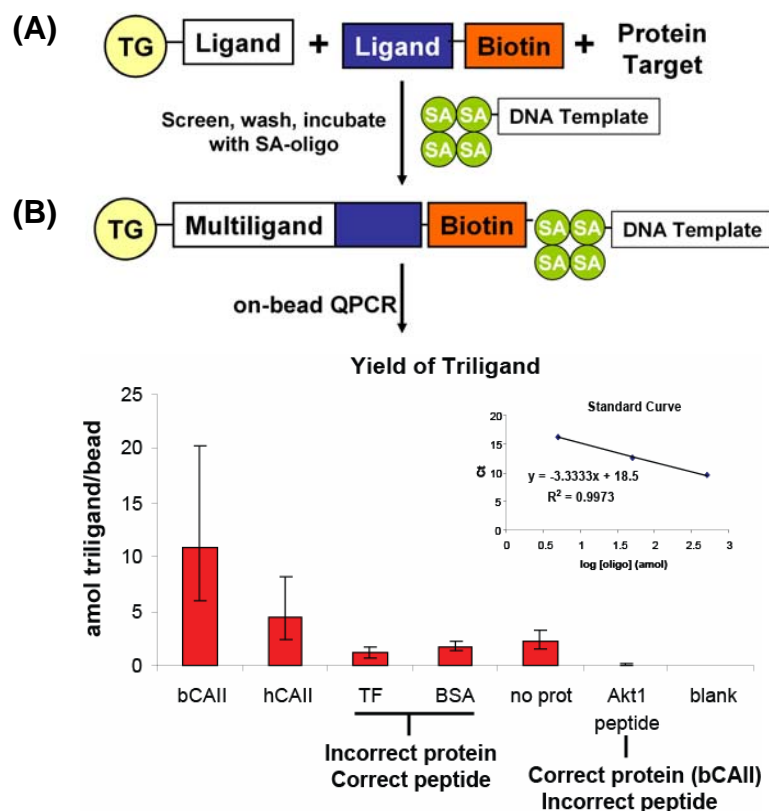


**Figure 4.2.** (A) General method for detecting on-bead multi-ligand by QPCR. (B) In a specific example, the results of a QPCR assay quantifying the yield of biotinylated triligand from the protein-catalyzed in situ click reactions of Figure 4.1 are illustrated. Results are expressed by bar graph in units of mean amol triligand/bead for 5-bead samples ( $N = 3$ ). The Ct values for a series of known template concentrations were used to generate a linear standard curve (inset), from which the concentration of streptavidin-oligo reagent in each 5-bead sample was extrapolated.

display a uniform loading of 100 pmol/bead. It is interesting that while bCAII apparently makes 2 times more triligand product per QPCR assay than hCAII, the triligand displays a slightly higher binding affinity for hCAII (see Chapter 3). Out of the controls, the “no protein” control displays the consistently higher background reaction than the BSA and Tf controls. It is possible that BSA and Tf are blocking reactive azides on the bead and attenuating the background click reaction. It is also interesting that the Akt1 peptide control displayed the least background, showing nearly no triligand formation, and is comparable with blank beads. Here, bCAII is evidently binding to the bead but not to the Akt1 peptide, and azides on these beads are blocked more effectively with bCAII than with BSA or Tf.

### **4.3.3 Strategies for Improving Signal-to-Noise Ratio during**

#### **In Situ Click/OBOC Screens**

Based on the success of the colorimetric assay in Figure 4.1, a new method for visualization of hits from the in situ click/OBOC screens emerged. Rather than stratifying hit beads based on fluorescence (via binding of a fluorescently labeled protein target, see Chapter 2), it became apparent that the assay of Figure 4.1 could be easily modified to accommodate screening of an entire bead library rather than a single sequence. This colorimetric approach removed dependence on a fluorescence microscope (or array scanner) for identification of hits, and allowed the researcher to pick the hits in real time while monitoring the BCIP development with a standard light microscope. Furthermore, the intrinsic autofluorescence<sup>13,14</sup> of TentaGel S-NH<sub>2</sub> beads was no longer a potential challenge to the signal-to-noise ratio. It also should be noted that the more delicate of protein targets (such as phospho-Akt), which were previously

intolerant to covalent modification with fluorophores, now became candidates for multi-ligand capture agent development.

We were surprised by the extremely low yield of the protein-catalyzed click reaction. Such a low-frequency event may potentially be surrounded by a high level of background. A major source of background would arise from the binding of protein target to the bead, but without any click reaction occurring. Since our methods of Chapter 2 relied on protein detection (by way of the fluorophore), “background hits” would not have been distinguished from “true hits.” Thus, the general concept of multi-stage screening was explored (see Figures 4.3-4.4).

For the most important cancer-specific protein biomarkers, antibodies are available. Therefore, primary and AP-labeled secondary antibodies initially could serve as reagents to detect bead-bound protein from a simple OBOC screen, as shown in Figure 4.3A and Figure 4.4A, all the way to the in situ click/OBOC screen (see Figure 4.5A for a specific example). This antibody-based screening approach is essentially a sandwich (ELISA-like) assay, but with the solid support being a bead rather than a microwell of a 96-well plate. As an added bonus, this approach also selects for those hit beads and peptides that can eventually form a multi-ligand capture agent that, together with the antibody, form an ELISA pair.

The antibody-based screening approach also allowed for improvement of the signal-to-noise ratio, through pairing each screen with an anti-screen. Figure 4.3B illustrates an anti-screen which would be performed following the 1° ligand screen of Figure 4.3A. This screen eliminates “background hits” which would represent natural antibody-binding epitopes. Figure 4.4B illustrates an anti-screen which would be performed following the *epitope-targeted* 1° ligand screen of Figure 4.4A. This screen

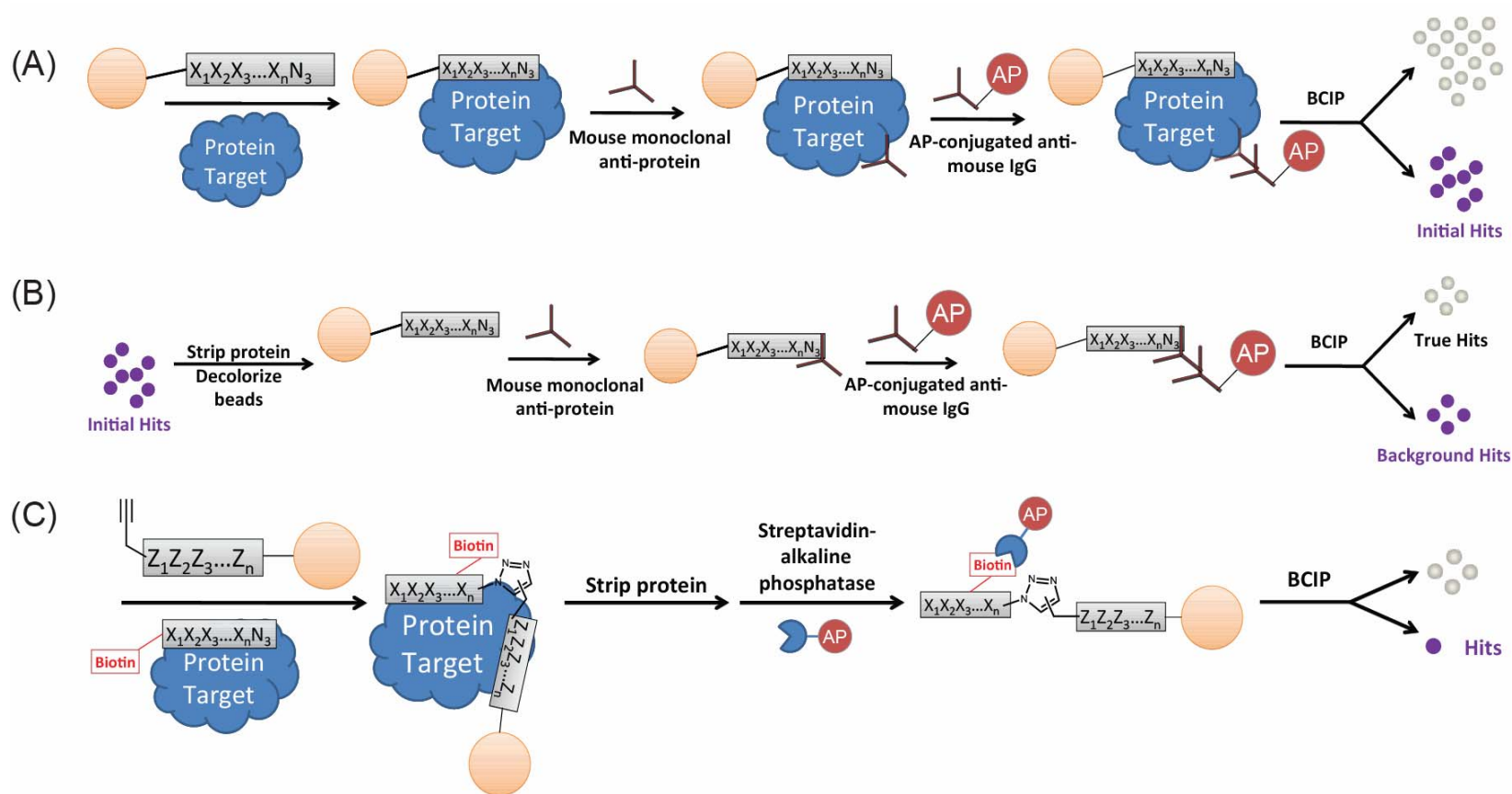


**Figure 4.3.** General screening strategies to improve signal-to-noise ratio and reduce number of false positives in OBOC selections.

**(A)** Colorimetric antibody screen for initial hits. This screen can be used at any level of multi-ligand discovery (i.e., anchor, biligand, etc.), as only bound protein is detected. **(B)** Anti-screen for removing background hits. **(C)** Direct detection of on-bead biligand.

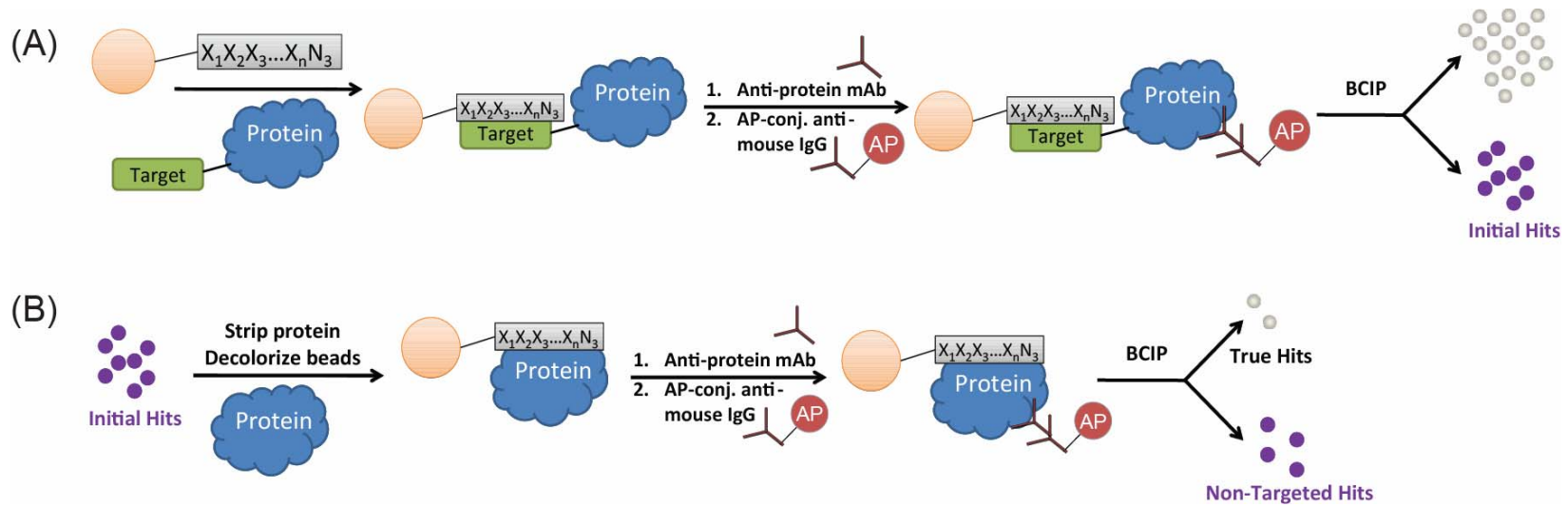


**Figure 4.4.** (A) Screening and (B) anti-screening strategies to target a particular protein epitope or modification.

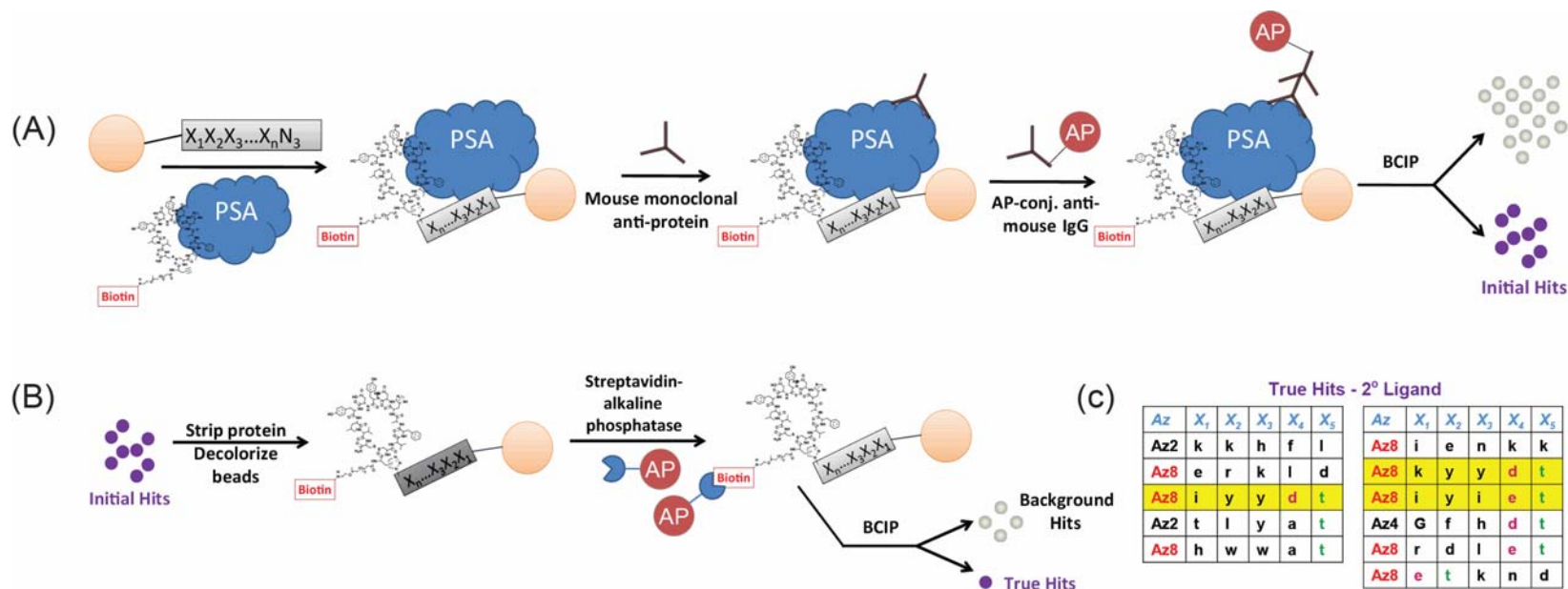


**Figure 4.5.** Two-stage in situ/click OBOC screening strategy to identify a biligand capture agent for PSA using a previously identified cyclic peptide Biotin-(EG)<sub>5</sub>-Pra-cy(CVFAHNYDYLVLC) as the anchoring unit. It should be noted that this strategy is a specific application of Figures 4.3A,C. (A) Probing for bound PSA. (B) Probing for on-bead, protein-catalyzed biligand. (C) True hits displaying a high degree of sequence homology.

eliminates “background hits” which would represent non-targeted peptides. Figure 4.5B illustrates the specific case of an anti-screen that results in direct detection of the bead-bound biligand products of the protein-catalyzed click reaction. Through detection of the biotin label, we can parse out the false-positive beads which bind to PSA (in the Figure 4.5A screen) but do not undergo in situ click reaction with the biotinylated anchor ligand. A general screen for direct detection of protein-catalyzed in situ hits is shown in Figure 4.3C, and this is simply the whole-library extension of the Figure 4.1 assay.

#### **4.3.4 Selection of Biligand Capture Agent for Prostate-Specific Antigen**

The in situ click/OBOC selection of an epitope-targeted biligand capture agent against prostate-specific antigen was explored as a feasibility demonstration for the antibody- and biotin-based multi-stage screening strategies.

**Prostate-specific antigen.** PSA is a 30-kDa serum glycoprotein and protein biomarker for detection and management of prostate cancer. This protein is present in normal prostatic tissue, but increased levels of PSA are a reliable indicator of prostate cancer and are widely used as a marker of potential cancerous growths or disease status.<sup>15</sup> Differences in concentration between the active form of PSA and enzymatically inactive versions (e.g., proPSA, nicked inactive PSA, ACT-PSA complex) may provide distinguishing information between cancer and benign prostatic hyperplasia (BPH), which is a common misdiagnosis. Additionally, PSA has a single N-oligosaccharide chain attached to Asn-45, and it has been reported that one can distinguish PSA origin (healthy vs. tumor) through differences in glycosylation patterns.<sup>16</sup> Creating specific

multi-ligands that target these minor variants of PSA may potentially facilitate more accurate diagnosis of prostatic diseases.

**Preparation of anchor (1°) ligand.** Due to its relevance in the diagnosis and monitoring of human prostate cancer, PSA is a well studied protein target for ligand development. Phage display,<sup>1,17</sup> polysome selection,<sup>18</sup> and *in silico* structure-guided design<sup>19,20</sup> have all been used to isolate peptide ligands of  $\mu\text{M}$  to nM binding affinity against PSA. It was our idea that the multi-ligand discovery process can be expedited through implementation of one of these peptides as the anchor (1°) ligand. Indeed, the 1° ligand OBOC screen is the most challenging step of Figure 2.1 since only weak binding interactions are probed. After evaluating several of these reported peptides, we chose the optimized phage-derived cyclic sequence cy(CVFAHNYDYLVLC) as the 1° ligand for the rapid selection of a multi-ligand capture agent against PSA.<sup>1</sup> SPR measurement determined that this peptide displays a binding affinity of  $K_D \approx 2.4 \mu\text{M}$  for its interaction with PSA. As this  $K_D$  value is approximately the same affinity as our *biligand* for bCAII, we concluded that cy(CVFAHNYDYLVLC) was an excellent starting point for building a multi-ligand capture agent that specifically recognizes the active site of PSA.

Cyclic peptides, due to their conformational rigidity, lose less entropy and free energy upon binding to targets than their linear counterparts.<sup>21</sup> This translates to enhancements in receptor-binding affinity, specificity, and stability. To illustrate this point, we determined that cy(CVFAHNYDYLVLC) binds to the active site of PSA when cyclized, but does not bind as a linear sequence (SPR, data not shown).

In order to prepare the peptide cy(CVFAHNYDYLVLC) for in situ click chemistry, the artificial amino acid L-propargylglycine was installed on the N-terminus during solid-phase peptide synthesis of the linear sequence. Following the coupling of L-propargylglycine, two other chemical modifications were made. First, Fmoc-NH-(PEG)<sub>5</sub>-COOH (22 atoms) (Novabiochem) was installed to impart better water solubility to the cyclic anchor ligand. Second, biotin was added to cap the N-terminus, thus providing the label for performing the two-stage in situ click/OBOC screen with direct detection of on-bead protein-catalyzed biligand. Peptide cyclization by formation of a disulfide bond was achieved by an oxygen/Cu(II)(1,10-phenanthroline)<sub>3</sub> system.<sup>22</sup> The final structure of cyclic anchor ligand Biotin-(EG)<sub>5</sub>-Pra-cy(CVFAHNYDYLVLC) is shown in Figure 4.7A. Results from SPR determined that the addition of these linker moieties did not affect the overall binding affinity of the anchor to PSA. It was found that this modified cyclic anchor ligand had an affinity of 2.1 μM (Figure 4.7C). A kinetic fit of the data yielded  $k_d = 0.09 \text{ s}^{-1}$  and  $k_a = 4.5 \times 10^4 \text{ M}^{-1}\text{s}^{-1}$  (for 1:1 binding interaction).

Binding specificity for the cyclic anchor ligand of Figure 4.7A was characterized by sandwich (ELISA-like) assays on streptavidin-functionalized microtiter plates. Similar to Chapter 3, the cyclic anchor (1° capture agent) was paired with a commercial mouse monoclonal anti-PSA antibody (2° capture agent) for quantification of captured PSA. For a sandwich assay performed with PSA presented in 10% porcine serum, the analytical sensitivity was ~2 μM (~60 μg/mL), further confirming the SPR result of Figure 4.7C even in a high protein background.

Cyclic peptides were prepared in bulk by solid-phase synthesis, purified by HPLC, and analyzed by MS prior to use. Their characterization is as follows:

*cy(CVFAHNYDYLVLC)*. MALDI-MS of the purified cyclic peptide gave a peak at  $m/z$  1443.2 for  $[M + H]^+$ .

*Biotin-(EG)<sub>5</sub>-Pra-cy(CVFAHNYDYLVLC)* (Figure 4.7A). MALDI-MS of the purified biotinylated cyclic anchor gave a peak at  $m/z$  2100.0 for  $[M + H]^+$ .

**Two-stage in situ click/OBOC screen for biligand capture agent using a biotinylated anchor ligand.** The two-stage in situ click/OBOC screening approach for selection of a biligand capture agent against PSA is shown in detail in Figures 4.5A-B. Note that this screening procedure is an application of the general methods in Figure 4.3. For these screens, a single comprehensive library of  $3 \times 18^5$  hexamers was used (Library X): Az-X<sub>1</sub>X<sub>2</sub>X<sub>3</sub>X<sub>4</sub>X<sub>5</sub>-TentaGel, where Az = azidoalkyl amino acids Az2,<sup>23</sup> Az4, or Az8, and X = all D-amino acids except D-Cys and D-Met. In the first stage (Figure 4.5A), two antibodies were applied to detect and amplify the binding of PSA to the bead library during an in situ/click OBOC screen. Binding of monoclonal anti-PSA antibody to the PSA-bound bead was visualized by probing with an AP-labeled secondary anti-IgG, followed by treatment with BCIP. The percentage of hits (purple beads) following this first screen was 10%, a value which indicated that a significant number of “background hits” were likely selected along with the “true hits.” This first screen may be optimized to achieve a more manageable number of hits, through modulating antibody and/or PSA concentrations, or by testing different blocking buffers. Instead, we chose to perform a second screen, against only the initial hits from the first screen (Figure 4.5B). Because a biotinylated cyclic anchor ligand was applied in the first screen, we have a label for direct monitoring of the in situ click hits, representing protein-catalyzed conjugation of 1°

ligand to bead-bound 2° ligands. In the second screen, AP-SA followed by BCIP treatment allowed visualization of only the in situ click biligand hits. Surprisingly, only 10% of the initial hits were “true hits” in this assay. This result confirms the practical importance of the multi-stage screening method to enrich for the best hits.

A representative image of the beads in this second screen is depicted in Figure 4.6, and it illustrates the high signal-to-noise ratio that may be achieved by colorimetric detection. Edman sequencing of the true hits (i.e., in situ click biligands) yielded the table of results shown in Figure 4.5C. There is an incredible sequence homology displayed by these biligand hits. All hits demonstrate an extremely high preference for  $X_5 = t$  and significant propensity for  $Az = Az8$ . Also, two sequences show the homology of “yy” in positions  $X_2$  and  $X_3$ . This motif was reinforced by two additional occurrences of y at these positions. The 2° ligand motif  $Az8-X_1yydt$  was observed twice ( $X_1 = k, i$ ).

**Validation of PSA-binding cyclic biligands.** Based on the Edman sequencing results (Figure 4.5C), the cyclic biligands comprised of  $Az8-iiydt$ ,  $Az8-kyydt$ , and  $Az8-iyiet$  were chosen as candidates to test for binding affinity by SPR. The best-binding cyclic biligand was Biotin-(EG)<sub>5</sub>-Tz1-cy(CVFAHNYDYLVLC)-kyydt, whose structure is shown in Figure 4.7B. SPR measurement determined that this peptide displays a binding affinity of  $K_D \approx 140$  nM for its interaction with PSA, which is a factor of ~15 improvement from the cyclic anchor (Figure 4.7D). Biligands Biotin-(EG)<sub>5</sub>-Tz1-cy(CVFAHNYDYLVLC)-iiydt and Biotin-(EG)<sub>5</sub>-Tz1-cy(CVFAHNYDYLVLC)-iyiet displayed affinities of  $K_D \approx 480$  nM and  $K_D \approx 5$  μM, respectively (data not shown). Thus,

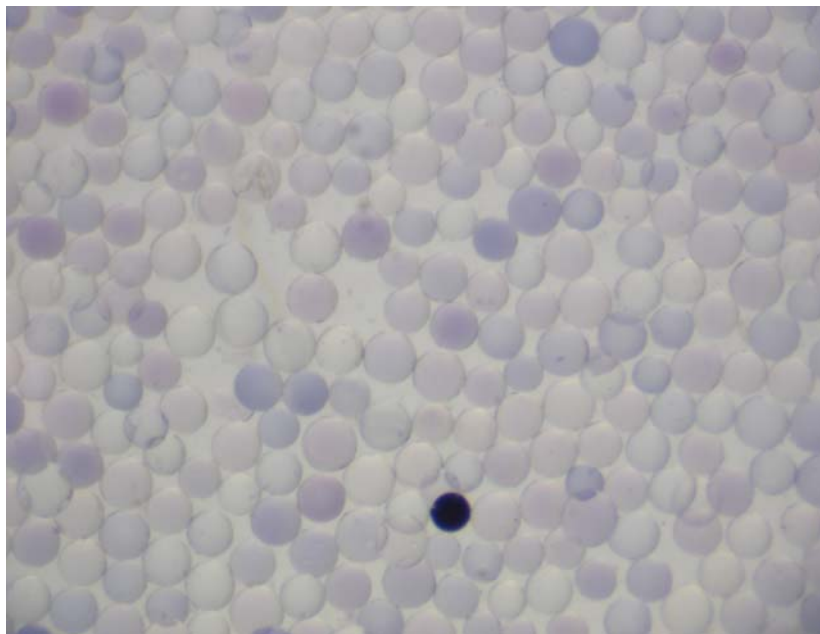


**Figure 4.6.** Representative image of an in situ click/OBOC screen with enzymatic amplification. In a single assay,  $>10^6$  TentaGel beads (90- $\mu\text{m}$  diameter) present individual 2° ligands to a solution of PSA and the biotinylated cyclic anchor (of Figure 4.7A). Specific binding by PSA and formation of in situ click product (purple color) is visualized by treatment with AP-SA and the chromogenic substrate BCIP.

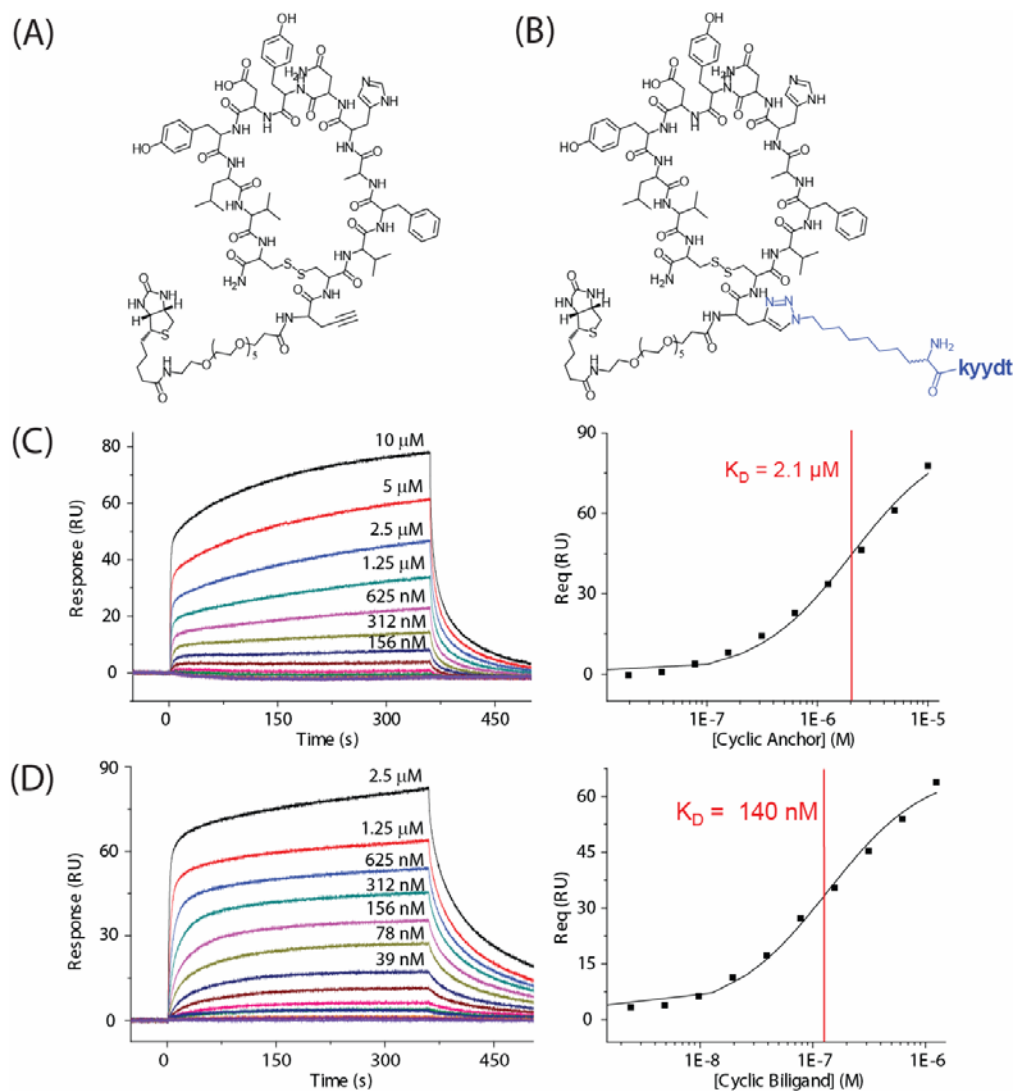


**Figure 4.7.** Structures of active site targeted cyclic anchor (A) and cyclic biligand (B) against PSA. Note that the anchor (black) is comprised of L-amino acids, while the 2<sup>o</sup> ligand (of the biligand) is composed of D-stereoisomers. (C) SPR response sensorgrams obtained with increasing concentration (1 nM to 10  $\mu$ M) of cyclic anchor demonstrate  $K_D \approx 2.1 \mu$ M binding affinity to immobilized PSA. (D) SPR response sensorgrams obtained with increasing concentration (0.3 nM to 2.5  $\mu$ M) of cyclic biligand display  $K_D \approx 140$  nM binding affinity to immobilized PSA.

it appears that the area proximal to the active site of PSA is negatively affected by binding of isoleucine.

To further evaluate the cyclic biligand of Figure 4.7B as a suitable capture agent for PSA, a sandwich (ELISA-like) assay will be performed in parallel with the standard commercial 2-antibody ELISA kit for PSA capture and detection. The analytical sensitivities will also be compared for cyclic anchor vs. cyclic biligand as 1° capture agents. Based on the high specificity of the cyclic anchor, we expected that its corresponding biligand will have sufficient affinity and specificity to capture the PSA from even undiluted serum.

#### **4.4 CONCLUSIONS**

To both qualitatively and quantitatively assess the formation of protein-templated multi-ligand products from in situ click/OBOC screens, two complementary assays were developed. First, the colorimetric assay employing AP-SA and the chromogenic substrate BCIP allowed detection of on-bead multi-ligands by simple visual inspection. Second, the QPCR assay employing a novel streptavidin-oligo reagent allowed accurate and direct determination of the on-bead in situ click products. The low-yielding, but detectable, products of in situ click chemistry inspired us to develop next-generation, multi-stage screening strategies to improve the signal-to-noise ratio and reduce the number of false positives in our screens. Next-generation screening formats included colorimetric antibody-based screens for initial hits, anti-screens for removing background hits, and direct screening of on-bead biligand. These methods dramatically improved the efficiency of the in situ click/OBOC multi-ligand discovery process. Furthermore, these

new colorimetric methods were easier to perform as they did not require sophisticated instrumentation (e.g., fluorescent microscopes or array scanners).

As a specific application of the multi-stage screening strategies, the rapid selection of a biligand capture agent for PSA was demonstrated. The biligand selection process was expedited through both use of a previously reported, phage-derived cyclic anchor ligand and a two-stage in situ click/OBOC screening method. The cyclic anchor was shown by SPR to have an affinity of  $K_D \approx 2.1 \mu\text{M}$ , and it was a viable capture agent in sandwich (ELISA-like) assays, pulling down  $2 \mu\text{M}$  ( $\sim 60 \mu\text{g/mL}$ ) PSA from dilute serum. After two screens, the initial pool of in situ click biligand hits was reduced to 10% true hits, and we obtained an extremely high sequence homology in these cyclic biligand sequences. The best cyclic biligand was shown by SPR to have an affinity of 140 nM. The sequence of this capture agent is unique in that it is a mixture of cyclic, L-chirality, and D-chirality components. Also, one can feasibly only obtain the resultant biligand from the in situ click/OBOC screening methodology described in this thesis. Using the cyclic biligand as a starting point, we next intend to synthesize a triligand capture agent of even higher affinity (e.g.,  $K_D \approx 1 \text{ nM}$ ) and specificity for PSA.

#### **4.5 ACKNOWLEDGEMENTS**

This work was completed in collaboration with Steven W. Millward, Gabriel A. Kwong, Kaycie M. Butler, Vanessa M. Burns, and Marrissa Barrientos.

**4.6 REFERENCES**

1. (a) Wu, P.; Leinonen, J.; Koivunen, E.; Lankinen, H.; Stenman, U.-H. *Eur. J. Biochem.* **2000**, *267*, 6212–6220. (b) Pakkala, M.; Jylhärinta, A.; Wu, P.; Leinonen, J.; Stenman, U. H.; Santa, H.; Vepsäläinen, J.; Peräkylä, M.; Närvänen, A. *J. Pept. Sci.* **2004**, *10*, 439–447. (c) Koistinen, H.; Närvänen, A.; Pakkala, P.; Hekim, C.; Aaltonen, J.; Zhu, L.; Laakkonen, P.; Stenman, U.-H. *Biol. Chem.* **2008**, *389*, 633–642.
2. G. Liu, K. S. Lam, in *Combinatorial Chemistry—A Practical Approach* (Fenniri, H., editor), Oxford University Press, USA, 2000, pp. 43–44.
3. Sano, T. and C. R. Cantor *Proc. Natl. Acad. Sci. USA* **1990**, *87*, 142–146.
4. Chan, T. R.; Fokin, V. V. *QSAR Comb. Sci.* **2007**, *26*, 1274–1279.
5. Lewis, W. G.; Green, L. G.; Grynszpan, F.; Radić, Z.; Carlier, P. R.; Taylor, P.; Finn, M. G.; Sharpless, K. B. *Angew. Chem. Int. Ed.* **2002**, *41*, 1053–1057.
6. Manetsch, R.; Krasinski, A.; Radić, Z.; Raushel, J.; Taylor, P.; Sharpless, K. B.; Kolb, H. C. *J. Am. Chem. Soc.* **2004**, *126*, 12809–12818.
7. Bourne, Y.; Kolb, H. C.; Radić, Z.; Sharpless, K. B.; Taylor, P.; Marchot, P. *Proc. Natl. Acad. Sci. USA* **2004**, *101*, 1449–1454.
8. Mocharla, V. P.; Colasson, B.; Lee, L. V.; Röper, S.; Sharpless, K. B.; Wong, C.-H.; Kolb, H. C. *Angew. Chem. Int. Ed.* **2005**, *44*, 116–120.
9. Whiting, M.; Muldoon, J.; Lin, Y.-C.; Silverman, S. M.; Lindstrom, W.; Olson, A. J.; Kolb, H. C.; Finn, M. G.; Sharpless, K. B.; Elder, J. H.; Fokin, V. V. *Angew. Chem. Int. Ed.* **2006**, *45*, 1435–1439.
10. Klein, D. *Trends Mol. Med.* **2002**, *8*, 257–260.

11. Bustin, S. A. *J. Mol. Endocrinol.* **2000**, *25*, 169–193.
12. Klein, D.; Leutenegger, C. M.; Bahula, C.; Gold, P.; Hofmann-Lehmann, R.; Salmons, B.; Lutz, H.; Gunzburg, W. H. *J. Acquir. Immune Defic. Syndr.* **2001**, *26*, 8–20.
13. Alluri, P. G.; Reddy, M. M.; Bachhawat-Sikder, K.; Olivos, H. J.; Kodadek, T. *J. Am. Chem. Soc.* **2003**, *125*, 13995–14004.
14. George, J.; Tear, M. L.; Norey, C. G.; Dougal Burns, D. *J. Biomol. Screening* **2003**, *8*, 72–80.
15. Jeong, S.; Lee, S.-W. *J. Microbiol. Biotechnol.* **2007**, *17*, 840–846.
16. Peracaula, R.; Tabarés, G.; Royle, L.; Harvey, D. J.; Dwek, R. A.; Rudd, P. M.; de Llorens, R. *Glycobiology* **2003**, *13*, 457–470.
17. Ferrieu-Weisbuch, C.; Michel, S.; Collomb-Clerc, E.; Pothion, C.; Deleage, G.; Jolivet-Reynaud, C. *J. Mol. Recognit.* **2006**, *19*, 10–20.
18. Gersuk, G. M.; Corey, M. J.; Corey, E.; Stray, J. E.; Kawasaki, G. H.; Vessella, R. *L. Biochem. Biophys. Res. Comm.* **1997**, *232*, 578–582.
19. (a) Hassan, M. D.; Hassan, I.; Kumar, V.; Somvanshi, R. K.; Dey, S.; Singh, T. P.; Yadav, S. *J. Pept. Sci.* **2007**, *13*, 849–855. (b) Kumar, V.; Hassan, Md. I.; Singh, A. K.; Dey, S.; Singh, T. P.; Yadav, S. *Clin. Chim. Acta* **2009**, *403*, 17–22.
20. Denmeade, S. R.; Lou, W.; Lövgren, J.; Malm, J.; Lilja, H.; Isaacs, J. T. *Cancer Res.* **1997**, *57*, 4924–4930.
21. Joo, S. H.; Xiao, Q.; Ling, Y.; Gopishetty, B.; Pei, D. *J. Am. Chem. Soc.* **2006**, *128*, 13000–13009.
22. Careaga, C. L.; Falke, J. J. *J. Mol. Biol.* **1992**, *226*, 1219–1235.

23. Roice, M.; Johannsen, I.; Meldal, M. *QSAR Comb. Sci.* **2004**, *23*, 662–673.

## **Chapter 5**

A Non-Oxidative Approach toward Chemically and Electrochemically Functionalizing

Si(111)

## 5.1 INTRODUCTION

Semiconductor devices and semiconductor processing are playing an increasingly large role in biotechnology applications. Examples include silicon nanowires (SiNWs)<sup>1</sup> and nanocantilevers<sup>2,3</sup> for label-free biomolecular sensors, nanofluidics for biomolecular separations,<sup>4-7</sup> and microfabricated lab-on-a-chip technologies.<sup>8,9</sup> Coupled with these developments has been the emergence of mechanical,<sup>10-12</sup> chemical, and electrochemical approaches for functionalizing and/or selectively activating surfaces. For sensing applications, electrochemical activation of surfaces is particularly relevant since it is only limited by the size of electronically addressable features (which can be much denser than what can be spotted with an inkjet, for example). Electrochemical activation of metal surfaces has been pioneered by Mrksich and co-workers,<sup>13-16</sup> and applications of that chemistry toward the spatially selective biofunctionalization of semiconductor nanowires has been demonstrated by at least two groups.<sup>17,18</sup>

For silicon surfaces, the chemistry is particularly challenging because unprotected silicon forms a native oxide (SiO<sub>2</sub>) layer. This native oxide layer can limit the use of silicon electrodes for electrochemical functionalization. Moreover, the native oxide on silicon has a low isoelectric point (~2). Therefore, SiO<sub>2</sub> surfaces are negatively charged under physiological conditions (= pH 7.4).<sup>19</sup> These surface charges can potentially limit the sensitivity of SiNW field effect biosensors through Debye screening<sup>20</sup> by the localized ionic concentration at the sensor surface. Additionally, the native oxide layer contains electrical defect sites at the Si-SiO<sub>2</sub> interface.<sup>21</sup> These electrical defect sites can detrimentally affect carrier recombination rates leading to decreased transistor or sensor performance in silicon-based nanoelectronic devices.<sup>22</sup>

For high surface area devices, such as SiNWs, this phenomenon can reduce charge carrier mobilities significantly.<sup>21</sup> Thus, the ideal biofunctionalization strategy for electrochemically activating silicon surfaces should begin with non-oxidized silicon. For sensing applications, the functionalization approach should provide continued protection of the silicon surface against further oxidation and limit the number of surface defect sites that can increase carrier recombination rates.

Several methods for attaching organic molecules onto non-oxidized silicon surfaces have been reported. One class of schemes relies on the direct covalent attachment of terminal alkenes on hydrogen-terminated surfaces by thermal induction, ultraviolet (UV) light, or catalysis.<sup>23–30</sup> The resulting alkyl monolayers reflect the atomic flatness of the underlying silicon,<sup>31,32</sup> and they provide partial chemical passivation of silicon via the formation of a Si-C bond. However, the alkyl monolayers prepared by the above strategies have not been demonstrated to give long-term protection to the silicon surface against oxidation due to limited molecular packing densities.

The Lewis group has developed techniques to alkylate chlorine-terminated Si(111) surfaces using alkylmagnesium and alkyllithium reagents.<sup>33–38</sup> A limitation of these methods is that a 100% surface coverage can only be obtained with a methylated Si(111) surface, as confirmed by low-temperature STM.<sup>34,39</sup> By comparison, the surface coverage achieved by the ethylation of chlorine-terminated Si(111) is limited by steric effects and corresponds to 80% of the atop silicon sites.<sup>40</sup> For more complex long-chain organic molecules, surface coverages will most certainly be lower, and the resistance to oxidation of the Si(111) surface will be reduced. It is therefore necessary to develop a surface chemistry method that will fully passivate the Si(111) surface, provide resistance

to oxide growth, and offer a chemical handle for the attachment of a variety of molecules. No methods have yet been demonstrated that protect the more technologically relevant Si(100) surface against oxidation.

This chapter describes the development of a versatile and robust strategy for chemically passivating Si(111) surfaces in a manner that stabilizes the underlying Si against native oxidation and allows for both chemical and electrochemical functionalization of the surface. Based on our previous work on methylated and ethylated Si(111),<sup>33-40</sup> the more chemically versatile acetylenylation of chlorine-terminated Si(111) was explored. Work by Nemanick<sup>41</sup> and Lewis' group<sup>42,43</sup> indicated that the chlorination/alkylation chemistry for acetylenylating Si(111) could proceed to completion. The footprint of the linear *sp*-hybridized acetylene group (-C≡CH) on Si(111) should be as small or smaller than the -CH<sub>3</sub> group, and so a high surface coverage should be possible. Equally important is that the -C≡CH group also provides a chemical handle for additional functionalization via the Cu(I) catalyzed Huisgen 1,3-dipolar cycloaddition ('click' reaction<sup>44,45</sup>) between an azide and the surface-bound alkyne. In particular, we designed an azide-functionalized, modified benzoquinone for attachment, via the click reaction, to the surface-bound acetylenyl groups to form a 1,2,3-triazole. The click reaction is useful because azides and acetylenes are synthetically easy to introduce, compatible with a variety of solvents and species, and tolerant against other functionalities (highly specific, coupling can only occur between these two groups). Our work here follows reports that have demonstrated that different molecules can be clicked onto gold and SiO<sub>2</sub> surfaces in a variety of solvent and pH conditions.<sup>46-54</sup>

We previously reported on the electrochemistry of hydroquinones on Si(111) and Si(100) surfaces, attached via the UV-activation of H-terminated Si.<sup>17</sup> In that work, the hydroquinones could be reversibly oxidized to form benzoquinones (the ‘activated’ surface) which could then react by way of either Diels-Alder cycloaddition<sup>13,15</sup> or Michael addition chemistries,<sup>55,56</sup> leading to a selectively biofunctionalized silicon microwire or nanowire surface. However, while the hydroquinone coverage on the Si(111) surface did yield at least some protection for that surface against oxidation, the electrochemical step to oxidize the hydroquinone also led to oxidation of the underlying Si(111). Thus, in this work, we have designed and synthesized a benzoquinone that can be clicked onto the acetylenylated silicon surface. The surface-bound benzoquinone may be then activated via electrochemical *reduction* to produce an amine terminus.<sup>14,57,58</sup> We demonstrate that the entire chemical process may be accomplished in a fashion that greatly reduces the oxidation of the underlying silicon. We also demonstrate the selective attachment of ferrocene onto an electrochemically activated Si(111) surface, as well as the model biomolecule, biotin.

## 5.2 MATERIALS AND EXPERIMENTAL METHODS

### 5.2.1 Chemicals

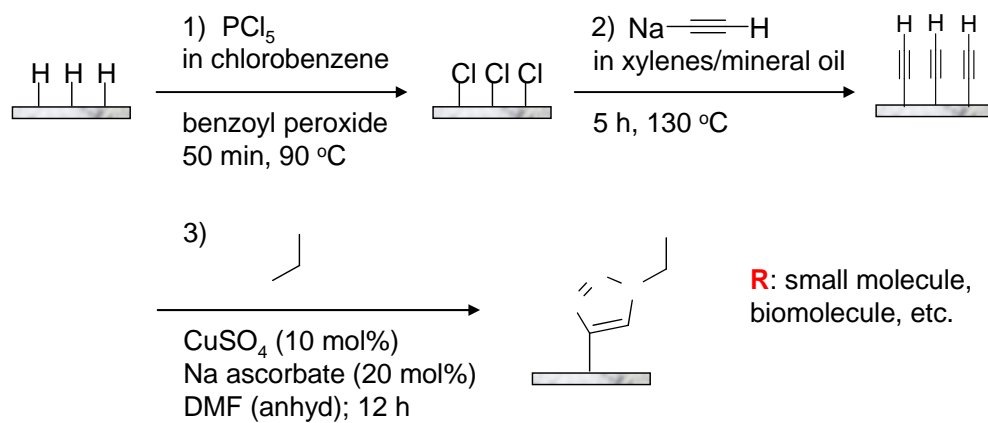
Anhydrous methanol and anhydrous tetrahydrofuran (THF, inhibitor-free) were obtained from Aldrich and exclusively stored and used in a N<sub>2</sub>(g)-purged glove box. Chlorobenzene, benzoyl peroxide, and sodium acetylide (18 wt% in xylenes/light mineral oil) were purchased from Aldrich and were stored and used in the glove box. Phosphorus pentachloride (PCl<sub>5</sub>) was acquired from Riedel-de Haën (Seelze, Germany). The 40% NH<sub>4</sub>F(aq) solution was obtained from Transene Co. (Rowland, MA) and was

used as received. The  $\text{CuSO}_4 \cdot 5\text{H}_2\text{O}$  was obtained from Spectrum Chemical Mfg. Corp. (Gardena, CA). Sodium ascorbate, ferrocene carboxylic acid, and anhydrous  $N,N'$ -dimethylformamide (DMF) were obtained from Aldrich.  $N,N'$ -Diisopropylcarbodiimide (DIC) was purchased from AnaSpec (San Jose, CA). Dulbecco's Phosphate Buffered Saline (DPBS) (2.7 mM KCl, 1.5 mM  $\text{KH}_2\text{PO}_4$ , 137 mM NaCl, 8 mM  $\text{Na}_2\text{HPO}_4$ ) pH 7.4 was purchased from Sigma. EZ-Link NHS-Biotin was obtained from Pierce Biotechnology (Rockford, IL). Nanogold Streptavidin was purchased from Invitrogen (Carlsbad, CA). GoldEnhance-EM kit for Nanogold amplification was bought from Nanoprobes (Yaphank, NY).

### 5.2.2 Acetylenylation of Si(111)

Scheme 5.1 shows the strategy utilized for functionalization of Si(111), using a two-step chlorination/alkylation method followed by Cu(I)-catalyzed click chemistry. The acetylene passivation leads to a high coverage of atop sites on an unreconstructed Si(111) surface ( $97 \pm 5\%$ ), which resists native oxidation of the surface.<sup>39,40</sup> Another advantage is the ability to use the terminal alkyne to attach a variety of molecules via click chemistry.

The starting surfaces used in these experiments were single crystal, polished Si(111) wafers that were 500 to 550  $\mu\text{m}$  thick, phosphorus-doped (n-type), with 0.005 to 0.02  $\Omega\text{-cm}$  resistivity, and a miscut angle of  $3^\circ$ - $4^\circ$  (Montco Silicon Technologies; Spring City, PA). Prior to use, the Si wafers (1 cm  $\times$  1 cm) were cleaned by successive sonications in acetone, methanol, and isopropanol. Substrates were then rinsed with Millipore (18 M $\Omega$ ) water and then placed into basic piranha solution (5:1:1 =  $\text{H}_2\text{O}:\text{H}_2\text{O}_2$ :



**Scheme 5.1.** Strategy for the functionalization of Si(111).

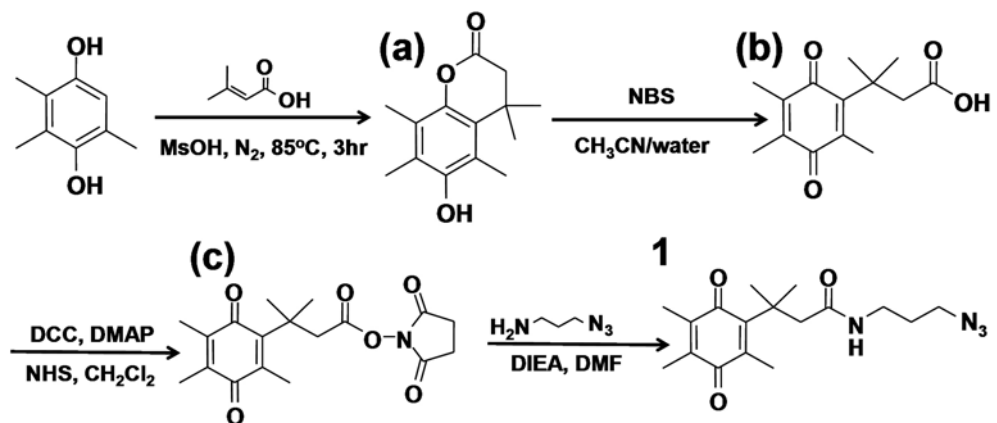
NH<sub>4</sub>OH *warning: caustic!*) at 80 °C for 5 min. The samples were removed from piranha solution, rinsed with copious amounts of Millipore water and dried under streaming N<sub>2</sub>(g). The samples were immediately placed in degassed NH<sub>4</sub>F(aq) solution for 15 min. The samples were subsequently removed from the NH<sub>4</sub>F(aq), rinsed copiously with water, dried under streaming N<sub>2</sub>(g), and immediately loaded into a glove box.

Chlorination of the Si(111) surfaces (Scheme 5.1, Step 1) was carried out in a N<sub>2</sub>(g)-purged glove box, according to published methods.<sup>33-40</sup> A saturated solution of PCl<sub>5</sub> in chlorobenzene was prepared and heated for 1 h before use to ensure complete dissolution of the PCl<sub>5</sub>. The Si substrate was added with a grain of benzoyl peroxide to this solution and heated to 90 °C for 50 min. Subsequently, the samples were rinsed with anhydrous THF several times and immediately used for the acetylenylation step.

Acetylenylation of the chlorinated Si(111) surfaces (Scheme 5.1, Step 2) was performed inside the N<sub>2</sub>(g)-purged glove box. The chlorinated wafers were immersed in a sodium acetylide (18 wt% in xylenes/light mineral oil) suspension and heated to 130 °C for 5 h.<sup>43</sup> After reaction, the samples were removed from solution, rinsed copiously with anhydrous THF, and then rinsed with anhydrous methanol. The samples were then immersed into a fresh volume of anhydrous methanol, removed from the glove box into air, sonicated for 10 min, and then dried in a stream of N<sub>2</sub>(g).

### 5.2.3 Synthesis of Electroactive Benzoquinone 1

Scheme 5.2 describes the synthetic procedure for making the electroactive benzoquinone **1** used for all surface click reactions.<sup>57</sup> A 2,3,5-trimethylhydroquinone was treated with dimethylacrylic acid to give a lactone (**a**) by a Friedel-Crafts type



**Scheme 5.2.** Synthesis of electroactive benzoquinone **1**.

addition reaction. The quinone acid (**b**) was prepared by oxidation of the resulting lactone (**a**) with aqueous N-bromosuccinimide (NBS). The acid was activated with an N-hydroxysuccinimidyl (NHS) group to give (**c**), which was then subjected to 3-azidopropylamine to afford **1**.

**6-Hydroxy-4,4,5,7,8-peptamethyl-chroman-2-one (a).** 2,3,5-Trimethylhydroquinone (2 g, 13.1 mmol) was mixed with 3,3-dimethylacrylic acid (1.45 g, 14.5 mmol) and methanesulfonic acid (10 mL). The mixture was stirred at 85 °C under nitrogen for 3 h and then cooled to room temperature. To the mixture, 100 g of ice was added with stirring. The precipitate was extracted with ethyl acetate (4 × 50 mL). The combined organic layer was washed with saturated NaHCO<sub>3</sub> (2 × 50 mL) and water (2 × 50 mL), and dried over MgSO<sub>4</sub>. After filtration and evaporation, an obtained residue was recrystallized from hexane and ethyl acetate (2:1, v/v) to give 2.6 g (84%) of the desired product as a white solid. <sup>1</sup>H NMR 300 MHz (CDCl<sub>3</sub>) δ 4.69 (s, 1H), 2.56 (s, 2H), 2.37 (s, 3H), 2.23 (s, 3H), 2.9 (s, 3H), 1.46 (s, 6H).

**3-Methyl-3-(2,4,5-trimethyl-3,6-dioxocyclohexa-1,4-dienyl)butanoic acid (b).** To a solution of the lactone **a** (1.58 g, 6.74 mmol) in a mixture of acetonitrile (15 mL) and water (3 mL) was added N-bromosuccinimide (1.26 g, 7.08 mmol) in portions with stirring at room temperature. After 30 min, the organic solvents were evaporated under reduced pressure, and the remaining solution was extracted with CH<sub>2</sub>Cl<sub>2</sub> (2 × 30 mL). The combined organic layer was dried over MgSO<sub>4</sub>, and reduced solvent to give 1.65 g (98%) of a yellow oily product, which was used without further purification. <sup>1</sup>H NMR 300 MHz (CDCl<sub>3</sub>) δ 3.04 (s, 2H), 2.15 (s, 3H), 1.96 (m, 3H), 1.94 (m, 3H), 1.45 (s, 6H).

**3-Methyl-3-(2,4,5-trimethyl-3,6-dioxocyclohexa-1,4-dienyl)butanoic acid, N-hydroxysuccinimidyl ester (c).** To a solution of acid **b** (326 mg, 1.30 mmol) and N-hydroxysuccinimide (152 mg, 1.32 mmol) in CH<sub>2</sub>Cl<sub>2</sub> (15 mL), was added 1,3-dicyclohexylcarbodiimide (DCC, 270 mg, 1.31 mmol) portionwise, followed by a catalytic amount of *N,N*-dimethylaminopyridine (DMAP). The reaction mixture was stirred for 1 h. The white precipitate was filtered and the filtrate was concentrated. The residue was redissolved in cold ethyl acetate (5 mL) and insoluble impurities were filtered. Solvent was removed to give 419 mg (93%) of a yellow foamy solid product. <sup>1</sup>H NMR 300 MHz (CDCl<sub>3</sub>) δ 3.27 (s, 2H), 2.77 (s, 4H), 2.15 (s, 3H), 1.94 (s, 6H), 1.51 (s, 6H).

**N-(3-azidopropyl)-3-methyl-3-(2,4,5-trimethyl-3,6-dioxocyclohexa-1,4-dienyl) butanamide (1).** To a solution of **c** (443 mg, 1.28 mmol) in DMF (5 mL) was added diisopropylethylamine (DIEA, 523 μL, 3.06 mmol), followed by 3-azidopropylamine (153 mg, 1.53 mmol). The reaction mixture was stirred overnight at 50 °C, diluted with ethyl acetate (30 mL), washed with NH<sub>4</sub>Cl and brine, and dried over MgSO<sub>4</sub>. Solvent was reduced and the residue was purified by silica gel chromatography (hex/EtOAc, 2:1) to give 370 mg (87%) of product as a yellow solid. <sup>1</sup>H NMR 300 MHz (CDCl<sub>3</sub>) δ 3.30 (t, J = 6.6, 2H), 3.23 (q, J = 6.6, 2H), 2.81 (s, 2H), 2.12 (s, 3H), 1.96 (m, 3H), 1.94 (m, 3H), 1.70 (quint, J = 6.6, 2H), 1.41 (s, 6H). Mass (ES) m/z 333.0 ([M + H]<sup>+</sup>).

#### 5.2.4 Click Reaction to Attach **1** onto Acetylene-Terminated Si(111)

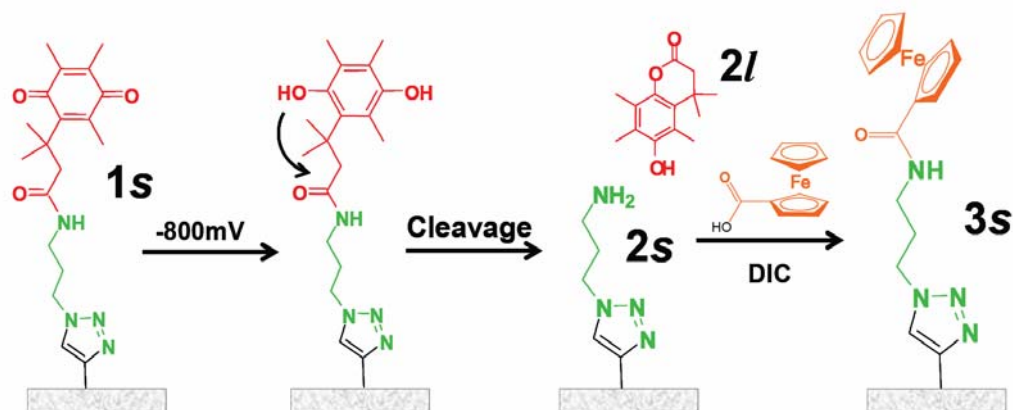
The click reaction of acetylene-terminated Si(111) (Scheme 5.1, Step 3) with **1**

(Scheme 5.2) was carried out in anhydrous DMF. Relative to the azide, 20 mol% sodium ascorbate was added, followed by 10 mol% of  $\text{CuSO}_4 \cdot 5\text{H}_2\text{O}$ , and a 10 mM azide solution of **1** in DMF. The reaction was run for 12 h in the glove box. After the reaction, the surface was sonicated in DMF for  $3 \times 5$  min and then rinsed with methanol and blow dried under  $\text{N}_2(\text{g})$ .

### 5.2.5 Electrochemical Activation to Attach Ferrocene Carboxylic Acid and Biotin

**1** was attached to acetylene-terminated Si(111) using the Cu(I)-catalyzed click reaction (Scheme 5.1, Step 3), to form **1s** (Scheme 5.3). Reductive electrochemistry ( $-800$  mV referenced to Ag/AgCl) was performed to convert the modified benzoquinone to hydroquinone in degassed DPBS (pH 7.4). The hydroquinone then underwent an intramolecular cyclization reaction, leaving a free amine on the surface (**2s**) and releasing a lactone species (**2l**). This amine terminus allows for a variety of subsequent reactions, including amide coupling chemistry, which is commonly utilized to attach biomolecules to surfaces. We first illustrated the use of this electrochemical reduction process to attach ferrocene carboxylic acid to the surface, to form **3s**, via amide coupling chemistry. Ferrocene carboxylic acid (0.02 M) and *N,N'*-diisopropylcarbodiimide (DIC) (0.13 M) in DMF were added to the free amine surface. The amide coupling reaction was run overnight covered in an  $\text{N}_2$ -purged glove box. The surface was then sonicated three times in DMF, then MeOH, and then blown dry.

Similarly, biotin (0.02 M) and DIC (0.13 M) in DMF were added to the free amine surface **2s**. The amide coupling reaction was run overnight in an  $\text{N}_2$ -purged glove box at  $50$  °C. The surface was then sonicated three times in DMF, then MeOH, and blow dried. Subsequently, the Nanogold streptavidin (10 pM in 0.05% Tween20/DPBS)



**Scheme 5.3.** The chemical and electrochemical steps involved in non-oxidatively activating Si(111) surfaces. The molecules or molecular components are colored to highlight their different functions. **1s** represents the surface-bound benzoquinone that resulted from the click reaction of **1** to the acetylene-modified Si(111) surface (reacted acetylene group drawn in black). Upon reduction at  $-800\text{ mV}$  (vs. Ag/AgCl) of the benzoquinone to the hydroquinone, an intramolecular cyclization reaction ensues to produce **2l** (red lactone leaving group) and **2s** (the green triazole ring with an amine terminus). This represents the activated surface. The ferrocene carboxylic acid (orange), a second electrochemically active molecule, is then coupled to the Si(111) surface.

was introduced for 15 min. The surface was sonicated in 0.05% Tween20/DPBS for 25 min and then water for 5 min. The gold particles were then amplified with gold enhancement reagents for 10 min and then sonicated in water for 5 min.

## **5.3 SURFACE CHARACTERIZATION**

### **5.3.1 X-ray Photoelectron Spectroscopy**

X-ray photoelectron spectroscopy (XPS) was utilized to characterize many of the steps of both Schemes 5.1 and 5.3. All XPS measurements were performed in an ultra-high vacuum chamber of an M-probe surface spectrometer that has been previously described.<sup>59</sup> All measurements were taken on the center of the sample at room temperature. Monochromatic Al K $\alpha$  X-rays (1486.6 eV) were incident at 35° from the sample surface and were used to excite electrons from samples. The emitted electrons were collected by a hemispherical analyzer at a take-off angle of 35° from the plane of the sample surface.

ESCA-2000 software was employed to collect and analyze the data. To get an overview of the species present in the sample, survey scans were run from 0 to 1000 binding eV (BeV). The Si 2p (97-106 BeV), Cl 2p (196-206 BeV), C 1s (282-292 BeV), N 1s (393-407 BeV), Fe 2p (695-745 BeV), and Au 4f (77-97 BeV) regions were investigated in detail.

### **5.3.2 Contact Angle Goniometry**

The sessile contact angle of water on the functionalized Si(111) surface was utilized as a measurement of the fidelity of the monolayer for all surfaces of Schemes 5.1 and 5.3 except H- and Cl-terminated Si(111). Contact angle measurements were

obtained with an NRL C.A. Goniometer Model #100-00 (Rame-Hart) at room temperature. Contact angles,  $\theta$ , were measured from sessile drops by lowering a 1  $\mu$ L drop from a syringe needle onto the surface. This was repeated three times and averaged to obtain the  $\theta$  for the surface.

### 5.3.3 Electrochemical Characterization of Surface Coverages

Reductive electrochemistry was performed on **1s** in a custom-made cell using a VMP Multi-Potentiostat (Princeton Applied Research, Oak Ridge, TN) (Figure 5.3). Dulbecco's Phosphate Buffered Saline (DPBS) was used as the electrolyte, with silicon as a working electrode, a Pt coil as a counter electrode, and an Ag/AgCl reference electrode. Cyclic voltammetry was carried out at a rate of 100 mV/s. Molecular coverage was obtained by integrating the cathodic peak of the first scan in which all the modified benzoquinone was reduced to hydroquinone.

### 5.3.4 Fourier-Transform Infrared Spectroscopy

The H- and H-C $\equiv$ C-terminated Si(111) surfaces were characterized by Attenuated Total Reflection Fourier Transform Infrared Spectroscopy (ATR-FTIR). The Si(111) surfaces were prepared from single-crystal, polished Si(111), miscut 3°-4°, boron-doped (p-type), 500 to 550  $\mu$ m thick, and with 4 to 20  $\Omega$ -cm resistivity (Addison Engineering; San Jose, CA). Samples were cut into (2 cm  $\times$  2 cm) pieces. Samples underwent the acetylenylation and click reactions as described above. Samples were mounted on a Germanium ATR crystal (GATR, Harrick Scientific Products) for a grazing angle of 65°. The sample was placed in a Vertex 70 FT-IR spectrometer (Bruker

Optics) for measurements. In an air-purged sample chamber, 512 or 1024 scans were taken, with background scans of air subtracted from the spectra. Spectra were fitted with a linear baseline prior to analysis.

## 5.4 RESULTS

### 5.4.1 XPS Survey Scans and Contact Angle Measurements

XPS survey scans revealed the progression of the acetylenylation and click chemistry steps. For a freshly prepared, H-terminated Si(111) surface (H-[Si(111)]), Si 2p and Si 2s peaks were observed, at 100 BeV and 150 BeV, respectively. Additional small C 1s and O 1s peaks, corresponding to adventitiously adsorbed carbon and oxygen on the surface, were also detected. After chlorination of H-[Si(111)] by PCl<sub>5</sub>, two new peaks at 200 BeV and 270 BeV appeared in the XPS spectrum, representing the Cl 2p and Cl 2s electrons, respectively. Upon a treatment with sodium acetylide, the chlorine peaks disappeared completely and a pronounced C 1s appeared at 285 BeV, verifying that the acetylene-terminated Si(111) surface (H-C≡C-[Si(111)]) has been generated. Other adsorbed carbon can contribute to the C 1s peak intensity for this scan. After the click reaction with electroactive quinone **1**, a new N 1s peak appears at 400 BeV.

Sessile contact angles were also quantified for the various surface functionalization steps described in Schemes 5.1 and 5.3, and those values are listed in Table 5.1.

### 5.4.2 High-Resolution XPS Measurements

High-resolution XPS measurements were utilized to quantitate the chemical steps of Schemes 5.1 and 5.3. In particular, the Si 2p region was used to monitor the growth

**Table 5.1.** Measured contact angles for various Si(111) surfaces.

Surfaces	Contact Angle (°)
H-C≡C-[Si(111)]	$77 \pm 2$
<b>1s</b>	$68 \pm 2$
<b>2s</b>	$60 \pm 2$
<b>3s</b>	$59 \pm 2$

of silicon oxides as a function of exposure time to air (Figure 5.1) and as a function of the chemical and electrochemical steps of Scheme 5.3 (Figure 5.2A) in two sets of experiments. For both measurements, a Shirley baseline was applied to each spectrum before the peaks were fitted. Peak line shapes for bulk Si  $2p_{3/2}$  and  $2p_{1/2}$  were fitted to Voigt functions fixed at 95% Gaussian and 5% Lorentzian, with a 15% asymmetry. The Si  $2p_{1/2}$  and  $2p_{3/2}$  peaks were fitted with the two peaks held 0.6 BeV apart, the full width at half maximum (FWHM) was fixed at 1, and the integrated area ratio of the  $2p_{1/2}/2p_{3/2}$  peaks was fixed at 0.51, as has been previously described.<sup>33–35,42</sup> The broad peak between 100 and 104 BeV was assigned as  $\text{Si}^+$  to  $\text{Si}^{4+}$  oxides and was fitted to a third peak. The positions of the three peaks and the width of the third peak were optimized to obtain the best fit to the experimental spectrum. For very thin oxide layers, the oxide coverage was calculated from the  $\text{SiO}_x:\text{Si}$  2p peak area ratio. This was determined by dividing the area under the third peak by the total area of the Si  $2p_{3/2}$  and  $2p_{1/2}$  peaks.<sup>35</sup> The  $\text{SiO}_x:\text{Si}$  2p peak area ratio was then divided by a normalization constant of 0.21 for Si(111) to estimate the fraction of surface atoms that was oxidized.<sup>33–35</sup>

We estimated that there were approximately 0.25 equivalent monolayers of  $\text{SiO}_x$  on the acetylene-terminated Si(111) surface after 6 days' exposure to air (Figure 5.1). This is consistent with other results that have shown stability toward oxidation for as long as 60 days in air.<sup>43</sup> Following the formation of **1s** and the reduction of **1s** to **2s** at  $-800$  mV (Scheme 5.3) in aqueous electrolyte, the amount of  $\text{SiO}_x$  was calculated to be 0.29 and 0.34 equivalent monolayers, respectively.

The  $\text{H-C}\equiv\text{C}[\text{Si}(111)]$  surface was also characterized using high-resolution C 1s XPS (Figure 5.2B). The resulting spectrum was deconvoluted and fitted to three peaks, the silicon-bonded carbon at 283.8 BeV, the carbon-bonded carbon at 284.9 BeV,

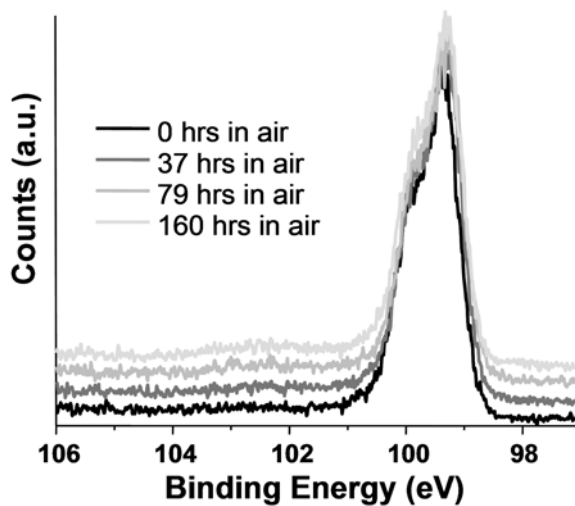


**Figure 5.1.** XPS data of H-C≡C-[Si(111)], collected in the Si 2p region, and taken after exposure to air for up to 160 h. The peaks for SiO<sub>x</sub> species should appear between 100 and 104 BeV. The amount of oxidation of the Si(111) can be estimated from this data to be about 0.25 equivalent monolayers. The Si 2p features are normalized to the same height for all three scans. The 37, 79, 160 h scans are shown offset from the 0 h scan to reveal the spectral detail.

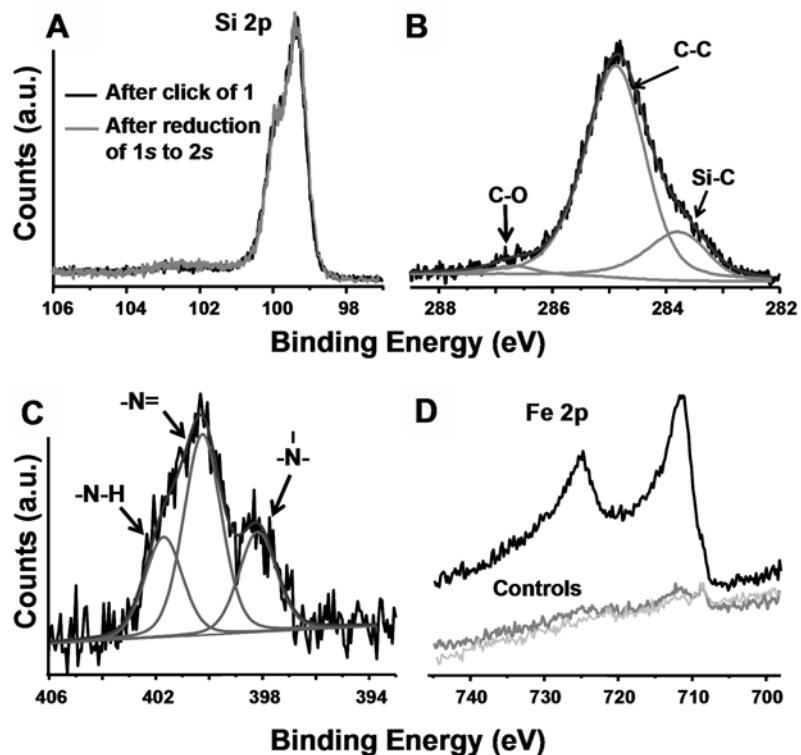


**Figure 5.2.** High-resolution XPS spectra of H-C≡C-[Si(111)], and of that surface following the click reaction to form **1s** and the reduction of **1s** to **2s**. **(A)** Si 2p region revealing the near absence of oxide growth during the Cu(I)-catalyzed click reaction, and during the reductive transformation of **1s** to **2s**. **(B)** Scan of the C 1s region of H-C≡C-[Si(111)]. The Si-C peak is unique to H-C≡C-[Si(111)] surfaces. The C-C peak contains contributions from the C≡C bond and adventitious carbon from the environment. The C-O peak present also arises from adventitious hydrocarbons. **(C)** Scan of the N 1s region of **1s**, validating the click formation of **1s**. The area ratio of the three peaks is 1:2:1, respectively. **(D)** Scan of the Fe 2p region showing the formation of **3s** via the amide coupling of ferrocene carboxylic acid to **2s**. The control plots are of **1s** (dark grey) and the H-C≡C-[Si(111)] surface (light grey) after exposure to ferrocene carboxylic acid under the same conditions.

and the oxygen-bonded carbon at 286.8 BeV. As developed by Nemanick,<sup>41,42</sup> peaks were fitted to Voigt functions having 70% Gaussian and 30% Lorentzian line shapes. The peak center-to-center distances were fixed at 1.1 BeV between the Si-C and C-C peaks, and at 2.9 BeV between the Si-C and O-C peaks. To calculate the surface coverage of the acetylene, the integrated area under the silicon-bonded carbon peak was ratioed to the total integrated area of the Si 2p<sub>3/2</sub> and 2p<sub>1/2</sub> peaks and normalized with respect to scan time. The ratio calculated was referenced to a methyl-terminated Si(111) surface that was scanned under the same conditions. The effective coverage of acetylene on the Si surface was  $97 \pm 5 \%$ , consistent with other measurements of such surfaces.<sup>43</sup> The statistical uncertainty in this number is largely determined by the signal-to-noise ratio of the XPS data (~30:1).

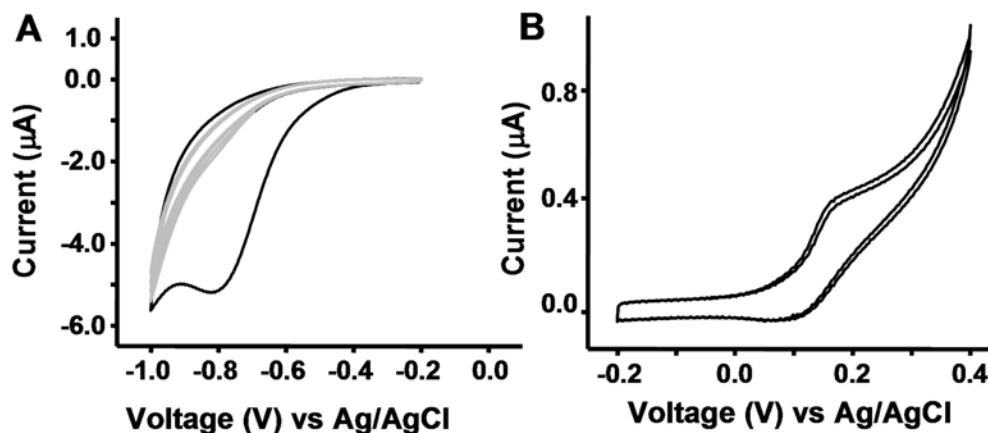
The high-resolution N 1s spectrum of **1s** illustrates the attachment of the benzoquinone (**1**) via click chemistry (Figure 5.2C). There is no peak at 405 BeV, signifying the absence of free azide. This result indicates that the azide-modified electroactive benzoquinone is not just freely adsorbed but covalently bonded to the surface.<sup>52</sup> The N 1s spectrum was deconvoluted and fitted to three peaks, each composed of 80% Gaussian and 20% Lorentzian line shapes.<sup>60</sup> The three peaks correspond to the amide nitrogen at 401.7 BeV, the doubly bonded nitrogen atoms (in the 1,2,3-triazole ring) at 400.3 BeV, and the singly bonded nitrogen (in the 1,2,3-triazole ring) at 398.2 BeV, respectively. The ratio of peak areas was found to be 1:2:1, consistent with the structure of **1s**. After electrochemical cleavage to **2s**, the N 1s region remained unchanged.

Figure 5.2D is a high-resolution scan of the Fe 2p region that demonstrates the attachment of ferrocene carboxylic acid onto **2s** to form **3s**. The Fe 2p<sub>3/2</sub> and 2p<sub>1/2</sub> peaks

occur at 711.3 and 724.8 BeV, respectively. It is difficult to quantify the amount of iron from such data because the peak shape is highly asymmetric and hard to deconvolute with a single Gaussian/Lorentzian function due to the strong multiplet splitting.<sup>60</sup> However, as discussed below, the surface coverage of **3s** can be estimated from cyclic voltammetry measurements. Figure 5.2D also shows two control experiments. Although a trace amount of ferrocene residue was detected on the controls, this measurement does confirm that the large majority of ferrocene is the result of the covalent bond formation between carboxylic acid of the ferrocene and the free amine of **2s**.

#### 5.4.3 Electrochemical Measurements

Figure 5.3A depicts the cyclic voltammogram (CV) for **1s**. The prominent cathodic peak in the first scan confirms the presence of electroactive benzoquinone and, therefore, that the click reaction proceeded. Molecular coverage was obtained by integrating the cathodic peak of the first scan, where all the modified benzoquinone was reduced to hydroquinone. Complete conversion of **1s** to **2s** accompanied by the release of **2I** (Scheme 5.3) was achieved at potentials below  $-0.9$  V. Consecutive CV scans demonstrated that no detectable benzoquinone remained. For the determination of coverage, the area under the cathodic peak was obtained after subtracting the non-Faradaic current. This area was converted to the number of molecules by a stoichiometric ratio of 2 electrons to 1 electroactive molecule. Then, the number of molecules was divided by the electrode surface area and then normalized to the Si atop atom surface density ( $7.8 \times 10^{14}$  /cm<sup>2</sup> for Si(111)).<sup>17</sup> The coverage calculated for **1s** on the H-C≡C-[Si(111)] was  $6.7 \pm 0.3$  %.



**Figure 5.3.** Cyclic voltammograms (CVs) for **1s** and **3s**. **(A)** The electrochemical activation of **1s** to **2s**. The black trace is of the first scan, and the grey traces are of two subsequent scans, indicating nearly complete conversion of benzoquinone to hydroquinone during the first scan. **(B)** The reversible oxidation of **3s**. Two subsequent scans are shown. CVs were performed at a rate of 100 mV/s with voltages relative to Ag/AgCl.

The amine terminus presented by **2s** provides a handle for subsequent reaction, including amide coupling chemistry, which is commonly utilized to attach biomolecules to surfaces. An exemplary surface is **3s**, the product of the amide coupling of ferrocene carboxylic acid with **2s**. The CVs of **3s** (Figure 5.3B) display reversible  $\text{Fc}^{0/+}$  redox behavior, as expected for ferrocene oxidation. The peak spacing confirms that ferrocene is covalently attached (but not adsorbed) onto the surface. The coverage was calculated by integrating the anodic peak after subtracting the non-Faradaic current. The number of molecules was divided by the electrode surface area and normalized to Si atom surface density which is  $7.8 \times 10^{14}/\text{cm}^2$  for Si(111).<sup>17</sup> The coverage calculated for **3s** was 0.5%. We do not fully understand the low coverage of ferrocene molecules. A likely possibility is that the time and/or temperature conditions for the coupling reaction were not optimal. It is also possible that degradation of the surface by oxidative potential treatments might also reduce the coverage of ferrocene.

## 5.5 DISCUSSION

The coverage values for H-C $\equiv$ C-[Si(111)], surface **1s**, and surface **3s** are summarized in Table 5.2, calculated with respect to all atop sites on an unreconstructed Si(111) surface.

The 97% coverage of the H-C $\equiv$ C-[Si(111)] surface is consistent with the Si 2p XPS in Figure 5.1 (and other studies<sup>43</sup>) that indicated little surface-bound SiO<sub>x</sub>. The acetylene carbons are *sp*-hybridized, implying a perpendicular attachment to the Si(111) surface. The atomic radius for C is smaller than that for Si (0.70 Å versus 1.10 Å), and there is a 3.8-Å spacing between atop sites on Si(111). These values support the notion

**Table 5.2.** The molecular surface coverages for various Si(111) surfaces, as measured by XPS or electrochemistry (EC).

Surfaces	Coverage (%)
H-C≡C-[Si(111)]	97 ± 5 (XPS)
<b>1s</b> – benzoquinone	6.7 ± 0.3 (EC)
<b>3s</b> – ferrocene	0.5 (EC)

that a 100% passivation of Si(111) surfaces can be achieved using the approach we described here.

Additional support for 100% acetylenylation of Si(111) comes from the ATR-FTIR measurements of H-[Si(111)] and H-C≡C-[Si(111)] (Figure 5.4; black and grey traces, respectively). Whereas XPS allows analysis of the elemental composition of surfaces, infrared spectroscopy (IR) gives information about the types of chemical functionality on a surface. The spectra shown in Figure 5.4 are expanded to highlight the region containing the signature Si-H ( $2083\text{ cm}^{-1}$ ) stretching frequency that is observed for the H-[Si(111)]. The Si-H stretch is strong and sharp, indicating that the surface sites are passivated with one hydrogen atom per atop site. This is expected for a H-[Si(111)] freshly prepared by an  $\text{NH}_4\text{F(aq)}$  etch.<sup>61</sup> For H-C≡C-[Si(111)], the  $2083\text{ cm}^{-1}$  vibration has quantitatively disappeared, again consistent with 100% acetylenylation and with other work.<sup>43</sup> A weak C≡C stretch might be expected in this region ( $2120$  to  $2175\text{ cm}^{-1}$ ),<sup>43,49</sup> although we have not observed it. When H-[Si(111)] is ethylated through a similar chlorination/alkylation procedure, the coverage of ethyl groups on the atop sites of the Si(111) surface is reduced by steric interactions to approximately 80%.<sup>40</sup> Following the Grignard alkylation of Si(111), no Cl is detected on the surface,<sup>33</sup> and FTIR data indicates that the remaining Si(111) atop sites are hydrogenated.<sup>62</sup> For the ethylated surface, the  $2083\text{ cm}^{-1}$  feature is broadened, shifted (to  $2070\text{ cm}^{-1}$ ) and reduced in intensity to 14% of that observed for the H-[Si(111)] surface.<sup>62</sup>

The coverage of the electroactive benzoquinone **1** on Si(111) to form **1s** was calculated to be ~7% of all available Si(111) atop sites. We previously reported on electrochemically activating Si(111) and Si(100) surfaces through the use of protected

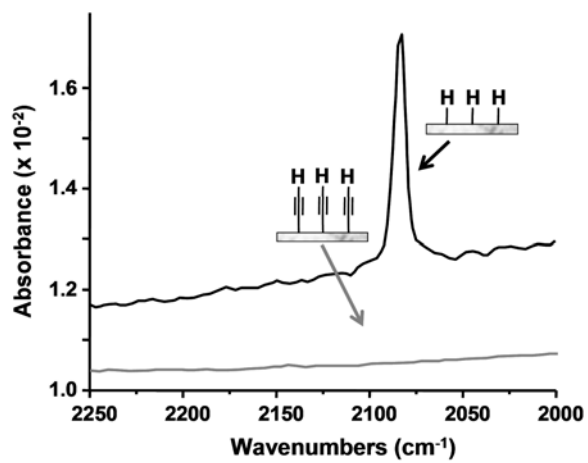


**Figure 5.4.** ATR-FTIR characterization of a H-[Si(111)] and H-C≡C-[Si(111)], in the region of the 2083 cm<sup>-1</sup> Si-H mode.

hydroquinones that were attached to H-terminated Si surfaces via UV activation.<sup>17</sup> For those molecules, coverages of up to 23% were achievable on Si(111), although bulkier protection groups on the hydroquinone led to slightly reduced surface coverages, implying steric interactions played at least some role in limiting coverage. It is likely that steric interactions play a dominating role in determining the efficiency of the click reaction to form **1s**. While the acetylene footprint may be approximated by the van der Waals radius of the carbon atom, the 1,2,3-triazole ring formed upon the click reaction will obviously be much larger. In fact, it is possible that the click chemistry is only effective at the step edges of the Si(111) surface. We have extensively characterized various Si(111) surfaces that have been alkylated using the two-step chlorination/alkylation chemistry using high-resolution Scanning Tunneling Microscopy (STM). For both methylated<sup>34,39</sup> and ethylated<sup>40</sup> Si(111), we find that about 10% of the Si surface atoms lie at step edges. This arises from etch pits that are apparently formed during the chlorination step, implying that the H-C≡C-[Si(111)] surface likely shares a similar morphology. In that case, acetylene groups located at step edges would not have the steric constraints that would limit the formation of the triazole ring. It is interesting that the 7% coverage of **2s** is similar to the number of Si atop sites that would reside at step edges. We are currently investigating the H-C≡C-[Si(111)] and **1s** surfaces using high-resolution STM to test this hypothesis.

We observed minimal oxide growth on an acetylenylated surface even after 6 days' exposure to air, indicating nearly 100% passivation of the surface (Figure 5.1). Following the formation of **1s** and electrochemical reduction of **1s** to **2s** to reveal the free amine, the amount of SiO<sub>x</sub> was slightly increased to 0.29 and 0.34 equivalent monolayers, respectively. The oxidation growth observed was due to the click chemistry

on acetylenylated surfaces that were minimally exposed to air during cleaning and preparation for reaction, and the electrochemistry which was carried out in an ambient (and aqueous) environment. It is notable that the limited oxide growth on the silicon even after all surface modifications afforded well-behaved electrodes.

There have been several reported examples of click reactions on metal surfaces, although relatively few papers have attempted to report quantitative coverage values. Chidsey's group<sup>51-53</sup> has reported on coverages of up to 55% of ferrocene molecules clicked onto  $\text{N}_3\text{-(CH}_2\text{)}_n\text{-S-[Au]}$  SAMs. On gold, each organic group has approximately twice the area available to it, as compared with the area available to each acetylene group on Si(111) [ $21.4 \text{ \AA}^2/\text{molecule}$  for gold and  $12.8 \text{ \AA}^2/\text{molecule}$  for Si(111)].<sup>17,63,64</sup> However, even for the much more loosely packed SAM, steric interactions were attributed as the reason for the incomplete (55%) yield of the click reaction.

The stated goal of this work was to develop a general strategy for electrochemically directing the biofunctionalization of Si(111) surfaces without oxidizing the underlying Si(111). To this end, we demonstrated the electrochemical activation and subsequent attachment of the model biomolecule, biotin, using a modification of the chemistry described in Scheme 5.3 (see Experimental Methods). To detect surface-bound biotin, we utilized Au nanoparticle-labeled streptavidin (strept-Au) and followed through with electroless amplification of the Au to produce particles that were imaged using Scanning Electron Microscopy (SEM). Representative data from this experiment, shown in Figure 5.5, indicate that the selectivity for attachment of strept-Au onto **2s** is about 100-fold greater than on two control surfaces,  $\text{H-C}\equiv\text{C-[Si(111)]}$  and **1s**, both of which were also treated with biotin and exposed to strept-Au.

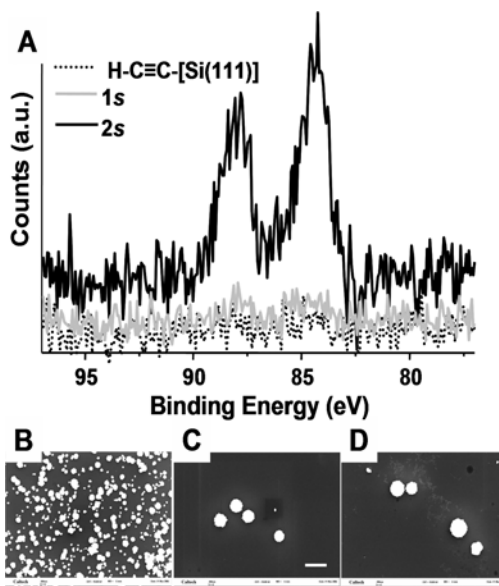


**Figure 5.5.** Demonstration of bioattachment to acetylenylated Si(111) through reductive formation of **2s** followed by the amide coupling of biotin. **(A)** XPS of the biotinylated Si(111) surface following exposure to strept-Au, but prior to the electroless Au amplification. The Au 4f region is comprised of two spin-orbit coupled peaks: Au 4f<sub>7/2</sub> (~84 BeV) and Au 4f<sub>5/2</sub> (~88 BeV). The dotted trace is from H-C≡C-[Si(111)], and the grey trace is from **1s**, each exposed to biotin and strept-Au as controls. The three SEM images **(B, C, D)** are of the activated and biofunctionalized surface, plus two controls. All images were taken following the electroless amplification step. The scale bar is 1 μm. **(B)** **2s**, incubated with biotin, and exposed to strept-Au. **(C)** H-C≡C-[Si(111)] incubated with biotin, and exposed to strept-Au. **(D)** **1s** incubated with biotin, and exposed to strept-Au. There are at least 500 Au nucleation sites on B, 5 on C, and 7 on D.

## 5.6 CONCLUSIONS

Acetylenylation of the Si(111) surface via the two-step chlorination/alkylation procedure was combined with click chemistry to provide a non-oxidative approach for adding chemical functionality to a silicon surface. Si(111) surfaces can be nearly 100% passivated with acetylene groups. A specifically designed, electroactive benzoquinone molecule has been immobilized to the H-C≡C-[Si(111)] surface. A 7% coverage of the benzoquinone was found, suggesting that the click reaction may have occurred at step edges on the H-C≡C-[Si(111)] surface. The attachment of an electroactive benzoquinone was highly selective and was accomplished with only a minimal amount of oxidation of the underlying Si(111). The electroactive benzoquinone was reduced and cleaved from the surface to produce an amine terminus. In separate experiments, ferrocene carboxylic acid and biotin were selectively and covalently immobilized to the electrochemically activated surface.

We believe this approach can be employed as a general platform to prepare functional surfaces for various applications and can be extended toward the selective biopassivation of arrays of various types of nanomechanical and/or nanoelectronic sensor devices.

## 5.7 ACKNOWLEDGEMENTS

This work was completed in collaboration with Rosemary D. Rohde, Woon-Seok Yeo, and Ryan C. Bailey. The XPS measurements were carried out at the Molecular Materials Research Center of the Beckman Institute at Caltech. We thank Professor Nate Lewis, Dr. Bruce Brunshwig, Dr. Pat Hurley, and Dr. Joseph Nemanick for kind advice and help regarding the acetylenylation of Si(111).

**5.8 REFERENCES**

1. Zheng, G.; Patolsky, F.; Cui, Y.; Wang, W. U.; Lieber, C. M. *Nat. Biotechnol.* **2005**, *23*, 1294–1301.
2. Beckmann, N.; Zahnd, C.; Huber, F.; Bietsch, A.; Plückthun, A.; Lang, H.-P.; Güntherodt, H.-J.; Hegner, M.; Gerber, C. *Proc. Natl. Acad. Sci. USA* **2005**, *102*, 14587–14592.
3. Yue, M.; Lin, H.; Dedrick, D. E.; Satyanarayana, S.; Majumdar, A.; Bedekar, A. S.; Jenkins, J. W.; Sundaram, S. *J. Microelectromech. Syst.* **2004**, *13*, 290–299.
4. Reccius, C. H.; Mannion, J. T.; Cross, J. D.; Craighead, H. G. *Phys. Rev. Lett.* **2005**, *95*, 268101.
5. Stavis, S. M.; Edel, J. B.; Li, Y. G.; Samiee, K. T.; Luo, D.; Craighead, H. G. *J. Appl. Phys.* **2005**, *98*, 044903.
6. Fan, R.; Karnik, R.; Yue, M.; Li, D. Y.; Majumdar, A.; Yang, P. D. *Nano Lett.* **2005**, *5*, 1633–1637.
7. Karnik, R.; Castelino, K.; Fan, R.; Yang, P.; Majumdar, A. *Nano Lett.* **2005**, *5*, 1638–1642.
8. (a) Craighead, H. G.; James, C. D.; Turner, A. M. P. *Curr. Opin. Solid State Mater. Sci.* **2001**, *5*, 177–184. (b) Jung, D. R.; Kapur, R.; Adams, T.; Giuliano, K. A.; Mrksich, M.; Craighead, H. G.; Taylor, D. L. *Crit. Rev. Biotechnol.* **2001**, *21*, 111–154.
9. For example, (a) Woolley, A. T.; Hadley, D.; Landre, P.; deMello, A. J.; Mathies, R. A.; Northrup, M. A. *Anal. Chem.* **1996**, *68*, 4081–4086. (b) Pantoja, R.; Nagarah, J. M.; Starace, D. M.; Melosh, N. A.; Blunck, R.; Bezanilla, F.; Heath, J. R. *Biosens. Bioelectron.* **2004**, *20*, 509–517.

10. Piner, R. D.; Zhu, J.; Xu, F.; Hong, S.; Mirkin, C. A. *Science* **1999**, *283*, 661–663.
11. Lee, K.-B.; Park, S.-J.; Mirkin, C. A.; Smith, J. C.; Mrksich, M. *Science* **2003**, *295*, 1702–1705.
12. Jung, H.; Dalal, C. K.; Kuntz, S.; Shah, R.; Collier, C. P. *Nano Lett.* **2004**, *4*, 2171–2177.
13. Yousaf, M.; Mrksich, M. *J. Am. Chem. Soc.* **1999**, *121*, 4286–4287.
14. Hodneland, C. D.; Mrksich, M. *J. Am. Chem. Soc.* **2000**, *122*, 4235–4236.
15. Yeo, W.-S.; Yousaf, M. N.; Mrksich, M. *J. Am. Chem. Soc.* **2003**, *125*, 14994–14995.
16. Yeo, W.-S.; Mrksich, M. *Adv. Mater.* **2004**, *16*, 1352–1356.
17. Bunimovich, Y. L.; Ge, G.; Beverly, K. C.; Ries, R. S.; Hood, L.; Heath, J. R. *Langmuir* **2004**, *20*, 10630–10638.
18. Curreli, M.; Li, C.; Sun, Y.; Lei, B.; Gundersen, M. A.; Thompson, M. E.; Zhou, C. *J. Am. Chem. Soc.* **2005**, *127*, 6922–6923.
19. (a) Hu, K.; Fan, F.-R. F.; Bard, A. J.; Hillier, A. C. *J. Phys. Chem. B* **1997**, *101*, 8298–8303. (b) Yeganeh, M. S.; Dougal, S. M.; Pink, H. S. *Phys. Rev. Lett.* **1999**, *83*, 1179–1182.
20. (a) Israelachvili, J. *Intermolecular and Surface Forces* (London: Academic Press, 1985). (b) Lud, S. Q.; Nikolaidis, M. G.; Haase, I.; Fischer, M.; Bausch, A. R. *ChemPhysChem* **2006**, *7*, 379–384. (c) Neff, P. A.; Wunderlich, B. K.; Lud, S. Q.; Bausch, A. R. *Phys. Status Solidi A* **2006**, *203*, 3417–3423.
21. Buriak, J. M. *Chem. Rev.* **2002**, *102*, 1271–1308.

22. Yablonovitch, E.; Allara, D. L.; Chang, C. C.; Gmitter, T.; Bright, T. B. *Phys. Rev. Lett.* **1986**, *57*, 249–252.
23. Sung, M. M.; Kluth, G. J.; Yauw, O. W.; Maboudian, R. *Langmuir* **1997**, *13*, 6164–6168.
24. Sieval, A. B.; Demirel, A. L.; Nissink, J. W. M.; Linford, M. R.; van der Maas, J. H.; de Jeu, W. H.; Zuilhof, H.; Sudhölter, E. J. R. *Langmuir* **1998**, *14*, 1759–1768.
25. Effenberger, F.; Gotz, G.; Bidlingmaier, B.; Wezstein, M. *Angew. Chem. Int. Ed.* **1998**, *37*, 2462–2464.
26. Boukherroub, R.; Wayner, D. D. M. *J. Am. Chem. Soc.* **1999**, *121*, 11513–11515.
27. Linford, M. R.; Fender, P.; Eisenberger, P. M.; Chidsey, C. E. D. *J. Am. Chem. Soc.* **1995**, *117*, 3145–3155.
28. Cicero, R. L.; Linford, M. R.; Chidsey, C. E. D. *Langmuir* **2000**, *16*, 5688–5695.
29. Buriak, J. M.; Allen, M. J. *J. Am. Chem. Soc.* **1998**, *120*, 1339–1340.
30. Stewart, M. P.; Buriak, J. M. *J. Am. Chem. Soc.* **2001**, *123*, 7821–7830.
31. Boukherroub, R.; Morin, S.; Bensebaa, F.; Wayner, D. D. M. *Langmuir* **1999**, *15*, 3831–3835.
32. Zhang, L.; Li, L.; Chen, S.; Jiang, S. *Langmuir* **2002**, *18*, 5448–5456.
33. Webb, L. J.; Nemanick, E. J.; Biteen, J. S.; Knapp, D. W.; Michalak, D. J.; Traub, M. C.; Chan, A. S. Y.; Brunshwig, B. S.; Lewis, N. S. *J. Phys. Chem. B* **2005**, *109*, 3930–3937.
34. Yu, H. B.; Webb, L. J.; Ries, R. S.; Solares, S. D.; Goddard, W. A.; Heath, J. R.; Lewis, N. S. *J. Phys. Chem. B* **2005**, *109*, 671–674.
35. Webb, L. J.; Lewis, N. S. *J. Phys. Chem. B* **2003**, *107*, 5404–5412.

36. Bansal, A.; Li, X. L.; Yi, S. I.; Weinberg, W. H.; Lewis, N. S. *J. Phys. Chem. B* **2001**, *105*, 10266–10277.
37. Royea, W. J.; Juang, A.; Lewis, N. S. *Appl. Phys. Lett.* **2000**, *77*, 1988–1990.
38. Bansal, A.; Lewis, N. S. *J. Phys. Chem. B* **1998**, *102*, 4058–4060.
39. Solares, S. D.; Yu, H.; Webb, L. J.; Lewis, N. S.; Heath, J. R.; Goddard, W. A., III. *J. Am. Chem. Soc.* **2006**, *128*, 3850–3851.
40. Yu, H.; Webb, L. J.; Solares, S. D.; Cao, P.; Goddard, W. A., III; Heath, J. R.; Lewis, N. S. *J. Phys. Chem. B* **2006**, *110*, 23898–23903.
41. Nemanick, E. J. Chemical and electrical passivation of single crystal silicon surfaces through covalently bound organic monolayers. Ph.D. thesis: California Institute of Technology, 2005.
42. Nemanick, E. J.; Hurley, P. T.; Brunschwig, B. S.; Lewis, N. S. *J. Phys. Chem. B* **2006**, *110*, 14800–14808.
43. Hurley, P. T.; Nemanick, E. J.; Brunschwig, B. S.; Lewis, N. S. *J. Am. Chem. Soc.* **2006**, *128*, 9990–9991.
44. Kolb, H. C.; Finn, M. G.; Sharpless, K. B. *Angew. Chem. Int. Ed.* **2001**, *40*, 2004–2021.
45. Bock, V. D.; Hiemstra, H.; van Maarseveen, J. H. *Eur. J. Org. Chem.* **2006**, 51–68.
46. Zhang, Y.; Luo, S.; Tang, Y.; Yu, L.; Hou, K.-Y.; Cheng, J. P.; Zeng, X.; Wang, P. G. *Anal. Chem.* **2006**, *78*, 2001–2008.
47. Lummerstorfer, T.; Hoffmann, H. *J. Phys. Chem. B* **2004**, *108*, 3963–3966.
48. Lee, J. K.; Chi, Y. S.; Choi, I. S. *Langmuir* **2004**, *20*, 3844–3847.

49. Li, H.; Cheng, F.; Duft, A. M.; Adronov, A. *J. Am. Chem. Soc.* **2005**, *127*, 14518–14524.
50. Zirbs, R.; Kienberger, F.; Hinterdorfer, P.; Binder, W. H. *Langmuir* **2005**, *21*, 8414–8421.
51. Collman, J. P.; Devaraj, N. K.; Chidsey, C. E. D. *Langmuir* **2004**, *20*, 1051–1053.
52. Collman, J. P.; Devaraj, N. K.; Eberspacher, T. P. A.; Chidsey, C. E. D. *Langmuir* **2006**, *22*, 2457–2464.
53. Devaraj, N. K.; Dinolfo, P. H.; Chidsey, C. E. D.; Collman, J. P. *J. Am. Chem. Soc.* **2006**, *128*, 1794–1795.
54. Devaraj, N. K.; Miller, G. P.; Ebina, W.; Kakaradov, B.; Collman, J. P.; Kool, E. T.; Chidsey, C. E. D. *J. Am. Chem. Soc.* **2005**, *127*, 8600–8601.
55. Giovanelli, D.; Lawrence, N. S.; Jiang, L.; Jones, T. G. J.; Compton, R. G. *Anal. Lett.* **2003**, *36*, 2941–2959.
56. Rousell, C.; Rohner, T. C.; Jensen, H.; Girault, H. H. *ChemPhysChem* **2003**, *4*, 200–206.
57. Zheng, A.; Shan, D.; Binghe, W. *J. Org. Chem.* **1999**, *64*, 156–161.
58. Yeo, W.-S.; Hodneland, C. D.; Mrksich, M. *ChemBioChem* **2001**, *2*, 590–593.
59. Haber, J. A.; Lewis, N. S. *J. Phys. Chem. B* **2002**, *106*, 3639–3656.
60. Babić-Samardžija, K.; Lupu, C.; Hackerman, N.; Barron, A. R.; Luttge, A. *Langmuir* **2005**, *21*, 12187–12196.
61. Dumas, P.; Chabal, Y. J.; Higashi, G. S. *Phys. Rev. Lett.* **1990**, *65*, 1124–1127.
62. Webb, L. J.; Rivillon, S.; Michalak, D. J.; Chabal, Y. J.; Lewis, N. S. *J. Phys. Chem. B* **2006**, *110*, 7349–7356.

63. Strong, L.; Whitesides, G. M. *Langmuir* **1988**, *4*, 546–558.
64. Chidsey, C. E. D.; Bertozzi, C. R.; Putvinski, T. M.; Muzsca, A. M. *J. Am. Chem. Soc.* **1990**, *112*, 4301–4306.

## **Appendix A**

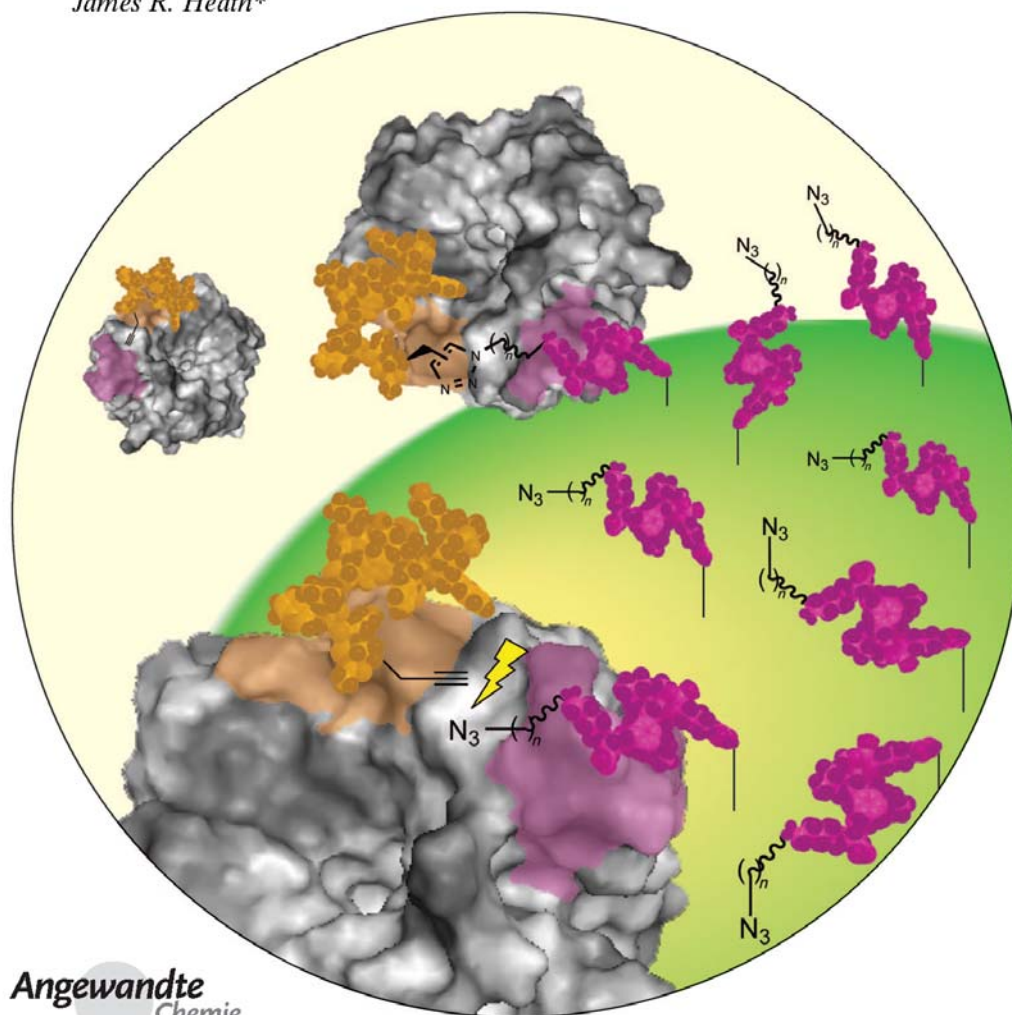
Iterative In Situ Click Chemistry Creates Antibody-Like Protein Capture Agents

Reproduced from

*Angewandte Chemie International Edition* **2009**, *48*, 4944–4948

## Iterative In Situ Click Chemistry Creates Antibody-like Protein-Capture Agents\*\*

Heather D. Agnew, Rosemary D. Rohde, Steven W. Millward, Arundhati Nag, Woon-Seok Yeo, Jason E. Hein, Suresh M. Pitram, Abdul Ahad Tariq, Vanessa M. Burns, Russell J. Krom, Valery V. Fokin, K. Barry Sharpless, and James R. Heath\*



Angewandte  
Chemie

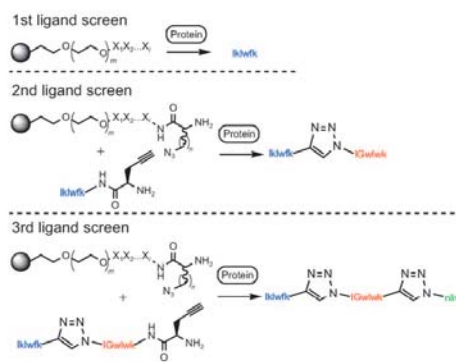
4944  InterScience

© 2009 Wiley-VCH Verlag GmbH & Co. KGaA, Weinheim

Angew. Chem. Int. Ed. 2009, 48, 4944–4948

Most protein-detection methods rely upon antibody-based capture agents.<sup>[1]</sup> A high-quality antibody exhibits high affinity and selectivity for its cognate protein. However, antibodies are expensive and can be unstable towards dehydration, pH variation, thermal shock, and many other chemical and biochemical processes.<sup>[2,3]</sup> Several alternative protein-capture agents, including oligonucleotide aptamers and phage-display peptides, have been reported, each of which has advantages as well as significant limitations.<sup>[4–10]</sup> A further alternative is the use of one-bead-one-compound (OBOC) peptide or peptide-mimetic libraries.<sup>[11–15]</sup> An advantage of OBOC libraries is that chemical stability, water solubility, and other desired properties may be designed into the compounds. However, OBOC libraries contain typically only  $10^3$ – $10^6$  elements, and so significant trade-offs are made between peptide length and library chemical diversity. Herein we report the use of *in situ* click chemistry as a screening approach towards the construction of multi-ligand protein-capture agents (Scheme 1). We harnessed the method to produce a triligand capture agent against human and bovine carbonic anhydrase II (h(b)CAII) as a model system.

*In situ* click chemistry has been utilized previously for the rapid identification of small-molecule enzymatic inhibitors.<sup>[16–20]</sup> These studies implemented libraries of small-molecule building blocks functionalized with either azide or acetylene groups. During the screening of the target protein with the molecular libraries, the protein plays an active role in the selection and covalent assembly of a new inhibitor. In these systems, the protein accelerates the Huisgen 1,3-dipolar cycloaddition by holding the two fragments—azide and acetylene—in proximity. The protein exhibits exquisite selectivity; it promotes the formation of a 1,2,3-triazole (Tz) between those library elements that can be brought into a



**Scheme 1.** Representation of an *in situ* screen based on click chemistry for the preparation of a multi-ligand protein-capture agent. 1st: A comprehensive OBOC peptide library on TentaGel (TG) beads ( $x_i$ : variable region) is incubated together with a fluorescently labeled protein target. Hit beads are identified on the basis of their fluorescence intensity. 2nd: A hit peptide from the 1st screen is employed as the anchor ligand and incubated in the presence of the OBOC peptide library, in which the peptides are now appended with an azide linker ( $n=4, 8$ ). 3rd: The process is repeated, but with the biligand from the 2nd screen as the new anchor unit to enable the rapid identification of higher-order multi-ligand capture agents.

precise relative molecular orientation on the protein surface. The result is a biligand inhibitor with an affinity that approaches the full product of the affinities of the individual molecular components. Furthermore, the triazole itself can contribute to the binding affinity observed for this inhibitor.

The advances we report herein are manifold. First, the production of the capture agent does not require prior knowledge of affinity agents against the target protein. Our anchor ligand was a relatively weakly binding short heptapeptide comprised of non-natural D-amino acids and a terminal, acetylene-containing amino acid (D-propargylglycine, D-Pra). It was identified by using a standard, two-generation OBOC screen against bCAII; the peptide sequence on the hit beads was identified by Edman degradation (see the Supporting Information). This first anchor ligand, kklwfk-(D-Pra), exhibited an approximately 500  $\mu\text{M}$  affinity for bCAII (see the Supporting Information). The second advance is that the *in situ* click screen (Scheme 1) samples a very large chemical space. Our OBOC library consisted of short-chain peptides and was comprehensive. We utilized five copies of a  $2 \times 10^7$ -element library of D stereoisomers:  $Az_n-x_2-x_3-x_4-x_5-x_6-Az_n$  ( $Az_n$  = azide-containing amino acids ( $n=4, 8$ );  $x_i$  = any D-amino acid except Cys).  $Az_n$  building blocks were prepared by published methods (see the Supporting Information).<sup>[21–23]</sup>

The third advance is that the process can be repeated. Once a biligand has been identified, that biligand can serve as the anchor ligand. The same OBOC library is employed to identify a triligand, and so forth (Scheme 1). Upon the addition of each ligand to the capture agent, the affinity and the selectivity of the capture agent for its cognate protein

[\*] H. D. Agnew, R. D. Rohde, Dr. S. W. Millward, A. Nag, Dr. W.-S. Yeo,<sup>[†]</sup> A. A. Tariq, V. M. Burns, R. J. Krom, Prof. J. R. Heath  
Division of Chemistry and Chemical Engineering  
California Institute of Technology  
1200 East California Boulevard, Pasadena, CA 91125 (USA)  
Fax: (+1) 626-395-2355  
E-mail: heath@caltech.edu  
Homepage: <http://www.its.caltech.edu/~heathgrp>

Dr. J. E. Hein, Dr. S. M. Pitram, Prof. V. V. Fokin, Prof. K. B. Sharpless  
Department of Chemistry and  
The Skaggs Institute for Chemical Biology  
The Scripps Research Institute  
10550 North Torrey Pines Road, La Jolla, CA 92037 (USA)

[†] Current address: Department of Bioscience and Biotechnology  
Konkuk University, Seoul, 143-701 (Korea)

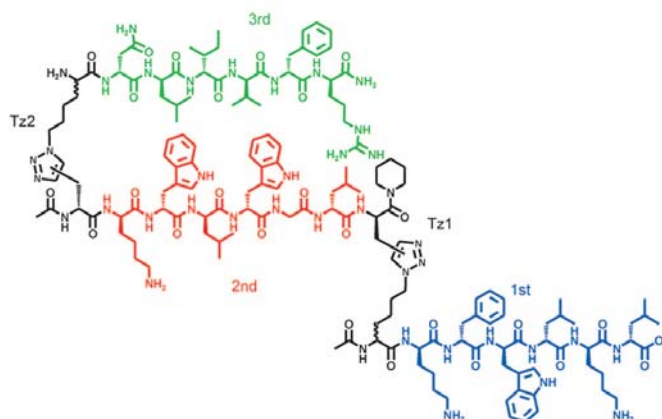
[\*\*] This research was supported by the National Cancer Institute, grant No. 5U54 CA119347 (J.R.H.), the W. M. Keck Foundation (K.B.S.), and a subcontract from the MITRE Corporation (J.R.H.). Postdoctoral and graduate fellowships were provided by the NSF and PEO (H.D.A.), the Gates Foundation (R.D.R.), the NSERC (J.E.H.), and the NCI (S.W.M.). We also acknowledge H. C. Kolb, S. S. Lee, J. Cha, J. Lim, S. Tan, S. Y. Yeo, A. Srivastava, M. Barrientos, E. Johnson Chavarria, A. Stuparu, J. Vielmetter, and C. S. Parker for useful discussions and assistance.

Supporting information for this article is available on the WWW under <http://dx.doi.org/10.1002/anie.200900488>.

## Communications

increase rapidly. With lklwfk-(D-Pra) as the anchor ligand, we used the screen in Scheme 1, followed by a more focused screen against a much smaller OBOC library, to identify the biligand (D-Pra)-kwlwGI-Tz1-kfwlkl against bCAII. This biligand exhibited a  $3 \mu\text{M}$  binding affinity for bCAII, as measured by surface plasmon resonance (SPR). With this biligand as the new anchor unit, we repeated the screen in Scheme 1, followed again by a focused screen in situ, to identify a triligand, rfviln-Tz2-kwlwGI-Tz1-kfwlkl (Scheme 2), which exhibited 64 and 45 nM binding affinities against bCAII and hCAII, respectively, as determined by SPR.<sup>[24]</sup> The triligand can be prepared in bulk quantities by standard solid-phase synthesis of the individual heptapeptides followed by ligation through the copper(I)-catalyzed azide-alkyne cycloaddition (CuAAC).<sup>[25]</sup> Details of all screening conditions and OBOC libraries are in the Supporting Information.

In the case of previously reported screens based on in situ click chemistry, the triazole product, or biligand inhibitor, was identified by chromatographic separation followed by mass spectrometry.<sup>[16–20]</sup> In the screen in Scheme 1, the triazole product represents a very small fraction of the peptide on the bead, and so only the variable region of the peptide is



**Scheme 2.** Triligand capture agent for the protein b(h)CAII. The triazoles (Tz1, Tz2) can be either 1,4 (*anti*) or 1,5 (*syn*) isomers since the protein-templated reaction can produce both products.

identified during the peptide-sequencing step. Thus, we sought to confirm the validity of the in situ screen in multiple ways.

For triligand screens, we generated a histogram to chart the position-dependent frequency of amino acids observed on the hit beads (Figure 1). On the basis of this histogram, we constructed two focused OBOC libraries. The first library contained only the 3rd-ligand variable region and was used in an in situ screen. The second library contained the same 3rd-ligand variable region and was coupled by CuAAC (Tz2;

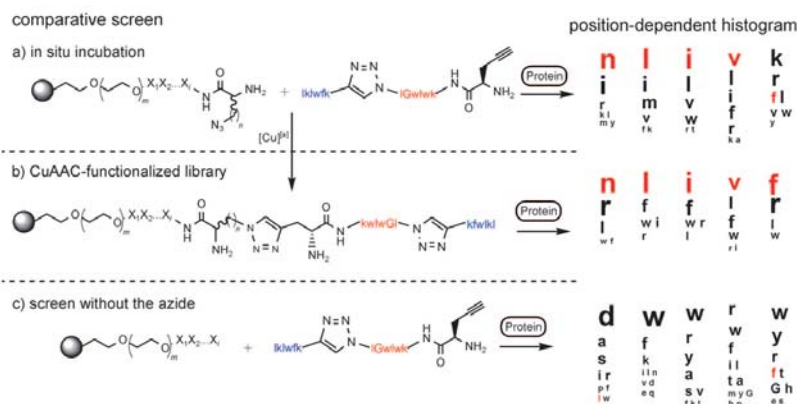


**Figure 1.** Position-dependent histograms for the first-generation in situ click screens (for peptides with (a) and without (c) an azide-containing amino acid) to generate a triligand. a) For the in situ screen, a third of the beads had no azide group at the  $x_1$  and  $x_2$  positions, but all hit beads contained an azide group. b) First- and second-generation CuAAC-library screens yielded independent validation of the result obtained in the in situ screens. The final, consensus triligand sequence is indicated by red font. c) In the absence of the azide functionality, completely different hit sequences were obtained. Sample size: in situ, 25 hits; in situ, no azide, 24 hits; CuAAC library, 21 hits. [a] See the Supporting Information for CuAAC conditions.

Scheme 2), to the biligand. This on-bead triligand screen and the in situ screen both yielded the same consensus sequence. This result confirmed the equivalence of the two screen types. We also carried out a third in situ screen in which the Az<sub>n</sub> (azide-containing) amino acid was not included in the OBOC library. The formation of a triazole linkage was thus prohibited. This screen generated a very different, and much less homologous, set of hit sequences (Figure 1). This result confirmed the importance of the triazole linkage in the formation of a multiligand species.

Finally, we developed an enzyme-linked colorimetric assay for detecting the on-bead, protein-templated multiligand inhibitor (Figure 2a). For this assay, we prepared a biotin conjugate of the biligand anchor (biotin-(EG)<sub>5</sub>-(D-Pra)-kwGf-Tz1-kfwkI; EG = ethylene glycol), which was then employed in an in situ OBOC screen (Scheme 1) with beads appended with the single consensus 3rd ligand Az4-nlvfr. After the screen, alkaline phosphatase-streptavidin (AP-SA) was introduced to bind to any potential bead-bound biotinylated triligand. Excess AP-SA was removed, and the beads were incubated with 5-bromo-4-chloro-3-indoyl phosphate (BCIP), a chromogenic substrate for AP (Figure 2b; see the Supporting Information for details).<sup>[26]</sup> The purple color is a positive indicator for an on-bead triligand. The triligand was only formed in the presence of the protein b(h)CAII, and not when the protein substrate was transferrin (Tf), bovine serum albumin (BSA), or absent. Similarly, the on-bead triligand was not obtained when the incorrect biligand anchor sequence was used.

For the first-generation biligand and triligand screens, a striking result was the extremely high sequence homology that was observed for the hit beads. For example, for the first 17 hit beads sequenced from the initial biligand in situ screen (with five copies of a  $2 \times 10^7$ -element OBOC library), two peptides were identical, and a third peptide differed by only a single amino acid (see the Supporting Information). For the initial triligand screen (against the same library), the most commonly observed amino acids by position (Figure 1) reflect

the consensus sequence identified in the second-generation (focused) screen almost exactly. Such sequence homology is unique to the in situ screens and suggests that these screens generate highly selective hits. Thus, multiligand capture agents identified in this way should exhibit high selectivity. In a dot-blot experiment, b(h)CAII was detected selectively by the triligand in 10% porcine serum with a detection limit of 20 ng of the protein (Figure 3; see the Supporting Information for details). The sequence identity of the proteins bCAII and hCAII is greater than 80% (PDB ID: 1CA2, 1V9E).

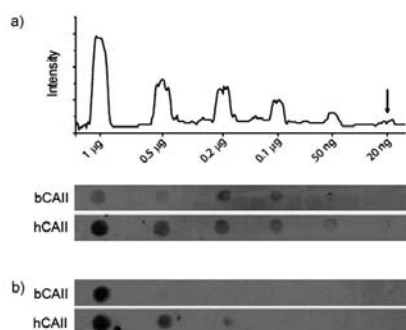


**Figure 3.** a) Dot blot illustrating the limit of detection by the triligand for b(h)CAII in 10% porcine serum. b) When the biligand anchor (D-Pra)-kwGf-Tz1-kfwkI was used as the capture agent in 0.1% serum, the sensitivity was reduced more than 10-fold.

The protein bCAII is also known to have intrinsic esterase activity. It catalyzes the hydrolysis of 4-nitrophenyl acetate (4-NPA) to the chromophore 4-nitrophenol (4-NP).<sup>[27]</sup> Thus, we utilized the 4-NPA assay to determine whether the triligand binds to the active site (see the Supporting Information). The

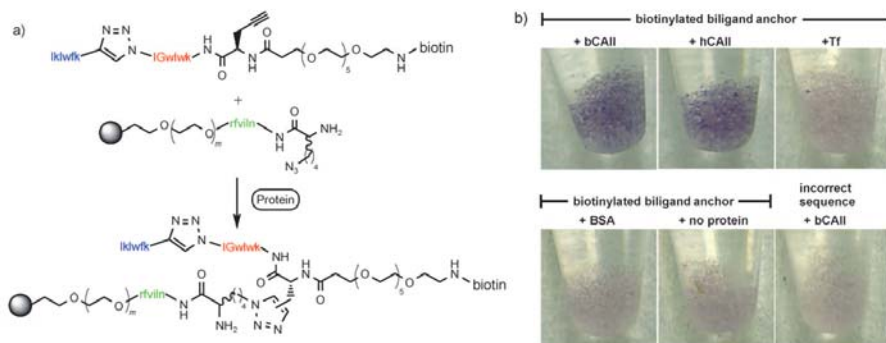


**Figure 2.** a) Scheme for the in situ click assay for on-bead triazole formation with a biotinylated biligand anchor (biotin-(EG)<sub>5</sub>-(D-Pra)-kwGf-Tz1-kfwkI). b) After treatment with AP-SA then BCIP, purple beads are a positive indicator of triazole formation. The triligand was only formed by the in situ process in the presence of b(h)CAII, and not when the protein was Tf, BSA, or absent. The on-bead triligand was not observed when the biligand anchor sequence was incorrect.

## Communications

triligand did not interfere with the enzyme activity of bCAII; it apparently binds away from the active site, or at least does not interfere with the normal catalysis of the active site. Such off-site, yet highly selective, binding is common for natural antibodies raised against proteins and bodes well for the scope of the technique we have described.

We are currently exploring the limits of the binding affinity that can be attained with these multiligand inhibitors and developing multiligand capture agents against other proteins so as to demonstrate the generality and/or limitations of this approach.

Received: January 26, 2009  
Published online: March 19, 2009

**Keywords:** click chemistry · combinatorial chemistry · inhibitors · peptides · protein-capture agents

- [1] C. A. K. Borrebaeck, *Immunol. Today* **2000**, *21*, 379.
- [2] T. Kodadek, M. M. Reddy, H. J. Olivos, K. Bachhawat-Sikder, P. G. Alluri, *Acc. Chem. Res.* **2004**, *37*, 711.
- [3] N. Blow, *Nature* **2007**, *447*, 741.
- [4] G. P. Smith, V. A. Petrenko, *Chem. Rev.* **1997**, *97*, 391.
- [5] J. C. Cox, A. Hayhurst, J. Hesselberth, T. S. Bayer, G. Georgiou, A. D. Ellington, *Nucleic Acids Res.* **2002**, *30*, 108e.
- [6] T. G. McCauley, N. Hamaguchi, M. Stanton, *Anal. Biochem.* **2003**, *319*, 244.
- [7] J. F. Lee, J. R. Hesselberth, L. A. Meyers, A. D. Ellington, *Nucleic Acids Res.* **2004**, *32*, 95D.
- [8] L. Gold, B. Polisky, O. Uhlenbeck, M. Yarus, *Annu. Rev. Biochem.* **1995**, *64*, 763.
- [9] P. E. Burnmeister, S. D. Lewis, R. F. Silva, J. R. Preiss, L. R. Horwitz, P. S. Pendergrast, T. G. McCauley, J. C. Kurz, D. M. Epstein, C. Wilson, A. D. Keefe, *Chem. Biol.* **2005**, *12*, 25.
- [10] D. Proske, M. Blank, R. Buhmann, A. Resch, *Appl. Microbiol. Biotechnol.* **2005**, *69*, 367.
- [11] K. S. Lam, M. Lebl, V. Krchňák, *Chem. Rev.* **1997**, *97*, 411.
- [12] A. Furka, F. Sebestyen, M. Asgedom, G. Dibo, *Int. J. Pept. Protein Res.* **1991**, *37*, 487.
- [13] H. M. Geysen, T. J. Mason, *Bioorg. Med. Chem. Lett.* **1993**, *3*, 397.
- [14] P. G. Alluri, M. M. Reddy, K. Bachhawat-Sikder, H. J. Olivos, T. Kodadek, *J. Am. Chem. Soc.* **2003**, *125*, 13995.
- [15] a) M. M. Reddy, K. Bachhawat-Sikder, T. Kodadek, *Chem. Biol.* **2004**, *11*, 1127; b) D. G. Udugamasooriya, S. P. Dineen, R. A. Brekken, T. Kodadek, *J. Am. Chem. Soc.* **2008**, *130*, 5744.
- [16] W. G. Lewis, L. G. Green, F. Grynszpan, Z. Radić, P. R. Carlier, P. Taylor, M. G. Finn, K. B. Sharpless, *Angew. Chem.* **2002**, *114*, 1095; *Angew. Chem. Int. Ed.* **2002**, *41*, 1053.
- [17] R. Manetsch, A. Krasniński, Z. Radić, J. Raushel, P. Taylor, K. B. Sharpless, H. C. Kolb, *J. Am. Chem. Soc.* **2004**, *126*, 12809.
- [18] Y. Bourne, H. C. Kolb, Z. Radić, K. B. Sharpless, P. Taylor, P. Marchot, *Proc. Natl. Acad. Sci. USA* **2004**, *101*, 1449.
- [19] V. P. Mocharla, B. Colasson, L. V. Lee, S. Röper, K. B. Sharpless, C.-H. Wong, H. C. Kolb, *Angew. Chem.* **2005**, *117*, 118; *Angew. Chem. Int. Ed.* **2005**, *44*, 116.
- [20] M. Whiting, J. Muldoon, Y.-C. Lin, S. M. Silverman, W. Lindstrom, A. J. Olson, H. C. Kolb, M. G. Finn, K. B. Sharpless, J. H. Elder, V. V. Fokin, *Angew. Chem.* **2006**, *118*, 1463; *Angew. Chem. Int. Ed.* **2006**, *45*, 1435.
- [21] H. K. Chenault, J. Dahmer, G. M. Whitesides, *J. Am. Chem. Soc.* **1989**, *111*, 6354.
- [22] J. C. M. van Hest, K. L. Kiick, D. A. Tirrell, *J. Am. Chem. Soc.* **2000**, *122*, 1282.
- [23] H.-S. Lee, J.-S. Park, B. M. Kim, S. H. Gellman, *J. Org. Chem.* **2003**, *68*, 1575.
- [24] Although we have not yet been able to determine which regioisomer of the in situ click product was formed, the authentic triligand synthesized by CuAAC to test affinity and selectivity was definitely the 1,4-triazole.
- [25] V. V. Rostovtsev, L. G. Green, V. V. Fokin, K. B. Sharpless, *Angew. Chem.* **2002**, *114*, 2708; *Angew. Chem. Int. Ed.* **2002**, *41*, 2596.
- [26] G. Liu, K. S. Lam in *Combinatorial Chemistry—A Practical Approach* (Ed.: H. Fenniri), Oxford University Press, USA, **2000**, pp. 43–44.
- [27] Y. Pocker, J. T. Stone, *Biochemistry* **1967**, *6*, 668.

**Appendix B**

Complete Hit Sequencing Results

	X <sub>1</sub>	X <sub>2</sub>	X <sub>3</sub>	X <sub>4</sub>	X <sub>5</sub>
hit1	r	r	y	h	r
hit2	m/v	r	w	k	r
hit3	k	r	w	y	y
hit4	w	k	k	k	w
hit5	h	f	f	f	r
hit6	s	r	--	r	r
hit7	r	r	w	h	y
hit8	r	k	w	w	w
hit9	r	w	s	f	r
hit10	r	r	g	w	r
hit11	g	f	r	r	w
hit12	r	t	r	r	w
hit13	m	r	w	k	r
hit14	y	r	k	r	w
hit15	a	--	--	--	--
hit16	r	r	i	r	w
hit17	--	--	k/l	w	--
hit18	r	w	--	--	r
hit19	k/l	r	--	w	r
hit20	w	r	f	r	y
hit21	d/p	y	y	r	r
hit22	r	y	w	k	k
hit23	k/l	r	r	r	w
hit24	y	r	r	k	w
hit25	r	k/l	f	y	r
hit26	r	w	w	k	r

	X <sub>1</sub>	X <sub>2</sub>	X <sub>3</sub>	X <sub>4</sub>	X <sub>5</sub>
hit27	w	r	--	y	r
hit28	h	r	w	r	r
hit29	w	y	r	k	r
hit30	l	r	f	r	r
hit31	w	k	r	k	k
hit32	r	r	r	w	s/m
hit33	r	r	k	f	w
hit34	r	r	w	r	y
hit35	w	r	h	y	k
hit36	r	r	y	f	r
hit37	w	r	k	w	r
hit38	w	y	--	r	r
hit39	y	r	r	r	h
hit40	y	r	r	r	w
hit41	p	f	y	w	r
hit42	k	y	w	r	k
hit43	r	y	w	h	k
hit44	r	w	h	w	n
hit45	r	h	f	h	h/f
hit46	r	r	--	h	r
hit47	r	y	r	r	r
hit48	y	f	h	h/w	w
hit49	r	r	r	w	y
hit50	w	r	r	r	r/--
hit51	r	w	k	f	h

**Table B.1.** First-generation anchor ligand screen **An1** results.

	X <sub>1</sub>	X <sub>2</sub>	X <sub>3</sub>	X <sub>4</sub>	X <sub>5</sub>	X <sub>6</sub>
<b>hit1</b>	y	r	w	f	k	f
<b>hit2</b>	h/r	h/r	f	l	l/r	r
<b>hit3</b>	f	r	f	y	y	r
<b>hit4</b>	h/r	f	f	k	l	--
<b>hit5</b>	k	l	f	l	k	l
<b>hit6</b>	l	f	l	w	l	k
<b>hit7</b>	f	f	f	r	y	--
<b>hit8</b>	h/r	f	f	f	r	--
<b>hit9</b>	r	w	w	l	k	f
<b>hit10</b>	h/r	f	f	r	y	y
<b>hit11</b>	l	k	l	f	l	k
<b>hit12</b>	f	r	r	w	w	k
<b>hit13</b>	h/r	y	f	f	k	l
<b>hit14</b>	l	k	f	f	f	k
<b>hit15</b>	h/r	f	f	r	r	--

(A)

	X <sub>1</sub>	X <sub>2</sub>	X <sub>3</sub>	X <sub>4</sub>	X <sub>5</sub>	X <sub>6</sub>
<b>hit1</b>	h	l	y	f	l	r
<b>hit2</b>	l	k	l	w	f	k

(B)

**Table B.2.** Second-generation anchor ligand screen (A) **An2a** and (B) **An2b** results.

The two anchor ligand candidates (hlyflr and lklwfk) are highlighted in yellow.

	Az <sub>n</sub>	x <sub>2</sub>	x <sub>3</sub>	x <sub>4</sub>	x <sub>5</sub>	x <sub>6</sub>	Az <sub>n</sub>
<b>hit1</b>	<b>Az4</b>	<b>k</b>	<b>i</b>	<b>w</b>	<b>i</b>	<b>G</b>	
hit2	Az8	r	l	w	v	G	Az4
hit3	Az8	r	r	r	k	r	Az8
hit4	Az4	l	l	v	i	k	Az4
hit5	Az4	m	i	l	i	k	
hit6	Az8	i	i	i	m	r	Az4
hit7	Az8	i	i	i	w	r	Az8
hit8	Az4	n	v	i	i	f	
hit9	Az4	i	f	l	v	k	Az8
<b>hit10</b>	<b>Az4</b>	<b>k</b>	<b>i</b>	<b>w</b>	<b>i</b>	<b>G</b>	<b>Az8</b>
hit11	Az4	r	r	k	f	r	Az8
hit12	Az4	r	v	w	l	r	Az8
hit13	Az8	k	y	r	r	r	Az4
hit14	Az8	r	r	k	v	w	Az4
hit15	Az4	i	f	l	v	k	Az8
hit16		k	r	k	r	f	Az4
<b>hit17</b>	<b>Az8</b>	<b>k</b>	<b>i</b>	<b>w</b>	<b>i</b>	<b>k</b>	
hit18	Az8	y	r	k	f	k	
hit19	Az4	i	f	f	r	v	Az8
hit20		a	r	k	k	y	Az4
hit 21		r	k	r	t	i	Az4
hit 22	Az8	k	m	v	f	k	Az4
hit23	Az4	l	i	m	k	i	Az4

**Table B.3.** In situ biligand screen **Bi1** results. Potential 2° ligand candidates are highlighted in orange.

hit1	f	k	l	w	i	k
hit2	v	w	l	w	G	G
hit3	f	w	f	w	G	G
hit4	k	w	f	w	G	G
hit5	f	k	l	w	l	k
hit6	k	w	f	w	G	G
hit7	w	w	i	w	G	G
hit8	k	G	w	l	w	G
hit9	k	l	w	i	w	G
hit10	l	w	i	w	G	l
hit11	f	k	G	f	l	i
hit12	f	w	i	w	G	k
hit13	l	w	l	w	G	i
hit14	i	i	v	l	w	k
hit15	l	i	i	f	v	
hit16	v	k	f	i	l	l
hit17	l	G	f	f	w	i
hit18	k	k	l	k	k	l
hit19	f	k	l	w	i	k
hit20	w	i	w	G	G	f
hit21	f	f	l	l	v	k
hit22	k	f	k	f	w	k
hit23	l	i	k	l	f	v
hit24	l	w	f	w	G	v
hit25	f	w	f	w	G	i
hit26	G	w	f	w	G	v
hit27	G	w	i	w	G	k

(A)

	x <sub>1</sub>	x <sub>2</sub>	x <sub>3</sub>	x <sub>4</sub>	x <sub>5</sub>	x <sub>6</sub>
hit1	k	w	i	w	G	w
hit2	k	w	i	w	G	v
hit3	k	w	l	w	G	l
hit4	k	w	i	w	G	l
hit5	k	w	i	w	G	w
hit6	k	w	l	w	G	l
hit7	G	w	i	w	G	i
hit8	k	i	f	k	i	f

(B)

**Table B.4.** On-bead biligand screen (A) **Bi2a** and (B) **Bi2b** results. Potential 2° ligand candidates are highlighted in yellow/green. Consensus motif w-x<sub>3</sub>-w-G (where x<sub>3</sub> = hydrophobic amino acid) is highlighted in red font.

	Az <sub>n</sub>	x <sub>2</sub>	x <sub>3</sub>	x <sub>4</sub>	x <sub>5</sub>	x <sub>6</sub>	Az <sub>n</sub>
hit1	Az4	n	i	i	i	v	
hit2	Az4	i	i	l	l	k	Az4
hit3	Az4	n	i	i	v	l	
hit4	Az4	n	m	i	f	l	Az4
hit5	Az4	n	v	l	v	l	
hit6	Az4	n	l	i	l	f	Az4
hit7	Az4	n	l	i	l	f	Az4
hit8	Az8	r	l	w	i	r	Az4
hit9	Az4	n	l	i	v	f	Az4
hit10	Az4	r	m	w	v	k	Az8
hit11	Az4	i	i	l	l	k	Az8
hit12	Az4	i	l	v	v	r	Az4
hit13	Az4	n	l	l	f	l	Az4
hit14	Az4	n	i	i	v	y	
hit15		m	k	r	k	k	Az8
hit16	Az4	i	l	i	r	w	Az4
hit17	Az8	i	i	v	f	r	Az8
hit18	Az8	y	f	t	r	r	
hit19	Az4	n	m	i	i	v	Az4
hit20	Az8	i	l	i	a	k	Az4
hit21	Az4	i	l	l	r	w	
hit22	Az8	i	v	v	f	r	Az4
hit23	Az4	l	l	l	v	k	Az4
hit24	Az4	k	v	w	i	k	Az4
hit25	Az4	i	m	v	l	r	Az4

**Table B.5.** First-generation in situ triligand screen **Tri1** results. Potential 3° ligand candidates are highlighted in orange.

	X <sub>2</sub>	X <sub>3</sub>	X <sub>4</sub>	X <sub>5</sub>	X <sub>6</sub>	X <sub>7</sub>
<b>hit1</b>	r	l	w	l	r	f
<b>hit2</b>	r	l	w	l	r	l
<b>hit3</b>	r	f	f	f	r	f
<b>hit4</b>	r	l	f	l	r	f
<b>hit5</b>	l	f	f	w	f	r
<b>hit6</b>	l	w	f	f	f	r
<b>hit7</b>	l	f	l	w	f	r
<b>hit8</b>	l	w	l	f	f	r
<b>hit9</b>	l	f	f	w	l	r
<b>hit10</b>	r	r	r	l	w	r
<b>hit11</b>	r	l	w	l	r	f
<b>hit12</b>	w	r	r	r	r	w
<b>hit13</b>	r	f	r	f	r	w
<b>hit14</b>	f	w	f	f	w	r

**Table B.6.** First-generation on-bead triligand screen **Tri2** results. Recall that the focused Library E was used for this screen. Potential 3° ligand candidates are highlighted in orange.

	x <sub>2</sub>	x <sub>3</sub>	x <sub>4</sub>	x <sub>5</sub>	x <sub>6</sub>	x <sub>7</sub>
<b>hit1</b>	n	l	i	v	f	r
<b>hit2</b>	n	l	i	v	l	r
<b>hit3</b>	n	i	i	l	l	r
<b>hit4</b>	i	l	f	l	f	r
<b>hit5</b>	n	l	i	v	l	r
<b>hit6</b>	n	i	i	l	w	r
<b>hit7</b>	n	l	i	v	f	r
<b>hit8</b>	n	l	i	v	f	r

(A)

	x <sub>2</sub>	x <sub>3</sub>	x <sub>4</sub>	x <sub>5</sub>	x <sub>6</sub>	x <sub>7</sub>
<b>hit1</b>	n	l	i	v	f	r
<b>hit2</b>	n	l	i	v	f	r
<b>hit3</b>	n	i	i	v	f	r
<b>hit4</b>	n	i	i	v	f	r
<b>hit5</b>	n	i	i	l	l	r
<b>hit6</b>	n	l	i	v	l	r
<b>hit7</b>	n	l	i	v	f	r

(B)

**Table B.7.** Results of second-generation triligand screens: (A) **Tri3** (in situ) and (B)

**Tri4** (on-bead). The final 3<sup>o</sup> ligand sequence is highlighted in orange.

	X <sub>1</sub>	X <sub>2</sub>	X <sub>3</sub>	X <sub>4</sub>	X <sub>5</sub>
<b>hit1</b>	w	f	r	r	r
<b>hit2</b>	s	w	v	w	G
<b>hit3</b>	p	v	y	f	w
<b>hit4</b>	d	d	y	w	G
<b>hit5</b>	i	w	a	y	w
<b>hit6</b>	d	n	w	G	f
<b>hit7</b>	a	w	w	a	t
<b>hit8</b>	r	f	r	r	f
<b>hit9</b>	d	w	w	h	t
<b>hit10</b>	r	f	r	w	r
<b>hit11</b>	d	e	w	p	h
<b>hit12</b>	a	w	w	l	w
<b>hit13</b>	a	w	w	a	y
<b>hit14</b>	d	k	k	i	y
<b>hit15</b>	d	w	s	i	e
<b>hit16</b>	s	w	w	f	y
<b>hit17</b>	d	w	l	r	y
<b>hit18</b>	s	w	a	f	y
<b>hit19</b>	d	l	f	l	w
<b>hit20</b>	d	w	a	t	w
<b>hit21</b>	f	k	y	r	s
<b>hit22</b>	d	q	r	w	r
<b>hit23</b>	i	w	s	t	h
<b>hit24</b>	l	i	v	m	w

**Table B.8.** Azide-free in situ triligand screen **TriX** results (control). Note the poor hit homology, and the lack of resemblance with nlivfr.

## **Appendix C**

### Custom Edman Degradation

To allow for resolution of artificial azide-containing amino acids by Edman degradation, the **Pulsed-Liquid cLC extended** method was utilized (Figure C.1A) on the model 494 Proclise cLC sequencing system (Applied BioSystems, Foster City, CA). It includes a modified gradient, **Normal 1 cLC extended** (Figure C.1B), and a flask cycle extended by 5 min (**Flask Normal extended**, Figure C.2).

The chromatograms corresponding to elution of Az2, Az4, Az6 and Az8 following Edman degradation are shown in Figure C.3 and demonstrate a 6-min retention time increase for every two methylene units added to the azidoalkyl side chain. Fmoc-Az2-OH was synthesized according to literature protocol,<sup>1</sup> while Fmoc-Az6-OH was synthesized from 1,6-dibromohexane according to Scheme 2.1.

(A)

Cycle #	Cartridge Cycle	Flask Cycle	Gradient
Default	Cart-PL 6mmGFF cLC	Flask Normal extended	Normal 1 extended
1	None	Prepare Pump cLC	Prepare Pump cLC
2	None	Flask Blank cLC	Normal 1 extended
3	Cart Begin cLC	Flask Standard cLC	Normal 1 extended

(B)

Time	%B	uL/min	Event	Cum. Volume A	Cum. Volume B
0.0	8	40	12	0.00	0.00
0.4	12	40	1	14.40	1.60
4.0	20	40	1	135.36	24.64
22.0	45	40	1	621.36	258.64
34.0	60	40	1	849.36	510.64
35.0	90	40	1	859.36	540.64
39.0	90	60	0	883.36	756.64
40.0	50	20	0	889.36	770.64

**Figure C.1. (A) Pulsed-Liquid cLC extended method and (B) Normal 1 cLC extended gradient.**

Cycle or Procedure :

Cycle/Procedure

- Prepare Pump cLC
- Run Gradient cLC
- Flask Normal extended**
- User Defined Cycle Template

Step	Function Name	Fn #	Value	Global	El. Tin
51	Load Position	226	0	<input type="checkbox"/>	31:16
52	Bubble Flask	212	5	<input type="checkbox"/>	31:21
53	Empty Flask	215	20	<input type="checkbox"/>	31:41
54	Del S4, Flask	171	10	<input type="checkbox"/>	31:51
55	Dry Flask	213	10	<input type="checkbox"/>	32:01
56	Bubble Flask	212	5	<input type="checkbox"/>	32:06
57	Flush Flask/Injector	222	40	<input type="checkbox"/>	32:46
58	Flush Injector	221	20	<input type="checkbox"/>	33:06
59	Wait	257	850	<input type="checkbox"/>	47:16
60	Wait	257	360	<input type="checkbox"/>	53:16
61	End	259	0	<input type="checkbox"/>	53:16

**Figure C.2.** Final steps of **Flask Normal extended** flask cycle.

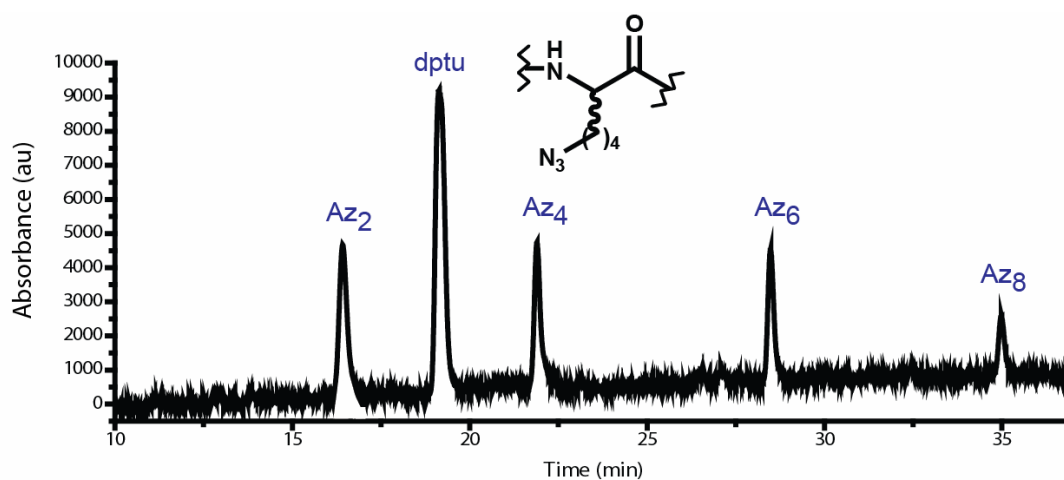


**Figure C.3.** Edman traces for artificial azide-containing amino acids.

## REFERENCES

1. Roice, M.; Johannsen, I.; Meldal, M. *QSAR Comb. Sci.* **2004**, *23*, 662–673.

**Appendix D**

A Non-Oxidative Approach toward Chemically and Electrochemically Functionalizing

Si(111)

Reproduced from

*Journal of the American Chemical Society* **2006**, *128*, 9518–9525

## A Non-Oxidative Approach toward Chemically and Electrochemically Functionalizing Si(111)

Rosemary D. Rohde, Heather D. Agnew, Woon-Seok Yeo, Ryan C. Bailey, and James R. Heath\*

*Contribution from the Division of Chemistry and Chemical Engineering, MC 127-72, California Institute of Technology, Pasadena, California 91125*

Received March 23, 2006; E-mail: heath@caltech.edu

**Abstract:** A general method for the non-oxidative functionalization of single-crystal silicon(111) surfaces is described. The silicon surface is fully acetylenylated using two-step chlorination/alkylation chemistry. A benzoquinone-masked primary amine is attached to this surface via Cu(I)-catalyzed Huisgen 1,3-dipolar cycloaddition ("click" chemistry). The benzoquinone is electrochemically reduced, resulting in quantitative cleavage of the molecule and exposing the amine terminus. Molecules presenting a carboxylic acid have been immobilized to the exposed amine sites. X-ray photoelectron spectroscopy (XPS), Fourier transform infrared spectroscopy (FTIR), cyclic voltammetry (CV), and contact angle goniometry were utilized to characterize and quantitate each step in the functionalization process. This work represents a strategy for providing a general platform that can incorporate organic and biological molecules on Si(111) with minimal oxidation of the silicon surface.

### Introduction

Semiconductor devices and semiconductor processing are playing an increasingly large role in biotechnology, with applications that include nanowires (NWs)<sup>1</sup> and nanocantilevers<sup>2,3</sup> for label-free biomolecular sensors, nanofluidics for biomolecular separations,<sup>4-7</sup> and a host of microfabricated lab-on-a-chip technologies.<sup>8,9</sup> Coupled with these emerging nano- and microtechnologies has been the emergence of mechanical,<sup>10-12</sup> chemical, and electrochemical approaches for functionalizing and/or selectively activating surfaces. Electrochemical activation of surfaces is particularly relevant because it is shape conformal and is only limited by the size of electronically addressable features (which can be much denser than what can be spotted with an inkjet, for example). Electrochemical activation of metal

surfaces has been pioneered by Mrksich,<sup>13-16</sup> and applications of that chemistry toward the biofunctionalization of semiconductor nanowires has been demonstrated by at least two groups.<sup>17,18</sup> For Si surfaces, the chemistry is particularly challenging: without protection, Si will form a native oxide that can prevent the use of silicon electrodes for electrochemical functionalization. The native oxide on silicon also has a low isoelectric point, meaning that under physiological conditions (pH 7.4), SiO<sub>2</sub> surfaces are negatively charged.<sup>19</sup> These surface charges can potentially limit the sensitivity of certain nanoelectronic biomolecular sensor devices through Debye screening<sup>20</sup> of the biomolecular probe/target binding event to be sensed. Furthermore, the native oxide of Si can detrimentally impact carrier recombination rates.<sup>21</sup> For high surface area devices, such as Si NWs, this can likely result in a degradation of electrical properties. Thus, the ideal biofunctionalization strategy for electrochemically activating Si surfaces should begin with non-oxidized Si. The approach should also provide continued protection of the Si surface against subsequent oxidation and should limit the number of surface traps that can increase carrier recombination rates.

- (1) Zheng, G.; Patolsky, F.; Cui, Y.; Wang, W. U.; Lieber, C. M. *Nature Biotechnol.* **2005**, *23*, 1294, and references therein.
- (2) Beckmann, N.; Zahid, C.; Huber, F.; Bitsch, A.; Plneckthun, A.; Lang, H.-P.; Güntherodt, H.-J.; Hegner, M.; Gerber, C. *Proc. Natl. Acad. Sci. U.S.A.* **2005**, *102*, 14587.
- (3) Yue, M.; Lin, H.; Dedrick, D. E.; Satyanarayana, S.; Majumdar, A.; Bedekar, A. S.; Jenkins, J. W.; Sundaram, S. *J. Microelectromech. Syst.* **2004**, *13*, 290.
- (4) Reccius, C. H.; Mannoni, J. T.; Cross, J. D.; Craighead, H. G. *Phys. Rev. Lett.* **2005**, *95*, 268101.
- (5) Stavris, S. M.; Edel, J. B.; Li, Y. G.; Samiee, K. T.; Luo, D.; Craighead, H. G. *J. Appl. Phys.* **2005**, *98*, 044903.
- (6) Fan, R.; Karnik, R.; Yue, M.; Li, D. Y.; Majumdar, A.; Yang, P. D. *Nano Lett.* **2005**, *5*, 1633.
- (7) Karnik, R.; Castellino, K.; Fan, R.; Yang, P.; Majumdar, A. *Nano Lett.* **2005**, *5*, 1638.
- (8) Craighead, H. G.; James, C. D.; Turner, A. M. P. *Curr. Opin. Solid State Mater. Sci.* **2001**, *5*, 177.
- (9) Jung, D. R.; Kapur, R.; Adams, T.; Giuliano, K. A.; Mrksich, M.; Craighead, H. G.; Taylor, D. L. *Crit. Rev. Biotechnol.* **2001**, *21*, 111.
- (10) Piner, R. D.; Zhu, J.; Xu, F.; Hong, S.; Mirkin, C. A. *Science* **1999**, *283*, 661.
- (11) Lee, K.-B.; Park, S.-J.; Mirkin, C. A.; Smith, J. C.; Mrksich, M. *Science* **2003**, *295*, 1702.
- (12) Jung, H.; Dalal, C. K.; Kuntz, S.; Shah, R.; Collier, C. P. *Nano Lett.* **2004**, *4*, 2171.

- (13) Yousaf, M.; Mrksich, M. *J. Am. Chem. Soc.* **1999**, *121*, 4286.
- (14) Hodneland, C. D.; Mrksich, M. *J. Am. Chem. Soc.* **2000**, *122*, 4235.
- (15) Yeo, W.-S.; Yousaf, M. N.; Mrksich, M. *J. Am. Chem. Soc.* **2003**, *125*, 14994.
- (16) Yeo, W.-S.; Mrksich, M. *Adv. Mater.* **2004**, *16*, 1352.
- (17) Bunimovich, Y. L.; Ge, G.; Beverly, K. C.; Ries, R. S.; Hood, L.; Heath, J. R. *Langmuir* **2004**, *20*, 10630.
- (18) Curci, M.; Li, C.; Sun, Y.; Lei, B.; Gundersen, M. A.; Thompson, M. E.; Zhou, C. *J. Am. Chem. Soc.* **2005**, *127*, 6922.
- (19) Hu, K.; Fan, F.-R. F.; Bard, A. J.; Hillier, A. C. *J. Phys. Chem. B* **1997**, *101*, 8298.
- (20) Israelachvili, J. *Intermolecular and Surface Forces*; Academic Press: London, 1985.
- (21) Yablonovitch, E.; Allara, D. L.; Chang, C. C.; Gmitter, T.; Bright, T. B. *Phys. Rev. Lett.* **1986**, *57*, 249.

Several methods for attaching organic molecules onto non-oxidized Si surfaces have been reported. One class of schemes relies upon the direct covalent attachment of alkene terminated molecules to H-terminated surfaces by thermal induction, ultraviolet (UV) light, or catalysis.<sup>22–29</sup> These strategies have not been demonstrated as giving long-term protection to the Si surface against oxidation. Lewis' group has developed the two-step chlorination/alkylation procedure for Si(111) surfaces that is based upon Grignard chemistry.<sup>30–35</sup> A limitation of these approaches is that, thus far, only the methylated Si(111) surface (using Lewis' chemistry) can be 100% covered.<sup>34,36</sup> For example, the coverage that can be achieved through the ethylation of Cl-terminated Si(111) is limited by steric effects and is about 80% of the atop sites.<sup>37</sup> For larger organic molecules, surface coverages will most certainly be lower, and resistance to oxidation will be reduced. To fully passivate the Si(111) surface, generate resistance to oxide growth, and provide for a chemically versatile surface, different surface chemistries are needed. It is relevant to note that no surface chemistry has yet been demonstrated that yields protection of the much more technologically relevant Si(100) surface against oxidation.

In this paper, we describe a versatile and robust strategy for chemically passivating Si(111) surfaces in a manner that stabilizes the underlying Si against oxidation and allows for both chemical and electrochemical functionalization of the surface. Upon the basis of our previous work on methylated and ethylated Si(111),<sup>30–37</sup> we chose to explore the more chemically versatile acetylenylation of chlorine-terminated Si(111). Work by Nemanick<sup>38</sup> and Lewis' group<sup>39,40</sup> indicated that the chlorination/alkylation chemistry for acetylenylating Si(111) could proceed to completion. The footprint of the  $\text{—C}\equiv\text{CH}$  on Si(111) should be as small or smaller than the  $\text{—CH}_3$  group, and so a high surface coverage should be possible. Equally important is that the  $\text{—C}\equiv\text{CH}$  group also provides a chemical handle for additional functionalization via the Cu(I) catalyzed Huisgen 1,3-dipolar cycloaddition ("click" reaction<sup>41,42</sup>) between an azide and the surface-bound alkyne. In particular, we

designed an azide-functionalized, modified benzoquinone for attachment, via the click reaction, to the surface-bound acetylenyl groups to form a 1,2,3-triazole. The click reaction is useful because azides and acetylenes are synthetically easy to introduce, compatible with a variety of solvents and species, and tolerant against other functionality (highly specific, coupling can only occur between these two groups). Our work here follows recent reports that have demonstrated that different molecules can be clicked onto gold and  $\text{SiO}_2$  surfaces in a variety of solvent and pH conditions.<sup>43–51</sup>

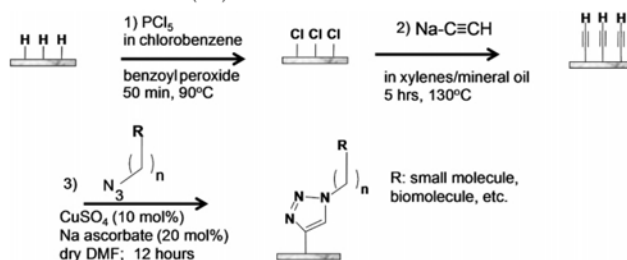
We previously reported on the electrochemistry of hydroquinones on Si(111) and Si(100) surfaces, attached via the UV-activation of H-terminated Si.<sup>17</sup> In that work, the hydroquinones could be reversibly oxidized to form benzoquinones (the "activated" surface), which could then react by way of either Diels–Alder cycloaddition<sup>13,15</sup> or Michael addition chemistries,<sup>32,53</sup> leading to a selectively bifunctionalized Si microwire or nanowire surface. However, although the hydroquinone coverage on the Si(111) surface did yield at least some protection for that surface against oxidation, the electrochemical step to oxidize the hydroquinone also led to oxidation of the underlying Si(111). Thus, in this work, we have designed and synthesized a benzoquinone that can be clicked onto the acetylenylated Si surface. The surface-bound benzoquinone may be then activated via electrochemical *reduction* to produce an amine terminus.<sup>14,54,55</sup> We demonstrate that the entire chemical process may be accomplished in a fashion that greatly reduces the oxidation of the underlying Si. We also demonstrate the selective attachment of ferrocene onto an electrochemically activated Si(111) surface, as well as the model biomolecule, biotin.

## Experimental Methods

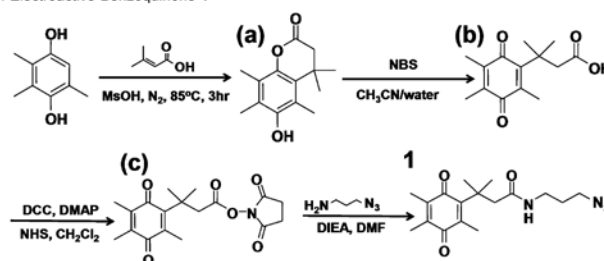
**Chemicals.** Anhydrous methanol and anhydrous tetrahydrofuran (THF, inhibitor-free) were obtained from Aldrich and exclusively stored and used in a  $\text{N}_2$ (g)-purged glovebox. Chlorobenzene, benzoyl peroxide, and sodium acetylide (18 wt % in xylenes/light mineral oil) were purchased from Aldrich and were stored and used in the glovebox. Phosphorus pentachloride ( $\text{PCl}_5$ ) was acquired from Riedel-de Haën (Seelze, Germany). The 40%  $\text{NH}_4\text{F}$ (aq) solution was obtained from Transene Co. (Rowland, MA) and was used as received. The  $\text{CuSO}_4 \cdot 5\text{H}_2\text{O}$  was obtained from Spectrum Chemical Mfg. Corp. (Gardena, CA). Sodium ascorbate, ferrocene carboxylic acid, and anhydrous *N,N*-dimethylformamide (DMF) were obtained from Aldrich. *N,N*-Diisopropylcarbodiimide (DIC) was purchased from Anaspec (San Jose, CA).

- (22) Sung, M. M.; Kluth, G. J.; Yauw, O. W.; Maboudian, R. *Langmuir* 1997, 13, 6164.  
 (23) Sieval, A. B.; Demirel, A. L.; Nissink, J. W. M.; Linford, M. R.; van der Maas, J. H.; de Jeu, W. H.; Zuilhof, H.; Sudhölter, E. J. R. *Langmuir* 1998, 14, 1759.  
 (24) Effenberger, F.; Gotz, G.; Bidlingmaier, B.; Wezstein, M. *Angew. Chem., Int. Ed.* 1998, 37, 2462.  
 (25) Boukherroub, R.; Wayner, D. D. M. *J. Am. Chem. Soc.* 1999, 121, 11513.  
 (26) Linford, M. R.; Fender, P.; Eisenberger, P. M.; Chidsey, C. E. D. *J. Am. Chem. Soc.* 1995, 117, 3145.  
 (27) Cicera, R. L.; Linford, M. R.; Chidsey, C. E. D. *Langmuir* 2000, 16, 5688.  
 (28) Buriak, J. M.; Allen, M. J. *J. Am. Chem. Soc.* 1998, 120, 1339.  
 (29) Stewart, M. P.; Buriak, J. M. *J. Am. Chem. Soc.* 2001, 123, 7821.  
 (30) Webb, L. J.; Nemanick, E. J.; Biteson, J. S.; Knapp, D. W.; Michalak, D. J.; Traub, M. C.; Chan, A. S. Y.; Brunschwig, B. S.; Lewis, N. S. *J. Phys. Chem. B* 2005, 9, 3930.  
 (31) Yu, H. B.; Webb, L. J.; Ries, R. S.; Solares, S. D.; Goddard, W. A.; Heath, J. R.; Lewis, N. S. *J. Phys. Chem. B* 2005, 109, 671.  
 (32) Webb, L. J.; Lewis, N. S. *J. Phys. Chem. B* 2003, 107, 5404.  
 (33) Bansal, A.; Li, X. L.; Yu, S. I.; Weinberg, W. H.; Lewis, N. S. *J. Phys. Chem. B* 2001, 105, 10266.  
 (34) Royea, W. J.; Jung, A.; Lewis, N. S. *Appl. Phys. Lett.* 2000, 77, 1988.  
 (35) Bansal, A.; Lewis, N. S. *J. Phys. Chem. B* 1998, 102, 4058.  
 (36) Solares, S. D.; Yu, H.; Webb, L. J.; Lewis, N. S.; Heath, J. R.; Goddard, W. A., III. *J. Am. Chem. Soc.* 2006, 128, 3850.  
 (37) Yu, H.; Webb, L. J.; Heath, J. R.; Lewis, N. S. *Appl. Phys. Lett.* (in press, 2006).  
 (38) Nemanick, E. J. *Chemical and Electrical Passivation of Single Crystal Silicon Surfaces through Covalently Bound Organic Monolayers*; Caltech Ph.D. Thesis, 2005.  
 (39) Nemanick, E. J.; Hurley, P. T.; Brunschwig, B. S.; Lewis, N. S. *J. Phys. Chem. B* 2006, in press.  
 (40) Hurley, P. T.; Nemanick, E. J.; Brunschwig, B. S.; Lewis, N. S., submitted.  
 (41) Kolb, H. C.; Finn, M. G.; Sharpless, K. B. *Angew. Chem., Int. Ed.* 2001, 40, 2004.  
 (42) Bock, V. D.; Hiemstra, H.; van Maarseveen, J. H. *Eur. J. Org. Chem.* 2006, 51, and references therein.  
 (43) Zhang, Y.; Luo, S.; Tang, Y.; Yu, L.; Hou, K.-Y.; Cheng, J. P.; Zeng, X.; Wang, P. G. *Anal. Chem.* 2006, 78, 2001.  
 (44) Lumerstorfer, T.; Hoffmann, H. *J. Phys. Chem. B* 2004, 108, 3963.  
 (45) Lee, J. K.; Chi, Y. S.; Choi, I. S. *Langmuir* 2004, 20, 3844.  
 (46) Li, H.; Chang, F.; Dutt, A. M.; Adronov, A. *J. Am. Chem. Soc.* 2005, 127, 14518.  
 (47) Zirbs, R.; Kienberger, F.; Hinterdorfer, P.; Binder, W. H. *Langmuir* 2005, 21, 8414.  
 (48) Collman, J. P.; Devaraj, N. K.; Chidsey, C. E. D. *Langmuir* 2004, 20, 1051.  
 (49) Collman, J. P.; Devaraj, N. K.; Eberspacher, T. P. A.; Chidsey, C. E. D. *Langmuir* 2006, 22, 2457.  
 (50) Devaraj, N. K.; Dinolfo, P. H.; Chidsey, C. E. D.; Collman, J. P. *J. Am. Chem. Soc.* 2006, 128, 1794.  
 (51) Devaraj, N. K.; Miller, G. P.; Ebina, W.; Kakaradov, B.; Collman, J. P.; Kool, E. T.; Chidsey, C. E. D. *J. Am. Chem. Soc.* 2005, 127, 8600.  
 (52) Giovannelli, D.; Lawrence, N. S.; Jiang, L.; Jones, T. G. J.; Compton, R. G. *Anal. Lett.* 2003, 36, 2941.  
 (53) Rousell, C.; Rohner, T. C.; Jensen, H.; Girault, H. H. *ChemPhysChem* 2003, 4, 200.  
 (54) Zheng, A.; Shan, D.; Binghe, W. *J. Org. Chem.* 1999, 64, 156.  
 (55) Yeo, W.-S.; Hodneland, C. D.; Mirksich, M. *ChemBioChem* 2001, 590.

Scheme 1. Strategy for the Functionalization of Si(111)



Scheme 2. Synthesis of Electroactive Benzoquinone 1



Dulbecco's Phosphate Buffered Saline (DPBS) (2.7 mM KCl, 1.5 mM  $\text{KH}_2\text{PO}_4$ , 137 mM NaCl, 8 mM  $\text{Na}_2\text{HPO}_4$ , pH 7.4) was purchased from Sigma. EZ-Link NHS–Biotin was obtained from Pierce Biotechnology, Inc. (Rockford, IL). Nanogold Streptavidin was purchased from Invitrogen (Carlsbad, CA). GoldEnhance-EM kit for Nanogold amplification was bought from Nanoprobes (Yaphank, NY).

**Acetylenylation of Si(111).** Scheme 1 shows the strategy used for functionalization of Si(111), using a two-step chlorination/alkylation method followed by Cu(I)-catalyzed click chemistry. The acetylene passivation leads to a high coverage of atop sites on an unreconstructed Si(111) surface ( $97 \pm 5\%$ ), which resists native oxidation of the surface.<sup>39,40</sup> Another advantage is the ability to use the terminal alkyne to attach a variety of molecules via click chemistry.

The starting surfaces used in these experiments were single-crystal, polished Si(111) wafers, that were 500–550  $\mu\text{m}$  thick, phosphorus-doped (n-type), with 0.005–0.02  $\Omega\text{-cm}$  resistivity and a miscut angle of 3–4° (Monteco Silicon Technologies (Spring City, PA)). Prior to use, the Si wafers (1 cm  $\times$  1 cm) were cleaned by successive sonications in acetone, methanol, and 2-propanol. Substrates were then rinsed with Millipore (18 M $\Omega$ ) water and then placed into basic piranha solution (5:1:1 =  $\text{H}_2\text{O}/\text{H}_2\text{O}_2/\text{NH}_4\text{OH}$  warning: caustic!) at 80 °C for 5 min. The samples were removed from piranha solution, rinsed with copious amounts of Millipore water, and dried under streaming  $\text{N}_2(\text{g})$ . The samples were immediately place in degassed  $\text{NH}_4\text{F}(\text{aq})$  solution for 15 min. The samples were subsequently removed from the  $\text{NH}_4\text{F}(\text{aq})$ , rinsed copiously with water, dried under streaming  $\text{N}_2(\text{g})$ , and immediately loaded into a glovebox.

Chlorination of the Si(111) surfaces (Scheme 1, Step 1) was carried out in a  $\text{N}_2(\text{g})$ -purged glovebox, according to published methods.<sup>30–37</sup> A saturated solution of  $\text{PCl}_5$  in chlorobenzene was prepared and heated for 1 h before use to ensure complete dissolution of the  $\text{PCl}_5$ . The Si substrate was added with a grain of benzoyl peroxide to this solution and heated to 90 °C for 50 min. Subsequently, the samples were rinsed with anhydrous THF several times and immediately used for the acetylenylation step.

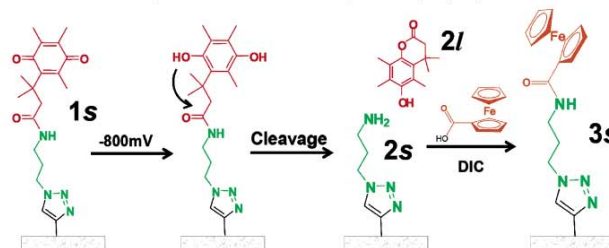
Acetylenylation of the chlorinated Si(111) surfaces (Scheme 1, Step 2) was performed inside the  $\text{N}_2(\text{g})$ -purged glovebox. The chlorinated wafers were immersed in a sodium acetylide (18 wt % in xylenes/light mineral oil) suspension and heated to 130 °C for 5 h.<sup>40</sup> After reaction, the samples were removed from solution, rinsed copiously with anhydrous THF, and then rinsed with anhydrous methanol. The samples were then immersed into a fresh volume of anhydrous methanol, taken out of the glovebox into air, sonicated for 10 min, and then dried in a stream of  $\text{N}_2(\text{g})$ .

**Synthesis of Electroactive Benzoquinone 1.** Scheme 2 describes the synthetic procedure for making the electroactive benzoquinone 1 used for all surface click reactions.<sup>54</sup> A 2,3,5-trimethylhydroquinone was treated with dimethylacrylic acid to give a lactone **a** by a Friedel–Crafts type addition reaction. The quinone acid **b** was prepared by oxidation of the resulting lactone **a** with aqueous *N*-bromosuccinimide (NBS). The acid was activated with an *N*-hydroxysuccinimide (NHS) group to give **c**, which was then subjected to 3-azidopropylamine to afford **1**.

**6-Hydroxy-4,4,5,7,8-peptamethyl-chroman-2-one (a).** 2,3,5-Tri-methylhydroquinone (2 g, 13.1 mmol) was mixed with 3,3-dimethylacrylic acid (1.45 g, 14.5 mmol) and methanesulfonic acid (10 mL). The mixture was stirred at 85 °C under nitrogen for 3 h and then cooled to room temperature. To the mixture was added 100 g of ice with stirring. The precipitate was extracted with ethyl acetate (4  $\times$  50 mL). The combined organic layer was washed with saturated  $\text{NaHCO}_3$  (2  $\times$  50 mL) and water (2  $\times$  50 mL) and dried over  $\text{MgSO}_4$ . After filtration and evaporation, an obtained residue was recrystallized from hexane and ethyl acetate (2:1, v/v) to give 2.6 g (84%) of the desired product as a white solid.  $^1\text{H NMR}$  300 MHz ( $\text{CDCl}_3$ )  $\delta$  4.69 (s, 1H), 2.56 (s, 2H), 2.37 (s, 3H), 2.23 (s, 3H), 2.9 (s, 3H), 1.46 (s, 6H).

**3-Methyl-3-(2,4,5-trimethyl-3,6-dioxocyclohexa-1,4-dienyl)butanoic Acid (b).** To a solution of the lactone **a** (1.58 g, 6.74 mmol) in a mixture of acetonitrile (15 mL) and water (3 mL) was added *N*-bromosuccinimide (1.26 g, 7.08 mmol) in portions with stirring at room temperature. After 30 min, the organic solvents were evaporated

Scheme 3. Chemical and Electrochemical Steps Involved in Non-oxidatively Activating Si(111) Surfaces\*



\* The molecules or molecular components are colored to highlight their different functions: **1s** represents the surface-bound benzoquinone that resulted from the click reaction of **1** to the acetylene-modified Si(111) surface (reacted acetylene group drawn in black). Upon reduction at  $-800$  mV (vs Ag/AgCl) of the benzoquinone to the hydroquinone, an intramolecular cyclization reaction ensues to produce **2l** (red lactone leaving group) and **2s** (the green triazole ring with an amine terminus). This represents the activated surface. The ferrocene carboxylic acid (orange), a second electrochemically active molecule, is then coupled to the Si(111) surface.

under reduced pressure, and the remaining solution was extracted with  $\text{CH}_2\text{Cl}_2$  ( $2 \times 30$  mL). The combined organic layer was dried over  $\text{MgSO}_4$ , and the solvent was removed to give 1.65 g (98%) of a yellow oily product, which was used without further purification.  $^1\text{H NMR}$  300 MHz ( $\text{CDCl}_3$ )  $\delta$  3.04 (s, 2H), 2.15 (s, 3H), 1.96 (m, 3H), 1.94 (m, 3H), 1.45 (s, 6H).

**3-Methyl-3-(2,4,5-trimethyl-3,6-dioxocyclohexa-1,4-dienyl)butanoic Acid, *N*-Hydroxysuccinimide Ester (c).** To a solution of acid **b** (326 mg, 1.30 mmol) and *N*-hydroxysuccinimide (152 mg, 1.32 mmol) in  $\text{CH}_2\text{Cl}_2$  (15 mL) was added 1,3-dicyclohexylcarbodiimide (DCC, 270 mg, 1.31 mmol) portionwise, followed by a catalytic amount of *N,N*-(dimethylamino)pyridine (DMAP). The reaction mixture was stirred for 1 h. The white precipitate was filtered, and the filtrate was concentrated. The residue was redissolved in cold ethyl acetate (5 mL), and insoluble impurities were filtered. Solvent was removed to give 419 mg (93%) of a yellow, foamy solid product.  $^1\text{H NMR}$  300 MHz ( $\text{CDCl}_3$ )  $\delta$  3.27 (s, 2H), 2.77 (s, 4H), 2.15 (s, 3H), 1.94 (s, 6H), 1.51 (s, 6H).

***N*-(3-azidopropyl)-3-methyl-3-(2,4,5-trimethyl-3,6-dioxocyclohexa-1,4-dienyl)butanamide (1).** To a solution of **c** (443 mg, 1.28 mmol) in DMF (5 mL) was added diisopropylethylamine (DIEA, 523  $\mu\text{L}$ , 3.06 mmol), followed by 3-azidopropylamine (153 mg, 1.53 mmol). The reaction mixture was stirred overnight at  $50^\circ\text{C}$ , diluted with ethyl acetate (30 mL), washed with  $\text{NH}_4\text{Cl}$  and brine, and dried over  $\text{MgSO}_4$ . Solvent was reduced, and the residue was purified by silica gel chromatography (hex/EtOAc, 2:1) to give 370 mg (87%) of product as a yellow solid.  $^1\text{H NMR}$  300 MHz ( $\text{CDCl}_3$ )  $\delta$  3.30 (t,  $J = 6.6$ , 2H), 3.23 (q,  $J = 6.6$ , 2H), 2.81 (s, 2H), 2.12 (s, 3H), 1.96 (m, 3H), 1.94 (m, 3H), 1.70 (quint,  $J = 6.6$ , 2H), 1.41 (s, 6H). Mass (ES)  $m/z$  333.0 ( $[\text{M} + 1]^+$ ).

**Click Reaction to Attach 1 onto Acetylene-Terminated Si(111).** The click reaction of acetylene-terminated Si(111) (Scheme 1, Step 3) with **1** (Scheme 2) was carried out in anhydrous DMF. Relative to the azide, 20 mol % sodium ascorbate was added, followed by 10 mol % of  $\text{CuSO}_4 \cdot 5\text{H}_2\text{O}$ , and a 10 mM azide solution of **1** in DMF. The reaction was run for 12 h in the glovebox. After the reaction, the surface was sonicated in DMF for 5 min three times and then rinsed with methanol and blow dried under  $\text{N}_2$ (g).

**Electrochemical Activation to Attach Ferrocene.** **1** was attached to acetylene-terminated Si(111) using the Cu(I)-catalyzed click reaction (Scheme 1, Step 3), to form **1s** (Scheme 3). Reductive electrochemistry ( $-800$  mV referenced to Ag/AgCl) was performed to convert the modified benzoquinone to hydroquinone in degassed DPBS (pH 7.4). The hydroquinone then underwent an intramolecular cyclization reaction, leaving a free amine on the surface (**2s**), releasing a lactone species (**2l**). This amine terminus allows for a variety of subsequent reactions, including amide coupling chemistry, which is commonly

utilized to attach biomolecules to surfaces. We first illustrated the use of this electrochemical reduction process to attach ferrocene carboxylic acid to the surface, to form **3s**, via amide coupling chemistry. Ferrocene carboxylic acid (0.02 M) and *N,N*-diisopropylcarbodiimide (DIC) (0.13 M) in DMF were added to the free amine surface. The amide coupling reaction was run overnight covered in an  $\text{N}_2$ -purged glovebox. The surface was then sonicated three times in DMF, then MeOH, and then blown dry.

**Electrochemical Activation to Attach Biotin.** Biotin (0.02 M) and DIC (0.13 M) in DMF were added to the free amine surface **2s**. The amide coupling reaction was run overnight in an  $\text{N}_2$ -purged glovebox at  $50^\circ\text{C}$ . The surface was then sonicated three times in DMF, then MeOH, and blow dried. Subsequently, the Nanogold streptavidin (10 pM in 0.05% Tween20/DPBS) was introduced for 15 min. The surface was sonicated in 0.05% Tween20/DPBS for 25 min and then water for 5 min. The gold particles were then amplified with gold enhancement reagents for 10 min and then sonicated in water for 5 min.

**Surface Characterization Methods. X-ray Photoelectron Spectroscopy.** X-ray photoelectron spectroscopy (XPS) was utilized to characterize many of the steps of both Schemes 1 and 3. All XPS measurements were performed in an ultrahigh vacuum chamber of an M-probe surface spectrometer that has been previously described.<sup>56</sup> All measurements were taken on the center of the sample at room temperature. Monochromatic Al K $\alpha$  X-rays (1486.6 eV) were incident at  $35^\circ$  from the sample surface and were used to excite electrons from samples. The emitted electrons were collected by a hemispherical analyzer at a takeoff angle of  $35^\circ$  from the plane of the sample surface.

ESCA-2000 software was used to collect and analyze the data. To get an overview of the species present in the sample, survey scans were run from 0 to 1000 binding eV (BeV). The Si 2p (97–106 BeV), Cl 2p (196–206 BeV), C 1s (282–292 BeV), N 1s (393–407 BeV), Fe 2p (695–745 BeV), and Au 4f (77–97 BeV) regions were investigated in detail.

**Contact Angle Measurements.** The sessile contact angle of water on the functionalized Si(111) surface was used to check the fidelity of the monolayer for all surfaces of Schemes 1 and 3 except H- and Cl-terminated Si(111). Contact angle measurements were obtained with an NRL C.A. Goniometer Model #100-00 (Rame-Hart, Inc.) at room temperature. Contact angles,  $\theta$ , were measured from sessile drops by lowering a 1  $\mu\text{L}$  drop from a syringe needle onto the surface. This was repeated three times and averaged to obtain the  $\theta$  for the surface.

**Electrochemical Characterization of Surface Coverages.** Electrochemistry was performed in a custom-made cell using a VMP Multi-Potentiostat (Princeton Applied Research, Oak Ridge, TN). Dulbecco's phosphate buffered saline (DPBS) was used as the electrolyte, with

(56) Haber, J. A.; Lewis, N. S. *J. Phys. Chem. B* 2002, 106, 3639.

**Table 1.** Measured Contact Angles for Various Si(111) Surfaces

surfaces	contact angle (deg)
H-C≡C-[Si(111)]	77 ± 2
1s	68 ± 2
2s	60 ± 2
3s	59 ± 2

silicon as a working electrode, a Pt coil as a counter electrode, and an Ag/AgCl reference electrode. Cyclic voltammetry was carried out at a rate of 100 mV/s. Molecular coverage was obtained by integrating the cathodic peak of the first scan in which all the modified benzoquinone was reduced to hydroquinone.

**Infrared Surface Characterization.** The H- and H-C≡C-terminated Si(111) surfaces were characterized by attenuated total reflection Fourier transform infrared spectroscopy (ATR-FTIR). The Si(111) surfaces were prepared from single-crystal, polished Si(111), miscut 3–4°, boron-doped (p-type), 500–550 μm thick, and with 4–20 Ω-cm resistivity (Addison Engineering, Inc., San Jose, CA). Samples were cut into (2 cm × 2 cm) pieces. Samples underwent the acetylenylation and click reactions as described above. Samples were mounted on a Germanium ATR crystal (GATR, Harick Scientific Products, Inc.) for a grazing angle of 65°. The sample was placed in a Vertex 70 FT-IR spectrometer (Bruker Optics Inc.) for measurements. In an air-purged sample chamber, 512 or 1024 scans were taken, with background scans of air subtracted from the spectra. Spectra were fitted with a linear baseline prior to analysis.

## Results

**XPS Survey Scans and Contact Angle Measurements.** XPS survey scans revealed the progression of the acetylenylation and click chemistry steps. For a freshly prepared, H-terminated Si(111) surface (H-[Si(111)]), Si 2p and Si 2s peaks were observed, at 100 BeV and 150 BeV, respectively. Additional small C 1s and O 1s peaks, corresponding to adventitiously adsorbed carbon and oxygen on the surface, were also detected. After chlorination of H-[Si(111)] by PCl<sub>5</sub>, two new peaks at 200 BeV and 270 BeV appeared in the XPS spectrum, representing the Cl 2p and Cl 2s electrons, respectively. Upon a treatment with sodium acetylide, the chlorine peaks disappeared and a pronounced C 1s appeared at 285 BeV, verifying that the acetylene-terminated Si(111) surface (H-C≡C-[Si(111)]) has been generated. Other adsorbed carbon can contribute to the C 1s peak intensity for this scan. After the click reaction, a new N 1s peak appears at 400 BeV.

Sessile contact angles were also quantified for the various surface functionalization steps described in Schemes 1 and 3, and those values are listed in Table 1.

**High-Resolution XPS Measurements.** High-resolution XPS measurements were utilized to quantitate the chemical steps of Schemes 1 and 3. In particular, the Si 2p region was used to monitor the growth of silicon oxides as a function of exposure time to air (Figure 1) and as a function of the chemical and electrochemical steps of Scheme 3 (Figure 2A) in two sets of experiments. For both measurements, a Shirley baseline was applied to each spectrum before the peaks were fitted. Peak line shapes for bulk Si 2p<sub>3/2</sub> and 2p<sub>1/2</sub> were fitted to Voigt functions fixed at 95% Gaussian and 5% Lorentzian, with a 15% asymmetry. The Si 2p<sub>1/2</sub> and 2p<sub>3/2</sub> peaks were fitted with the two peaks held 0.6 BeV apart, the full width at half-maximum (fwhm) was fixed at 1, and the integrated area ratio of the 2p<sub>1/2</sub>/2p<sub>3/2</sub> peaks was fixed at 0.51, as has been previously described.<sup>30–32,39</sup> The broad peak between 100 and 104 BeV

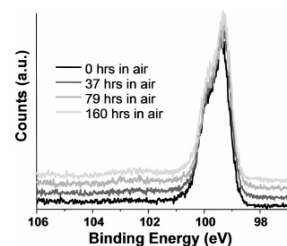


**Figure 1.** XPS data of H-C≡C-[Si(111)], collected in the Si 2p region and taken after exposure to air for up to 160 h. The peaks for SiO<sub>x</sub> species should appear between 100 and 104 BeV. The amount of oxidation of the Si(111) can be estimated from these data to be about 0.25 equivalent monolayers. The Si 2p features are normalized to the same height for all three scans. The 37, 79, 160 h scans are shown offset from the 0 h scan to reveal the spectral detail. For the 4 scans, the amount of SiO<sub>x</sub>, as extracted from fits to the spectra, are 0.0, 0.18, 0.21, and 0.25 equiv monolayers, with increasing time.

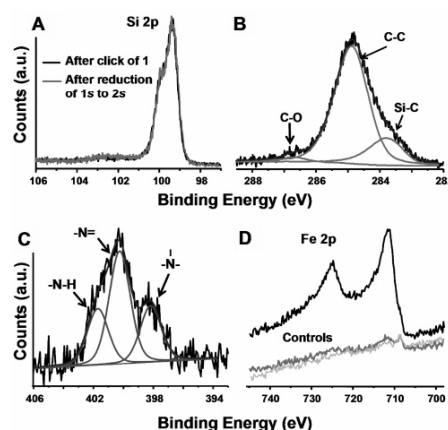


**Figure 2.** High-resolution XPS spectra of H-C≡C-[Si(111)], and of that surface following the click reaction to form 1s and the reduction of 1s to 2s. (A) Si 2p region revealing the near absence of oxide growth during the Cu(I)-catalyzed click reaction, and during the reductive transformation of 1s to 2s. (B) Scan of the C 1s region of H-C≡C-[Si(111)]. The Si-C peak is unique to H-C≡C-[Si(111)] surfaces. The C-C peak contains contributions from the C≡C bond and adventitious carbon from the environment. The C-O peak present also arises from adventitious hydrocarbons. (C) Scan of the N 1s region of 1s, validating the click formation of 1s. The area ratio of the three peaks is 1:2:1, respectively. (D) Scan of the Fe 2p region showing the formation of peaks of 1s via the amide coupling of ferrocene carboxylic acid to 2s. The control plots are of 1s (dark gray) and the H-C≡C-[Si(111)] surface (light gray) after exposure to ferrocene carboxylic acid under the same conditions.

was assigned as Si<sup>+</sup> to Si<sup>2+</sup> oxides and was fitted to a third peak. The positions of the three peaks and the width of the third peak were optimized to get the best fit to the experimental spectrum. For very thin oxide layers, the oxide coverage was calculated from the SiO<sub>x</sub>/Si 2p peak area ratio. This was determined by dividing the area under the third peak by the total area of the Si 2p<sub>3/2</sub> and 2p<sub>1/2</sub> peaks.<sup>32</sup> The SiO<sub>x</sub>/Si 2p peak area ratio was then divided by a normalization constant of 0.21 for Si(111) to estimate the fraction of surface atoms that were

oxidized.<sup>30–32</sup> We estimated that there were approximately 0.25 equivalent monolayers of SiO<sub>x</sub> on the acetylene-terminated Si(111) surface after 6 days exposure to air (Figure 1). This is consistent with other results that have shown stability toward oxidation for as long as 60 days in air.<sup>40</sup> Following the formation of **1s** and the reduction of **1s** to **2s** at  $-800$  mV (Scheme 3) in aqueous electrolyte, the amount of SiO<sub>x</sub> was calculated to be 0.29 and 0.34 equivalent monolayers, respectively.

The H–C≡C–[Si(111)] surface was also characterized using high-resolution XPS of the C 1s spectrum (Figure 2B). This spectrum was deconvoluted and fitted to three peaks, the silicon-bonded carbon at 283.8 BeV, the carbon-bonded carbon at 284.9 BeV, and the oxygen-bonded carbon at 286.8 BeV. As developed by Nemanick,<sup>38,39</sup> peaks were fitted to Voigt functions having 70% Gaussian and 30% Lorentzian line shapes. The peak center-to-center distances were fixed at 1.1 BeV between the Si–C and C–C peaks, and at 2.9 BeV between the Si–C and O–C peaks. To calculate the surface coverage of the acetylene the integrated area under the silicon-bonded carbon peak was ratioed to the total integrated area of the Si 2p<sub>3/2</sub> and 2p<sub>1/2</sub> peaks and normalized with respect to scan time. The ratio calculated was referenced to a methyl terminated Si(111) surface that was scanned under the same conditions. The effective coverage of acetylene on the Si surface was  $97 \pm 5\%$ , consistent with other measurements of such surfaces.<sup>40</sup> The statistical uncertainty in this number is largely determined by the signal-to-noise ratio of the XPS data ( $\sim 30:1$ ).

The high-resolution N 1s spectrum of **1s** illustrates the attachment of the benzoquinone (**1**) via click chemistry (Figure 2C). The spectrum was deconvoluted and fitted to three peaks, each composed of 80% Gaussian and 20% Lorentzian line shapes.<sup>57</sup> The three peaks correspond to the amide nitrogen at 401.7 BeV, the doubly bonded nitrogen atoms (in the triazole ring) at 400.3 BeV, and the singly bonded nitrogen (in the triazole ring) at 398.2 BeV, respectively. The ratio of peak areas was found to be 1:2:1, consistent with the structure of **1s**. After electrochemical cleavage to **2s**, the N 1s region remained unchanged.

Figure 2D is a high-resolution scan of the Fe 2p region that demonstrates the attachment of ferrocene carboxylic acid onto **2s** to form **3s**. The Fe 2p<sub>3/2</sub> and 2p<sub>1/2</sub> peaks occur at 711.3 and 724.8 BeV, respectively. It is difficult to quantify the amount of iron from such data because the peak shape is highly asymmetric and hard to deconvolute with a single Gaussian/Lorentzian function due to the strong multiplet splitting.<sup>57</sup> However, as discussed below, the surface coverage of **3s** can be estimated from cyclic voltammetry measurements. Figure 2D also shows two control experiments. Although a trace amount of ferrocene residue is detected on the controls, this measurement does confirm that the large majority of ferrocene is the result of the covalent bond formation between carboxylic acid of the ferrocene and the free amine of **2s**.

**Electrochemical Measurements.** Figure 3A depicts the cyclic voltammogram (CV) for **1s**. The prominent cathodic peak in the first scan confirms the presence of electroactive benzoquinone and, therefore, that the click reaction proceeded. Molecular coverage was obtained by integrating the cathodic peak of the first scan in which all the modified benzoquinone

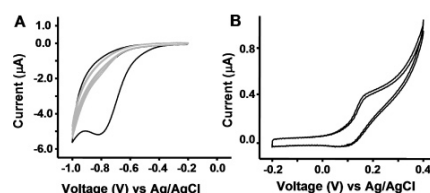


**Figure 3.** Cyclic voltammograms (CVs) for **1s** and **3s**. (A) The electrochemical activation of **1s** to **2s**. The black trace is of the first scan, and the gray traces are of two subsequent scans, indicating nearly complete conversion of benzoquinone to hydroquinone during the first scan. (B) The reversible oxidation of **3s**. Two subsequent scans are shown. CVs were performed at a rate of 100 mV/s with voltages relative to Ag/AgCl.

**Table 2.** Measured Molecular Surface Coverages for Various Si(111) Surfaces, as Measured by XPS or Electrochemistry (EC)

surfaces	coverage (%)
H–C≡C–[Si(111)]	$97 \pm 5$ (XPS)
<b>1s</b> –benzoquinone	$6.7 \pm 0.3$ (EC)
<b>3s</b> –ferrocene	0.5 (EC)

was reduced to hydroquinone. Complete conversion of **1s** to **2s** accompanied by the release of **2l** (Scheme 3) was achieved at potentials below  $-0.9$  V. Consecutive CV scans show that no detectable benzoquinone remained. For the determination of coverage, the area under the cathodic peak was obtained after subtracting the non-Faradaic current. This area was converted to the number of molecules by a stoichiometric ratio of 2 electrons to 1 electroactive molecule. Then the number of molecules was divided by the electrode surface area and then normalized to the Si atop atom surface density ( $7.8 \times 10^{14}/\text{cm}^2$  for Si(111)).<sup>17</sup> The coverage calculated for **1s** on the H–C≡C–[Si(111)] was  $6.7 \pm 0.3\%$ .

Figure 3B represents a CV of **3s**, the product of the amide coupling of ferrocene carboxylic acid with **2s**. The CV shows reversible Fe<sup>0/+</sup> redox behavior, as expected for ferrocene oxidation. The peak spacing confirms that ferrocene is covalently attached (but not adsorbed) onto the surface. The coverage was calculated by integrating the anodic peak after subtracting the non-Faradaic current. The number of molecules was divided by the electrode surface area and normalized to Si atom surface density which is  $7.8 \times 10^{14}/\text{cm}^2$  for Si(111).<sup>17</sup> The coverage calculated for **3s** was 0.5%. We do not fully understand the low coverage of ferrocene molecules. A likely possibility is that the time and/or temperature conditions for the coupling reaction were not optimal. It is also possible that degradation of the surface by oxidative potential treatments might also reduce the coverage of ferrocene.

## Discussion

The coverage values for H–C≡C–[Si(111)], surface **1s**, and surface **3s** are summarized in Table 2, calculated with respect to all atop sites on an unreconstructed Si(111) surface.

The 97% coverage of the H–C≡C–[Si(111)] surface is consistent with the Si 2p XPS in Figure 1 (and other studies<sup>40</sup>) that indicated little surface-bound SiO<sub>x</sub>. The acetylene carbons are sp-hybridized, implying a perpendicular attachment to the Si(111) surface. The atomic radius for C is smaller than that for Si (0.70 Å versus 1.10 Å), and there is a 3.8-Å spacing between atop sites on Si(111). These values support the notion

(57) Babjić-Samarđžija, K.; Lupu, C.; Hackerman, N.; Barron, A. R.; Lutge, A. *Langmuir* 2005, 21, 12187.

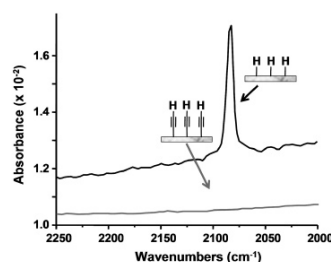


**Figure 4.** ATR-FTIR characterization of a H-[Si(111)] and H-C≡C-[Si(111)] in the region of the 2083  $\text{cm}^{-1}$  Si-H mode.

that a 100% passivation of Si(111) surfaces can be achieved using the approach we described here.

Additional support for 100% acetylenylation of Si(111) comes from the ATR-FTIR measurements of H-[Si(111)] and H-C≡C-[Si(111)] (Figure 4; black and gray traces, respectively). Whereas XPS allows analysis of the elemental composition of surfaces, infrared spectroscopy (IR) gives information about the types of chemical functionality on a surface. The spectra shown in Figure 4 are expanded to highlight the region containing the signature Si-H ( $2083 \text{ cm}^{-1}$ ) stretching frequency that is observed for the H-[Si(111)]. The Si-H stretch is strong and sharp, indicating that the surface sites are passivated with one hydrogen atom per atop site. This is expected for a H-[Si(111)] freshly prepared by an  $\text{NH}_4\text{F}(\text{aq})$  etch.<sup>58</sup> For H-C≡C-[Si(111)], the  $2083 \text{ cm}^{-1}$  vibration has quantitatively disappeared, again consistent with 100% acetylenylation and with other work.<sup>40</sup> A weak C=C stretch might be expected in this region ( $2120\text{--}2175 \text{ cm}^{-1}$ ),<sup>40,46</sup> although we have not observed it. When H-[Si(111)] is ethylated through a similar chlorination/alkylation procedure, the coverage of ethyl groups on the atop sites of the Si(111) surface is limited by steric interactions to be approximately 80%.<sup>37</sup> Following the Grignard alkylation of Si(111), no Cl is detected on the surface,<sup>30</sup> and FTIR data indicates that the remaining Si(111) atop sites are hydrogenated.<sup>59</sup> For the ethylated surface, the  $2083 \text{ cm}^{-1}$  feature is broadened, shifted (to  $2070 \text{ cm}^{-1}$ ), and reduced in intensity to 14% of that observed for the H-[Si(111)] surface.<sup>59</sup>

The coverage of the electroactive benzoquinone **1** on Si(111) to form **1s** was calculated to be  $\sim 7\%$  of all available Si(111) atop sites. We previously reported on electrochemically activating Si(111) and Si(100) surfaces through the use of protected hydroquinones that were attached to H-terminated Si surfaces via UV activation.<sup>17</sup> For those molecules, coverages of up to 23% were achievable on Si(111), although bulkier protection groups on the hydroquinone led to slightly reduced surface coverages, implying steric interactions played at least some role in limiting coverage. It is likely that steric interactions play a dominating role in determining the efficiency of the click reaction to form **1s**. Although the acetylene footprint may be approximated by the van der Waals radius of the carbon atom, the triazole ring formed upon the click reaction will obviously be much larger. In fact, it is possible that the click chemistry is only effective at the step edges of the Si(111) surface. We have

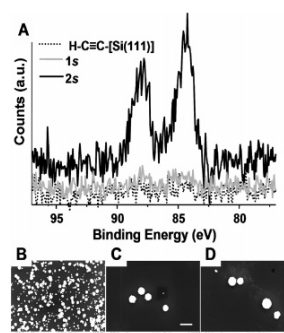


**Figure 5.** Demonstration of bioattachment to acetylenylated Si(111) through reductive formation of **2s** followed by the amide coupling of biotin. (A) XPS of the biotinylated Si(111) surface following exposure to strept-Au, but prior to the electroless Au amplification. The Au 4f region is comprised of two spin-orbit coupled peaks: Au  $4f_{7/2}$  ( $\sim 84 \text{ eV}$ ) and Au  $4f_{5/2}$  ( $\sim 88 \text{ eV}$ ). The dotted trace is from H-C≡C-[Si(111)], and the gray trace is from **1s**, each exposed to biotin and strept-Au as controls. The three SEM images (B, C, and D) are of the activated and biofunctionalized surface, plus two controls. All images were taken following the electroless amplification step. The scale bar is  $1 \mu\text{m}$ . (B) **2s**, incubated with biotin, and exposed to strept-Au. (C) H-C≡C-[Si(111)] incubated with biotin, and exposed to strept-Au. (D) **1s** incubated with biotin, and exposed to strept-Au. There are at least 500 Au nucleation sites on B, 5 on C, and 7 on D.

extensively characterized various Si(111) surfaces that have been alkylated using the two-step chlorination/alkylation chemistry using high-resolution scanning tunneling microscopy (STM). For both methylated<sup>31,36</sup> and ethylated<sup>37</sup> Si(111), we find that about 10% of the Si surface atoms lie at step edges. This arises from etch pits that are apparently formed during the chlorination step, implying that the H-C≡C-[Si(111)] surface likely has a similar morphology. In that case, acetylene groups located at step edges would not have the steric constraints that would limit the formation of the triazole ring. It is interesting that the 7% coverage of **2s** is similar to the number of Si atop sites that would reside at step edges. We are currently investigating the H-C≡C-[Si(111)] and **1s** surfaces using high-resolution STM in an effort to test this hypothesis.

We observed that minimal oxide growth on an acetylenylated surface even after 6 days exposure to air, indicating nearly 100% passivation of the surface (Figure 1). Following the formation of **1s** and electrochemical reduction of **1s** to **2s** to reveal the free amine, the amount of  $\text{SiO}_x$  was slightly increased to 0.29 and 0.34 equivalent monolayers, respectively. The oxidation growth observed was due to the click chemistry on acetylenylated surfaces that were minimally exposed to air during cleaning and preparation for reaction, and the electrochemistry which was carried out in an ambient (and aqueous) environment. It is notable that the limited oxide growth on the silicon even after all surface modifications afforded well-behaved electrodes.

There have been several reported examples of click reactions on metal surfaces, although relatively few papers have attempted to report quantitative coverage values. Chidsey's group<sup>48–50</sup> has reported on coverages of up to 55% of ferrocene molecules clicked onto  $\text{N}_3\text{-(CH}_2\text{)}_n\text{-S-[Au]}$  SAMs. On gold, each organic group has approximately twice the area available to it (21.4

(58) Dumas, P.; Chabal, Y. J.; Higashi, G. S. *Phys. Rev. Lett.* **1990**, *65*, 1124.  
(59) Webb, L. J.; Rivillon, S.; Michalak, D. J.; Chabal, Y. J.; Lewis, N. S. *J. Phys. Chem. B* **2006**, *110*, 7349.

$\text{\AA}^2/\text{molecule}$  for gold and  $12.8 \text{ \AA}^2/\text{molecule}$  for Si(111))<sup>17,60,61</sup> as compared with the area available to each acetylene group on Si(111). However, even for the much more loosely packed SAM, steric interactions were attributed as the reason for the incomplete (55%) yield of the click reaction.

The stated goal of this work was to develop a general strategy for electrochemically directing the bifunctionalization of Si(111) surfaces without oxidizing the underlying Si(111). To this end, we demonstrated the electrochemical activation and subsequent attachment of the model biomolecule, biotin, using a modification of the chemistry described in Scheme 3 (see Experimental Methods). To detect surface-bound biotin, we utilized Au nanoparticle-labeled streptavidin (strept-Au) and followed through with electroless amplification of the Au to produce particles that were imaged using scanning electron microscopy (SEM). Representative data from this experiment, shown in Figure 5, indicates that the selectivity for attachment of strept-Au onto **2s** is about 100-fold greater than on two control surfaces, H-C≡C-[Si(111)] and **1s**, both of which were also treated with biotin and exposed to strept-Au.

### Conclusions

Acetylenylation of the Si(111) surface via the two-step chlorination/alkylation procedure was combined with click chemistry to provide a non-oxidative approach for adding chemical functionality to a silicon surface. Si(111) surfaces can be nearly 100% passivated with acetylene groups. A specifically designed, electroactive benzoquinone molecule has been im-

mobilized to the H-C≡C-[Si(111)] surface. A 7% coverage of the benzoquinone was found, which suggests that the click reaction may have occurred at step edges on the H-C≡C-[Si(111)] surface. The attachment of an electroactive benzoquinone was highly selective and was accomplished with only a minimal amount of oxidation of the underlying Si(111). The electroactive benzoquinone was reduced and cleaved from the surface to produce an amine terminus. In separate experiments, ferrocene carboxylic acid and biotin were selectively and covalently immobilized to the electrochemically activated surface.

We believe this approach can be used as a general platform to prepare functional surfaces for various applications and can be extended toward the selective biopassivation of arrays of various types of nanomechanical and/or nanoelectronic sensor devices.

**Acknowledgment.** R.D.R. thanks the Hispanic Scholarship Fund and the Bill and Melinda Gates Foundation. H.D.A. is supported by the National Science Foundation Graduate Research Fellowship. We acknowledge support from the National Cancer Institute, the Institute for Collaborative Biotechnologies funded by the Army Research Office, and a subcontract from the MITRE Corporation for support of this research. The XPS measurements were carried out at the Molecular Materials Research Center of the Beckman Institute at Caltech. We thank Professor Nate Lewis, Dr. Pat Hurley, and Dr. Joe Nemanick for kind advice and help regarding the acetylenylation of Si(111).

JA062012B

(60) Strong, L.; Whitesides, G. M. *Langmuir* **1988**, *4*, 546.  
 (61) Chidsey, C. E. D.; Bertozzi, C. R.; Putvinski, T. M.; Muijsce, A. M. *J. Am. Chem. Soc.* **1990**, *112*, 4301.